Journal of Pharmaceutical and Biomedical Analysis 60 (2012) 1–6

Contents lists available at SciVerse ScienceDirect

Journal of Pharmaceutical and Biomedical Analysis

journal homepage: www.elsevier.com/locate/jpba

Isoxyl assays in plasma

Chenchen Wang[a,b], Lucila Garcia-Contreras[a,c], Pavan Muttil[a,d], Anthony J. Hickey[a,*]

[a] Eshelman School of Pharmacy, University of North Carolina at Chapel Hill, Division of Molecular Pharmaceutics, Campus Box #7571, 1310 Kerr Hall, Chapel Hill, NC 27599, USA
[b] Allergan, 2525 Dupont Dr., Irvine, CA 92612, USA
[c] 1110 N. Stonewall Ave., Suite 321, PO Box 26901, Oklahoma City, OK 73126-0901, USA
[d] Department of Pharmaceutical Sciences, College of Pharmacy, University of New Mexico, Albuquerque, NM 87131, USA

ARTICLE INFO

Article history:
Received 8 August 2011
Received in revised form 21 October 2011
Accepted 28 October 2011
Available online 4 November 2011

Keywords:
Tuberculosis
Isoxyl
Method validation
Metabolism
Minimum inhibitory concentration

ABSTRACT

Isoxyl is an effective drug to treat multi-drug resistant (MDR) tuberculosis but was abandoned due to failure in some clinical outcomes. The aim of this study was to develop and validate a reverse-phase high-performance liquid chromatographic (HPLC) method for determination of isoxyl concentrations in plasma, a prerequisite for understanding poor in vivo behavior of the drug. In the method, isoxyl was extracted from guinea pig plasma with acetonitrile and quantified by a Hewlett Packard 1100 series HPLC coupled with a Spherisorb 5 μm ODS2 (2 × 100 mm) column and UV detection at 270 nm. The mobile phase was 70% ACN in 20 mM ammonium acetate buffer. The isoxyl peak was eluted at 4.8 min with no interference with the peaks of impurities from plasma and internal standard. Recovery of isoxyl from guinea pig plasma was >68%, and LOQ (Limit of Quantification) was 0.25 μg/ml which was 8 times lower than the reported minimal inhibitory concentration (MIC, 2 μg/ml). The HPLC method was sensitive, reproducible, and accurate for quantification of isoxyl in guinea pig plasma according to FDA guidance for bioanalytical method validation. The method was utilized to quantify isoxyl plasma concentrations following oral administration of the drug to guinea pigs. The results suggest that the poor clinical outcomes of the drug may have been caused by the extremely low isoxyl plasma concentrations which were far below the MIC for action on *Mycobacterium tuberculosis*.

1. Introduction

Tuberculosis remains a serious infectious disease resulting in the death of more than two million people annually. Disturbingly, the incidence of multiple drug resistance to the first and second line agents employed to treat tuberculosis is increasing globally. New drugs are desperately needed to respond to this major challenge to public health internationally. Assessment of drugs that have previously shown some promise would help in this endeavor. Isoxyl (thiocarlide) (Fig. 1A) is an effective antituberculosis drug used to treat various multi-drug resistant (MDR) strains (MIC = 1–10 μg/ml). However, the drug was abandoned forty years ago due to failure of early clinical trials. Since a sensitive and accurate quantitative method is absent for the drug, the studies of in vivo exposure to isoxyl were rare and unreliable. The exact mechanism of poor clinical outcomes remains unclear.

Most studies of isoxyl were conducted in 1960s and 1970s. Only two quantitative analytical methods, microbiological [1–5] and radiochemical (S35 labeled isoxyl) [3–6], have been used to quantify isoxyl concentrations in body fluids. The microbiological activity method was insensitive and the radioactive labeling method could not distinguish between intact drug and metabolites. Consequently, limited in vivo exposure to isoxyl was reported and the data were inconsistent. Published isoxyl blood levels after oral administration are summarized in Table 1 [1–4]. The isoxyl plasma peak concentrations varied from 5.5 μg/ml to 128 μg/ml, and rates of absorption and elimination were very different in these studies. Also, since these studies were carried out under several different conditions, such as dose, dose regimen, dosage form, fasting vs. non-fasting, healthy subjects vs. tuberculosis patients, small vs. large population sample sizes, and serum vs. blood samples, comparison is difficult. Further reliable studies are necessary to elucidate the in vivo disposition of isoxyl.

Recent development of Chromatographic method allows for more accurate quantification of in vivo exposure to isoxyl. Dover et al. [7] and Kordulakova et al. [8] employed a reverse phase HPLC and a LC–MS, respectively, to understand in vitro metabolism of isoxyl by incubating the drug with mycobacterial flavin-containing monooxygenase "EthA". Dover et al. [7] used a linear gradient containing 0.05% formic acid in water and acetonitrile, and measured absorbance of isoxyl at 254 nm. Kordulakova et al. [8] utilized a linear gradient containing 0.07% ammonium formate in methanol–water. However, no development and validation of the chromatographic method to quantify isoxyl in body fluids was

* Corresponding author. Tel.: +1 919 962 0223; fax: +1 919 966 0197.
E-mail address: ahickey@unc.edu (A.J. Hickey).

0731-7085/$ – see front matter © 2011 Elsevier B.V. All rights reserved.
doi:10.1016/j.jpba.2011.10.029

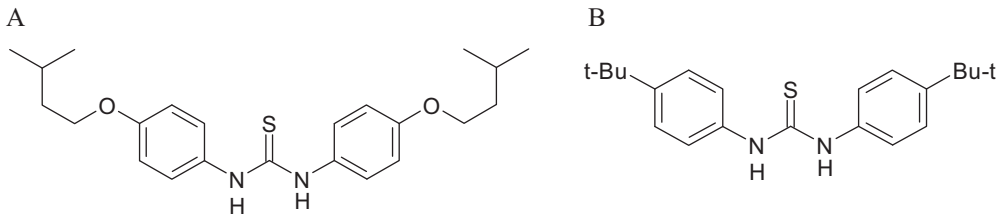

Fig. 1. The chemical structures of isoxyl (A) and N,N′-bis[4-(1,1-dimethylethyl)phenyl]-thiourea (B).

reported. The aim of the study was to develop and validate an HPLC method to determine the isoxyl concentrations in plasma. The in vivo exposure of the drug following i.v. and oral administration to guinea pigs was also reported.

Guinea pig plasma was selected in consideration of low costs and future application to preclinical animal experiments. The guinea pig develops disease and an immune response similar to the human after exposure to low inocula of mycobacteria [9]. Therefore, it will be an excellent model for future pharmacokinetic and efficacy studies of isoxyl.

2. Materials and methods

2.1. Materials

Isoxyl was purchased from Cayman Chemical Co. (Ann Arbor, Michigan). Acetonitrile (HPLC grade) and ammonium acetate (HPLC grade) were obtained from Acros Organics and Fisher Scientific, respectively. N,N′-bis[4-(1,1-dimethylethyl)phenyl]-thiourea was from Ryan Scientific, Inc. (Mt. Pleasant, South Carolina). Ethanol was purchased from Sigma (200 proof, ≥99.5%). Dunkin–Hartley guinea pigs were purchased from Hilltop Lab Animals Inc. (Scottsdale, PA). Plasma samples from guinea pigs were withdrawn and then stored at −80 °C until use. Ultrapure water was obtained from Barnstead Nanopure Infinity Ultrapure Water System (Dubuque, IA, USA).

2.2. Preparation of the standards and quality control (QC) samples

A 2 mg quantity of isoxyl was weighed accurately and then transferred to a 2 ml volumetric flask containing ethanol. The stock solutions of isoxyl at concentrations of 0.1, 0.01, 0.001 mg/ml were made by a series of 10-fold dilutions using volumetric flasks. These solutions were stored at −20 °C until use. From these stock solutions, concentrations of 0.05, 0.1, 0.25, 0.5, 1, 2.5, 5, 10, 25, 50 μg/ml isoxyl were made freshly using either 50% ACN in 20 mM ammonium acetate buffer (pH 7.0) or guinea pig plasma to obtain the standards. Three quality controls were made by spiking plasma with isoxyl to prepare solutions at low (0.4 μg/ml), medium (6 μg/ml) and high (40 μg/ml) concentrations. The standards and quality controls in plasma were stored at −80 °C until analysis.

2.3. Analytical conditions

The analysis was performed using a Hewlett Packard 1100 series HPLC (Agilent Technologies, Santa Clara, CA) with a binary pump, an autosampler, a Waters Spherisorb 5 μm ODS2 (2 × 100 mm) preceded by a Nova-Pak C18 4 μm precolumn cartridge, and a UV detector set at 270 nm (the absorption maximum wavelength of isoxyl in acetonitrile). The narrow-bore column was employed owing to its higher detectability, less consumption of solvents, and short run time. Mobile phase was screened by varying ratios of acetonitrile to water. Flow rate was 0.5 ml/min. The optimal analysis condition was determined.

2.4. Extraction of isoxyl from plasma

N,N′-bis[4-(1,1-dimethylethyl)phenyl]-thiourea (Fig. 1B), having similar structure to isoxyl, was chosen as an internal standard (IS) to compensate for variations in sample preparation and injection procedures. Internal standard (0.102 mg/ml) of 5 μl was spiked in 100 μl of the standards, QCs, blank plasma controls and samples. Acetonitrile of 400 μl was then added to precipitate proteins. The samples were vortexed for 2 min and centrifuged at 12,000 rpm for 10 min. The supernatants were pipetted into microcentrifuge tubes and dried in a Savant ISS110 Speedvac concentrator (Thermo Fisher Scientific, Waltham, MA). Each pellet was dissolved in 100 μl of 50% acetonitrile in 20 mM ammonium acetate buffer from which 50 μl was injected.

2.5. Method validation

The method was validated according to FDA guidance for bioanalytical method validation (http://www.fda.gov/downloads/Drugs/GuidanceComplianceRegulatoryInformation/Guidances/UCM070107.pdf). Briefly, the standards containing pure isoxyl in either 50% ACN and 50% 20 mM ammonium acetate buffer or guinea pig plasma were used to determine linearity of the drug in a range of concentrations from the limit of quantification to 20 times of minimum inhibitory concentration (MIC). The standard

Table 1
Summary of blood levels of isoxyl delivered orally in human subjects [1–4].

Author	Robinson et al.	Eule et al.	Lambelin et al.
Route (form)	Oral (not mentioned)	Oral (tablets)	Oral (tablets)
Dose	Single, 9 g	2× 3 g (6 h)	2× 3 g (4 h)
No. of patients	9	31	6
Subjects	Healthy, fasting	Patients	Healthy, non-fasting
Samples	Blood	Serum	Blood
Method	Microbiological	Microbiological	Microbiological and radioactive
MIC	0.4 μg/ml	0.6–0.8 μg/ml	1.2–1.4 μg/ml
Time (C < MIC)	>24 h	<24 h	>24 h
C_{max} (T_{max})	>128 μg/ml (2 h) in 5 subjects 8–24 μg/ml (2–6 h) in 4 subjects	5.5 μg/ml (9 h after first dose)	8–11 μg/ml (∼10 h after first dose)

curve was plotted by peak area ratios of isoxyl to internal standard against isoxyl concentrations. The best fit line was obtained by the least square regression method and the regression coefficient (R) was calculated. Background levels were measured and the limit of detection (LOD) was determined by signal to background ratio of 3. Specificity was evaluated by separation of the isoxyl peak from the peaks of impurities from plasma and internal standard. Intraday precision and accuracy of the HPLC method were evaluated by assaying at least four replicates of standard plasma solutions at three concentrations, low (0.4 μg/ml), medium (6 μg/ml) and high (40 μg/ml) in one day. The inter-day variation was determined by assaying these three concentrations on each of five consecutive days. The accuracy of the measurement was the mean percentage recovery of isoxyl at each concentration. The precision of the measurement was the coefficient of variation which was calculated by the ratio of standard deviations of replicates to the mean concentrations. The limit of quantification (LOQ) was measured by determining precision and accuracy of five replicates of four low concentrations, 0.05, 0.1, 0.25, and 0.5 μg/ml. The measurements for the LOQ should have a precision of 20% and an accuracy of 80–120% according to FDA guidance.

2.6. Recovery evaluation

Extraction efficiency was determined by comparing the amount of the drug extracted from plasma with the amount of drug in the reference standards. Samples of 0.4, 6, 40 μg/ml in triplicate were extracted and analyzed by HPLC as described in above. To prepare the reference standards, drug free plasma of 100 μl was extracted with 400 μl acetonitrile. The supernatant was collected and dried in the same way as described in above. Isoxyl and 50% acetonitrile in 20 mM ammonium acetate buffer were added to the blank extraction pellets to prepare standards of 0.4, 6, 40 μg/ml. All the standards were assayed in triplicate. An internal standard was introduced into each sample and standards. The recovery of isoxyl from plasma was evaluated by comparing peak area ratios of isoxyl to internal standard measured in samples with those of the reference standards of the respective concentrations.

2.7. Stability studies

The stability of isoxyl was evaluated by determining the drug concentration change in quality control samples (QCs) during storage. Triplicate QCs were stored at room temperature for 5.5 h or underwent three freeze–thaw cycles according to FDA guidance. For long-term stability, the standards were stored at −80 °C for a month (30 days).

2.8. Preliminary in vivo exposure studies

Male Dunkin–Hartley guinea pigs (808–961 g) were employed. All of the animal experiments were consist with the policies of the UNC-CH Institutional Animal Care and Use Committee. The right external jugular vein of each guinea pig was cannulated using silicone polymer tubing connected to polyethylene PE-50 tubing to facilitate collection of blood samples. Two guinea pigs received a dose of 10 mg/kg or 20 mg/kg by intravenous administration through the cannular implanted in the jugular vein. Blood samples were collected at various time points and drug concentrations were determined by the HPLC assay. For oral delivery, isoxyl was suspended in 1% carboxymethyl cellulose (CMC) and ground in a mortar with a pestle. The suspensions were fed orally to guinea pigs (non-fasting) in duplicate at a dose of 100 mg/kg. The plasma samples were collected and isoxyl concentrations were determined by the HPLC method.

Table 2
Determination of Limit of Quantification (LOQ) (n = 5).

Conc. (μg/ml)	Precision (%)	Accuracy (%)
0.05	43	259
0.1	40	108
0.25	11	87
0.5	12	100

3. Results

Optimization of chromatographic methods was conducted using samples containing the pure drug solution in 50% ACN and 50% 20 mM ammonium acetate buffer (pH 7.0). The optimized mobile phase contained 70% ACN and 30% 20 mM ammonium acetate buffer (pH 7.0). The flow rate was 0.5 ml/min. The retention times of the IS and isoxyl were 3.5 and 4.5 min, respectively (Fig. 2A). As the percentage of ACN in mobile phase increased to 75%, isoxyl peak merged with internal standard peak. Decrease of ACN resulted in the longer retention time (T_R). When 10 μl of the samples was injected onto the HPLC column, a linear calibration plot of isoxyl ranging from 0.1 μg/ml to 50.6 μg/ml was obtained. The regression equation and correlation coefficiency were determined: Peak Area Ratio (Isoxyl/Internal Standard) = 0.173 × Concentration − 0.0044 and R = 0.9980. The limit of detection (LOD) of the method was determined to be 20 ng/ml injected.

For plasma samples, isoxyl was extracted by ACN and analyzed by HPLC. Isoxyl peak (4.8 min) was separated well from the peaks of internal standard (3.8 min) and impurities from serum (1.2 min) (Fig. 2B). The chromatogram of blank guinea pig plasma showed only the peak of impurities from plasma (Fig. 2C). The LOQ was determined to be 0.25 μg/ml and the recovery of isoxyl extracted by ACN was above 68% (Tables 2 and 3). The standard curve of isoxyl was linear from 0.25 μg/ml to 50 μg/ml in plasma: Peak Area Ratio (Isoxyl/Internal Standard) = 0.20 × isoxyl concentration − 0.023 and R = 0.9979.

As shown in Table 4, the HPLC method was validated for determining isoxyl concentrations in plasma: (1) intra-day and inter-day precision of the method were between 6.8 and 14% for 0.4 μg/ml and between 6.0 and 8.0% for 6 and 40 μg/ml; and (2) intra-day and inter-day accuracy of the method were between 115 and 119% for 0.4 μg/ml and between 85 and 99% for 6 and 40 μg/ml. HPLC analysis demonstrated that isoxyl was stable under the conditions employed. Isoxyl concentrations in the plasma samples did not change after being frozen and thawed for three cycles or kept at room temperature for 5.5 h (Table 5). Also, isoxyl was stable after the plasma samples were stored at −80 °C for one month (Table 5).

Preliminary study of in vivo exposure was first determined by intravenous administration of isoxyl to guinea pigs. Two doses of isoxyl (10 and 20 mg/kg) exhibited the same plasma concentration vs. time profiles: the initial concentration of isoxyl in blood circulation was 12–14 μg/ml and the drug was rapidly eliminated to a concentration below MIC (2 μg/ml) in 1 h (Fig. 3A). When isoxyl was administered orally, the drug plasma concentrations at various time points were far below the reported MIC (2 μg/ml). Most of them were also below the limit of quantification (LOQ) (Fig. 3B).

Table 3
Determination of extraction efficiencies in three concentrations (n = 3).

Conc. (μg/ml)	Recovery (%)
0.40	77 ± 13
6.0	68 ± 13
40.3	96 ± 5.2

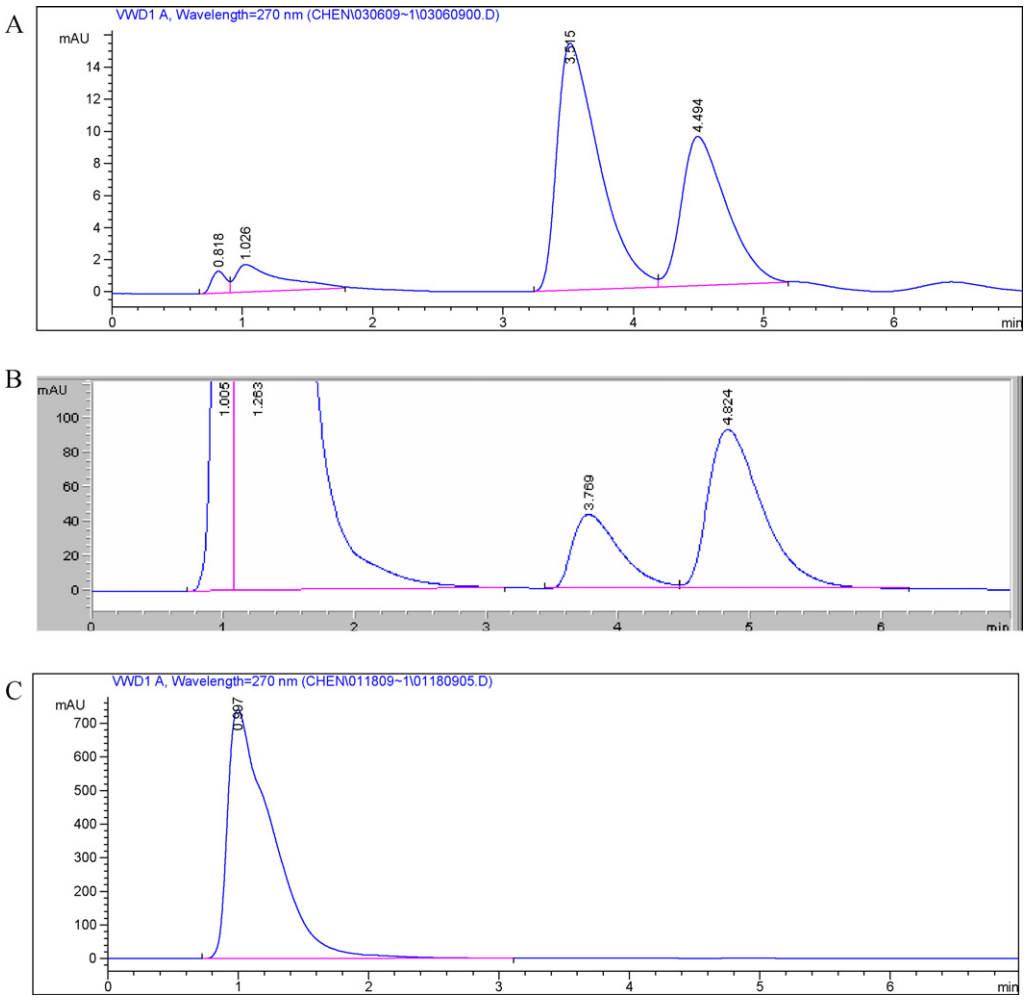

Fig. 2. (A) A chromatograph of isoxyl (4.5 min) and internal standard (3.5 min) dissolved in ethanol. (B) A representative chromatogram of isoxyl (4.8 min) and internal standard (3.8 min) extracted from guinea pig plasma (wavelength = 270 nm). (C) A chromatogram of blank guinea pig plasma.

4. Discussion

An optimized reverse-phase HPLC method was developed to determine isoxyl concentrations in plasma. The method was a simple procedure with good peak resolution and short run-time. The method was precise, accurate and robust with low limit of quantification as defined by the FDA guidance.

The HPLC method was utilized to determine preliminarily the in vivo exposure of isoxyl after it was given to guinea pigs by intravenous administration. Isoxyl has been shown to be active in animals and humans at an oral dose of 100 mg/kg [10–12]. Indeed, some reports suggest that a dose of 50 mg/kg is effective in therapy [13]. However, in the present study, an oral dose of isoxyl at 100 mg/kg did not approach the MIC for *Mycobacterium tuberculosis* in the circulation, as estimated from drug concentrations in plasma. Even for direct i.v. administration, the low and high doses exhibited the overlapped isoxyl plasma concentration vs. time profiles with relatively low initial concentrations (12–14 μg/ml), and the plasma concentrations decreased to below MIC in 1 h. Therefore, it is inferred that the equivocal therapeutic outcome observed in some clinical trials may be a result of low in vivo exposure of isoxyl following oral delivery. Isoxyl is highly hydrophobic drugs. It is not surprising that poor aqueous solubility might limit absorption of the drug. This is consistent with the previous reports that majority of administered dose was cleared via feces [5,14,15]: about 60% of isoxyl was recovered in feces in 3 days after an oral dose of 200 mg/kg was administered to rabbits [16].

The present results seem inconsistent with the previous reports that detected much higher drug concentrations than the MIC where the peaks of isoxyl concentrations in plasma varied from 5 to 108 μg/ml following oral administration [1–4]. In the literature studies, either the microbiological or radiochemical method was

Table 4
Intra-day and inter-day variations ($n = 4$ for each concentration).

Spiked conc. (μg/ml)	Intra-day			Inter-day		
	Measured conc. (μg/ml)	Precision (%)	Accuracy (%)	Measured conc. (μg/ml)	Precision (%)	Accuracy (%)
0.41	0.47	6.8	115	0.49	14	119
6.2	5.6	7.5	89	5.22	6.0	85
41.2	39.0	7.3	95	41.0	8.0	99

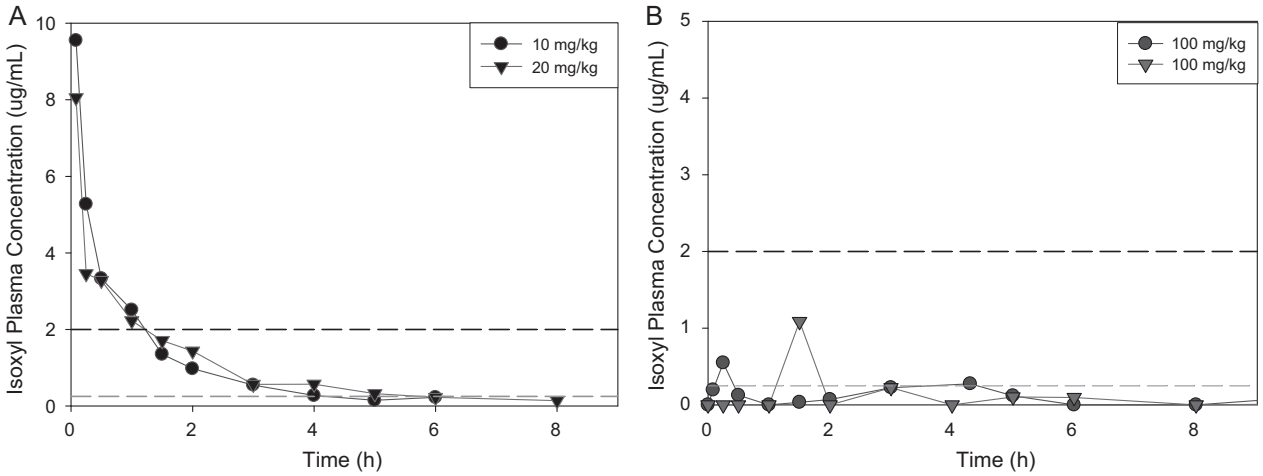

Fig. 3. In vivo exposure studies of isoxyl after it was given by i.v. administration (A), and by the oral route (B). The dotted line in black represents MIC and that in dark gray is limit of quantification (LOQ).

Table 5
Stability of isoxyl.

	Time period	Spiked conc. (μg/ml)	% of Control
Benchtop ($n=3$)	5.5 h	0.41	115 ± 21
		6.12	85 ± 1.5
		41.2	104 ± 3.2
Freeze/thaw ($n=3$)	3 cycles	0.41	105 ± 12
		6.12	112 ± 12
		41.2	107 ± 10
Storage at −80 °C	One month	0.5	82
		10	119
		25	96
		50	114

employed. The radiochemical method cannot distinguish metabolites of isoxyl from the parent drug. This suggested that isoxyl might be transformed to some metabolites in vivo which cannot be detected by HPLC, since they may be hydrophilic and mixed with co-eluting impurities from plasma. If the microbiological method was accurate, which seems not always true, these metabolites should be active. In this scenario, depending on the activity of the metabolites, individual differences in patient metabolism of isoxyl may lead to the highly controversial conclusions regarding efficacy of isoxyl in the literature [11–13,15,17–19]. Further investigation needs to be performed to understand the in vivo metabolism of isoxyl.

The results suggested two possible explanations, (1) poor solubility and (2) rapid and variable metabolism, for this low in vivo exposure of isoxyl to guinea pigs following oral administration. The newly developed HPLC method will facilitate both developing novel formulations targeting to the main site of infection and identifying active metabolites with better physicochemical properties in the near future.

5. Conclusions

A reliable reverse-phase HPLC method was developed for determination of isoxyl concentrations in plasma. The method was used to perform preliminary in vivo exposure study of isoxyl after it was administered intravenously and orally. Interpretation of previous reports in the context of the initial in vivo study, suggests that previous therapeutic failures or conflicting clinical trial outcomes of isoxyl may have been due to either poor absorption of the drug or variation in formation of active drug metabolites. Development of novel formulations or active metabolites may be promising approaches to rescue this abandoned drug and render it an effective agent for treatment of the serious MDR TB disease. The HPLC method described form the basis for future work in treatment of infection.

Acknowledgement

We sincerely appreciate the guidance from Dr. Philip C. Smith, Eshelman School of Pharmacy, University of North Carolina at Chapel Hill, on the project.

References

[1] H. Eule, E. Werner, Thiocarlide (4′4-diisoamyloxythiocarbanilide) blood levels in patients suffering from tuberculosis, Tubercle 47 (1966) 214–219.
[2] O.P. Robinson, P.A. Hunter, Absorption and excretion studies with thiocarlide (4′4-diisoamyloxythiocarbanilide) in man, Tubercle 47 (1966) 207–213.
[3] G. Lambelin, Pharmacology and toxicology of isoxyl, Antibiot. Chemother. 16 (1970) 84–95.
[4] G. Lambelin, R. Roncucci, M.J. Simon, M. Gautier, A. Vincze, L. Verbist, Simultaneous determination of double labelled isoxyl (3H and 35S) blood levels in man, by radio- and bio-assays, Beitr. Klin. Erforsch. Tuberk. Lungenkr. 138 (1968) 161–172.
[5] E. Freerksen, Blood-level determinations after administration of isoxyl by microbiological methods and with radioactive labeled (35S) isoxyl in rabbits and humans, in: Trans. 24th Res. Conf. Pulm. Dis., 1965.
[6] P.A. Emerson, J.P. Nicholson, The absorption of 4-4-diisoamyloxythiocarbanilide (isoxyl) using radioactive material (S.35 tagged), Veterans Administration-Armed Forces, in: Trans. 24th Res. Conf. Pulm. Dis., 1965.
[7] L.G. Dover, A. Alahari, P. Gratraud, J.M. Gomes, V. Bhowruth, R.C. Reynolds, G.S. Besra, L. Kremer, EthA a common activator of thiocarbamide-containing drugs acting on different mycobacterial targets, Antimicrob. Agents Chemother. 51 (2007) 1055–1063.
[8] J. Kordulakova, Y.L. Janin, A. Liav, N. Barilone, T. Dos Vultos, J. Rauzier, P.J. Brennan, B. Gicquel, M. Jackson, Isoxyl activation is required for bacteriostatic activity against *Mycobacterium tuberculosis*, Antimicrob. Agents Chemother. 51 (2007) 3824–3829.
[9] U.D. Gupta, V.M. Katoch, Animal models of tuberculosis for vaccine development, Indian J. Med. Res. 129 (2009) 11–18.
[10] A.J. Crowle, R.S. Mitchell, T.L. Petty, The effectiveness of a thiocarbanilide (isoxyl) as a therapeutic drug in mouse tuberculosis, Am. Rev. Respir. Dis. 88 (1963) 716–717.
[11] E. Freerksen, Experiences with isoxyl in experimental therapy, in: Trans. 23th Res. Conf. Pulm. Dis., 1964.
[12] M. Rosenfeld, Rifampicin, myambutol, isoxyl, and capreomycin as combination partners in animal experiments, Antibiot. Chemother. 16 (1970) 501–515.
[13] I. Stahle, Monotherapy with 4-4′-diisoamyloxythio-carbanilide (isoxyl), Acta Tuberc. Pneumol. Scand. 44 (1964) 327–334.
[14] G.V.R. Born (Ed.), Antituberculosis Drugs, Springer-Verlag, 1988, pp. 185–189.

[15] R.S. Mitchell, T.L. Petty, W.E. Dye, Clinical and pharmacological studies of isoxyl, in: Trans. 23th Res. Conf. Pulm. Dis., 1964.
[16] G. Meissner, J. Meissner, Absorption and distribution of [3H]- and [35S]-4,4′-di(isoamyloxy)thiocarbanilide (thiocarlide) in rabbits, Nuklearmedizin. Supplementum. 8 (1970) 177–182.
[17] R. Urbancik, L. Trnka, Report on the antimicrobial activity of isoxyl on *M. tuberculosis* "in vitro" and "in vio", Acta Tuberc. Pneumol. Belg. 54 (1963) 66–86.
[18] Isoxyl, Tubercle 46 (1965) 298–300.
[19] J. Tousek, On the clinical effectiveness of isoxyl, Antibiot. Chemother. 16 (1970) 149–155.

Journal of Pharmaceutical and Biomedical Analysis 60 (2012) 7–13

Contents lists available at SciVerse ScienceDirect

Journal of Pharmaceutical and Biomedical Analysis

journal homepage: www.elsevier.com/locate/jpba

Development and validation of LC/ESI-MS method for the detection and quantification of exogenous ceramide NP in stratum corneum and other layers of the skin

Fitsum F. Sahle [a], Stefan Lange [b], Bodo Dobner [b], Johannes Wohlrab [c], Reinhard H.H. Neubert [a,*]

[a] Department of Pharmaceutical Technology and Biopharmaceutics, Institute of Pharmacy, Martin Luther University Halle-Wittenberg, Wolfgang-Langenbeck Str. 4, D-06120 Halle (Saale), Germany
[b] Department of Pharmaceutical Chemistry and Clinical Pharmacy, Institute of Pharmacy, Martin Luther University Halle-Wittenberg, Wolfgang-Langenbeck Str. 4, D-06120 Halle (Saale), Germany
[c] Department of Dermatology and Venereology, Medical Faculty, Martin Luther University Halle-Wittenberg, Ernst-Grube Str. 40, D-06120 Halle (Saale), Germany

ARTICLE INFO

Article history:
Received 25 July 2011
Received in revised form 27 October 2011
Accepted 28 October 2011
Available online 6 November 2011

Keywords:
Ceramide
Deuterated ceramide NP
Stratum corneum
Skin
LC/ESI-MS

ABSTRACT

Ceramides (CERs) are integral parts of the intercellular lipid lamellae of the stratum corneum (SC), which provide the barrier function of the skin. Administration of CERs deep into the SC may help to restore the barrier function in affected or aged skin. However, quantification of the amount of CER penetrated into the target site needs a selective and sensitive analytical method. Therefore, an LC/ESI-MS method was developed and validated for the detection and quantification of exogenous CER [NP] in the SC as well as other skin layers. The strategy involved synthesis of ceramide [NP]-D3-18 (deuterated CER [NP]) to distinguish it from the endogenous CER [NP] in MS on weight basis. The method was linear over 10–800 ng/ml and sensitive with a limit of detection (LOD) and limit of quantification (LOQ) of 3 and 10 ng/ml, respectively. It was also accurate with within-run and between-run percentage recoveries of 97.1–103.2 and 99.0–104.9, respectively. The within-run and between-run relative standard deviations (RSDs) were 0.9–5.4% and 2.1–7.4%, respectively, suggesting the method is precise. The method was highly selective and the matrix effect was too minimal with matrix factor (MF) mean and RSD values of 1.002 and 4.57%, respectively.

1. Introduction

Ceramides (CERs) are sphingolipids that contain a sphingosine (S), phytosphingosine (P), 6-hydroxysphingosine (H) or dihydrosphingosine (DS) moiety attached through an amide linkage to a nonhydroxy (N), α-hydroxy (A) or ester-linked ω-hydroxy (EO) long chain free fatty acid (FFA) [1–4]. "Ceramide XY" stands as the current rational nomenclature of CERs, where X and Y represent the type of the FFA moiety and the sphingoid base, respectively. Accordingly, CER [NP] is a sphingolipid that comprises a nonhydroxy acyl group linked with phytosphingosine moiety through an amide bond [1,3]. In addition, to date 11 CER classes, all the above possible sphingoid base and acyl group combinations except "CER EODS", are identified in human stratum corneum (SC) and each CER class further contains several types of CERs, which differ in their acyl group chain length and/or the type of esterified FFA in ω-esterified CERs [3,4].

CERs are integral parts of the intercellular lipid lamellae of the SC, which is responsible for the barrier function of the mammalian skin [1,5,6]. Many skin disease conditions, such as psoriasis [7], atopic dermatitis [8–10] and irritant/allergic contact dermatitis [8] are associated with depletion or disturbance of the level of CERs in the SC. Hence, administration of appropriate CER (s) into the lipid lamellae of the SC might help to prevent and treat such skin conditions and to that end there are many skin preparations on the market that contain CERs.

Some analytical methods were developed for the identification and quantification of CERs in the SC, which include LC/ESI-MS [11,12], LC/APCI-MS [13–15], AMD-HPTLC [16–18], LC-MS/MS [19,20] and HPTLC combined with LC/ESI-MS [21]. However, none of these methods can be used to discriminately identify and quantify the amount of exogenous CERs permeated into the SC, which is necessary for *ex vivo* or *in vivo* bioavailability studies that involve the skin.

Abbreviations: CER, ceramide; EEDQ, 2-ethoxy-1-ethoxycarbonyl-1,2-dihydrochinolin; FFA, free fatty acid; HAC, acetic acid; LOD, limit of detection; LOQ, limit of quantification; MF, matrix effect; SC, stratum corneum; SIM, selected ion monitoring; S/N, signal to noise ratio; RSD, relative standard deviation; THF, tetrahydrofuran.

* Corresponding author. Tel.: +49 345 5525000; fax: +49 345 5527292.
E-mail address: reinhard.neubert@pharmazie.uni-halle.de (R.H.H. Neubert).

0731-7085/$ – see front matter © 2011 Elsevier B.V. All rights reserved.
doi:10.1016/j.jpba.2011.10.032

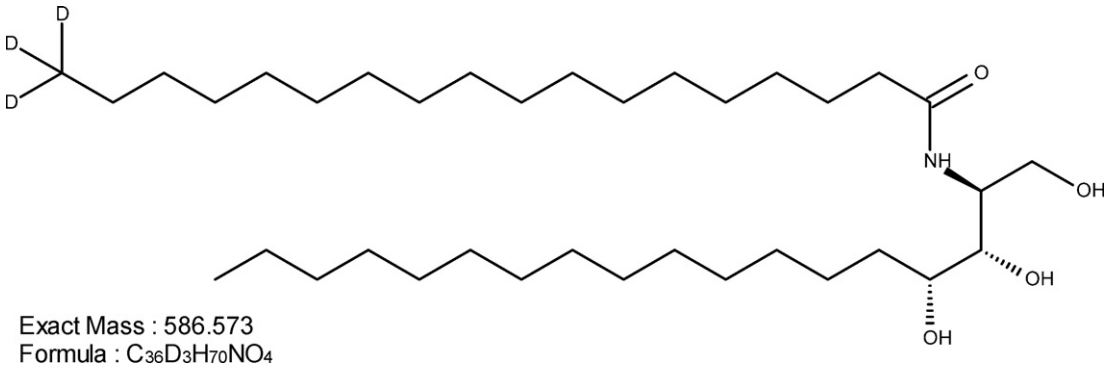

Fig. 1. Chemical structure of ceramide [NP]-D3-18 (deuterated CER [NP]).

LC/MS technique is a highly sensitive and selective technique that can be used for identification and quantification of minute quantities of analyte in biological fluids [22]. However, despite its sensitivity and specificity, it is not possible to differentiate between exogenous and endogenous compounds that have same chemical structures and molecular masses using LC/MS. Nonetheless, deuterated organic compounds can be detected using mass spectrometry with great sensitivity and are widely used to study the movement of drugs in the body [23].

Besides, quantification of compounds using LC/MS demands adequate degree of substance separation. Especially in ESI-MS lack of adequate degree of separation of compounds in a biological fluid might lead to a significant degree of ion suppression, which is referred as "matrix effect", and the reproducibility and accuracy of the method could be highly compromised [22,24]. Thus, analysis of biological fluids, such as SC extract, needs development of appropriate HPLC method for maximum separation of the substance to be quantified from the rest of the matrix.

Therefore, the aim of this work was to synthesize a deuterated CER NP (Fig. 1), which can be distinguished from the endogenous CER [NP] using a mass spectrometer and develop a sensitive and selective LC/ESI-MS method which helps to quantify trace amounts of the exogenous CER [NP] in SC and other skin layers.

2. Materials and methods

2.1. Materials

Octadecanoic-18,18,18-D3 acid was purchased from Dr. Ehrenstorfer GmbH, Augsburg, Germany. 2-Ethoxy-1-ethoxycarbonyl-1,2-dihydrochinolin (EEDQ) was obtained from Fluka, Buchs, Switzerland. Phytosphingosine (1,3,4-Octadecanetriol, 2-amino-, (2S, 3S, 4R)-) was generously donated by Evonik Goldschmidt GmbH, Essen, Germany. Chloroform and silica gel 60, 0.06–0.200 mm, were obtained from Merck KGaA, Darmstadt, Germany. HPLC grade tetrahydrofuran (THF) was supplied by Sigma-Aldrich, Steinheim, Germany. Acetic acid (HAC) was from Grüssing GmbH, Filsum, Germany. Hexane was purchased from NeoLab Migge GmbH, Heidelberg, Germany. HPLC grade methanol was purchased from VWR International, Darmstadt, Germany. Absolute ethanol was supplied by Bundesmonopolverwaltung für Branntwein, Offenbach, Germany. Double distilled water was used throughout the experiment. A human thigh skin was kindly donated by the Department of Dermatology and Venereology of the Faculty of Medicine, Martin Luther University Halle-Wittenberg after approval by the independent ethics committee of the Faculty.

2.2. Methods

2.2.1. Synthesis of deuterated CER [NP]

For the synthesis of the deuterated CER [NP] 0.98 mmol 18,18,18-D3-octadecanoic acid, 1.46 mmol EEDQ [25], and 0.98 mmol phytosphingosine were dissolved in 30 ml ethanol and stirred continuously for 24 h at 55 °C. Additional amount of EEDQ, equivalent to 1 mmol, was further added to the reacting mixture and was allowed to react for additional 12 h. TLC was used to control the reaction process and following completion of the reaction process, the reacting mixture was concentrated to 1/5 of its original volume and 52.5 ml chloroform-methanol (20:1, v/v) was added to the mixture. Subsequently, the mixture was transferred into a separatory funnel and 100 ml of 3% HCl (36% v/v) aqueous solution was added and the mixture was thoroughly shaken. The formed emulsion was broken through filtration and the filter was rinsed twice with two 25 ml portions of warm chloroform. Finally, the two layers were allowed to equilibrate in a separatory funnel and the organic layer was removed, dried for 24 h over sodium sulfate, filtered and the organic solvent was evaporated leaving the synthesized deuterated CER [NP]. Chloroform was dried by refluxing over P_2O_5 for 2 h before use.

2.2.2. Column chromatography

Following its synthesis, the deuterated CER [NP] was purified using a column chromatographic technique. The column was filled with silica gel at a stationary phase to substance ratio of 100:1 (m/m) and was conditioned using chloroform. Then the substance to be purified was dissolved in chloroform and was slowly poured into the column. Increasing percentage of methanol in chloroform (200 ml 0%, 1%, 2%, 3%, 4% and 5% methanol in chloroform) was used as a mobile phase and about 30 ml chromatographic fractions were collected. The collected fractions were monitored using TLC technique. Chloroform was refluxed over P_2O_5 for 2 h before use.

2.2.3. Thin layer chromatography

TLC development was carried out by applying samples and reference substances on a TLC plate (TLC silica gel 60 F_{254} (5 cm × 10 cm), Merck KGaA, Darmstadt, Germany) using capillary tubes. The reference substance was dissolved in chloroform before application. The TLC plate was developed in a saturated chromatographic chamber containing chloroform-methanol (9:1, v/v) until the solvent front reached to the end of the TLC plate. Finally, the plate was removed from the chamber, dried and sprayed with aqueous solution of bromothymol blue as an indicator, which formed a yellowish molecular complex that turned blue when fumigated with ammonia. Whenever detection of the florescent active EEDQ was necessary, the TLC plate was observed under UV-lump before spraying it with the bromothymol blue solution. The Rf values of

the samples were compared with that of the reference substance for the purpose of identification.

2.2.4. LC/ESI-MS

Separation and quantification of deuterated CER [NP] in the samples was performed using an Agilent Technologies 1200 series HPLC (Agilent Technologies, Waldbronn, Germany) coupled with an Agilent Technologies 6120 Quadrapole MS (Agilent Technologies, Waldbronn, Germany). A reversed phase Nucleosil® C-18 HPLC column, 125 mm × 2 mm, 120-3 (Macherey-Nagel, Düren, Germany), fitted with a C-18 precolumn, maintained at 25 °C was used as a stationary phase while an isocratic system comprising methanol-THF-water-HAC (80:10:10:0.2, v/v/v/v) was used as a mobile phase at a flow rate of 0.2 ml/min. Samples for injection were prepared in methanol and the injection volume was set at 10 μl. ESI-MS was used as a detector with negative ion mode and optimum sensitivity was attained at fragmentor voltage of 180; capillary voltage of 4000 V; nebulizer pressure of 20 psig; drying gas flow rate of 11 l/min and drying gas temperature of 350 °C. N_2 was used as both nebulizer and drying gas.

2.2.5. Extraction of SC lipids

From postoperatively cleaned excised human skin, remaining from plastic surgery in which the subcutaneous tissue was mechanically dissected and discarded, the SC layer was removed by tape striping over an area of 2.0106 cm^2 (10 tape strips, each representing two layers of the SC). Then three 0.6 cm discs were punched out from the skin sample using a Kromayer punch (Stiefel-Laboratorium, Offenbach, Germany) and several slices were cut out using a cryo-microtome (Jung, Heidelberg, Germany). The first four slices, each 20 μm thick, were considered as the epidermal layer and then another twenty 40 μm thick slices and the remaining corium layers were considered as the dermal layer. Each layer was sonicated at 50 °C for 2 h in 5 ml Hexane/ethanol (2:1) (1.5 ml for the epidermis layer) and was left overnight for maximum lipid extraction. Finally, the mixtures were filtered, the supernatants were evaporated at 60 °C under a stream of N_2 gas and the residues were reconstituted in 1 ml methanol constituting skin layer extracts.

2.2.6. Method validation

2.2.6.1. Calibration curve and linearity. The calibration curve was constructed using 7 concentrations (10, 50,100, 200, 400, 600 and 800 ng/ml) of the deuterated CER [NP] in methanol. The linearity of the plot, concentration against peak area, was tested using linear regression analysis. The correlation coefficient, the slope and the intercept describing the calibration curve were calculated. The calibration curve standards were back calculated by plugging the peak areas obtained from the standards into the regression equation and the mean accuracy values of the standards were calculated.

2.2.6.2. Limits of detection (LOD) and quantification (LOQ). Estimation of LOD and LOQ was made according to the 1996 analytical detection limit guidance [26]. Consequently, the peak areas of eleven deuterated CER [NP] solutions (10 ng/ml) were determined and their concentrations were calculated to determine method LOD and LOQ.

2.2.6.3. Precision and accuracy. The within-run precision and accuracy of the method were determined by analyzing five replicates of the control sample containing 10, 30, 300 and 700 ng/ml solutions of deuterated CER [NP] in methanol. Five determinations of same concentrations were conducted over three runs on three different days to determine the between-run precision and accuracy of the method. The accuracy and precision of the method were reported as percentage recovery and relative standard deviation (RSD), respectively.

2.2.6.4. Selectivity. The selectivity of the method was determined through analysis of six SC extracts obtained from different sources. The Interactions of MS peaks of the extract with that of the pure deuterated CER [NP] was thoroughly investigated.

2.2.6.5. Carry-over. The carry-over effect of the method was analyzed by observing the occurrence of MS peak (s) within the retention window of deuterated CER [NP] after injecting blank samples preceded by running three samples of CER [NP] (800 ng/ml) dissolved in the SC extract.

2.2.6.6. Matrix effect. The matrix effect was investigated through analysis of six SC extracts obtained from different sources that are spiked with 30 ng/ml deuterated CER [NP]. For each analyte, the matrix factor (MF = peak area in the presence of matrix/peak area in the absence of matrix) was calculated and the mean and RSD of the MF were obtained.

3. Results and discussion

Over the last two decades, several analytical methods, mainly HPTLC and LC/MS techniques [11–21], have been developed for the identification and profiling of endogenous SC lipids. However, to date, to our knowledge, no analytical method has been developed to quantify exogenous SC lipids that permeate from pharmaceutical dosage forms into the different layers of the skin. In this study the potential use of isotopic forms of the lipids, exemplified by deuterated analogue of CER [NP], as a means of developing a selective and sensitive analytical method was assessed.

3.1. Synthesis and purification of deuterated CER [NP]

Deuterated organic compounds can be detected by MS with a high degree of sensitivity and have very low toxicity (especially compared with radioactive ones). Such drugs are very widely used in studies of metabolism and movement of drugs and toxic substances in humans and other animals [23]. Hence, the hydrogen atoms on the terminal carbon of the C-18 CER [NP] was replaced by deuterium, Fig. 1, to study the rate and extent of penetration of exogenous CER [NP] into the SC and other layers of the skin.

Synthesis of deuterated CER [NP] was attained through joining phytosphingosine with 18,18,18-D3-octadecanoic acid, a terminally deuterated stearic acid, through an amide bond using EEDQ as a condensing agent [25], Fig. 2. The reaction started as the nucleophilic carboxylate anion of the FFA attacks the electrophilic carbon atom of EEDQ ring at position 2. Since the formed intermediate product was extremely unstable it was broken down very rapidly into a mixed anhydride and quinoline. The formed mixed anhydride reacted with the amino group of phytosphingosine forming deuterated CER [NP]. In addition, the ethyl ester of carbonic acid, formed during the reaction process, was unstable and was rapidly broken down into carbon dioxide and ethanol.

Following its synthesis, the deuterated CER [NP] was purified from the remaining reactants and intermediate products using column chromatographic technique. A gradient system containing chloroform-methanol was used to efficiently separate the compounds and the CER was eluted at chloroform-methanol (95:5 v/v).

During both synthesis and purification steps, TLC was employed to detect and identify compounds of interest by comparing Rf values of the samples with the references. The identity and purity of the synthesized CER was finally reaffirmed using MS.

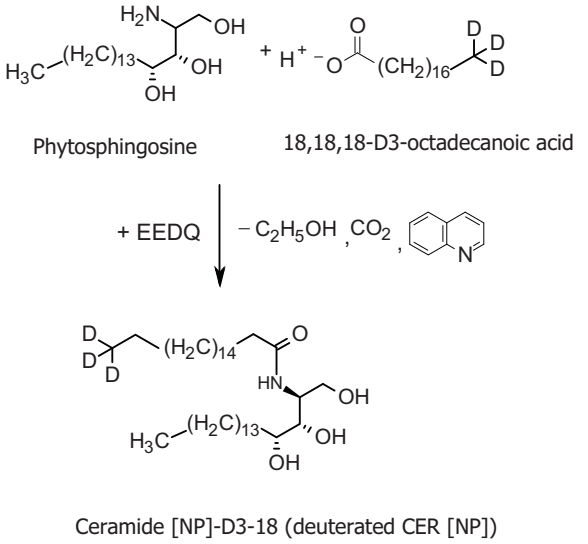

Fig. 2. Schematic representation of the mechanism by which phytosphingosine couples with octadecanoic-18,18,18-D3 acid to form deuterated CER [NP].

The deuterated analogue of CER [NP] (m/z = 585.5) was heavier than the endogenous CER [NP] (m/z = 582.5) and could easily be identified and quantified using LC/ESI-MS.

3.2. Lipid extraction

Mixtures of hexane-ethanol [12,14,17,21] or chloroform–methanol [13,15] were commonly employed to efficiently extract lipids from the SC. Consequently, preliminary studies were conducted to choose an appropriate extraction solvent with minimum matrix effect and maximum lipid extraction efficiency and hence *n*-hexane-ethanol (2:1, v/v) was chosen as an extraction solvent. Since solubility of CERs increases significantly with temperature, to attain maximum extraction the extraction process was subjected to 2 h of sonication at 50 °C and it was allowed overnight. After the extraction procedure, the *n*-hexane-ethanol (2:1, v/v) was evaporated and the lipid mixture was dissolved in methanol to dissolve the CERs leaving several other interfering lipophilic extracts undissolved.

3.3. Method development

Development of sensitive LC/MS method for quantification of traces of amounts of compounds in biological samples demands maximum separation of the compound from other interfering components of the matrix [22,24]. Consequently, an attempt was made to develop a sensitive and selective HPLC/ESI-MS method that can efficiently and adequately separate and quantify deuterated CER [NP] in SC extracts with minimum matrix effect.

In our case, a reasonable amount of deuterated CER was incorporated in the SC extract and the effect of the type of the stationary and mobile phases as well as other experimental parameters on the degree of chromatographic separation of the deuterated CER [NP] peak from other SC extracts peak was thoroughly investigated. Extensive optimizations were made to nullify the matrix effect. Three standard reversed phase C4, C8 and C18 HPLC columns were investigated as stationary phases and the results showed that higher degree of peak separation was obtained with the C18 column followed by the C8 column. Methanol was used as a principal mobile phase and raising the level of water and THF in methanol from 0% to 10%, each, resulted in a higher degree of peak separation. Any further change of THF or water percent resulted either in poor separation and/or increased peak retention time. Incorporation

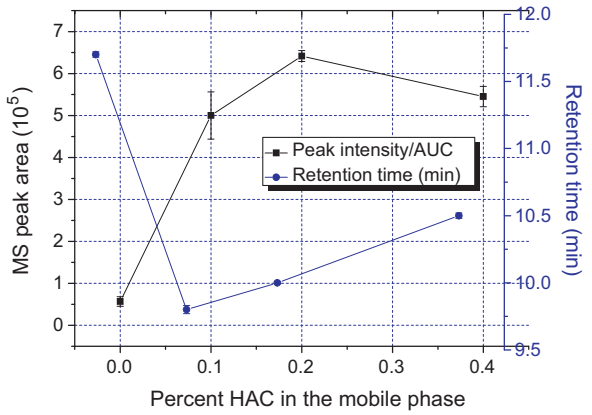

Fig. 3. Effect of percent HAC in the mobile phase on the deuterated CER [NP] LC/MS peak intensity and retention time.

of small percentage of HAC into the mobile phase reduced the retention time of the deuterated CER [NP] peak with better peak separation and tremendous increase in LC/MS peak intensity, Fig. 3. As can be seen in the figure, adding 0.1% HAC increased HPLC peak intensity about 10× and the retention time decreased by about 2 min. Increasing the level of HAC to 0.2% further improved peak intensity, with slight increase in retention time. However, any further addition of HAC reduced peak intensity and increased the retention time. Hence, methanol–THF–water–HAC (80:10:10:0.2, v/v/v/v) was selected as a mobile phase. The effect of temperature (25, 30, 35 and 40 °C) on peak separation was studied. Better peak separation was obtained at lower temperatures. Investigations on the effects of flow rate (1, 1.5, 2, 2.5 and 3 ml/min) and injection volume (5, 10 and 20 μl) on peak separation were made and well separated peaks were obtained at a flow rate of 0.2 ml/min and injection volume of 10 μl/min. Using the same chromatographic conditions, sufficient degree of CER [NP] peak separation was obtained in other skin layer extracts.

Like the HPLC conditions the effect of the MS parameters on peak intensity was investigated. At a low fragmentor voltage of 60, HAC (M. Wt = 60) interacted with deuterated CER [NP] (m/z = 585.5) to form adduct (m/z = 645.5 Da). No deuterated CER [NP] peak was observed on the MS. However, as the fragmentor voltage increases the CER [NP] peak dominated and at a fragmentor voltage of 180 only trace amount of adduct was detected, Fig. 4F. Higher degree of ionization was attained at higher temperature (350 °C), higher capillary voltage (4 kV), lower nebulizer pressure (20 psig) and higher drying gas flow rate (11 l/min). Since SIM mode is highly sensitive, quantification of deuterated CER [NP] was performed in SIM mode.

3.4. Method validation

The analytical method developed was validated according to the EMA guideline on validation of bioanalytical methods [27].

Table 1
Back calculated concentrations of the calibration standards and their calculated mean accuracy values obtained for the LC/ESI-MS method.

Nominal concentration (ng/ml)	Back calculated concentration (ng/ml)	Calculated mean accuracy value (%)	RSD (%) (n = 3)
10	8.9	89.2	6.2
50	48.4	96.7	3.0
100	97.2	97.2	7.0
200	209.6	104.8	2.0
400	398.6	99.6	3.7
600	597.8	99.6	2.2
800	792.6	99.1	1.4

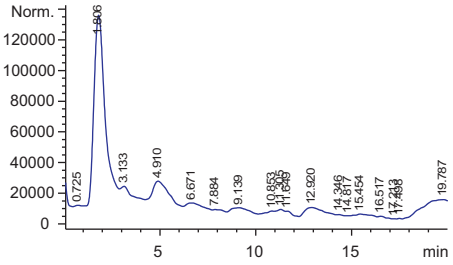

(A) LC/ESI-MS chromatogram of SC extract obtained in full ion monitoring mode [m/z=300-1000 Da]

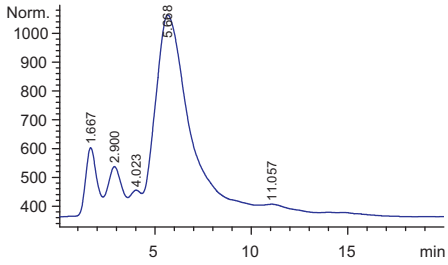

(B) LC/ESI-MS chromatogram of SC extract obtained in SIM mode [m/z=585.5 Da]

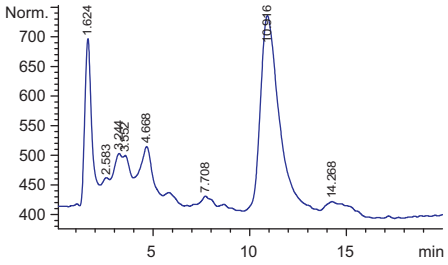

(C) LC/ESI-MS chromatogram of SC extract obtained in SIM mode [m/z=582.5 Da]

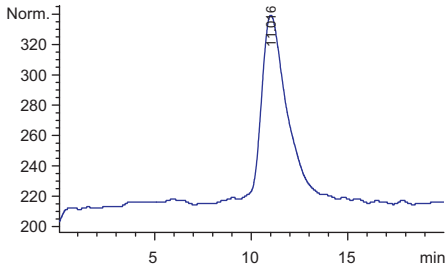

(D) LC/ESI-MS chromatogram of deuterated CER [NP] (10 ng/ml) in methanol obtained in SIM mode [m/z=585.5 Da]

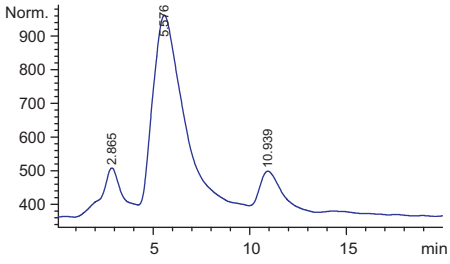

(E) LC/ESI-MS chromatogram of deuterated CER [NP] (10 ng/ml) in SC extract obtained in SIM mode [m/z=585.5 Da]

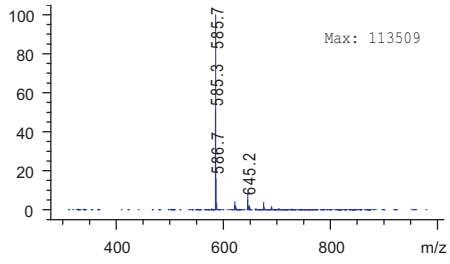

(F) MS of deuterated CER [NP] peak obtained in fullion monitoring mode [m/z=300-1000 Da]

Fig. 4. LC/ESI-MS chromatograms and spectrum of deuterated CER [NP] and SC extracts obtained in negative ionization mode.

3.4.1. Selectivity

Since the method is envisaged to quantify the amount of CER [NP] permeated, *ex vivo* or *in vitro*, from various pharmaceutical formulations into the skin, the chromatographic method was adequately tuned in such a way that it separates several SC components and possibly other pharmaceutical ingredients in pharmaceutical dosage forms. To further validate the selectivity of the method the LC/MS chromatograms of six SC extracts obtained from different sources were obtained. One representative chromatogram of the SC extracts and some other related LC/MS chromatograms are depicted in Fig. 4. The SC extract chromatogram in full ion monitoring mode, Fig. 4A, shows spectral of compounds that are present in the extract. However, the chromatogram obtained in SIM mode (m/z = 585.5 Da), Fig. 4B, showed no chromatographic peak within the retention window of the deuterated CER [NP], which is 10–12 min (Fig. 4D). Interesting to mention, SIM chromatogram at m/z = 582.5 Da resulted in a sharp peak within the retention window of CER [NP], Fig. 4C, representing the endogenous CER [NP]. Further investigation of the SC extract spiked with very low concentration (10 ng/ml) of deuterated CER [NP] gave a separate and sharp deuterated CER [NP] peak within its retention window, Fig. 4E. The MS of the deuterated CER [NP] peak, from a chromatogram obtained in full ion monitoring mode [300–1000 Da], is shown in Fig. 4F and was used to confirm the identity of the deuterated CER [NP] and its corresponding acetic acid adduct (m/z = 645.2 Da). HAC was used as part of the mobile phase. Therefore, the chromatographic peaks showed that the method is selective with no chromatographic peak detected within the retention window of CER [NP] in all the six SC extracts analyzed in SIM mode and only deuterated CER [NP] peak was obtained when the extracts were spiked with the deuterated CER.

Table 2
Values depicting the precision and accuracy of the LC/ESI-MS method for quantification of exogenous CER [NP] in SC and other skin layers.

Nominal concentration (ng/ml)	Calculated concentration (ng/ml) ($n = 5$)		Deuterated CER [NP] recovered (%)		RSD (%) ($n = 5$)	
	Within-run	Between-run	Within-run	Between-run	Within-run	Between-run
10	10.3	10.2	103.2	102.1	2.3	2.5
30	29.7	31.5	98.8	104.9	5.4	7.4
300	306.3	307.6	102.1	102.5	2.1	2.5
700	679.5	693.2	97.1	99.0	0.9	2.1

3.4.2. Carry-over

The appearance of no peak within the retention window of CER [NP] after injection of blank samples, preceded by running of three high concentration (800 ng/ml) deuterated CER [NP] in the SC extract, suggests that the solvent used could wash the column efficiently and the method is not affected by carry-over effect.

3.4.3. Calibration curve linearity and range

As the method was extensively optimized to nullify the matrix effect it was not necessary to prepare the calibration curve within the matrix. It was also supported by the results of validation of the matrix effect, see Section 3.4.6. Thus, a calibration curve describing the relationship between peak area and concentration was constructed ($n = 3$) for deuterated CER [NP] in methanol. A linear regression analysis was performed on the calibration curves and a linear relationship between concentration (ng/ml) and peak area was obtained over 10–800 ng/ml ($R^2 = 0.9993 \pm 0.0004$). The slope and intercept describing the relationship were found to be 268.9 ± 7.44 and 2884 ± 524.2, respectively. At higher concentrations, a polynomial relationship between concentration and peak area was observed.

In addition, the concentrations of the calibration standards were back calculated and the results are presented in Table 1 together with the calculated mean accuracy values. As has been shown in the table the calculated mean accuracy value ranged 89.2–104.8% suggesting the calibration curve is linear and can be employed for the quantification of deuterated CER [NP] within the range selected.

3.4.4. LOD and LOQ

LOD and LOQ of the method were determined based on "the Analytical Detection Limit Guidance – April 1996" [26] at spike level of 10 ng/ml and using 11 replicas. The concentrations obtained were checked for outliers using high and low sided *t*-test and no value was an outlier. The average concentration and the standard deviation (s) of the samples were 10.6 ng/ml and 1.0, respectively, and were used to calculate the LOD and the LOQ. The LOD was calculated as (LOD = (s) (*t*-value)) where *t* is Student's *t* value. For 11 replicas and 10 degrees of freedom the *t* value is 2.764 and LOD was 3.0 ng/ml. The signal to noise ratio (S/N = Average/SD) was found to be 9.82. Since LOD < spike level < 10 time LOD, S/N is between 2.5 and 10 and the percentage recovery was 106%, which is reasonable, the obtained spike level was appropriate. The LOQ of the method was calculated as (LOQ = $10 \times$ S) and hence was found to be 10 ng/ml. Therefore, the LOD and the LOQ of the method are 3 and 10 ng/ml, respectively.

3.4.5. Precision and accuracy

The precision and accuracy of the method were determined by analyzing four concentrations of the deuterated CER [NP] solutions in methanol (at the LOD, 3 times the LOD, medium and high concentrations) in five replicas (4×5). The results obtained are shown in Table 2. As can be seen in the table, the accuracy, expressed as the percentage deuterated CER [NP] recovered as calculated from the nominal value, ranged from 97.1% to 103.2% and 99.0% to 104.9% for within-run and between-run experiments, respectively. Whereas the precision of the method, expressed as RSD, ranged from 0.9% to 9.4% and 2.1% to 7.4% for within-run and between-run experiments, respectively. The results showed that the LC/ESI-MS method is accurate and precise and can be used for the quantification of deuterated CER [NP].

3.4.6. Matrix effect

As has been shown under Section 3.4.1 the LC/ESI-MS method is very selective. In addition, the development and optimization of the method was highly focused on avoiding the matrix effect rather than using the matrix during calibration curve preparation. To further assess the matrix effect the method was validated using six lots of SC extracts obtained from different sources. The extracts were spiked with 30 ng/ml of deuterated CER [NP] (3 times the LOD) and the amount of deuterated CER [NP] in the samples was quantified and the mean and the RSD of the MF were calculated to be not 100.2% and 4.57%, respectively. Thus the obtained MF close to 100% showed that the matrix has no or little effect on the ionization of the CER and hence the method can be used for quantification deuterated CER [NP] in SC extract without the need to construct the calibration curve in the matrix. The RSD value also suggests that the obtained results are not highly affected by the presence of the matrix. The chromatograms in Fig. 4 also showed that the developed chromatographic method could efficiently separates the matrix from the CER and corroborate the conclusion that the matrix effect can be neglected in the method developed.

4. Conclusion

A very simple but highly sensitive, accurate, precise and selective LC/ESI-MS method was developed and validated for the identification and quantification of exogenous CER [NP] in SC and deeper layers of the skin. The method should enable to study the permeability profile of CER [NP] from various pharmaceutical dosage forms and cosmetic preparations. The concept of the method can be extrapolated for quantification of other CERs and SC lipids in the skin.

Acknowledgements

The authors would like to thank Manuela Woigk and Ursula Schramm for their excellent technical assistance. Fitsum F. Sahle greatly acknowledges the financial support provided by the German Academic Exchange Service (DAAD).

References

[1] S. Wartewig, R.H. Neubert, Properties of ceramides and their impact on the stratum corneum structure: a review. Part 1. Ceramides, Skin Pharmacol. Physiol. 20 (2007) 220–229.
[2] M.E. Stewart, D.T. Downing, A new 6-hydroxy-4-sphingenine-containing ceramide in human skin, J. Lipid Res. 40 (1999) 1434–1439.
[3] Y. Masukawa, H. Narita, E. Shimizu, N. Kondo, Y. Sugai, T. Oba, R. Homma, J. Ishikawa, Y. Takagi, T. Kitahara, Y. Takema, K. Kita, Characterization of overall ceramide species in human stratum corneum, J. Lipid Res. 49 (2008) 1466–1476.
[4] Y. Mizutani, S. Mitsutake, K. Tsuji, A. Kihara, Y. Igarashi, Ceramide biosynthesis in keratinocyte and its role in skin function, Biochimie 91 (2009) 784–790.

[5] J. Mutanu Jungersted, L.I. Hellgren, J.K. Hogh, T. Drachmann, G.B. Jemec, T. Agner, Ceramides and barrier function in healthy skin, Acta Derm. Venereol. 90 (2010) 350–353.
[6] M.A. Lampe, M.L. Williams, P.M. Elias, Human epidermal lipids: characterization and modulations during differentiation, J. Lipid Res. 24 (1983) 131–140.
[7] Y. Cho, B.L. Lew, K. Seong, N.I. Kim, An inverse relationship between ceramide synthesis and clinical severity in patients with psoriasis, J. Korean Med. Sci. 19 (2004) 859–863.
[8] E. Berardesca, M. Barbareschi, S. Veraldi, N. Pimpinelli, Evaluation of efficacy of a skin lipid mixture in patients with irritant contact dermatitis, allergic contact dermatitis or atopic dermatitis: a multicenter study, Contact Dermatitis 45 (2001) 280–285.
[9] M. Loden, The skin barrier and use of moisturizers in atopic dermatitis, Clin. Dermatol. 21 (2003) 145–157.
[10] E. Proksch, J.M. Jensen, P.M. Elias, Skin lipids and epidermal differentiation in atopic dermatitis, Clin. Dermatol. 21 (2003) 134–144.
[11] K. Raith, R.H.H. Neubert, Liquid chromatography-electrospray mass spectrometry and tandem mass spectrometry of ceramides, Anal. Chim. Acta 403 (2000) 295–303.
[12] J.P. Vietzke, M. Strassner, U. Hintze, Separation and identification of ceramides in the human stratum corneum by high-performance liquid chromatography coupled with electrospray ionization mass spectrometry and electrospray multiple-stage mass spectrometry profiling, Chromatographia 50 (1999) 15–20.
[13] H. Farwanah, P. Nuhn, R. Neubert, K. Raith, Normal-phase liquid chromatographic separation of stratum corneum ceramides with detection by evaporative light scattering and atmospheric pressure chemical ionization mass spectrometry, Anal. Chim. Acta 492 (2003) 233–239.
[14] H. Farwanah, J. Wohlrab, R.H. Neubert, K. Raith, Profiling of human stratum corneum ceramides by means of normal phase LC/APCI-MS, Anal. Bioanal. Chem. 383 (2005) 632–637.
[15] J. van Smeden, L. Hoppel, R. van der Heijden, T. Hankemeier, R.J. Vreeken, J.A. Bouwstra, LC/MS analysis of stratum corneum lipids: ceramide profiling and discovery, J. Lipid Res. 52 (2011) 1211–1221.
[16] F. Bonte, P. Pinguet, J.M. Chevalier, A. Meybeck, Analysis of all stratum corneum lipids by automated multiple development high-performance thin-layer chromatography, J. Chromatogr. B Biomed. Appl. 664 (1995) 311–316.
[17] H. Farwanah, R. Neubert, S. Zellmer, K. Raith, Improved procedure for the separation of major stratum corneum lipids by means of automated multiple development thin-layer chromatography, J. Chromatogr. B Analyt. Technol. Biomed. Life Sci. 780 (2002) 443–450.
[18] G.A. Cordis, T. Yoshida, D.K. Das, HPTLC analysis of sphingomylein, ceramide and sphingosine in ischemic/reperfused rat heart, J. Pharm. Biomed. Anal. 16 (1998) 1189–1193.
[19] M. Scherer, K. Leuthauser-Jaschinski, J. Ecker, G. Schmitz, G. Liebisch, A rapid and quantitative LC-MS/MS method to profile sphingolipids, J. Lipid Res. 51 (2010) 2001–2011.
[20] E. Kindt, J. Wetterau, S.B. Mueller, C. Castle, C.M. Boustany-Kari, Quantitative sphingosine measurement as a surrogate for total ceramide concentration-preclinical and potential translational applications, Biomed. Chromatogr. 24 (2010) 752–758.
[21] J.P. Vietzke, O. Brandt, D. Abeck, C. Rapp, M. Strassner, V. Schreiner, U. Hintze, Comparative investigation of human stratum corneum ceramides, Lipids 36 (2001) 299–304.
[22] L.L. Jessome, D.A. Volmer, Ion suppression: a major concern in mass spectrometry, LCGC N. Am. 24 (2006) 498–511.
[23] D.J. Kushner, A. Baker, T.G. Dunstall, Pharmacological uses and perspectives of heavy water and deuterated compounds, Can. J. Physiol. Pharmacol. 77 (1999) 79–88.
[24] T.M. Annesley, Ion suppression in mass spectrometry, Clin. Chem. 49 (2003) 1041–1044.
[25] B. Belleau, G. Malek, A new convenient reagent for peptide syntheses, J. Am. Chem. Soc. 90 (1968) 1651–1652.
[26] W.D.o.N. Resources, Analytical Detection Limit Guidance & Laboratory Guide for Determining Method Detection Limits, Wisconsin Department of Natural Resources Laboratory Certification Program, 1996.
[27] EMEA, Draft Guideline on Validation of Bioanalytical Methods, European Medicines Agency, London, 2009.

Journal of Pharmaceutical and Biomedical Analysis 60 (2012) 14–18

Contents lists available at SciVerse ScienceDirect

Journal of Pharmaceutical and Biomedical Analysis

journal homepage: www.elsevier.com/locate/jpba

Cloud point extraction combined with graphite furnace atomic absorption spectrometry for speciation of Cr(III) in human serum samples

Mei Sun [a,*], Qianghua Wu [b]

[a] Hefei National Laboratory for Physical Sciences on Microscale, University of Science and Technology of China, Hefei 230026, China
[b] Department of Polymer Science and Engineering, University of Science and Technology of China, Hefei 230026, China

ARTICLE INFO

Article history:
Received 25 August 2011
Received in revised form 18 October 2011
Accepted 31 October 2011
Available online 6 November 2011

Keywords:
Chromium speciation
Cloud point extraction
Graphite furnace atomic absorption spectrometry
Human serum

ABSTRACT

A cloud point extraction (CPE) method for the preconcentration of ultra-trace chromium speciation in human serum samples prior to determination by graphite furnace atomic absorption spectrometry (GFAAS) had been developed in this paper. In this method, Cr(III) reacts with 1-(2-pyridylazo)-2-naphthol (PAN) yielding a hydrophobic complex, which is then entrapped in the surfactant-rich phase, whereas Cr(VI) remained in aqueous phase. Thus, separation of Cr(III) and Cr(VI) could be realized. Total chromium was determined after the reduction of Cr(VI) to Cr(III) by using ascorbic acid as reducing reagent. PAN was used not only as chelating reagent in CPE, but also as chemical modifier in GFAAS. Triton X-114 non-ionic surfactant had been used as an extraction medium. The main factors affecting CPE efficiency, such as pH of solution, concentration and kind of complexing agent, concentration of non-ionic surfactant, equilibration temperature and time, were investigated in detail. An enrichment factor of 83.5 was obtained for the preconcentration of Cr(III) with 10 mL solution. Under the optimal conditions, the detection limit of Cr(III) was 0.02 $\mu g\,L^{-1}$. The relative standard deviation was 2.6% for intra-day assay precision ($n = 7$, $c = 10\,ng\,mL^{-1}$), values of recovery for chromium were from 92.0% to 94.7% for three samples. This method is simple, accurate, and sensitive and can be applied to determine ultra-trace chromium speciation in human serum.

1. Introduction

Chromium is an essential trace element in both humans and animals and plays an important role in the metabolism of glucose aiding in the process of degradation of sugar in the blood and in lipid and protein metabolism. Chromium deficiency leads to signs and symptoms of 2 diabetes mellitus and cardiovascular disease. Excessive amounts of chromium, particularly in the more toxic Cr(VI) valence state, are detrimental to health, as chromium may be involved in the pathogenesis of some diseases such as lung and gastrointestinal cancer [1]. Glucose Tolerance Factor (GTF) is a low molecular weight Cr binding polypeptide, consisted of glycine, cysteine, glutamic acid and aspartic acid and Cr(III) being its essential active center. GTF has been proven to play an important role in normal glucose homeostasis by many studies and it has become the focus of studies. So for medical purposes, the accurate and precise analytical determination of Cr(III) in human serum is of paramount importance.

Chromium evaluation in biological materials is an extremely difficult task to accomplish because of the very low concentration and complicated matrixes present. At the moment, the widely used analytical techniques for the detection of total chromium in samples are graphite furnace atomic absorption spectrometry (GFAAS) [2–5], flame atomic absorption spectrometry (FAAS) [6], X-ray fluorescence spectrometry [7], spectrophotometric [8], inductively coupled plasma mass spectrometry (ICP-MS) [9–12] and inductively coupled plasma optical emission spectrometry [13–15]. However, these methods can only yield total amount of chromium or are not accurately reliable for the determination of ultra-trace chromium. As a result, preliminary species separation and preconcentration is required before detection by above sensitive analytical techniques [16]. For the speciation of chromium, the separation methods reported in the literature are usually based on liquid–liquid extraction [17], solid phase extraction [5,7,9,13,15], ion chromatography [10], high performance liquid chromatography [11], coprecipitation [18] and dispersive liquid–liquid microextraction (DLLME) [19], etc.

Separation and preconcentration based on cloud point extraction (CPE) is becoming an important and practical application in the use of surfactants in analytical chemistry. The principle, advantages and applications of CPE have been well-established and identified in recent years. The use of preconcentration steps based on CPE offers a conventional alternative to more traditional extraction systems and permits the design of extraction schemes that are simple,

* Corresponding author. Tel.: +86 551 3602811; fax: +86 551 3602803.
E-mail address: sunmei@ustc.edu.cn (M. Sun).

0731-7085/$ – see front matter © 2011 Elsevier B.V. All rights reserved.
doi:10.1016/j.jpba.2011.10.034

Table 1
Optimum operating conditions for GFAAS.

Element	Cr
Lamp current (mA)	20
Wavelength (nm)	357.9
Slit (nm)	0.7
Measurement mode	Peak area
Chemical modifier	PAN
Graphite furnace	
Dry1 temp (°C)	110 (ramp 1 s, hold 30 s)
Dry2 temp (°C)	130 (ramp 15 s, hold 30 s)
Pyrolysis temp (°C)	1500 (ramp 10 s, hold 20 s)
Atomization temp (°C)	2300 (ramp 0 s, hold 5 s)
Cleaning temp (°C)	2450 (ramp 1 s, hold 3 s)
Ar flow rate ($mL\,min^{-1}$)	250 (stopped during atomizing)
Sample volume (μL)	20

cheap, of high efficiency and of lower toxicity than extractions that use organic solvents. To date, CPE has been used for the extraction and preconcentration of metal ions after the formation of sparingly water-soluble complexes, and then the complex in the surfactant-rich phase is determined by different spectrometric methods [20]. Any species that interacts with the micellar system, either directly or after a prerequisite derivatization reaction may be extraction from the initial solution and may also be preconcentrated [21].

GFAAS could, in this sense, combine all the benefits associated with CPE to a sensitive instrumental technique. In recent years, CPE as an extraction technique prior to the GFAAS determination of Cr speciation [5,21,22] had been widely studied. However, these papers were mostly focusing on water samples with simple matrix, the research work was focusing on human serum samples has not found by CPE coupled GFAAS at present.

In this paper, a new method for GFAAS speciation of chromium in human serum samples is proposed by CPE with 1-(2-pyridylazo)-2-naphthol (PAN) as the chelating agent and Triton X-114 as the extractant. Under the optimal conditions, the complex Cr(III)-PAN formed will be "in situ" entrapped in surfactant-rich phase at the temperature higher than the cloud point temperature and separated from Cr(VI) in aqueous phase. Following preconcentration, the analyte in surfactant-rich phase will be determined, PAN is also as the chemical modifier in GFAAS determination. Several experimental variables affecting the method sensitivity and stability have been investigated in detail. The proposed method has been applied for the determination of ultra-trace Cr(III) in human serum samples with satisfactory results. The simplicity, high efficiency and low-cost of performance are the other features of the proposed method.

2. Experimental

2.1. Apparatus

A PerkinElmer model AAnalyst 800 atomic absorption spectrometer including the AS-800 autosampler with Zeeman effect background correction was used, and chromium hollow-cathode lamp (General Research Institute for Non-ferrous Metals, China) as radiation sources. The optimized operating conditions for GFAAS are listed in Table 1. A HH-S11-2 thermostated bath (Xiamen Medical Treatment Electronic Instrument Co. Ltd., China) was maintained at the desired temperature and phase separation was assisted using a centrifuge (TDL-50B, Shanghai Anting Scientific instrument Co. Ltd., China). Milli Q water purification system (Millipore Corp., Bedford, MA, USA).

2.2. Reagents

All reagents used in this work were of analytical purity grade at least. Ultra-pure water with a resistivity of 18.2 MΩ cm was prepared by Milli Q water purification system. HNO_3 and $HClO_4$ (MOS grade, Tianjing Fengchuan Chemical Reagent Science and Technology Co. Ltd., China) were further purified by double distillation.

Cr(III) and Cr(VI) standard working solutions were prepared by serial dilutions with ultra-pure water from stock solution ($1000\,\mu g\,mL^{-1}$) of Cr(III) and Cr(VI) were prepared by dissolving $CrCl_3{\cdot}6H_2O$ (The first Reagent Factory, Shanghai, PR China) and $K_2Cr_2O_7$ (The first Reagent Factory, Shanghai, PR China) in $0.1\,mol\,L^{-1}$ hydrochloric acid, respectively; $1 \times 10^{-3}\,mol\,L^{-1}$ PAN (The first Reagent Factory, Shanghai, PR China) was prepared by dissolution in ethanol; the nonionic surfactant Triton X-114 (Belgium, USA); 10% aqueous ascorbic acid solution was prepared fresh daily; trichloroacetic acid (Sinopharm Chemical Reagent Co. Ltd., Shanghai, PR China); GBW(E)090006 bovine serum certified reference material (National Institute of Metrology, PR China).

Vessels used for trace analysis were kept in 50% (v/v) nitric acid for at least 24 h and were subsequently washed several times with deionized water and ultra-pure water.

2.3. Procedures

For the CPE, an analytical solution contained 10 mL of sample solution or standard solution, 0.25 mL of 2.0% (v/v) Triton X-114, 0.2 mL of $2 \times 10^{-3}\,mol\,L^{-1}$ PAN, 1.5 mL of buffer solution (pH 11.0), was kept in the thermostatic bath maintained at 50 °C for 20 min. Separation of the two phases was accelerated by centrifugation for 10 min at 4000 rpm. After cooling in an ice-water bath for 15 min, the surfactant-rich phase became viscous and retained at the bottom of the tube. The aqueous phase then was readily separated by inverting the tubes. To decrease the viscosity of the extract and allow its pipetting, a 0.1 mL of methanol solution containing $0.1\,mol\,L^{-1}$ HNO_3 was added to the surfactant-rich phase. The 20 μL of the diluted extract was introduced into the graphite furnace by autosampler. Calibration was performed against aqueous standards submitted to the same cloud point extraction procedure. A blank submitted to the same procedure was measured parallel to the samples and calibration solutions.

2.4. Preparation and analysis of samples

Frozen serum samples were obtained from local hospital, thawed and allowed to reach room temperature. To precipitate the protein contents of the human serum sample, 5 mL of serum sample with a small amount of trichloroacetic acid was centrifuged for 5 min at the rate of 4000 rpm. After decantation of the serum sample, it was diluted at 1:10 ratio with ultrapure water and extracted by using the CPE procedure.

Cr(III) determination: to a 10 mL of sample or standard solution, 0.25 mL of 2.0% (v/v) Triton X-114, 0.2 mL of $2 \times 10^{-3}\,mol\,L^{-1}$ PAN and 1.5 mL of buffer solution (pH 11.0) were added for CPE separation. After phase separation, 0.1 mL of methanol solution containing $0.1\,mol\,L^{-1}$ HNO_3 was added to the surfactant-rich phase. The final solution was determined by GFAAS.

Total chromium determination [21,23]: to a 10 mL of sample, 0.1 mL of 10% aqueous ascorbic acid was added, then it was operated as described above.

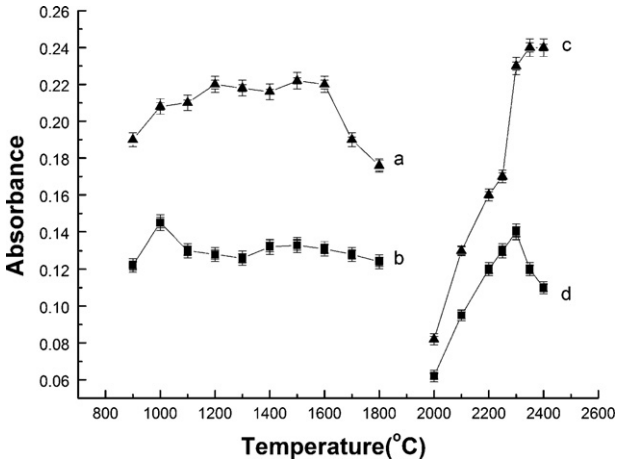

Fig. 1. Ashing and atomization curves for Cr(III) with CPE procedure. (a) Ashing curves (with CPE); (b) ashing curves (without CPE); (c) atomization curves (with CPE); (d) atomization curves (without CPE). 10 ng mL^{-1} Cr(III); 2×10^{-3} mol L^{-1} PAN; 2% (v/v) Triton X-114; pH 11.0.

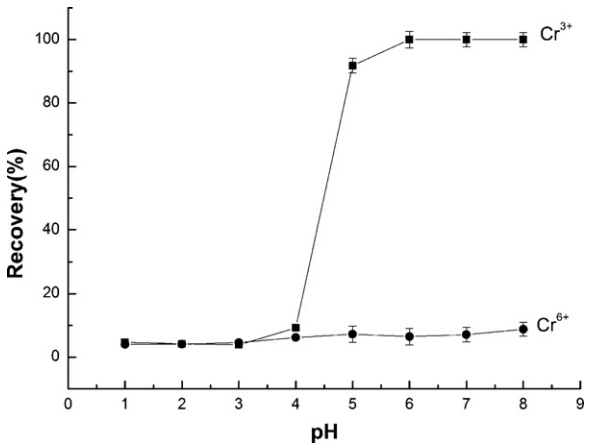

Fig. 2. Effect of pH on the extraction recoveries of Cr(III) and Cr(VI). Cr(III) 10 ng mL^{-1}; Cr(VI) 10 ng mL^{-1}; 2×10^{-3} mol L^{-1} PAN; 2% (v/v) Triton X-114.

3. Results and discussion

3.1. Ashing and atomization curves

In this work ashing and atomization curves were established using 10 ng mL^{-1} Cr(III) solutions submitted to CPE procedure. PAN was used not only as complexing agent for CPE but also as matrix modifier. The ashing and atomization curves of Cr(III) without CPE procedure were also studied. Fig. 1 shows the ashing and atomization curves for Cr(III) with and without CPE procedure. As can be seen, addition of matrix modifier, the pyrolysis temperature was increased to 1200 °C with considerable background reduction without losses of chromium and the atomization temperature was increased to 2350 °C. This is likely due to the fact that the chelate formation of Cr(III) with PAN prohibits the formation of Cr carbide and alters the atomization mechanism of chromium. So the optimal pyrolysis temperature and atomization temperature of 1200 °C and 2350 °C were chosen, respectively.

3.2. Effect of pH on CPE for Cr(III) and Cr(VI)

The formation of metal-chelate and its chemical stability are two important influencing factors for CPE. The pH, which plays a unique role on formation of the complex and subsequent extraction, is proved to be a main parameter for CPE. The effect of pH on the CPE efficiency of Cr(III) and Cr(VI) was studied and the results are shown in Fig. 2. It could be seen that extraction efficiency was higher for Cr(III) in the pH range of 9–12 and the extraction of Cr(VI) was negligible in the study pH range. This makes that it is possible to separate Cr(III) from Cr(VI) through the control of pH of the solution. In order to separate Cr(III) and Cr(VI), a pH of 11.0 was chosen for subsequent work.

3.3. Effect of complexing agent concentration

The effect of PAN concentration on the extraction yield of Cr(III) was studied. A 10 mL of solution containing 10 ng mL^{-1} Cr(III) and 10 ng mL^{-1} Cr(VI) in 2% (v/v) Triton X-114, at a medium buffer of pH 11 containing various amounts of PAN, was subjected to the CPE process. It could be found that the extraction efficiency was the highest when 2×10^{-3} mol L^{-1} PAN was used and the volume of PAN was kept constant at 0.2 mL. So 0.2 mL of 2×10^{-3} mol L^{-1} PAN solution was chosen for the subsequent experiment.

3.4. Effect of Triton X-114 concentration

A successful cloud point extraction should be able to maximize the extraction efficiency through minimizing the phase volume ratio ($V_{\text{surfactant-rich phase}}/V_{\text{aqueous phase}}$), so as to improve the preconcentration factor. Triton X-114 was chosen as the nonionic surfactant due to its lower cloud point temperature (22–25 °C) [24], which facilitates phase separation by centrifugation.

The variations of the analytical signal as a function of the concentration of Triton X-114 in the range 0.1–5% (v/v) were investigated when the volume of Triton X-114 was always kept at 0.25 mL. According to the results, Triton X-114 was found to have higher extraction efficiency for Cr(III) at surfactant concentration above 2.0% (v/v). So a concentration of 2.0% (v/v) was chosen as the optimum surfactant concentration in order to obtain the highest possible extraction efficiency.

3.5. Effects of equilibration temperature and time

It was desirable to employ the shortest equilibration time and the lowest possible equilibration temperature, as a compromise between completion of extraction and efficient separation of phases. The dependence of extraction recovery upon equilibration temperature and time were studied with a range 30–60 °C and 5–30 min, respectively. The results showed that an equilibration temperature 50 °C and a time of 20 min were adequate to achieve high quantitative extraction efficiency.

3.6. Interferences

The determination of Cr(III) in the presence of foreign ions was investigated. Cr(III) recovery was almost quantitative in the presence of other species with tolerance limits (error < 5%) indicated in Table 2. It can be seen that Cr(III) recoveries were essentially quantitative in the presence of foreign cations. Therefore these ions produce no interference in the cloud point extraction of Cr(III).

3.7. Characteristics of the method

The calibration graphs of Cr(III) were obtained by preconcentrating 10 mL of standard solutions containing known amounts of the analytes in the presence of PAN and Triton X-114 in a medium buffered at pH 11.0 for CPE. Under the optimal experimental conditions, the calibration curve for Cr(III) is linear up to 20 ng mL^{-1} with a correlation coefficient (r) of 0.9998. The relative standard deviation (R.S.D.) for seven replicate determinations of 10 ng mL^{-1}

Table 2
Tolerance limits of interfering species in the determination of 10 ng mL^{-1} of Cr(III).

Ion	Ion/Cr(III) ratio	Extraction recovery (%)
Na	5000	98.3
K	5000	98.5
Ca	1000	96.8
P	1000	98.2
Mg	1000	96.2
Zn	500	99.5
Cu	100	99.6
Mn	100	102.4
Hg	100	94.8
Al	50	92.1
Fe	50	95.7

Table 4
Analytical results of human serum samples.

	Sample	ρ (μg L^{-1})	
		Cr(total)	Cr(III)
Normal	Young group (n = 15)	0.88 ± 0.20	0.66 ± 0.15
	Middle group (n = 15)	1.402 ± 0.48	0.58 ± 0.18
	Seniors group (n = 15)	0.85 ± 0.26	0.52 ± 0.13
Diabetic cataracts	Young group (n = 10)	0.39 ± 0.12	0.28 ± 0.09
	Middle group (n = 10)	0.358 ± 0.12	0.22 ± 0.12
	Seniors group (n = 10)	0.43 ± 0.08	0.27 ± 0.10

standard solution was 2.6% for intra-day assay precision and 3.2% for inter-day assay precision during seven consecutive days. The enhancement factor [25], calculated as the ratio of slope of preconcentrated sample to that obtained without preconcentration, was 83.5 for chromium. The limit of detection (LOD) calculated as three times the standard deviation of the blank signal was 0.02 μg L^{-1}. The limit of quantitation was 0.07 μg L^{-1}.

Table 3 compares the characteristic data of the present method with those reported in literatures. Generally, the detection limit obtained by the present method is comparable to those reported methods; the enrichment factor and the relative standard deviation are better than most of them. It should be mentioned that the enrichment factor of our method can be improved by using larger volumes of initial solution and using less volumes of dilution solution.

3.8. Recovery study

The proposed CPE-GFAAS methodology was applied for the determination of Cr(III) in serum samples. In order to validate the proposed method, GBW(E)090006 bovine serum certified reference material was used. For total chromium, the obtained value is 0.23 ± 0.04 μg g^{-1} (n = 3), which is in good agreement with the certified value (0.21 μg g^{-1}); there is no distinctive difference.

When no appropriate serum standard reference materials with a certified content of Cr(III) are available, a recovery study can also be considered as a validation alternative. Serum recovery experiments were carried out by spiking the samples with different amounts of Cr(III) before any pretreatment. The serum samples were analyzed using the standard addition calibration and the percentages of recoveries were calculated. Recoveries ranged from 92.0% to 94.7%. The results indicated that the recoveries were reasonable for trace analysis and showed no matrix interference.

3.9. Sample analysis

The developed method was applied for the determination of Cr(III) and total chromium in different human serum samples. The analyzed results are shown in Table 4. It can be seen that Cr(III) is the dominating species in human serum samples; the content values of Cr(III) for diabetics are 0.22–0.28 μg L^{-1}, significantly lower than 0.52–0.66 μg L^{-1} for the normal people. So it is recommended to supplement a certain amount of chromium to the diabetics according to their nutritional level.

Table 3
Comparison of the published methods with the proposed method in this work.

Separation method	Detection method	Enrichment factor	Relative standard deviation (%)	Detection limit (ng mL^{-1})	Type of analyzed samples	References
–	ETAAS	–	15–18%	0.08 μg L^{-1}, 0.15 μg L^{-1}	Serum and urine	[2]
Magnetic solid phase extraction	FAAS	100	–	0.66 ng mL^{-1}	Water and human serum	[6]
CPE	ICP-DRC[a]-MS	10	–	0.01 ng mL^{-1} Cr(VI) 0.025 ng mL^{-1} Cr(III)	Natural waters	[12]
CPE	GFAAS	42	3.5%	21 ng L^{-1}	Water	[21]
CPE	STAT[b]-FAAS	50	–	0.082 μg L^{-1}	Soil	[26]
CPE	FAAS	48	5.5%	0.7 μg L^{-1}	Water	[27]
CPE	FAAS	35	3.4%	0.32 ng mL^{-1}	Water	[28]
CPE	ETV[c]-ICP-OES	–	3.8%	0.22 μg L^{-1}	Water	[29]
CPE	ICP-OES	20	3.2%	0.81 μg L^{-1}	Natural water	[30]
Solid-phase extraction	ICP-MS	–	5.0%	0.01 ng mL^{-1} Cr(III) 0.024 ng mL^{-1} Cr(VI)	Natural and waste water	[31]
Coprecipitation	FAAS	50	7.0%	1.33 μg L^{-1}	Natural water and food	[32]
Liquid–liquid extraction	Spectrophotometry	5	–	7.5 μg L^{-1}	Spiked river and tap water	[33]
CPE	GFAAS	83.5	2.6%	0.02 μg L^{-1}	Human serum	This method

[a] Dynamic reaction cell.
[b] Double-slotted quartz tube atom trap.
[c] Electrothermal vaporization.

4. Conclusions

In this work, the use of new micellar system as an alternative method to other methods about preconcentration of ultra-trace chromium speciation in human serum before detection by GFAAS offers several advantages including inexpensive, rapid, safe, lower-toxicity, high sensitivity, high recovery, low LOD and good precision. Triton X-114 was chosen for the formation of the surfactant-rich phase due to its excellent physicochemical characteristics: lower cloud point and higher density, which are easy to phase separation. The results of this study demonstrate the possibility of using the PAN-Triton X-114 system for preconcentration of ultra-trace chromium speciation in human serum samples with complicated matrixes.

Acknowledgements

This work was supported by the School Youth Research Fund of University of Science and Technology of China (KA2340000003), the Fund for Exploiting Apparatus Performance of Public Experimentation Center of University of Science and Technology of China (BJ2340000016) and the Fundamental Research Funds for the Central Universities (WK2340000028).

References

[1] J.L. Burguera, M. Burguera, C. Rondon, L. Rodriguez, P. Carrero, Y.P. de Pena, E. Burguera, Determination of chromium in urine by electrothermal atomic absorption spectrometry using different chemical modifiers, J. Anal. Atom. Spectrom. 14 (1999) 821–825.
[2] N. Todorovska, I. Karadjova, S. Arpadjan, T. Stafilov, On chromium direct ETAAS determination in serum and urine, Cent. Eur. J. Chem. 5 (2007) 230–238.
[3] M.R. Moghadam, S. Dadfarnia, A.M.H. Shabani, Speciation and determination of ultra trace amounts of chromium by solidified floating organic drop microextraction (SFODME) and graphite furnace atomic absorption spectrometry, J. Hazard. Mater. 186 (2011) 169–174.
[4] T. Inui, K. Fujita, M. Kitano, T. Nakamura, Determination of Cr(III) and Cr(VI) at sub-ppb levels in water with solid-phase extraction/metal furnace atomic absorption spectrometry, Anal. Sci. 26 (2010) 1093–1098.
[5] M. Ezoddin, F. Shemirani, R. Khani, Application of mixed-micelle cloud point extraction for speciation analysis of chromium in water samples by electrothermal atomic absorption spectrometry, Desalination 262 (2010) 183–187.
[6] Y.W. Wu, J. Zhang, J.F. Liu, Z.L. Deng, M.X. Han, F. Jiang, D.Z. Wang, H.K. Wang, H.Z. Yuan, Determination of chromium species in environmental water and human serum samples by FAAS after magnetic solid phase extraction, Atom. Spectrosc. 32 (2011) 41–47.
[7] P.R. Aranda, S. Moyano, L.D. Martinez, I.E. De Vito, Determination of trace chromium(VI) in drinking water using X-ray fluorescence spectrometry after solid-phase extraction, Anal. Bioanal. Chem. 398 (2010) 1043–1048.
[8] S.L. Narayana, S.A.N. Reddy, Y. Subbarao, H. Inseong, A.V. Reddy, A simple and highly sensitive spectrophotometric determination of Cr(VI) in food samples by using 3,4-dihydroxy-benzaldehydeisonicotinoylhydrazone (3,4-DHBINH), Food Chem. 121 (2010) 1269–1273.
[9] Y.F. Huang, Y. Li, Y. Jiang, X.P. Yan, Magnetic immobilization of amine-functionalized magnetite microspheres in a knotted reactor for on-line solid-phase extraction coupled with ICP-MS for speciation analysis of trace chromium, J. Anal. Atom. Spectrom. 25 (2010) 1467–1474.
[10] L.Y. Xing, D. Beauchemin, Chromium speciation at trace level in potable water using hyphenated ion exchange chromatography and inductively coupled plasma mass spectrometry with collision/reaction interface, J. Anal. Atom. Spectrom. 25 (2010) 1046–1055.
[11] H.J. Wang, X.M. Du, M. Wang, T.C. Wang, O.Y. Hong, B. Wang, M.T. Zhu, Y. Wang, G. Jia, W.Y. Feng, Using ion-pair reversed-phase HPLC ICP-MS to simultaneously determine Cr(III) and Cr(VI) in urine of chromate workers, Talanta 81 (2010) 1856–1860.
[12] N.N. Meeravali, S.J. Jiang, A novel cloud point extraction approach using cationic surfactant for the separation and pre-concentration of chromium species in natural water prior to ICP-DRC-MS determination, Talanta 80 (2009) 173–178.
[13] D.H. Chen, M. He, C.Z. Huang, B. Hu, Speciation of chromium in environmental water samples using chitosan-modified ordered mesoporous silica as solid phase extraction material and determination by inductively coupled plasma optical emission spectrometry, Atom. Spectrosc. 29 (2008) 165–171.
[14] K. Oktor, S. Yilmaz, G. Turker, E. Erkus, Speciative determination of Cr(III) and Cr(VI) in dyeing waste water of Dil Creek discharge to Izmit Gulf (Izmit-Kocaeli Turkey) by ICP-AES, Environ. Monit. Assess. 141 (2008) 97–103.
[15] J.S. Suleiman, B. Hu, C.Z. Huang, On-line speciation of Cr(III) and Cr(VI) using micro-column packed with immobilized used green tea leaves (UGTLs) and determination by ICP-OES in environmental water samples, Atom. Spectrosc. 28 (2007) 234–240.
[16] V. Gomez, M.P. Callao, Chromium determination and speciation since 2000, Trends Anal. Chem. 25 (2006) 1006–1015.
[17] A.S Beni, R. Karosi, J. Posta, Speciation of hexavalent chromium in waters by liquid–liquid extraction and GFAAS determination, Microchem. J. 85 (2007) 103–108.
[18] P.G. Krishna, J.M. Gladis, U. Rambabu, T.P. Rao, G.R.K. Naidu, Preconcentrative separation of chromium(VI) species from chromium(III) by coprecipitation of its ethyl xanthate complex onto naphthalene, Talanta 63 (2004) 541–546.
[19] P. Hemmatkhah, A. Bidari, S. Jafarvand, M.R.M. Hosseini, Y. Assadi, Speciation of chromium in water samples using dispersive liquid–liquid microextraction and flame atomic absorption spectrometry, Microchim. Acta 166 (2009) 69–75.
[20] A.B. Tabrizi, Cloud point extraction and spectrofluorimetric determination of aluminium and zinc in foodstuffs and water samples, Food Chem. 100 (2007) 1698–1703.
[21] P. Liang, H.B. Sang, Speciation of chromium in water samples with cloud point extraction separation and preconcentration and determination by graphite furnace atomic absorption spectrometry, J. Hazard. Mater. 154 (2008) 1115–1119.
[22] Y. Ebihara, T. Shimizu, K. Jinno, N. Uehara, Speciation of chromium (III) and chromium (VI) in river water by graphite furnace atomic absorption spectrometry after cloud point extraction with ammonium pyrrolidinedithiocarbamate, Bunseki Kagaku 56 (2007) 737–743.
[23] A.R. Turker, O. Yalcinkaya, A. Tunceli, Application of column solid phase extraction of chromium for indirect determination of ascorbic acid by flame atomic absorption spectrometry, J. Food Drug Anal. 16 (2008) 83–88.
[24] P. Liang, J. Li, Progress of the application of cloud point extraction to the separation and enrichment of metal ions and to the speciation analysis, PTCA (Part B: Chem. Anal.) (Chinese) 42 (2006) 582–587.
[25] J.L. Manzoori, G. Karim-Nezhad, Development of a cloud point extraction and pre-concentration method for Cd and Ni prior to flame atomic absorption spectrometric determination, Anal. Chim. Acta 521 (2004) 173–177.
[26] J.S. Lu, J.Y. Tian, H. Wu, C.C. Zhao, Speciation determination of chromium(VI) and chromium(III) in soil samples after cloud point extraction, Anal. Lett. 42 (2009) 1662–1677.
[27] G.D. Matos, E.B. dos Reis, A.C.S. Costa, S.L.C. Ferreira, Speciation of chromium in river water samples contaminated with leather effluents by flame atomic absorption spectrometry after separation/preconcentration by cloud point extraction, Microchem. J. 92 (2009) 135–139.
[28] Z.M. Sun, P. Liang, Determination of Cr(III) and total chromium in water samples by cloud point extraction and flame atomic absorption spectrometry, Microchim. Acta 162 (2008) 121–125.
[29] Y.J. Li, B. Hu, Z.C. Jiang, Y.W. Wu, Speciation of chromium in water samples by cloud point extraction combined with low temperature electrothermal vaporization ICP-OES, Anal. Lett. 39 (2006) 809–822.
[30] P. Liang, J. Li, Speciation of chromium with cloud point extraction separation and determination by ICP-OES, Atom. Spectrosc. 26 (2005) 89–93.
[31] S.Z. Chen, L. Zhu, D.B. Lu, X.L. Cheng, X.R. Zhou, Separation and chromium speciation by single-wall carbon nanotubes microcolumn and inductively coupled plasma mass spectrometry, Microchim. Acta 169 (2010) 123–128.
[32] O.D. Uluozlu, M. Tuzen, M. Soylak, Speciation and separation of Cr(VI) and Cr(III) using coprecipitation with Ni2+/2-nitroso-1-naphthol-4-sulfonic acid and determination by FAAS in water and food samples, Food Chem. Toxicol. 47 (2009) 2601–2605.
[33] W. Chen, G.P. Zhong, Z.D. Zhou, P. Wu, X.D. Hou, Automation of liquid–liquid extraction-spectrophotometry using prolonged pseudo-liquid drops and handheld CCD for speciation of Cr(VI) and Cr(III) in water samples, Anal. Sci. 21 (2005) 1189–1193.

Journal of Pharmaceutical and Biomedical Analysis 60 (2012) 19–25

Contents lists available at SciVerse ScienceDirect

Journal of Pharmaceutical and Biomedical Analysis

journal homepage: www.elsevier.com/locate/jpba

Development and validation of a bioanalytical LC–MS method for the quantification of GHRP-6 in human plasma

Jeovanis Gil[a,1], Ania Cabrales[b,1], Osvaldo Reyes[b], Vivian Morera[a], Lázaro Betancourt[a], Aniel Sánchez[a], Gerardo García[c], Galina Moya[c], Gabriel Padrón[a], Vladimir Besada[a], Luis Javier González[a,*]

[a] Department of Proteomics, Division of Physical-Chemistry, Center for Genetic Engineering and Biotechnology, PO Box 6162, Havana, Cuba
[b] Department of Chemical Synthesis, Division of Physical-Chemistry, Center for Genetic Engineering and Biotechnology, PO Box 6162, Havana, Cuba
[c] Quality Assurance Unit, Center for Genetic Engineering and Biotechnology, PO Box 6162, Havana, Cuba

ARTICLE INFO

Article history:
Received 31 August 2011
Received in revised form 28 October 2011
Accepted 7 November 2011
Available online 15 November 2011

Keywords:
GHRP-6
Internal standard
Plasma
Method validation
LC–MS

ABSTRACT

Growth hormone-releasing peptide 6 (GHRP-6, His-(DTrp)-Ala-Trp-(DPhe)-Lys-NH_2, MW = 872.44 Da) is a potent growth hormone secretagogue that exhibits a cytoprotective effect, maintaining tissue viability during acute ischemia/reperfusion episodes in different organs like small bowel, liver and kidneys. In the present work a quantitative method to analyze GHRP-6 in human plasma was developed and fully validated following FDA guidelines. The method uses an internal standard (IS) of GHRP-6 with ^{13}C-labeled Alanine for quantification. Sample processing includes a precipitation step with cold acetone to remove the most abundant plasma proteins, recovering the GHRP-6 peptide with a high yield. Quantification was achieved by LC–MS in positive full scan mode in a Q-Tof mass spectrometer. The sensitivity of the method was evaluated, establishing the lower limit of quantification at 5 ng/mL and a range for the calibration curve from 5 ng/mL to 50 ng/mL. A dilution integrity test was performed to analyze samples at higher concentration of GHRP-6. The validation process involved five calibration curves and the analysis of quality control samples to determine accuracy and precision. The calibration curves showed R^2 higher than 0.988. The stability of the analyte and its internal standard (IS) was demonstrated in all conditions the samples would experience in a real time analyses. This method was applied to the quantification of GHRP-6 in plasma from nine healthy volunteers participating in a phase I clinical trial.

1. Introduction

GHRP-6 (growth hormone-releasing peptide 6) is a six amino acid synthetic peptide (His-(DTrp)-Ala-Trp-(DPhe)-Lys-NH_2, MW = 872.44 Da) first described by Deghenghi et al. in 1994 [1]. It is a strong growth hormone secretagogue acting on specific G-protein-coupled receptors at the hypothalamus and the pituitary gland [2]. There are evidences that this synthetic derivative is related to sleep, food intake and neuroendocrine function in humans, rodents and sheep [3,4]. It exerts a potent cytoprotective effect by maintaining tissue viability during acute ischemia/reperfusion episodes in different organs like small bowel, liver and kidneys [5]. In preclinical experimental models, GHRP-6 exhibits antioxidant effects which may partially contribute to reduce myocardial ischemic damage [6]. This small synthetic peptide constitutes a promising therapeutic candidate not only for the treatment of growth disorders [7], but also as a cytoprotective agent.

Liquid chromatography coupled to mass spectrometry has been widely used to quantify drugs in biological matrices [8]. LC–MS analyses in combination with isotopic labeling have expanded their application to the absolute quantification of peptides and proteins in biological samples [9–12]. Generally, methods developed for absolute quantification use isotopically labeled compounds of known concentration as internal standards. The peptide and its IS have identical retention times in LC but different molecular masses. Extracted ion chromatograms of both compounds in MS analysis are therefore used to determine their relative abundances, calculating the absolute concentration of the compound under study based on the known amount of IS added earlier during sample processing.

Abbreviations: GHRP-6, growth hormone-releasing peptide 6; QCs, quality control samples; CSs, calibration standard samples; IS, internal standard; LC–MS, liquid chromatography coupled to mass spectrometry; ESI-MS, electrospray ionization mass spectrometry; LLOQ, lower limit of quantification; AUC, area under the curve; XIC, extracted ion chromatograms.

* Corresponding author.
E-mail addresses: jeovanis.gil@cigb.edu.cu (J. Gil), luis.javier@cigb.edu.cu (L.J. González).

[1] These authors contributed equally to this work.

0731-7085/$ – see front matter © 2011 Elsevier B.V. All rights reserved.
doi:10.1016/j.jpba.2011.11.007

This strategy was successfully applied to the quantification of large peptides like insulin [13] and Enfuvirtide [14]. Recently, new methods have also been reported for the analysis of other GHRP family members. Okano et al. developed a method for detection of GHRP-2 and its metabolite AA-3 in human urine samples after intravenous administration [15]. In addition, similar methods were implemented for the quantification of these molecules on drug testing [16] and doping control [17].

A sample cleanup step prior to LC–MS analysis is an absolute requirement to avoid potential interferences from substances present in complex matrixes. Mass spectrometric detection has been mainly used in selective ion monitoring (SIM) [18,19] or multiple reactions monitoring (MRM) modes [20,21]. Triple quadrupole and ion trap analyzers are the most commonly used mass spectrometers to quantify peptides in biological samples due to their high selectivity and sensitivity, their versatility in different scan modes and also their fast scanning speeds. However, Q-Tof mass spectrometers have been also employed for the analysis of short peptides (e.g. [Dmt1] DALDA, quantified by using an LC-Q-Tof system in MS/MS mode [22]).

Regulatory agencies (e.g. FDA and EMEA) require the validation of bioanalytical methods prior to the analysis of clinical samples in order to guarantee the reliability of their results. Validation assures that the method will provide accurate, precise, and reproducible data during analysis. According to the existing consensus, validating quantitative analytical methods entails, at least, the evaluation of selectivity, calibration curves, stability, accuracy and precision, and limits of quantification. Additional parameters which might be evaluated include limit of detection, recovery, reproducibility and ruggedness [23].

In this work, we developed a method to quantify the GHRP-6 peptide in human plasma. Sample cleanup includes an acetone precipitation step for highly abundant plasma proteins, using a monolithic column and a Q-Tof mass spectrometer in full scan mode for LC–MS analysis and employing ^{13}C-labeled Alanine GHRP-6 (MW = 875.42 Da) as internal standard. The three Daltons mass shift between the peptide and its internal standard (IS) was enough to separate their isotopic distributions, allowing the reliable quantification of the molecule. The method was fully validated and applied to clinical samples from a GHRP-6 pharmacokinetic study.

2. Materials and methods

2.1. Reagents and chemicals

All chemicals were HPLC grade. Acetone and acetonitrile were from Caledon (Canada), formic acid (FA) was from Sigma (USA) and 1,5-octyl-β-D-glucopyranoside was from Bachem (Switzerland). Water was ultrapure quality. GHRP-6 was supplied by BCN-peptide (Barcelona, Spain) with 99% purity. Blood was collected in 4 mL EDTA vaccutiners from Greiner Bio-One (Germany). Plasma samples were obtained from healthy volunteers under informed consent.

2.2. Equipment

LC–MS analysis was performed using an Agilent 1100 series nano-HPLC system (USA) coupled to a Q-Tof-2™ hybrid type orthogonal acceleration tandem mass spectrometer from Micromass (UK) equipped with a Z-spray nano-ESI ion source. A monolithic nano-column (200 μm × 5 cm) and a trap column (200 μm × 5 mm) from LC Packings (Netherlands) were used. Data acquisition and processing were accomplished with MassLynx 4.0 software (Waters, USA).

2.3. Synthesis of the internal standard (^{13}C-labeled Alanine GHRP-6)

The stable isotope-labeled internal standard for GHRP-6 was synthesized in solid phase by using the Fmoc/tBu strategy [24] with ^{13}C-labeled Alanine (isotopic purity 99%). It was purified to homogeneity by reversed-phase chromatography (>99% purity) at the Peptide Synthesis Laboratory of the Center for Genetic Engineering and Biotechnology (Havana, Cuba).

2.4. Amino acid analysis and extinction coefficient

The specific extinction coefficient of GHRP-6 was determined by triplicate using the methodology proposed by McEntire [25] in an LKB amino acid analyzer (Pharmacia, Sweden). Briefly, a peptide solution at a putative concentration of 1.0 mg/mL in water was prepared. The peptide was serially diluted in water, recording the absorbance of the dilutions at 280 nm. Aliquots corresponding to 30 nmol of peptide were taken for acid hydrolysis and subsequent amino acid analysis. The specific extinction coefficient (a_s) for peptide GHRP-6 at 280 nm yielded a value of 14.684 mL mg^{-1} cm^{-1}. This a_s value was used in all quantitative determinations of peptide content in stock solutions.

2.5. Calibration standards and quality control samples

Stock solutions of GHRP-6 and its internal standard were accurately prepared at 1 mg/mL by peptide content including 0.5% (w/v) of 1,5-octyl-β-D-glucopyranoside in water, in order to minimize adsorption problems [26]. Dilutions of stock solutions were prepared directly in water just before use. To prepare calibration standards (CSs) and quality control samples (QCs), 100 μL of plasma samples were spiked with 10 μL of sub-stock solutions. GHRP-6 concentrations for CSs were: 5, 10, 15, 20, 25, 30, 40 and 50 ng/mL and for QCs were: 10, 20 and 40 ng/mL. For all samples IS concentration was 15 ng/mL. Each calibration curve included a zero standard (without analyte) and a blank sample (processed control plasma). Samples for dilution integrity test were prepared at 75, 100, 450, 750 and 1500 ng/mL of GHRP-6. Before LC–MS analysis these samples were further diluted with plasma down to 15 ng/mL.

2.6. Sample processing

Sample cleanup included a precipitation step for plasma proteins. Briefly, 400 μL of cold acetone (−20 °C) were added to 1.5 mL Eppendorf tubes containing 100 μL of quality control or standard calibration samples. The tubes were vigorously mixed by vortexing for 3 min and then centrifuged at 12 000 rpm for 5 min. The supernatants (400 μL) were evaporated to dryness in a Speed Vac (SAVANT, USA) and stored at −20 °C until analysis. Each sample was dissolved in 100 μL of formic acid 0.1% (v/v), centrifuged at 12 000 rpm for 5 min and finally 40 μL of supernatant were analyzed by LC–MS.

2.7. LC–MS analysis

Mobile phase A was water:formic acid (100:0.1, v:v), and mobile phase B was acetonitrile–water–formic acid (80:20:0.1, v:v:v). Samples were loaded and desalted onto the trap column for 8 min (flow rate 20 μL/min). By valve switching the retained peptides were back-flushed and loaded onto the monolithic column. A linear gradient was ramped up from 10% to 50% of solvent B in 5 min at a flow rate of 0.8 μL/min to elute samples from the LC column. An additional time of 7 min was included to clean the column and restore initial conditions (50–100% B, 2 min; 100% B, 3 min; 100–10% B, 2 min). Total LC run time was about 20 min. ESI-MS

spectra were acquired in a Q-Tof-2™ mass spectrometer in the *m*/*z* range of 400–500 Th. The capillary and cone voltages were set at 2.5 kV and 40 V, respectively.

2.8. Analytical data processing

MassLynx v4.0 software was used for integrating the extracted ion chromatograms (XIC). The *m*/*z* ranges for integrating the signals corresponding to GHRP-6 and its IS were (437.0–438.0 Th) and (438.5–439.5 Th), respectively. The response in terms of concentration was calculated as: GHRP-6 area × (IS concentration/IS area). Axis logarithmic transformation was applied without weighting and linear regression was used to calculate the equation best fitting the curve. Statistical analysis based on coefficient of variation (C.V. %), relative error (R.E. %) and analysis of variance (ANOVA: single factor) was performed using the Microsoft Excel data analysis package.

3. Results and discussion

3.1. Method development

The proposed method was designed for rapid absolute quantification of GHRP-6 in human plasma (Fig. 1). To accurately determine the concentration of GHRP-6, an internal standard (IS) was synthesized with the same amino acid sequence but using ^{13}C-labeled Alanine. For the analysis, MS full scan was chosen instead of MS/MS because sensitivity in the latter mode is lower than in MS mode for Q-Tof mass spectrometers [27]. In addition, the elimination of possible interferences with GHRP-6 and its IS by sample cleanup minimizes the need for the more selective MS/MS mode.

The ionization conditions used in ESI-MS analysis permit the detection of both GHRP-6 and its IS almost exclusively as intense doubly-charged ions signals at *m*/*z* = 437.23 (Fig. 2A1) and *m*/*z* = 438.72 (Fig. 2A2), respectively. They facilitate using a narrow scanning range in positive full scan mode (*m*/*z* 400–500 Th) for LC–MS analysis, thus reducing considerably data storage requirements and speeding up the analysis. The experimental molecular masses agreed very well with the calculated values. Particularly, the ESI-MS spectrum shown in Fig. 2 B2 demonstrated the high isotopic purity of the synthesized IS. The three Daltons molecular mass shift between GHRP-6 and its IS was sufficient to separate both isotopic distributions, allowing the reliable absolute quantification of the analyte.

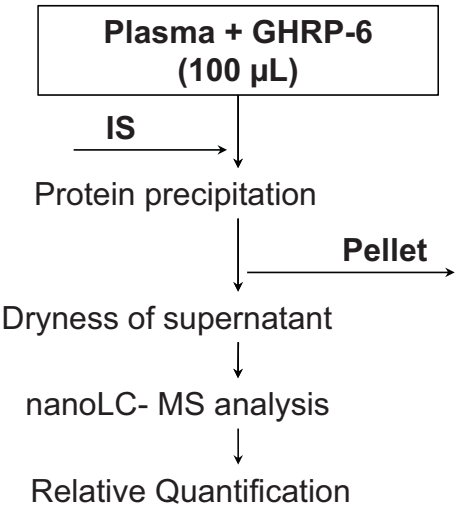

Fig. 1. Schematic representation of the bioanalytical method proposed for the analysis of GHRP-6 in human plasma.

The relative quantification of GHRP-6 and its IS was performed through the calculation of the area under the curve for the first two peaks of both isotopic ion distributions in the extracted ion chromatograms. The linearity of the response was evaluated up to 1 order of magnitude, so the maximum ratio between peptide and its IS in analyzed samples was not greater than 3.3-fold.

The choice of cold acetone precipitation for the removal of interfering plasma proteins was based on the high solubility of GHRP-6 in organic solvents. Peptide recovery was estimated during this process. Several ratios of acetone/plasma (v/v) from 2/1 to 9/1 were tested, keeping constant the concentration of GHRP-6. Peptide extraction efficiency was similar (around 85%) for all assayed conditions. However, with a ratio of 2/1 (acetone/plasma), plasma components that remain soluble after precipitation saturated the

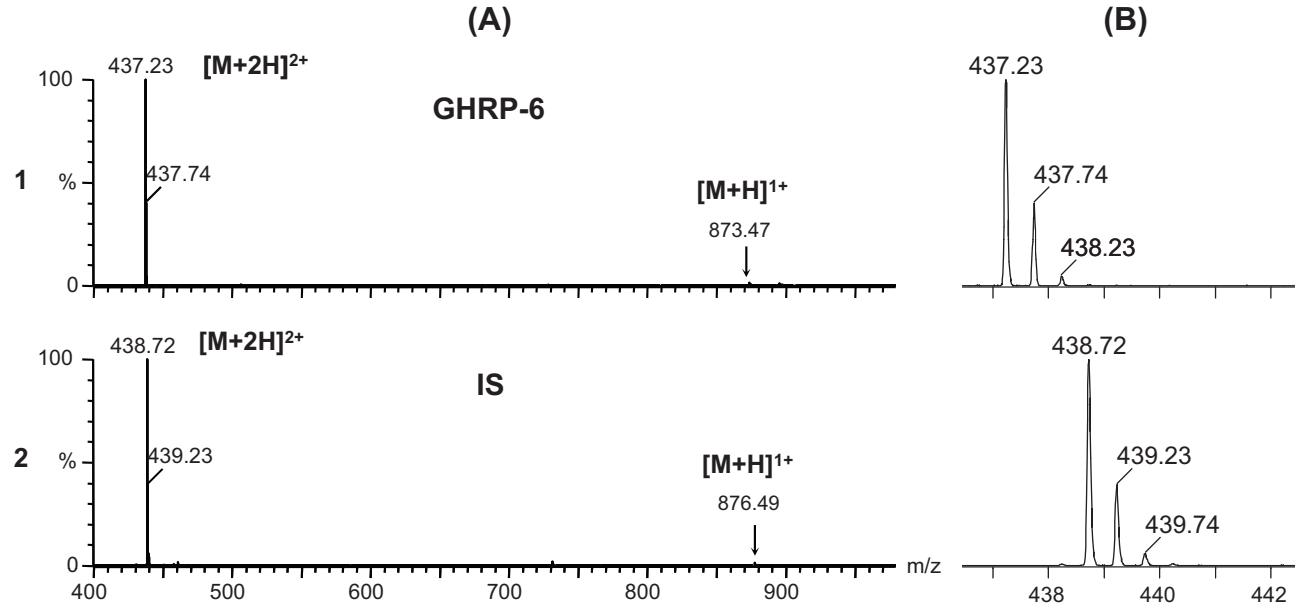

Fig. 2. ESI-MS spectra of GHRP-6 and its internal standard (IS). (A1) and (A2) full scan ESI-MS spectra of GHRP-6 and IS respectively. (B1) and (B2) are expanded regions with the isotopic ion distributions of both peptides.

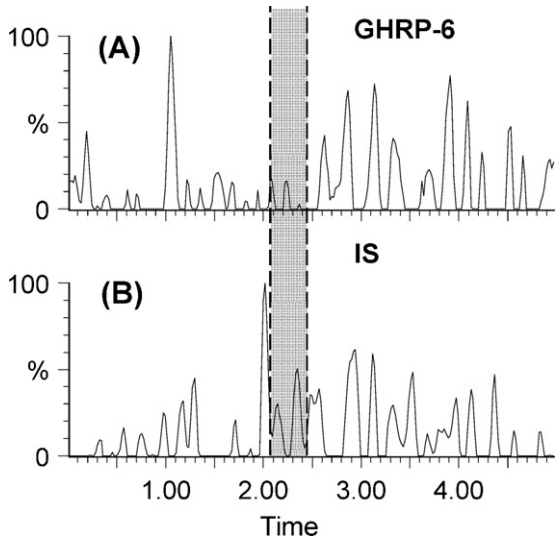

Fig. 3. Chromatograms of plasma without GHRP-6 or internal standard. (A) Extracted ion chromatogram for the two first components of the GHRP-6 isotopic distribution. (B) Extracted ion chromatogram for the two first components of the IS isotopic distribution.

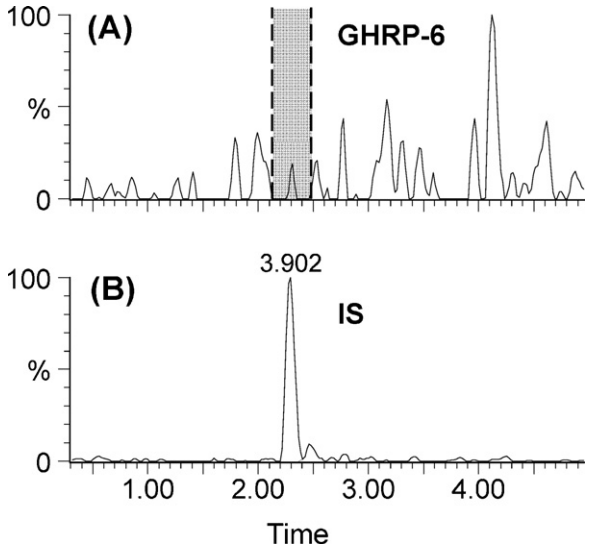

Fig. 4. Chromatograms of plasma with 0 ng/mL of GHRP-6 and 15 ng/mL of internal standard. (A) Extracted ion chromatogram for the two first components of the GHRP-6 isotopic distribution. (B) Extracted ion chromatogram for the two first components of the IS isotopic distribution. Peak label is the corresponding area under the curve (AUC).

column and decreased considerably peptide absorption, affecting overall sensitivity and the lifetime of the monolythic column as well. Higher ratios, starting from 4/1, did not affect peptide absorption onto the column; therefore 4/1 was chosen as optimum, given that higher acetone volumes increased considerably drying time. The latter parameter becomes critical when several samples are being processed.

Monolithic capillary columns were chosen for method development and validation because they provided high resolution (FWHM = 0.05 min) and a fast analysis for GHRP-6 (5 min acquisition window). The use of TFA as ion pair agent was discarded due to a considerable ion suppression in ESI-MS analysis, which compromised the overall sensitivity of the method even in combination with formic acid (FA). Therefore, 0.1% of FA was used exclusively in the mobile phase to preserve the sensitivity of the method without compromising resolution and peak shape. These conditions resulted in the detection of both GHRP6 and its IS as intense doubly-charged ion signals almost exclusively.

Blank plasma samples, without either analyte or IS were also analyzed, yielding no signal at the expected m/z for both peptides (Fig. 3). Samples prepared with 0 ng/mL of GHRP-6 and 15 ng/mL of IS were also analyzed and no detectable signal was observed in the extracted ion chromatogram for the analyte, but as expected, a prominent peak was detected at the m/z for the IS (Fig. 4). The sample clean up established in this method, was sufficient to eliminate potential interferences in the quantification process.

The recovery of the method was also evaluated for both peptides at three different concentrations covering the whole range of analysis. A schematic representation of the procedure is shown in Fig. 6. Plasma samples spiked with a known amount of GHRP-6 and IS were treated with cold acetone and centrifuged. The supernatant was dried and reconstituted in 0.1% FA in water. Before LC–MS analysis, the samples were spiked with an equal amount of either IS or GHRP-6 to calculate relative recovery, using the ratio of the areas under the curves from their corresponding extracted ion chromatograms. Eight replicates (4 for GHRP-6 and 4 for IS) were performed for each of the three concentration levels evaluated. The results were very similar (Table 1) among the three evaluated concentration levels (10, 20 and 40 ng/mL). In all cases the recoveries were consistent, precise and reproducible, with a

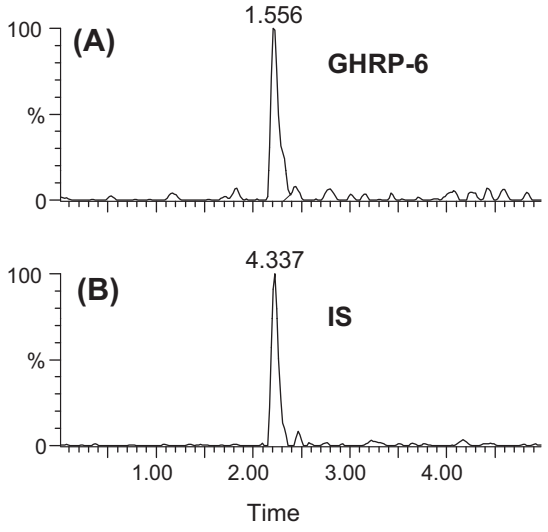

Fig. 5. Chromatograms of plasma with GHRP-6 at the lower limit of quantification (5 ng/mL) and 15 ng/mL of internal standard. (A) Extracted ion chromatogram for the two first components of the GHRP-6 isotopic distribution. (B) Extracted ion chromatogram for the two first components of the IS isotopic distribution. Peak label is the corresponding area under the curve (AUC).

Table 1
Relative recovery of analyte and its IS at three concentration levels. Eight replicates were analyzed in all cases.

	Relative recovery		
	10 ng/mL	20 ng/mL	40 ng/mL
Mean recovery (%)	67.1	58.0	57.9
C.V. %	10.9	13.2	11.2
N	8	8	8

coefficient of variation lower than 15%, as required by FDA guidance [28] (Table 1).

The matrix factor (MF) of processed plasma from 6 healthy volunteers was calculated in order to estimate possible interferences of plasma in the quantification of GHRP-6. An equimolar mixture of

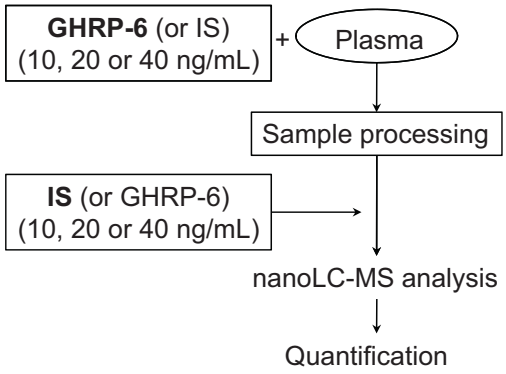

Fig. 6. Workflow for evaluating the recovery of GHRP-6 and IS in the current method. Three different concentrations of analyte and IS were examined, covering the whole range of analysis. GHRP-6 or IS were mixed with 100 μL of plasma, samples were processed (acetone precipitation and drying of supernatant), and after reconstitution they were mixed with equal amounts of the other peptide. Extraction efficiency was calculated from the AUC ratio of the extracted chromatograms for both peptides.

GHRP-6 and its IS was added to the processed plasma samples and were analyzed by LC–MS. On the other hand, the same amount of the equimolar mixture was analyzed by LC–MS in absence of matrix (processed plasma). The ratios between the areas of the extracted chromatograms for analyte and IS in presence or absence of processed plasma, were very similar. The coefficient of variation among all analyzed samples was 1.6%. The analysis of GHRP-6 and its IS in the context of processed plasma from 6 subjects did not exhibit a matrix effect.

3.2. Method validation

3.2.1. Sensitivity

The lower limit of quantification (LLOQ) of the analyte in plasma was experimentally determined. To establish the LLOQ with appropriate accuracy and precision, five replicates were analyzed, prepared with 5 ng/mL of GHRP-6 and 15 ng/mL of IS (Fig. 5). The relative error was calculated for all samples and it ranged between −9.7% and +9.1%, with a coefficient of variation of 8.7%. These results complied with previously established acceptance criteria [29].

3.2.2. Calibration range and response

During validation, five standard curves from 5 ng/mL to 50 ng/mL were analyzed. The R^2 coefficient was higher than 0.9879 for all curves assessed. The difference among curves showed a C.V. % lower than 10.5%. In order to estimate the differences introduced by sample sorting during validation batches [29], QCs, CSs and other validation samples were placed in different locations in the analysis run, without batch to batch differences. Carryover was estimated with blank samples analyzed after the most concentrated samples, and was lower than 6.3% of the response for the LLOQ sample.

Dilution integrity was also evaluated to mimic the analysis of the most concentrated clinical samples. Concentrated samples were prepared with equimolar mixes of both peptides at concentrations of 90 ng/mL, 450 ng/mL, 750 ng/mL and 1500 ng/mL. All samples were diluted in a single step with blank plasma prior to sample processing to reach a final concentration of 15 ng/mL, and the analysis was performed in duplicate. The coefficient of variation among all diluted samples was 2.1%, lower than the FDA acceptance criterion (15%) [28].

Table 2
Inter-day repeatability and variability of quality control samples from five validation batches.

	QCs, nominal concentrations		
	10 ng/mL	20 ng/mL	40 ng/mL
(a) Repeatability			
Mean (ng/mL)	9.0	19.8	40.2
C.V. %	4.8	5.6	3.1
R.E. %	−10.0	−1.0	+0.5
N	5	5	5
(b) Variability			
Mean (ng/mL)	9.6	19.5	40.1
C.V. %	8.8	5.0	5.1
R.E. %	−4.0	−2.5	+0.3
N	10	10	10

3.2.3. Accuracy and precision

To obtain statistical data on precision and accuracy, method validation was performed in five batches during three days. Ten replicates of QCs at three concentrations levels (10, 20 and 40 ng/mL) were scattered in between CSs. Repeatability and variability among days were also evaluated in terms of C.V. % and R.E. % (Table 2). Variability among days and analysts was calculated from calibration standards prepared by two different analysts for each independent validation batch (Table 3).

3.2.4. Sample stability

The stability of both analyte and its IS was tested under conditions similar to those that would be employed for the sample in a real time analysis. Following the validation requirements for bioanalytical methods based on LC–MS according to FDA Guidance [28], we evaluated: (a) stability of stock solutions, (b) post-preparative stability, (c) bench top stability, (d) freeze–thaw stability and (e) post-validation long-term stability at −80 °C.

Stock solutions for both peptides were prepared at 1 mg/mL. Their stability was evaluated immediately and after 6 h at room temperature. There was no variation on the concentrations and integrity of the peptides for two replicates. In post-preparative stability three concentration levels at three different incubation times were assessed. The first group of samples was analyzed immediately, another group at 12 h, and the last one at 24 h after processing. There were three replicates of the analysis and the incubated samples were compared against freshly prepared samples (Table 4). The results of this experiment showed that both the peptide and its internal standard were stable under the studied conditions ($p > 0.05$).

In the bench top stability study, the effect of keeping analyte and internal standard in unprocessed plasma for 4 h at room temperature was evaluated. The analysis was performed in triplicate at three different concentrations. No differences were found between

Table 3
Inter-day and inter-analyst variability of calibrator standard samples from five validation batches.

	Calibrator standards nominal concentrations							
	5 ng/mL	10 ng/mL	15 ng/mL	20 ng/mL	25 ng/mL	30 ng/mL	40 ng/mL	50 ng/mL
Mean	4.8	9.8	14.1	18.3	24.3	28.5	37.6	50.8
C.V. %	15.5	6.5	5.7	7.5	6.0	11.6	3.5	9.3
R.E. %	−4.4	−2.4	−6.3	−8.3	−2.6	−5.0	−6.1	1.6
N	5	5	5	5	5	5	5	5

Table 4
Evaluation of the stability of quality control samples.

	QCs nominal concentrations		
	10 ng/mL	20 ng/mL	40 ng/mL
(a) Post-preparative stability			
Mean (ng/mL)	10.4	19.6	37.8
C.V. %	7.3	7.7	8.0
P	0.75	0.07	0.48
(b) Bench top stability			
Mean (ng/mL)	10.5	18.6	41.3
C.V. %	4.3	6.0	10.6
P	0.68	0.90	0.68
(c) Freeze–thaw stability			
Mean (ng/mL)	10.4	19.5	39.8
C.V. %	6.6	9.2	6.0
P	0.24	0.20	0.76
(d) Long-term stability			
Mean (peak area)[a]	7.46 (7.22)	–	96.59 (102.11)
C.V. %	13.94	–	5.76
P	0.72	–	0.09

[a] To evaluate long-term stability, QC samples were prepared at 10 ng/ml and 50 ng/mL. The analysis was performed directly with the response (peak area). Values between parentheses correspond to the area of GHRP-6 in the extracted ion chromatogram from freshly prepared samples.

the samples incubated for 4 h and those analyzed immediately ($p > 0.05$) (Table 4).

For the freeze–thaw stability study three different concentrations of analyte in plasma were tested. A group of samples was submitted to three freeze–thaw cycles (−20 °C/25 °C) every 24 h. After the last cycle, the samples were processed and analyzed following the usual procedure. The results were compared to those of samples that were not subjected to freeze–thaw cycles, but processed immediately after thawing (Table 4). Both peptides were stable after three freeze–thaw cycles every 24 h ($p > 0.05$). To validate long-term stability, sufficient samples were prepared at two different analyte concentrations to perform triplicate analyses, and stored under the same conditions that would be used for clinical samples, at a temperature of −80 °C. The first group was analyzed at $t = 0$ (freshly prepared), and the remaining groups were analyzed at 7, 14 and 30 days. This experiment analyzed the direct response, rather than the concentration determined indirectly (Table 4). The result satisfied the acceptance criteria of FDA regulations ($p > 0.05$) guaranteeing sample stability during this time and storage conditions. The high stability demonstrated for GHRP-6 in human plasma, is probably due to the presence of two D-amino acids within the sequence. It is well known that D-amino acids increase the stability of peptides in biological fluids [30].

3.3. Application of the method

This method, after validation, was applied to the analysis of samples from a phase 1 clinical trial of GHRP-6. Selectivity and sensitivity were sufficient for detecting and quantifying this peptide in human plasma. The pharmacokinetic study involved nine healthy volunteers distributed into three groups corresponding to different dose levels (100, 200 and 400 μg/kg of weight), receiving the peptide as a single intravenous dose. Confident results were obtained from the analysis of clinical samples that required dilution at the early monitored times. LLOQ was reached in all cases after 12 h post-administration, so the method is sufficiently sensitive for modeling the pharmacokinetic profile of the peptide, as it includes more than 85% of AUC.

GHRP-6 exhibited a bi-phase pharmacokinetic profile of plasma concentration vs. time. Distribution phase was fast ($t_{1/2}\alpha_{(100\,\mu g/kg)} = 0.14$ h, $t_{1/2}\alpha_{(200\,\mu g/kg)} = 0.15$ h and $t_{1/2}\alpha_{(400\,\mu g/kg)} = 0.09$ h), this is typical for a peptide based drug. However, elimination phase was longer in time ($t_{1/2}\beta_{(100\,\mu g/kg)} = 2.96$ h, $t_{1/2}\beta_{(200\,\mu g/kg)} = 3.27$ h and $t_{1/2}\beta_{(400\,\mu g/kg)} = 1.15$ h). The clearance was very similar among the three dose levels (CL = 0.19 L/h kg). The maximum concentration (C_{max}) in all cases was reached 3 min after administration and was increased with dose ($C_{max(100\,\mu g/kg)} = 0.90$ μg/mL, $C_{max(200\,\mu g/kg)} = 2.37$ μg/mL and $C_{max(400\,\mu g/kg)} = 4.12$ μg/mL). Additionally, we found that the AUC was dose dependent, by increasing with the dose level. Complete results and analysis of this pharmacokinetic study will be published elsewhere.

4. Conclusions

A method based on LC–MS to quantify GHRP-6 in human plasma was developed and fully validated. The three Daltons mass shift between the analyte and its IS was sufficient for its absolute quantification. Protein precipitation via acetone and positive full scan mode acquisition, provide adequate selectivity and sensitivity to evaluate this peptide in human plasma. The calibration range was from 5 to 50 ng/mL, but dilution integrity tests demonstrated that more concentrated samples can be successfully analyzed. Sample stability evaluations showed that both the peptide and the internal standard were stable under the assayed conditions. The method was successfully applied to the analysis of GHRP-6 in clinical samples from pharmacokinetics study with this peptide, which will be the main objective of further work.

Acknowledgements

The authors would like to thank the Quality Assurance Unit of the Center for Genetic Engineering and Biotechnology for technical assistance during method development and validation; and Dr. Gilberto B. Domont for supporting the amino acid analysis and determination of the extinction coefficient of GHRP-6. We also thank Alejandro M. Martin from CIGB (Cuba) for critical review and English correction of the manuscript.

References

[1] R. Deghenghi, M.M. Cananzi, A. Torsello, C. Battisti, E.E. Muller, V. Locatelli, GH-releasing activity of hexarelin, a new growth hormone releasing peptide, in infant and adult rats, Life Sci. 54 (1994) 1321–1328.
[2] R.G. Smith, O.C. Palyha, S.D. Feighner, C.P. Tan, K.K. McKee, D.L. Hreniuk, L. Yang, G. Morriello, R. Nargund, A.A. Patchett, A.D. Howard, Growth hormone releasing substances: types and their receptors, Horm. Res. 51 (Suppl. 3) (1999) 1–8.
[3] T. Sugino, Y. Hasegawa, Y. Kurose, M. Kojima, K. Kangawa, Y. Terashima, Effects of ghrelin on food intake and neuroendocrine function in sheep, Anim. Reprod. Sci. 82–83 (2004) 183–194.
[4] P. Schuessler, M. Uhr, M. Ising, D. Schmid, J. Weikel, A. Steiger, Nocturnal ghrelin levels – relationship to sleep EEG, the levels of growth hormone, ACTH and cortisol – and gender differences, J. Sleep Res. 14 (2005) 329–336.
[5] D. Cibrián, H. Ajamieh, J. Berlanga, O.S. León, J.S. Alba, M.J. Kim, T. Marchbank, J.J. Boyle, F. Freyre, D. Garcia Del Barco, P. Lopez-Saura, G. Guillen, S. Ghosh, R.A. Goodlad, R.J. Playford, Use of growth-hormone-releasing peptide-6 (GHRP-6) for the prevention of multiple organ failure, Clin. Sci. (Lond.) 110 (2006) 563–573.
[6] J. Berlanga, D. Cibrian, L. Guevara, H. Dominguez, J. Alba, A. Seralena, G. Guillen, E. Lopez-Mola, P. Lopez-Saura, A. Rodriguez, B. Perez, D. Garcia, N.S. Vispo, Growth-hormone-releasing peptide 6 (GHRP6) prevents oxidant cytotoxicity and reduces myocardial necrosis in a model of acute myocardial infarction, Clin. Sci. (Lond.) 112 (2007) 241–250.
[7] F. Casanueva, C. Dieguez, Growth hormone secretagogues: physiological role and clinical utility, Trends Endocrinol. Metab. 10 (1999) 30–38.
[8] E. Gelpi, Biomedical and biochemical applications of liquid chromatography–mass spectrometry, J. Chromatogr. A 703 (1995) 59–80.
[9] J. Peng, S. Gygi, Proteomics: the move to mixtures, J. Mass Spectrom. 36 (2001) 1083.
[10] R. Aebersold, M. Mann, Mass spectrometry-based proteomics, Nature 422 (2003) 198–207.
[11] M. Washburn, D. Wolters, J.R. Yates, Large-scale analysis of the yeast proteome by multidimensional protein identification technology, Nat. Biotechnol. 19 (2001) 242–247.
[12] O. Stemmann, H. Zou, S. Gerber, S. Gygi, M. Kirschner, Dual inhibition of sister chromatid separation at metaphase, Cell 107 (2001) 715–726.
[13] S. Darby, M. Miller, R. Allen, M. LeBeau, A mass spectrometric method for quantitation of intact insulin in blood samples, J. Anal. Toxicol. 25 (2001) 8–14.

[14] D. Chang, S.J. Kolis, K.H. Linderholm, T.F. Julian, R. Nachi, A.M. Dzerk, P.P. Lin, J.W. Lee, S.K. Bansal, Bioanalytical method development and validation for a large peptide HIV fusion inhibitor (Enfuvirtide, T-20) and its metabolite in human plasma using LC–MS/MS, J. Pharm. Biomed. Anal. 38 (2005) 87–496.
[15] M. Okano, M. Sato, A. Ikekita, S. Kageyama, Determination of growth hormone secretagogue pralmorelin (GHRP-2) and its metabolite in human urine by liquid chromatography/electrospray ionization tandem mass spectrometry, Rapid Commun. Mass Spectrom. 24 (2010) 2046–2056.
[16] A. Thomas, M. Kohler, J. Mester, H. Geyer, W. Schänzer, M. Petrou, M. Thevis, Identification of the growth-hormone-releasing peptide-2 (GHRP-2) in a nutritional supplement, Drug Test Anal. 2 (2010) 144–148.
[17] A. Thomas, S. Höppner, H. Geyer, W. Schänzer, M. Petrou, D. Kwiatkowska, A. Pokrywka, M. Thevis, Determination of growth hormone releasing peptides (GHRP) and their major metabolites in human urine for doping controls by means of liquid chromatography mass spectrometry, Anal. Bioanal. Chem. 401 (2011) 507–516.
[18] H. Fouda, M. Nocerini, R. Schneider, C. Gedutis, Quantitative analysis by high-performance liquid chromatography atmospheric pressure chemical ionization mass spectrometry: the determination of the renin inhibitor CP-80, 794 in human serum, J. Am. Soc. Mass Spectrom. 2 (1991) 64–167.
[19] D. Wang-Iverson, M.E. Arnold, M. Jemal, A.I. Cohen, Determination of SQ 33,600, a phosphinic acid containing HMG CoA reductase inhibitor, in human serum by high-performance liquid chromatography combined with ionspray mass spectrometry, Biol. Mass Spectrom. 21 (1992) 189–194.
[20] T.R. Covey, E.D. Lee, J.D. Henion, High-speed liquid chromatography/tandem mass spectrometry for the determination of drugs in biological samples, Anal. Chem. 58 (1986) 2453–2460.
[21] B. Kaye, M.W.H. Clark, N.J. Cussans, P.V. Macrae, D.A. Stopher, The sensitive determination of abanoquil in blood by high-performance liquid chromatography/atmospheric pressure ionization mass spectrometry, Biol. Mass Spectrom. 21 (1992) 585–589.
[22] H. Wan, D.M. Desiderio, Quantification of [Dmt1] DALDA in ovine plasma by on-line liquid chromatography/quadrupole time-of-flight mass spectrometry, Rapid Commun. Mass Spectrom. 17 (2003) 538–546.
[23] D. Dadgar, P.E. Burnett, M.G. Choc, K. Gallicano, J.W. Hooper, Application issues in bioanalytical method validation, sample analysis and data reporting, J. Pharm. Biomed. Anal. 13 (1995) 89–97.
[24] G.B. Fields, R.L. Noble, Solid phase peptide synthesis utilizing 9-fluorenylmethoxycarbonyl amino acids, Int. J. Pept. Protein Res. 35 (1990) 161–214.
[25] J. McEntire, Selection and validation of analytical techniques, BioPharm 7 (1994) 68–80.
[26] H. John, M. Walden, S. Schafer, S. Genz, W.G. Forssmann, Analytical procedures for quantification of peptides in pharmaceutical research by liquid chromatography–mass spectrometry, Anal. Bioanal. Chem. 378 (2004) 883–897.
[27] R.H. Bateman, R. Carruthersa, J.B. Hoyesa, C. Jonesa, J.I. Langridgea, A. Millara, J.P.C. Vissersa, A novel precursor ion discovery method on a hybrid quadrupole orthogonal acceleration time-of-flight (Q-TOF) mass spectrometer for studying protein phosphorylation, J. Am. Soc. Mass Spectrom. 13 (2002) 92–803.
[28] FDA, Guidance for Industry, Bioanalytical Method Validation, May 2001.
[29] S. Bansal, A. DeStefano, Key elements of bioanalytical method validation for small molecules, AAPS J. 9 (2007) E109–E114.
[30] M.F. Powell, T. Stewart, L. Otvos, L. Urge, F.C.A. Gaeta, A. Sette, T. Arrhenius, D. Thomson, K. Soda, S.M. Colon, Peptide stability in drug development II: effect of single amino acid substitution and glycosylation on peptide reactivity in human serum, Pharm. Res. 10 (1993) 1268–1273.

Journal of Pharmaceutical and Biomedical Analysis 60 (2012) 26–31

Contents lists available at SciVerse ScienceDirect

Journal of Pharmaceutical and Biomedical Analysis

journal homepage: www.elsevier.com/locate/jpba

Determination of atomoxetine and its metabolites in conventional and non-conventional biological matrices by liquid chromatography–tandem mass spectrometry

Emilia Marchei[a,1], Esther Papaseit[b,c,d,1], Oscar Q. Garcia-Algar[c,d], Magi Farrè[b,c], Roberta Pacifici[a], Simona Pichini[a,*]

[a] Department of Therapeutic Research and Medicines Evaluation, Istituto Superiore di Sanità, Rome, Italy
[b] Human Pharmacology and Clinical Neurosciences Research Group, Hospital del Mar Research Institute-IMIM-Parc de Salut Mar, Barcelona, Spain
[c] Universitat Autonoma de Barcelona, Barcelona, Spain
[d] URIE, Department of Pediatrics, Hospital del Mar-Parc de Salut Mar, Barcelona, Spain

ARTICLE INFO

Article history:
Received 13 September 2011
Received in revised form 6 November 2011
Accepted 7 November 2011
Available online 17 November 2011

Keywords:
Atomoxetine
Tandem mass spectrometry
Oral fluid
Sweat
Plasma

ABSTRACT

A procedure based on liquid chromatography–tandem mass spectrometry (LC–MS/MS) is described for determination of atomoxetine (ATX) and its metabolites 4-hydroxyatomoxetine (4-OH-ATX) and N-des-methylatomoxetine (N-des-ATX) in plasma, urine, oral fluid and sweat using duloxetine as internal standard. Analytes were extracted from 0.5 mL biological fluids and sweat patch with 2 mL aliquots of tert-butyl methyl ether. The organic layer was evaporated and redissolved in mobile phase. Chromatographic separation was carried out on reverse-phase column and an isocratic mobile phase formed by 40% water and 60% 5 mM ammonium acetate, 47.2 mM formic acid, 4 mM trifluoroacetic acid in acetonitrile–water (85:15, v/v) at a flow rate of 0.5 mL/min. Separated analytes were identified and quantified by positive electrospray ionization tandem mass spectrometry and in multiple reaction monitoring acquisition mode. Limits of quantifications for the three analytes were 0.5 ng/mL plasma and oral fluid, 10 ng/mL urine and 1 ng/patch using 0.5 mL biological fluids or one sweat-patch per assay. Calibration curves were linear over the calibration ranges with $r^2 > 0.99$. At three concentrations spanning the linear dynamic range of the assay, mean recoveries in different biological matrices were always higher than 65%. This method was applied to therapeutic monitoring of ATX and its metabolites 4-OH-ATX and N-des-ATX in conventional and non-conventional biological matrices from individuals in drug treatment.

1. Introduction

Attention-deficit hyperactivity disorder (ADHD) affects 5–12% of children and adolescents worldwide and is associated with considerable morbidity and poorer outcomes later in life, representing the most frequent mental disorder diagnosed and treated in children [1–6]. Although multimodal treatment approaches are advocated, pharmacotherapy with psychostimulants remain the first-line treatment for ADHD [7–9]. In 2002, atomoxetine (ATX), a non stimulant drug was approved for the treatment of ADHD in children, adolescents, and adults as an alternative to methylphenidate (MPH) [10–12]. ATX is a potent inhibitor of the noradrenaline neuronal reuptake membrane transporter with minimal affinity for other monoamine transporters or receptors [13,14]. Following oral administration, ATX is well absorbed and metabolized predominantly in the liver by cytochrome P-450 enzyme pathway. ATX is mainly transformed by CYP2D6 isoenzyme to 4-hydroxyatomoxetine (4-OH-ATX), the primary pharmacologically active metabolite, further conjugated to 4-hydroxyatomoxetine-*O*-glucuronide (4-OH-ATX-G) and by CYP2C19 isoenzyme to N-desmethylatomoxetine (N-des-ATX), a less active metabolite [15,16]. Studies in healthy adults indicated that the pharmacokinetics of ATX is influenced by the CYP2D6 genetic polymorphic expression [17]. Thus, following drug administration, ATX and 4-OH-ATX are the principle circulating species in plasma from extensive metabolizers (EM), while in poor metabolizers ATX concentrations 5–10-fold higher than extensive metabolizers and N-des-ATX are predominantly found [18]. In addition, the administration of inhibitors of CYP 2D6 activity can reduce ATX metabolism as described in poor metabolizers [18].

There are different analytical methodologies available for measurement of ATX and its metabolites (4-OH-ATX, N-des ATX) in plasma and urine [17–23], but therapeutic drug monitoring of

* Corresponding author at: Department of Therapeutic Research and Medicines Evaluation, Istituto Superiore di Sanitá, V.le Regina Elena 299, 00161 Rome, Italy. Tel.: +39 0649903682; fax: +39 0649902016.
E-mail addresses: pichini@iss.it, simona.pichini@iss.it (S. Pichini).
[1] These authors contributed equally to the present article.

0731-7085/$ – see front matter © 2011 Elsevier B.V. All rights reserved.
doi:10.1016/j.jpba.2011.11.009

parent drug and its metabolites is essentially lacking. Monitoring compliance to therapeutic drugs especially in paediatric and adolescent population is more difficult to perform than in adults because the need for non invasive or less invasive, yet highly sensitive, analytical methods to assess drugs intake. Alternative biological matrices should be investigated for non-invasive assessment of short and long term drug use in paediatric and adolescent population.

Recently, we set up a procedure based on liquid chromatography–tandem mass spectrometry (LC–MS/MS) for the determination of ATX and its metabolites in hair of treated children and applied the method to monitor long-term drug compliance [24]. Subsequently, we sought to develop a simple and fast assay for the other conventional (blood and urine) and non-conventional (oral fluid and sweat) biological matrices. The aims of the study were: to develop and validate a simple LC–MS/MS method coupled with a minimum preparation of biological samples of small volumes (applicable to paediatric population) and to preliminarily verify if non-conventional, less invasive biological matrices could be used for therapeutic ATX monitoring.

2. Experimental

2.1. Materials

Standards of atomoxetine (ATX), N-desmethylatomoxetine (N-des-ATX) and 4-hydroxyatomoxetine (4-OH-ATX) were a kind gift from Eli Lilly and Company (Indianapolis, IN, USA). Duloxetine (used as internal standard, IS) was obtained from Cerillirant (Milan, Italy) and β-glucuronidase (10,000 units/mL) from Sigma–Aldrich (Milan, Italy). Ultrapure water and all other reagents of analytical grade were provided from Carlo Erba (Milan, Italy).

2.2. Biological samples

Blood, urine, oral fluid and sweat used for this study were obtained from two adolescents diagnosed for ADHD in treatment with ATX since the previous six months (one female of 14 years, 44 kg weight and 153 cm height taking 40 mg/day ATX and one male of 16 years, 57 kg weight, 179 cm height taking 60 mg/day ATX), attending the routine outpatient clinic at Hospital del Mar, Barcelona, Spain. The study was approved by the Ethical Committee of the Hospital. Parents of the two adolescents included in this study signed an informed consent and completed a structured questionnaire. Biological matrices were collected from the two adolescents coming for a routine control. Daily drug dose was administered during the visit. Blood and oral fluid samples were collected at peak time (2 h for ATX and 3 h for both metabolites) and 6 h post administration. Urine samples from 0 to 6 h post administration were collected. Sweat patches were applied on the back of the two individuals before taking medication and removing them 6 h post-application. Blood was immediately centrifuged and the obtained plasma was aliquoted into 0.5 mL plastic tubes. Drug-free plasma, oral fluid and urine were obtained from 20 different healthy donors, analyzed during method validation to exclude any source of chromatographic interferences and mixed to obtain a homogeneous pool of blank samples to be used for calibration standards and quality control (QC) samples. Drug-free sweat was collected by sweat patches applied to the back of healthy donors, after the skin had been cleaned with a 70% isopropyl alcohol swab, and removed 6 h post-application. One patch from the healthy individuals was checked for the absence of any interfering substance before using the other patches for calibration standards and QC samples. All biological samples were frozen at −20 °C until analysis. No preservatives were added to the specimens.

2.3. Calibration standards and quality control samples

Stock standard solutions (1 mg/mL) and working solutions (100, 10, 1 and 0.1 μg/mL) of ATX, 4-OH-ATX and N-des-ATX were prepared in methanol and stored at −20 °C until analysis. The IS working solution was used at a concentration of 0.1 μg/mL.

Calibration standards of ATX ranging from limit of quantification (LOQ) to 500 ng and from LOQ to 50 ng per mL plasma and oral fluid, respectively; from LOQ to 50 ng for 4-OH-ATX and N-des-ATX per mL plasma and oral fluid; from LOQ to 1000 ng for ATX and N-des-ATX and from LOQ to 2000 ng for 4-OH-ATX per mL urine and from LOQ to 50 ng per sweat patch for all analytes under investigation were prepared daily for each analytical batch by adding suitable amounts of methanol working solutions to 0.5 mL of pre-checked drug-free biological fluids or drug-free sweat patch. QC samples of 0.6 ng/mL (low), 20 ng/mL (medium) and 45 ng/mL (high) ATX in oral fluid or ng/patch and N-des-ATX and 4-OH-ATX in plasma, oral fluid or ng/patch; 0.6 ng/mL (low), 200 ng/mL (medium) and 450 ng/mL (high) ATX in plasma; 12 ng (low), 400 ng (medium) and 850 ng (high) ATX and N-des-ATX and 12 ng (low), 400 ng (medium) and 1500 ng (high) 4-OH-ATX per mL urine and samples at the limit of quantification (LOQ), were prepared, aliquoted, and stored at −20 °C. QC samples were included in each analytical batch to check calibration, accuracy, precision, matrix effect and stability of samples under storage conditions.

Blank urine containing 5000 ng/mL ATX and N-des-ATX and 10,000 and 20,000 ng/mL 4-OH-ATX were prepared as over-the curve samples, to be tested for accuracy and precision once diluted 5 and 10 times, respectively.

Since the standard of 4-OH-ATX-G was not available, the amount of urinary of 4-OH-ATX-G was obtained from the comparison of the concentration of 4-OH-ATX in un-hydrolyzed and hydrolyzed urine samples.

2.4. Sample preparation

Frozen plasma, oral fluid, and urine samples were allowed to thaw at room temperature. Before analysis, oral fluid was centrifuged to discard the mucous part, which accumulated at the bottom. Aliquots of 0.5 mL plasma, oral fluid and urine were added with 10 or 100 ng/mL IS and diluted with 500 μL water. After 30 s vortexing, analytes were extracted with two subsequent 2 mL aliquots tert-butyl methyl ether. After centrifugation at 3500 rpm for 3 min, the organic phase was evaporated to dryness under a stream of nitrogen and redissolved in 100 μl mobile phase.

An aliquot of urine samples, added with 500 μL of 10,000 units/mL β-glucuronidase was incubated overnight before extraction as reported above to measure total amount of 4-OH-ATX (free and glucuronated metabolite). The concentration difference between total amount of 4-OH-ATX and that of free metabolite allowed the calculation of glucuronated metabolite.

For ATX, 4-OH-ATX and N-des-ATX determination in sweat patch, the absorbent pad removed from the patch with clean tweezers and added to 10 ng IS and 0.5 mL water (covering the whole pad) in a clean tube was extracted twice with 2 mL tert-butyl methyl ether. After centrifugation at 3500 rpm for 3 min, the organic phase was evaporated to dryness under a stream of nitrogen and redissolved in 100 μl mobile phase.

A 15 μl volume of redissolved samples was injected into LC column.

2.4.1. Liquid chromatography–tandem mass spectrometry

Liquid chromatography–tandem mass spectrometry (LC–MS/MS) analyses were performed using an Alliance HPLC system (Waters, Etten-Leur, The Netherlands) interfaced to a Micromass Quattro micro API triple quadrupole mass spectrometer

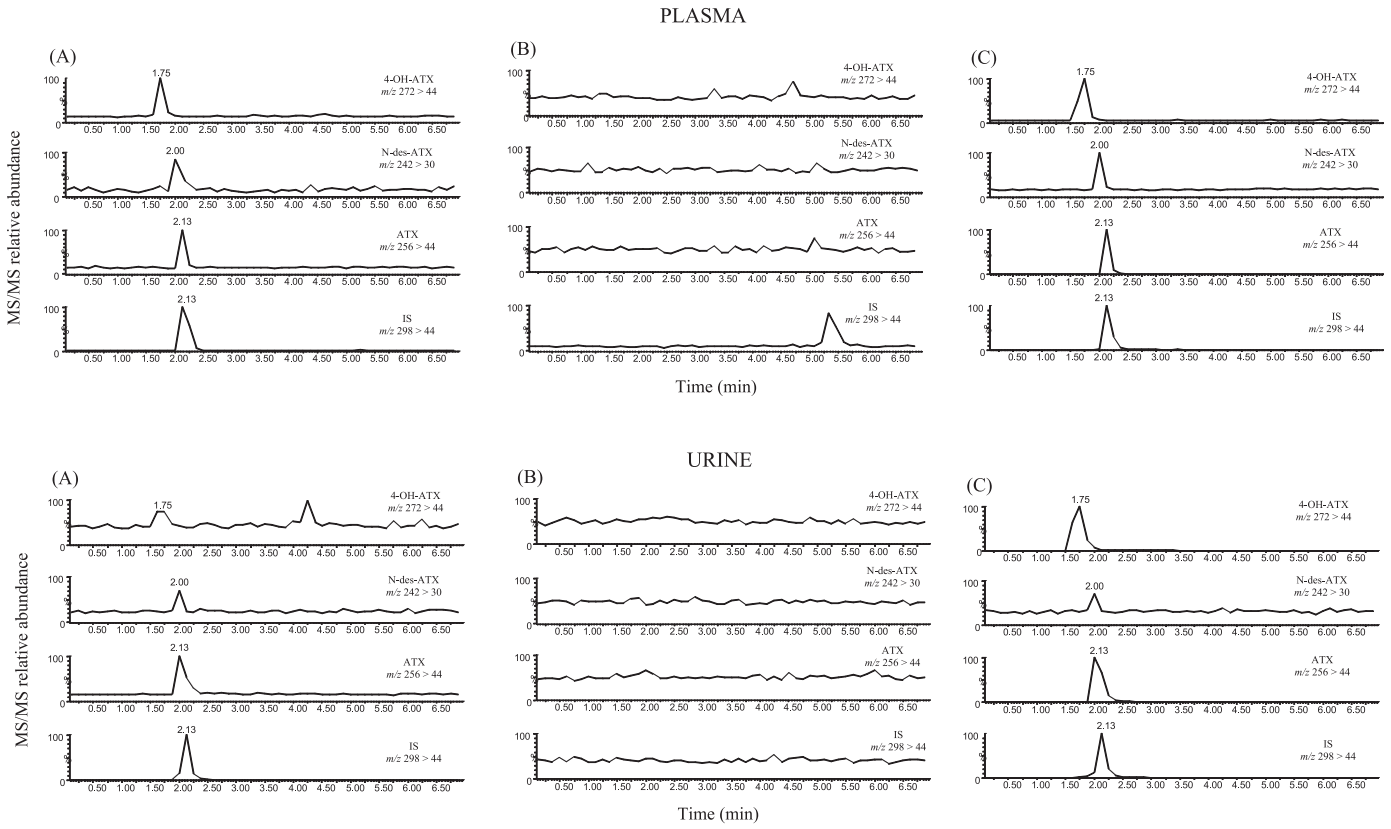

Fig. 1. LC–MS/MS chromatogram of an extract of (A) drug-free plasma (top) and urine (below) spiked with 0.6 and 12 ng/mL ATX, 4-OH-ATX and N-des-ATX, respectively, and 100 ng/mL IS; (B) drug-free plasma (top) and urine (below) samples; (C) plasma sample (top) containing 85.3 ng/mL ATX, 2.8 ng/mL 4-OH-ATX, 6.5 ng/mL N-des-ATX and urine sample (below) containing 0.2 μg/mL ATX, 29.8 μg/mL 4-OH-ATX, and 0.009 μg/mL N-des-ATX.

(Waters) equipped with an electrospray (ESI) ion source. Chromatographic separation was achieved by a YMC-Pack TMS column (40 mm × 4.6 mm i.d., 5–3 m particle size) (CPS analitica, Milan, Italy). Mobile phase was formed by solvent A (water) and solvent B (5 mM ammonium acetate, 47.2 mM formic acid, 4 mM trifluoroacetic acid in acetonitrile–water (85:15, v/v)). A mixture of 40% solvent A and 60% solvent B was used in isocratic conditions at a flow rate of 0.5 mL/min. The mass tandem spectrometer (Waters Quattro micro) was operated in positive electrospray ionization mode using multiple reaction monitoring (MRM) as acquisition mode. The following ESI conditions were applied: capillary voltage at 3 kV, source temperature, 120 °C and desolvation temperature, 420 °C. The cone and desolvation gas flows were set at 50 and 550 L/h, respectively. Cone voltage and collision energy were 20 V and 13 V, respectively. Acquisition was performed using multiple reaction monitoring (MRM) with the following transitions: ATX

Table 1
Calibration method for ATX, 4-OH-ATX and N-des-ATX in different biological matrices.

Analyte	Calibration line		Correlation coefficient (r^2)	Limit of detection (LOD)[b]	Limit of quantification (LOQ)[b]
	Slope[a]	Intercept[a]			
Plasma					
ATX	0.027 ± 0.010	−0.010 ± 0.081	0.999 ± 0.001	0.2	0.5
4-OH-ATX	0.031 ± 0.032	−0.045 ± 0.079	0.998 ± 0.002	0.1	0.5
N-des-ATX	0.002 ± 0.002	−0.001 ± 0.002	0.999 ± 0.001	0.2	0.5
Oral fluid					
ATX	0.322 ± 0.147	−0.193 ± 0.314	0.995 ± 0.001	0.2	0.5
4-OH-ATX	0.241 ± 0.119	−0.190 ± 0.335	0.992 ± 0.002	0.1	0.5
N-des-ATX	0.021 ± 0.008	−0.004 ± 0.014	0.990 ± 0.001	0.2	0.5
Urine					
ATX	0.002 ± 0.001	0.025 ± 0.078	0.999 ± 0.001	3.0	10
4-OH-ATX	0.0003 ± 0.0002	−0.002 ± 0.001	0.998 ± 0.001	3.0	10
N-des-ATX	0.002 ± 0.001	0.025 ± 0.001	0.999 ± 0.001	3.0	10
Sweat					
ATX	0.115 ± 0.013	−0.014 ± 0.003	0.993 ± 0.002	0.3	0.5
4-OH-ATX	0.114 ± 0.019	0.254 ± 0.130	0.993 ± 0.003	0.3	0.5
N-des-ATX	0.007 ± 0.003	0.005 ± 0.002	0.980 ± 0.010	0.3	0.5

[a] Mean and S.D. of three replicates.
[b] ng/mL for plasma, oral fluid and urine and ng/sweat patch for sweat.

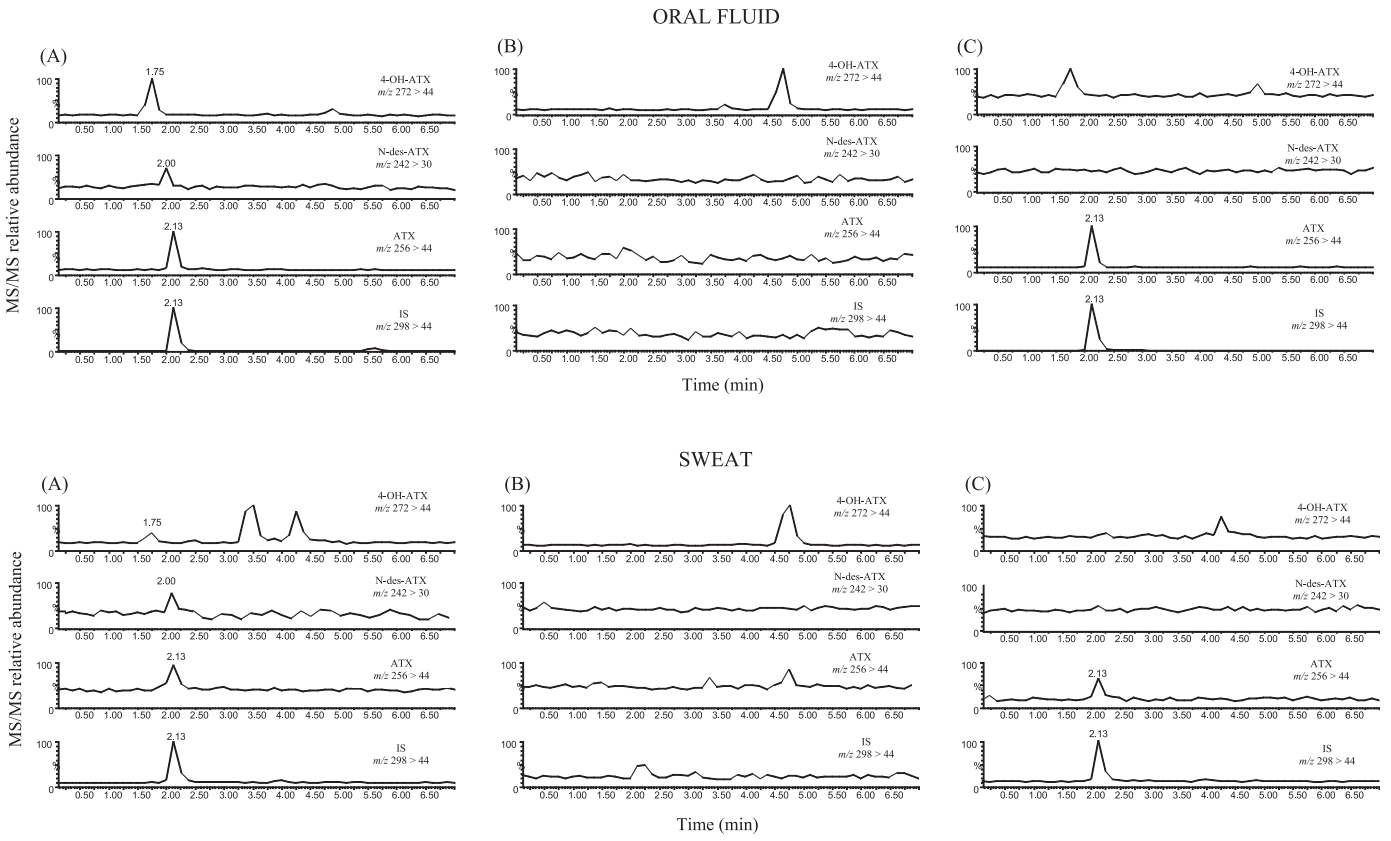

Fig. 2. LC–MS/MS chromatogram of an extract of (A) drug-free oral fluid (top) and sweat (below) spiked with 0.6 ng/mL ATX, 4-OH-ATX and N-des-ATX and 10 ng/mL IS; (B) drug-free oral fluid (top) and sweat (below) samples; (C) oral fluid sample (top) containing 0.8 ng/mL ATX, 0.5 ng/mL 4-OH-ATX and sweat sample (below) containing 3.4 ng/mL ATX.

m/z 256 → 148 and m/z 256 → 44, 4-OH-ATX m/z 272 → 148 and m/z 272 → 44, N-des-ATX m/z 242 → 134 and m/z 242 → 30 and duloxetine (IS) m/z 298 → 154 and m/z 298 → 44. The underlined transitions were selected for quantification.

2.4.2. Validation procedures

Prior to application to real samples, the method was tested in a validation protocol following the accepted criteria for bioanalytical method validation [25,26]. Selectivity, carryover, matrix effect, linearity, limits of detection and quantification, precision, accuracy, recovery, and stability were determined as previously reported [27].

3. Results and discussion

3.1. Chromatography and validation

Representative chromatograms obtained following the extraction of analytes under investigation spiked in 0.5 mL drug-free plasma, urine and oral fluid and one sweat patch spiked are shown in Figs. 1A and 2A. Separation of ATX, 4-OH-ATX and N-des-ATX was completed in 3 min. A 4 min equilibration time was necessary at the end of each run for elution of possible endogenous compounds.

When analyte concentration in urine samples was higher than those in the calibration curve, samples were re-processed once diluted 5 or 10 times (over-curve samples).

Samples following the one exceeding the linear range in the chromatographic run were re-injected to check for possible contamination by carryover. Nevertheless, there was no carryover observed in these cases nor, when drug-free urine samples were injected after the highest point of the calibration curve. No additional peaks due to endogenous substances that could have interfered with the detection of compounds of interest were observed after the injection of drug-free biological matrices (20 different samples per matrix) (Figs. 1B and 2B). Similarly, none of the principal drugs of abuse (opiates, cocaine, cannabinoids, amphetamines type-stimulants) or common ADHD comedications (antidepressants, benzodiazepines, methylphenidate, fluoxetine, paroxetine, sertraline, carbamazepine, risperidone) carried through the entire procedure, interfered with the assay and with the accurate quantification of the low QC samples in all the biological matrices.

No significant ion suppression (less than 10% analytical signal suppression) due to matrix effect, determined by dividing mean peak areas of QC solutions prepared in the mobile phase by blank biological matrices fortified with QC solutions after extraction multiplied by 100, occurred during chromatographic runs.

Linear calibration curves showed determination coefficients (r^2) equal to or higher than 0.99 in all cases. LODs and LOQs values, calculated from standard deviation (S.D.) of the mean noise level over the retention time window of each analyte were adequate for the purpose of the present study (Table 1). The calculated LOQ tested for precision and accuracy presented coefficients of variation always lower than 20%. The intra and inter-assay imprecision (measured as % relative standard deviation, RSD) and accuracy (measured as % error) values always lower than 20% were in accordance with the internationally established acceptance criteria (Table 2).

Over-curve samples, tested for imprecision and accuracy after diluting 5–10 times, gave values always lower than 10% relative standard deviation (RSD) and % error. Absolute analytical recoveries

Table 2
Intra-assay ($n = 5$) and inter-assay ($n = 20$) imprecision, accuracy ($n = 20$) and recovery of ATX, 4-OH-ATX and N-des-ATX in plasma, oral fluid, urine and sweat.

Analyte	Intra-assay imprecision (% RSD)			Inter-assay imprecision (% RSD)			Accuracy (% RSD)			Recovery (%)		
	Low QC	Medium QC	High QC	Low QC	Medium QC	High QC	Low QC	Medium QC	High QC	Low QC	Medium QC	High QC
Plasma												
ATX	11.7	3.6	3.2	7.3	9.8	9.0	5.8	8.5	3.1	93.6 ± 0.2	95.7 ± 0.5	87.4 ± 1.3
4-OH-ATX	5.3	5.4	4.5	5.6	11.8	17.2	16.2	9.3	11.1	73.5 ± 1.3	82.1 ± 2.1	76.0 ± 0.8
N-des-ATX	9.0	6.8	12.3	14.0	6.2	11.5	12.5	12.3	13.4	73.5 ± 0.7	75.9 ± 1.1	78.5 ± 1.2
Oral fluid												
ATX	10.4	3.1	4.0	5.7	3.0	5.0	15.0	8.4	3.4	89.6 ± 2.3	84.4 ± 0.4	83.1 ± 1.5
4-OH-ATX	13.5	6.7	3.8	14.7	3.0	11.4	8.2	6.6	11.0	70.3 ± 1.0	68.3 ± 2.5	78.4 ± 1.2
N-des-ATX	16.4	3.7	5.9	6.6	6.2	8.4	5.4	11.4	8.6	64.1 ± 3.5	61.6 ± 1.6	68.5 ± 0.6
Urine												
ATX	7.3	5.5	11.1	6.5	7.2	5.4	10.0	2.3	2.6	83.2 ± 0.3	79.1 ± 1.3	83.4 ± 1.5
4-OH-ATX	6.4	2.7	5.3	10.1	10.6	10.4	3.5	2.8	3.5	82.1 ± 1.5	85.1 ± 3.8	84.4 ± 0.3
N-des-ATX	10.7	6.5	6.9	9.1	5.6	6.3	6.0	3.7	7.1	70.5 ± 1.6	71.4 ± 1.7	70.1 ± 4.5
Sweat												
ATX	10.8	13.1	11.3	10.6	10.2	10.3	9.3	9.9	10.3	73.2 ± 3.6	74.4 ± 3.6	75.5 ± 4.8
4-OH-ATX	10.5	12.0	12.8	10.1	11.8	10.9	10.3	10.1	12.8	77.4 ± 2.5	70.5 ± 1.7	72.7 ± 1.5
N-des-ATX	7.05	9.6	10.8	9.4	10.0	7.6	11.1	15.7	11.8	72.5 ± 0.9	70.6 ± 1.3	71.6 ± 2.5

(mean ± S.D.) obtained after extraction procedure for the three different QC samples showed that there were no significant variations at different concentration levels for the analytes under investigation in different biological matrices (Table 2).

Regarding the freeze/thaw stability assays for quality control samples, no significant degradation was observed after any of the three freeze/thaw cycles; the differences in concentration compared to the initial concentration were lower that 10%. Similar results (differences always lower than 10%) were obtained in case of mid-term stability test, performed re-analyzing replicates of two real plasma, urine, oral fluid samples and two sweat patches, cut in four pieces, once a month for 6 months period, assuring the validity of stored samples analysis.

3.2. Analysis of clinical samples

The method of analysis described in this report is being used for samples obtained from children and adolescents (examples are reported in Figs. 1C and 2C), diagnosed for ADHD, in treatment with ATX at Hospital del Mar, Barcelona, Spain. Our goal is being to set up therapeutic drug monitoring (TDM) to assess drug compliance, to establish the relationship between drug and metabolite concentration in different biological matrices and clinical efficacy as well as possible side-effects and finally to test the possibility of using oral fluid or sweat as non-invasive alternative biological matrices for TDM in paediatrics.

Table 3 shows the concentrations of ATX and its metabolites (4-OH-ATX and N-des-ATX) in samples of different biological matrices analyzed during assay development, originating from two adolescents selected among the subjects attending outpatient clinics at Hospital del Mar. The adolescents were in treatment with 40 mg (subject 1) and 60 mg (subject 2) ATX (Strattera, Eli Lilly, Madrid, Spain). With respect to plasma samples, both at peak time and 6 h post administration, the parent drug was the analyte with the highest concentration with both metabolites were present in few ng/mL biological matrices.

ATX appeared in oral fluid in significantly lower concentrations than those in plasma. This is a surprising result considering the nature of the molecule, which is a weak base ($pK_a = 9.2$), such as the others amphetamine type-stimulants (3,4-methylerndioxymethamphetamine, methamphetamine) and methylphenidate shown to accumulate in oral fluid, which is more acidic than blood [28,29]. We hypothesize that the difference is due to extremely high protein-bound (98.7%) of ATX [30], as compared to that of 20% reported for the other molecules [28,29]. In case of the hydroxymetabolite, with a lower protein bound than the parent drug (around 66%), the OF/P ratio values were higher than those of ATX. Finally, since very low N-des-ATX concentrations were measured in plasma, it would not have been

Table 3
ATX, 4-OH-ATX and N-des-ATX concentration in samples of conventional and non-conventional matrices from subjects following oral administration of 40 mg (subject 1) and 60 mg (subject 2) of ATX.

Analyte	Plasma (ng/mL)		Oral fluid (ng/mL)		OF/P ratio		Amount excreted in urine in μg/mL (total amount in μg)	Sweat patch
	Peak time	6 h post-administration	Peak time	6 h post-administration	Peak time	6 h post-administration	0–6 h	6 h post-administration
Subject 1								
ATX	350.4	85.3	7.9	0.8	0.02	0.01	0.2 (36.5)	3.4
4-OH-ATX	4.4	2.8	0.9	0.5	0.2	0.2	29.8 (5365.1)	N.D.
4-OH-ATX-G[a]	–	–	–	–	–	–	56.0 (10,092.6)	–
N-des-ATX	16.3	6.5	N.D.	N.D.	N.D.	N.D.	0.009 (1.6)	N.D.
Subject 2								
ATX	268.6	100.4	26.0	9.7	0.1	0.1	0.2 (63.4)	2.7
4-OH-ATX	5.8	4.0	1.4	0.5	0.2	0.1	14.6 (5123.0)	N.D.
4-OH-ATX-G[a]	–	–	–	–	–	–	60.9 (21,342.3)	–
N-des-ATX	2.8	1.3	N.D.	N.D.	N.D.	N.D.	0.009 (3.1)	N.D.

N.D. not detected.
[a] 4-OH-ATX-G measured as difference between total amount of urinary 4-OH-ATX and free metabolite (this latter one measured without urine hydrolization).

possible to detect eventual minimal amounts present in oral fluid, at the sensitivity of the present assay. On one hand, these preliminary results evidence for the first time the passage of ATX and its hydroxyl-metabolite from plasma to oral fluid; on the other advocate for extended pharmacokinetic studies to clarify the potential of oral fluid for non invasive drug monitoring in paediatric patients.

Following oral administration of ATX in two subjects, around 50% of the administered dose was excreted in the urine in the first 6 h post-administration, primarily as 4-OH-ATX-G (25.2 and 35.6%, respectively) and 4-OH-ATX (13.4 and 8.5%, respectively), only 0.004 and 0.005%, as N-des-ATX respectively, and around 0.1% was excreted as parent compound.

Only the parent drug was found in sweat in a concentration range of few ng (around 3 ng) per sweat patch. This is in accordance with what we already reported for amphetamine-type stimulants such as MDMA and methylphenidate [29,31]. Taking into account these first observations and considering the total quantity of secreted sweat per body surface area, it can be postulated a non-negligible excretion of ATX in sweat, which can be of some use for forensic purposes.

4. Conclusion

The LC–MS/MS method reported allows the determination of ATX and its metabolites (4-OH-ATX and N-des-ATX) in conventional and non-conventional biological matrices. The rapid and simple extraction of analytes from different biological matrices, the minimum handling and time required, the high assay sensitivity and unequivocal detection render this method feasible for routine therapeutic monitoring of ATX and its metabolite in pharmaco-toxicological and clinical laboratories. For the first time, the possibility of drug monitoring in non-invasive biological matrices such as oral fluid and sweat was investigated, which has to be confirmed in a larger number of samples and in a complete kinetic study of different subjects treated with the drug.

Acknowledgments

The study was partly supported by grant of “Fondo per le Politiche Giovanili – Anno 2010 – Dipartimento della Gioventù”.

Dr. Oscar Garcia-Algar thanks Red SAMID, Instituto Carlos III (ISCIII), Madrid, Spain.

References

[1] D.P. Cantwell, Attention deficit disorder: a review of the past 10 years, J. Am. Acad. Child Adolesc. Psychiatry 35 (1996) 978–987.
[2] M. Dulcan, Practice parameters for the assessment and treatment of children, adolescents, and adults with attention-deficit/hyperactivity disorder, American Academy of Child and Adolescent Psychiatry, J. Am. Acad. Child Adolesc. Psychiatry 36 (1997) 85S–121S.
[3] J.M. Swanson, J.A. Sergeant, E. Taylor, E.J. Sonuga-Barke, P.S. Jensen, D.P. Cantwell, Attention-deficit hyperactivity disorder and hyperkinetic disorder, Lancet 351 (1998) 429–433.
[4] S.V. Faraone, J. Sergeant, C. Gillberg, J. Biederman, The worldwide prevalence of ADHD: is it an American condition? World Psychiatry 2 (2003) 104–113.
[5] G. Polanczyk, M.S. de Lima, B.L. Horta, J. Biederman, L.A. Rohde, The worldwide prevalence of ADHD: a systematic review and metaregression analysis, Am. J. Psychiatry 164 (2007) 942–948.
[6] R.G. Klein, S. Mannuzza, Long-term outcome of hyperactive children: a review, J. Am. Acad. Child Adolesc. Psychiatry 30 (1991) 383–387.
[7] M.K. Dulcan, R.S. Benson, AACAP Official Action. Summary of the practice parameters for the assessment and treatment of children, adolescents, and adults with ADHD, J. Am. Acad. Child Adolesc. Psychiatry 36 (1997) 1311–1317.
[8] L.S. Goldman, M. Genel, R.J. Bezman, P.J. Slanetz, Diagnosis and treatment of attention-deficit/hyperactivity disorder in children and adolescents. Council on Scientific Affairs, American Medical Association, JAMA 279 (1998) 1100–1107.
[9] J. Elia, P.J. Ambrosini, J.L. Rapoport, Treatment of attention-deficit-hyperactivity disorder, N. Engl. J. Med. 340 (1999) 780–788.
[10] F.A. Baughman, Treatment of attention-deficit/hyperactivity disorder, JAMA 281 (1999) 1490.
[11] D. Michelson, D. Faries, J. Wernicke, D. Kelsey, K. Kendrick, F.R. Sallee, T. Spencer, Atomoxetine in the treatment of children and adolescents with attention-deficit/hyperactivity disorder: a randomized, placebo-controlled, dose–response study, Pediatrics 108 (2001) E83.
[12] J.W. Witcher, A. Long, B. Smith, J.M. Sauer, J. Heilgenstein, T. Wilens, T. Spencer, J. Biederman, Atomoxetine pharmacokinetics in children and adolescents with attention deficit hyperactivity disorder, J. Child Adolesc. Psychopharmacol. 13 (2003) 53–63.
[13] D.T. Wong, P.G. Threlkeld, K.L. Best, F.P. Bymaster, A new inhibitor of norepinephrine uptake devoid of affinity for receptors in rat brain, J. Pharmacol. Exp. Ther. 222 (1982) 61–65.
[14] D.R. Gehlert, S.L. Gackenheimer, D.W. Robertson, Localization of rat brain binding sites for [3H]tomoxetine, an enantiomerically pure ligand for norepinephrine reuptake sites, Neurosci. Lett. 157 (1993) 203–206.
[15] B.J. Ring, J.S. Gillespie, J.A. Eckstein, S.A. Wrighton, Identification of the human cytochromes P450 responsible for atomoxetine metabolism, Drug Metab. Dispos. 30 (2002) 319–323.
[16] J.M. Sauer, G.D. Ponsler, E.L. Mattiuz, A.J. Long, J.W. Witcher, H.R. Thomasson, K.A. Desante, Disposition and metabolic fate of atomoxetine hydrochloride: the role of CYP2D6 in human disposition and metabolism, Drug Metab. Dispos. 31 (2003) 98–107.
[17] N.A. Farid, R.F. Bergstrom, E.A. Ziege, C.J. Parli, L. Lemberger, Single-dose and steady-state pharmacokinetics of tomoxetine in normal subjects, J. Clin. Pharmacol. 25 (1985) 296–301.
[18] D. Michelson, H.A. Read, D.D. Ruff, J. Witcher, S. Zhang, J. McCracken, CYP2D6 and clinical response to atomoxetine in children and adolescents with ADHD, J. Am. Acad. Child Adolesc. Psychiatry 46 (2007) 242–251.
[19] J.H. Mullen, R.L. Shugert, G.D. Ponsler, Q. Li, B. Sundaram, H.L. Coales, J.E. Yakupkovic, R.M. Lelacheur, W.J. Wheeler, F.J. Belas, J.M. Sauer, Simultaneous quantification of atomoxetine as well as its primary oxidative and O-glucuronide metabolites in human plasma and urine using liquid chromatography tandem mass spectrometry (LC/MS/MS), J. Pharm. Biomed. Anal. 38 (2005) 720–733.
[20] E. Choong, S. Rudaz, A. Kottelat, D. Guillarme, J.L. Veuthey, C.B. Eap, Therapeutic drug monitoring of seven psychotropic drugs and four metabolites in human plasma by HPLC–MS, J. Pharm. Biomed. Anal. 50 (2009) 1000–1008.
[21] H.J. Zhu, J.S. Wang, J.L. Donovan, C.L. DeVane, B.B. Gibson, J.S. Markowitz, Sensitive quantification of atomoxetine in human plasma by HPLC with fluorescence detection using 4-(4,5-diphenyl-1H-imidazole-2-yl) benzoyl chloride derivatization, J. Chromatogr. B: Analyt. Technol. Biomed. Life Sci. 846 (2007) 351–354.
[22] C. Patel, M. Patel, S. Rani, M. Nivsarkar, H. Padh, A new high performance liquid chromatographic method for quantification of atomoxetine in human plasma and its application for pharmacokinetic study, J. Chromatogr. B: Analyt. Technol. Biomed. Life Sci. 850 (2007) 356–360.
[23] W. Guo, W. Li, G. Guo, J. Zhang, B. Zhou B., Y. Zhai, C. Wang, Determination of atomoxetine in human plasma by a high performance liquid chromatographic method with ultraviolet detection using liquid–liquid extraction, J. Chromatogr. B: Analyt. Technol. Biomed. Life Sci. B 854 (2007) 128–134.
[24] E. Papaseit, E. Marchei, C. Mortali, G. Aznar, O. Garcia-Algar, M. Farrè, R. Pacifici, S. Pichini, Development and validation of a liquid chromatography–tandem mass spectrometry assay for hair analysis of atomoxetine and its metabolites: application in clinical practice, Forensic Sci. Int. (2011), Oct 22 [Epub ahead of print].
[25] Guidance for Industry, Bioanalytical of Health and Human Services, Food and Drug Administration, May 2001. Available from: http://www.fda.gov/cder/guidance/4252fnl.htm.
[26] ICH-Topic Q2B: Validation of Analytical Procedures: Methodology, International Conference on Harmonization of Technical Requirements for Registration of Pharmaceuticals for Human Use, Geneva, 1996.
[27] E. Marchei, D. Escuder, C.R. Pallas, O. Garcia-Algar, A. Gómez, B. Friguls, M. Pellegrini, S. Pichini, Simultaneous analysis of frequently used licit and illicit psychoactive drugs in breast milk by liquid chromatography tandem mass spectrometry, J. Pharm. Biomed. Anal. 55 (2011) 309–316.
[28] M. Navarro, S. Pichini, M. Farré, J. Ortuno, P.N. Roset, J. Segura, R. de la Torre, Usefulness of saliva for measurement of 3,4-methylenedioxymethamphetamine and its metabolites: correlation with plasma drug concentrations and effect of salivary pH, Clin. Chem. 47 (2001) 1788–1795.
[29] E. Marchei, M. Farré, R. Pardo, O. Garcia-Algar, M. Pellegrini, R. Pacifici, S. Pichini, Correlation between methylphenidate and ritalinic acid concentrations in oral fluid and plasma, Clin. Chem. 56 (2010) 585–592.
[30] J.M. Sauer, B.J. Ring, J.W. Witcher, Clinical pharmacokinetics of atomoxetine, Clin. Pharmacokinet. 44 (2005) 571–590.
[31] S. Pichini, M. Navarro, R. Pacifici, P. Zuccaro, J. Ortuno, M. Farré, P.N. Roset, J. Segura, R. de la Torre, Usefulness of sweat testing for the detection of MDMA after a single-dose administration, J. Anal. Toxicol. 27 (2003) 294–303.

Journal of Pharmaceutical and Biomedical Analysis 60 (2012) 32–43

Contents lists available at SciVerse ScienceDirect

Journal of Pharmaceutical and Biomedical Analysis

journal homepage: www.elsevier.com/locate/jpba

Intrarenal metabolomics reveals the association of local organic toxins with the progression of diabetic kidney disease

Tie Zhao[a,b], Haojun Zhang[a], Tingting Zhao[a], Xianglin Zhang[b], Jin Lu[b], Tingting Yin[c], Qionglin Liang[d], Yiming Wang[d], Guoan Luo[d], Huiyao Lan[e], Ping Li[a,*]

[a] Department of Pharmacology, Institute of Clinical Medical Sciences, China-Japan Friendship Hospital, Beijing, China
[b] Pharmacy Department, China-Japan Friendship Hospital, Beijing, China
[c] College of Pharmacy, Shenyang Pharmaceutical University, Shenyang, China
[d] Key Laboratory of Bioorganic Phosphorus Chemistry & Chemical Biology (Ministry of Education), Department of Chemistry, Tsinghua University, China
[e] Department of Medicine and Therapeutics, and Li Ka Shing Institute of Health Sciences, the Chinese University of Hong Kong, Hong Kong SAR, China

ARTICLE INFO

Article history:
Received 20 June 2011
Received in revised form 7 November 2011
Accepted 8 November 2011
Available online 17 November 2011

Keywords:
Diabetic kidney disease
Metabolomic
Organic toxins
Uremic toxin
Fosinopril

ABSTRACT

The pathological development of diabetic kidney disease (DKD) might involve metabolic perturbations in kidney tissue. The present study was designed to detect the systematic alterations of renal cortex metabolites thereby exploring the related mechanisms of DKD development and fosinopril treatment. Based on combined gas chromatography/time-of-flight mass spectrometry (GC–TOF MS) and liquid chromatography/time-of-flight mass spectrometry (UPLC–TOF MS) data acquiring platform, we have performed a metabolomic analysis of perfused renal cortex samples from the diabetic rats induced by streptozocin and treated with or without fosinopril, a pharmacological inhibitor of angiotensin II converting enzyme (ACEI). We identified a number of abnormal metabolites in the diabetic kidney, including groups of amino acids, carbohydrates, polyols, lyso-phospholipids, glucuronides and other unidentified metabolites. Of them, an increase in intrarenal organic toxins including uremic toxins, glucuronides and glucotocixity-associated metabolites are highly correlated with diabetic kidney injury including 24 h urinary protein levels and tubulointerstitial injury index. Treatment with fosinopril significantly attenuated diabetic kidney injury, and simultaneously blocked the intrarenal accumulation of these organic toxins, especially hippurate and glucuronides. These results indicate that intrarenal accumulation of organic toxins may be significant for the development of DKD and the related mechanisms deserve to be further investigated.

1. Introduction

Diabetic kidney disease (DKD) is a common microvascular complication of diabetic mellitus and one of the major causes of end-stage renal disease worldwide [1]. It occurs in up to one-third of patients with type1 diabetes and approximately 25% of patients with type2 diabetes [2]. The pathogenesis of DKD is complex with systemic metabolic abnormalities [3]. Although hyperglycemia is a well-known clinical prerequisite for DKD and many hypotheses for DKD etiology had been proposed in recent years [4], it remains unclear for the profound mechanisms of the development and progression of DKD.

Angiotensin converting enzyme inhibitors (ACEIs) have become a mainstay of adjunctive therapy for the prevention and amelioration of DKD [5]. Many clinical trials and animal studies have demonstrated that ACEIs are of specific benefit in reducing proteinuria [6] and preserving renal function. Although their renoprotective effects is considered to be the result of blood pressure control, much evidence recently have suggested that other mechanisms independent of lowering blood pressure might be involved [7,8].

Applications of metabolomics, characterized by holistic metabolic fingerprints or profiling analysis, in the research field of metabolic diseases including DM has aroused wide world concerns in the past few years [9–14]. However, most of them are based on blood/urinary samples. As far as DKD is concerned, more specific and explainable results will be achieved by metabolomics on the basis of renal tissue *vs* blood/urinary, since DKD is a secondary disease with unambiguous kidney damage. Accordingly, we utilized here an integrated gas chromatography/time-of-flight mass spectrometry (GC–TOF MS) and ultra performance liquid chromatography/time-of-flight mass spectrometry (UPLC–TOF MS) metabolomic platform to identify metabolic signatures in renal cortex of rats associated with pathological development and

* Corresponding author. Tel.: +86 1064227163; fax: +86 1084206084.
E-mail address: lp8675@yahoo.com.cn (P. Li).

0731-7085/$ – see front matter © 2011 Elsevier B.V. All rights reserved.
doi:10.1016/j.jpba.2011.11.010

fosinopril (an ACEI) intervention of DKD induced by streptozocin (STZ), which may provide new clues for the etiology of DKD as well as the pharmacological mechanisms of ACEIs.

2. Materials and methods

2.1. Animals experimental

Forty eight male Wistar rats weighing 200 ± 20 g, purchased from Beijing HFK Bio-Technology Co. Ltd. (Beijing, Certificate No. SCXK 2002-0010), were randomly divided into control group (n = 16) and diabetic group (n = 32). To accelerate the development of diabetic kidney disease, rats in diabetic group underwent a right uninephrectomy. One week after recovery, diabetes was induced by a single intraperitoneal injection of streptozocin [(STZ), Sigma, USA] at a dose of 40 mg/kg diluted in citrate buffer (0.1 mol/L, pH 4.0). Seventy-two hours after STZ injection, rats for blood glucose over 16.7 mmol/L were confirmed to be in diabetic state. Diabetic rats were then randomly assigned to model group (treatment with vehicle) and fosinopril treatment group. Rats in control group received sham operation and equal volume of citrate buffer one week later. Rats in fosinopril treatment group and rats in the other two groups were administrated with fosinopril or vehicle respectively by gavage daily for 20 weeks. The dose of fosinopril is 1.60 mg/kg. Four rats in model group and 1 rat in fosinopril group died of organ failure during the study. The final result of grouping was as follows: control group (n = 16), model group (n = 12) and fosinopril treatment (n = 15). At the end of the study, venous blood was collected from eye socket of each rat, and left kidney was harvested after *in situ* cardio-perfusion. Then, the removed kidney were weighed and cut into 2 pieces for the following histological and metabolomic study. During the experimental period, all the animals were kept in cages at a temperature of 20–25 °C, humidity of 65–69%, and were submitted to a 12-h light/dark cycle with free access to food and tap water. This study was approved by the Ethics Committee of China-Japan Friendship Institute of Clinical Medical science and performed in accordance with Guiding Principles for the Care and Use of Laboratory Animals.

2.2. Determination of body weight, blood sample and urinary protein

At the end of the experiment, body weight of rats was measured, and blood glucose values were determined by One-Touch Ultra glucometer (Lifescan, Milpitas, CA). The kidney weight index was calculated by dividing the kidney weight by the body weight. Rats were housed individually in metabolic cages (Fengshi, China) for 24-h urinary collection, and 24 h urinary protein was assessed by the Bradford method. The acquired venous blood was centrifuged at 3000 r/min for 15 min. Serum was separated and total cholesterol, triglycerides, blood urea nitrogen, serum creatinine, total protein, and albumin were measured using a CD-1600CS hematology analyzer (Abbott Labs, USA).

2.3. Renal histology

One piece of kidney was fixed in neutral buffered formalin (10%), embedded in paraffin, sectioned at 3 μm, and stained with periodic acid-Schiff (PAS). Twenty glomeruli were randomly selected from each rat, and the extent of mesangial extracellular matrix was identified by PAS-positive material in the mesangium. Glomeruli from the outer and middle thirds of the renal cortex were selected for area measurements, done with the aid of Image-Pro Plus 6.0 (Media Cybernetics, Silver Spring, MD). Care was taken to exclude juxtamedullary glomeruli [15]. Then, percentage of mesangial matrix occupying the selected glomerular tuft was calculated. Tubulointerstitial damage was assessed on PAS-stained paraffin sections at a magnification of 100× using a similar scoring system (0–4) as described previously in detail [16].

2.4. Metabolomic analysis

Renal cortex was isolated from another piece of removed kidney immediately and stored for metabolomic study. Renal cortex metabolomic analyses were obtained using combined GC–TOF MS and UPLC–TOF MS platform with identical method of sample extraction: fresh renal cortex tissue (60 mg) were weighed and underwent enzyme deactivation in liquid nitrogen before storing frozen at −80 °C until use, when each 800 μL methanol and 20 μL internal standard mixture (L-2-chlorophenylalanine and heptadecanoic acid at concentration level 0.5 mg/mL) was added into sample tube followed by homogenizing with a T10 basic homogenizer (IKA, Staufen, Germany) for 30 s twice in ice bath. The resultant homogenates were stored at 4 °C overnight and centrifuged at 12,000 rpm for 10 min at 4 °C, and then the supernatant were divided equally into two parts (each 300 μL) which were used to UPLC–TOF MS and GC–TOF MS analysis, respectively.

2.5. GC–TOF MS analysis

One part of 300 μL supernatant was transferred to an insert in a GC sampling vial and dried under nitrogen stream. After that, TMS derivatization was carried out. The derivatization procedure was conducted with minor modifications to our previous serum metabolomic study report [17]. Briefly, 50 μL methoxyamine (15 mg/mL in pyridine) was added to dry sample vials and vortexed for 30 s. Methoxymation was carried out at 30 °C for 16 h. After adding another 50 μL BSTFA (containing 1% TMCS) and vortexing for 30 s, silylation was carried out at 70 °C for 1 h. Each 1-μL derivatized sample was injected into an Agilent 6890 N gas chromatograph in splitless mode with time-of-flight mass spectrometry (Pegasus HT, Leco Co., CA, USA). Separation was achieved on a DB-5ms capillary column (30 m × 250 μm i.d., 0.25-μm film thickness; Agilent J&W Scientific, Folsom, CA, USA) using helium as the carrier gas, at a constant flow rate of 1.0 mL/min. The injector temperature was set at 270 °C. The GC oven temperature was set at 80 °C for the first two minutes, then programmed to ramp up 10 °C per minute to 180 °C, 5 °C per minute to 240 °C, 25 °C per minute to 290 °C, and finally maintained at 290 °C for nine minutes. Transfer line temperature and ion source temperature were set at 260 °C and 200 °C, respectively. The mass spectra were obtained with electron impact ionization (70 eV) at full scan mode (m/z 30–600).

2.6. UPLC–TOF MS analysis

Another part of 300 μL supernatant was transferred to a sampling vial pending for UPLC–TOF MS analysis. An Acquity Ultra Performance Liquid Chromatography system (Waters, USA) equipped with a 10 cm × 2.1 mm, 1.7 μm BEH C18 column (Waters, USA) was used in this study. The column, constant at 50 °C, was eluted with a linear gradient of 5–50% B over 0–3 min, 50–70% B over 3–10 min, 70–100% B over 10–15 min, the composition was held at 100% B for 5 min, where A = water with 0.1% ammonium formate and B = acetonitrile. The flow rate was 0.4 mL/min. Injection volume was 2 μL for positive ion mode (ES+) and 4 μl for negative ion mode (ES−), respectively. Samples were run Control-Model-Fosinopril alternately. All samples were kept at 4 °C during the analysis.

The mass spectrometric data was collected using a Micromass LCT Premier XE (Waters MS Technologies, Manchester, UK). The scan range was from 50 to 600 m/z with a scan time of 0.2 s and

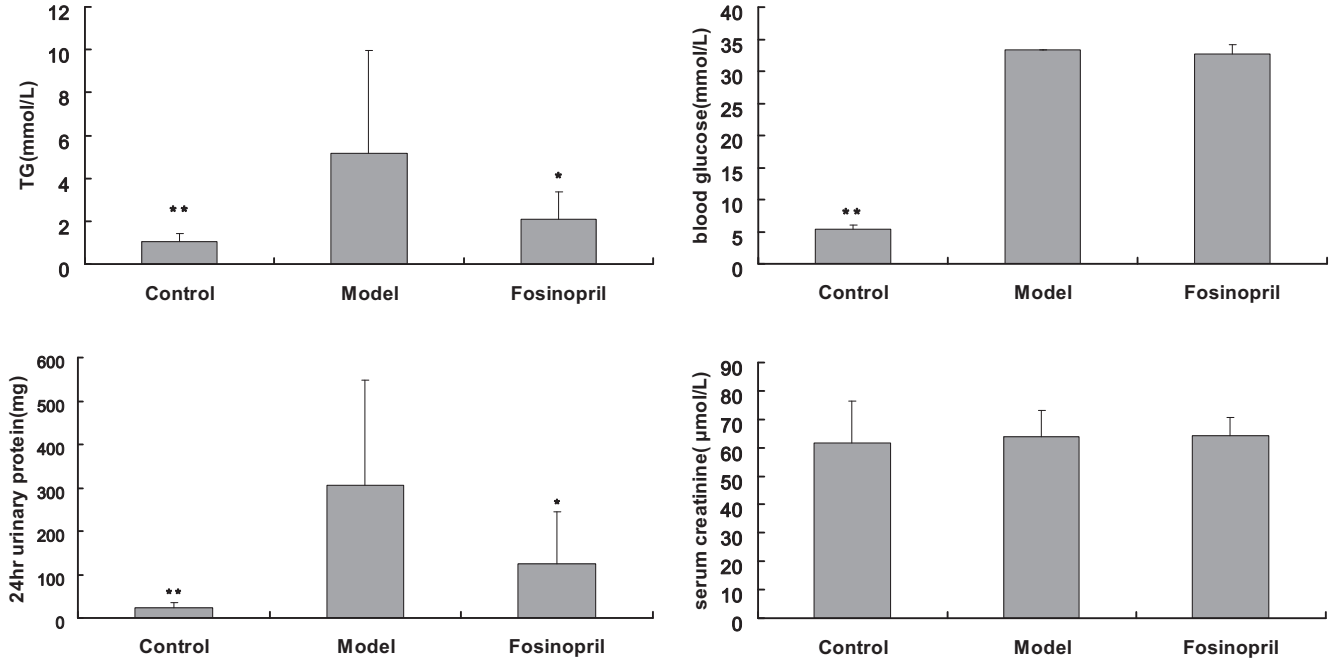

Fig. 1. The levels of individual biochemical index in DKD model and fosinopril intervention group. In the model group compared with the control group, the levels of blood glucose, triglycerides and 24 h urinary protein were increased. After fosinopril treatment, 24 h urinary protein and triglycerides were attenuated, but fosinopril have no effects on blood glucose. There is no difference in the serum creatinine among three groups. Data are shown as the mean ± SD. $^{*}p < 0.05$, $^{**}p < 0.01$, *vs* model group.

interscan delay of 0.05 s over a 28 min analysis time. The source temperature was set to 120 °C with a cone gas flow of 50 L/h. The desolvation gas flow was set to 600 L/h at a temperature of 350 °C. The capillary and cone voltage were set at 2.3 kV the 40 V, respectively. The mass spectrometry was operated in W optics mode with 12,000 resolution using dynamic range extension (DRE). Leucine enkephalin was used as the lock mass at a concentration of 2 μg/mL and flow rate of 20 μL/min, with a lockspray frequency of 10 s. MassLynx software (Waters) was used for system controlling and data acquisition.

2.7. Data process and statistical analyses

The acquired MS files from GC–TOF MS analysis were exported in NetCDF format by ChromaTOF software (v3.30, Leco Co., CA, USA). CDF files were extracted using custom scripts (revised

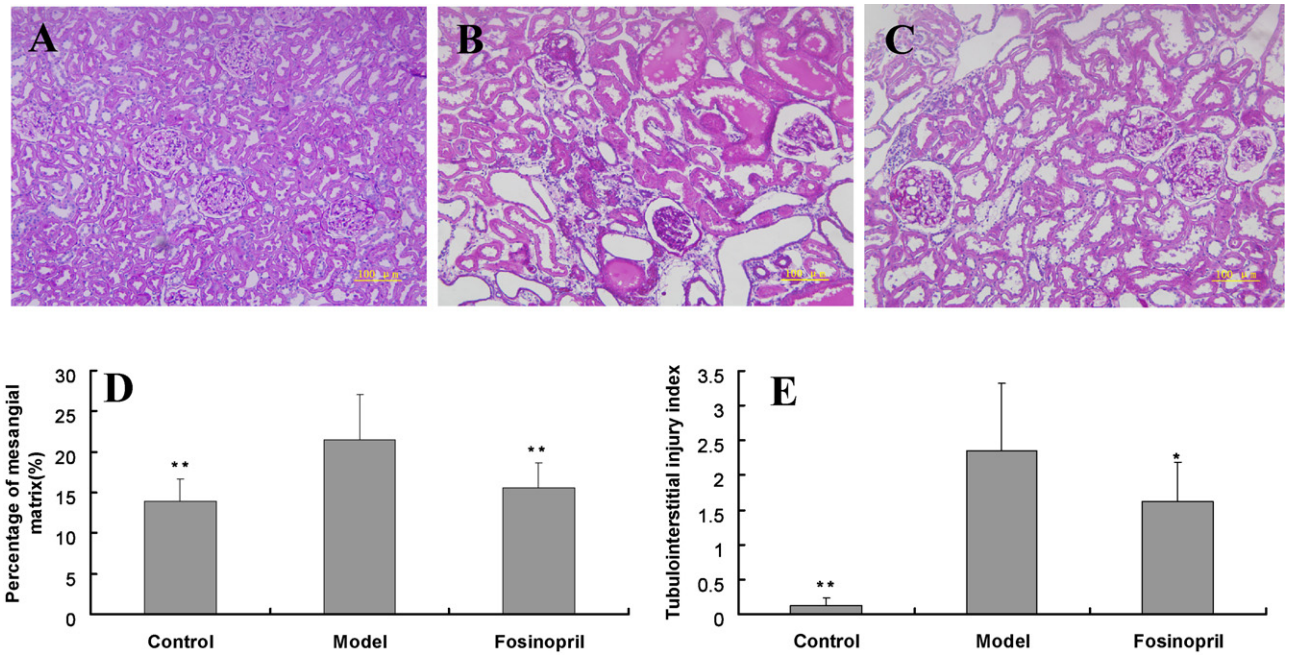

Fig. 2. Glomerular and interstitial changes in PAS-stained sections. The glomerular hypertrophy, mesangial matrix expansion and tubulointersitial injury were shown in model (B) and fosinopril treatment (C) groups except control group (A), and these pathological changes were improved in the fosinopril group compared with the model group (200×), D and E represent semi-quantitive analyses of mesangial matrix and interstitial injury in three groups respectively. Data are shown as the mean ± SD. $^{*}p < 0.05$, $^{**}p < 0.01$, *vs* model group.

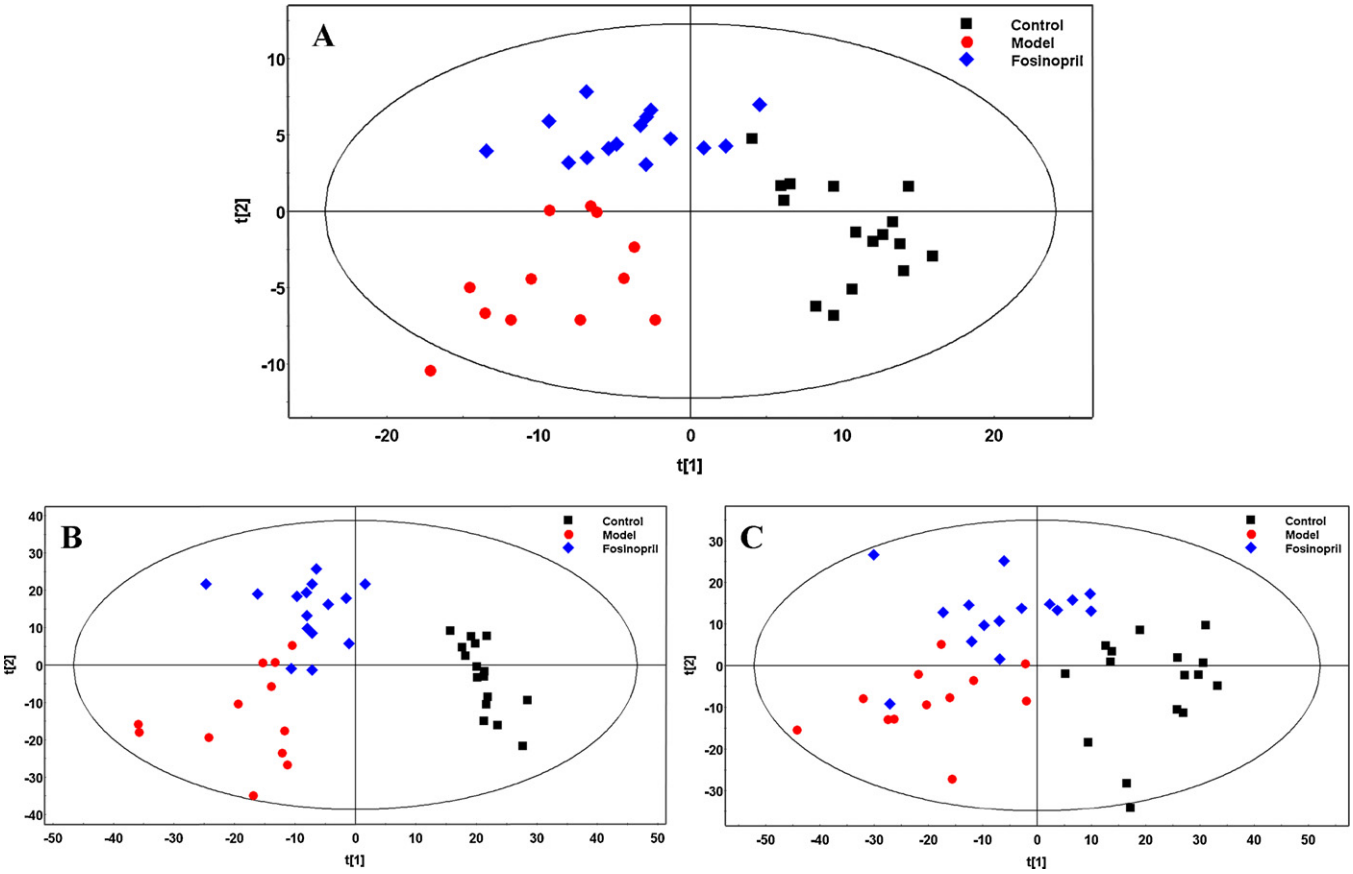

Fig. 3. Overview of global metabolic alterations in model and fosinpril treatment group by PLSDA model of data from metabolic fingerprints analysis (A) PLSDA score plot of data from GC–TOF MS based metabolomic analysis of all groups; (B) PLSDA score plot of data from UPLC–TOF MS (ESI-) based metabolomic analysis of all groups; (C) PLSDA scores plot of data from UPLC–TOF MS (ESI+) based metabolomic analysis of all groups.

Matlab toolbox hierarchical multivariate curve resolution (H-MCR), developed by Par Jonsson, et al. [18,19]) in the MATLAB 7.0 (The MathWorks, Inc, USA) for data pretreatment procedures such as baseline correction, de-noising, smoothing, alignment, time-window splitting, and multivariate curve resolution (based on multivariate curve resolution algorithm). The resulting three dimensional data set includes sample information, peak retention time and peak intensities. Internal standards and any known artificial peaks, such as peaks caused by noise, column bleed and BSTFA derivatization procedure, were removed from the data set.

The UPLC–TOF MS ES+ and ES− raw data were analyzed by the MarkerLynx Applications Manager version 4.1 (Waters, Manchester, U.K.). A list of the ion intensities of each peak detected was generated, using retention time (RT) and the m/z data pairs as the identifier for each ion. The resulting three-dimensional matrix contained arbitrarily assigned peak indices (retention time-m/z pairs), sample names (observations), and ion intensity information (variables). To obtain consistent differential variables, the resulting matrix was further reduced by removing any peaks with missing value (ion intensity = 0) in more than 30% of the samples from both model and control groups. The ion peaks generated by the internal standard were also removed.

Independent T test was used to compare differences with $p < 0.01$ for differential variables between control and model groups and $p < 0.05$ between model and fosinopril treatment group, respectively. The corresponding fold change was calculated for each variable to show how they varied between control and the model/fosinopril groups. Pearson correlation analyses between metabolites and biochemical/pathological parameters levels were performed by SPSS 15.0 (SPSS Inc., Chicago).

Compound identification in GC–TOF MS analysis was performed by comparing the mass fragments with NIST 08 standard mass spectral databases in NIST MS search 2.0 (NIST, Gaithersburg, MD) software with a similarity of more than 70% and finally verified by available reference compounds. Identification of differential metabolites from UPLC–TOF MS was performed comprehensively using accurate molecular weight, ES+ and ES− mode cross-assist analysis, source collision induced dissociation (sCID) technique, isotopic pattern comparison and free online database (HMDB, pubchem, metlin and lipidmaps). Three uremic toxin molecules (hippurate, indoxyl sulfate and 4-pyridoxic acid) were further validated by commercially available standard materials.

3. Results and discussion

3.1. Animal model of diabetic kidney disease and therapeutic effects of ACEI on kidney injury

As shown in Figs. 1 and 2, after the administration of STZ and right nephrotectomy, all rats developed hyperglycemia and diabetic kidney injury including heavy proteinuria, mesangial matrix expansion, glomerulosclerosis, protein cast, tubular dilation or atrophy, and infiltration of inflammatory cells, whereas an increase in blood urea nitrogen and serum creatinine did not reach to statistically significant levels. Meanwhile, diabetic rats treated with fosinopril displayed a significant inhibition of diabetic kidney injury including 59.0% lower proteinuria, 27.5% reduction in mesangial matrix expansion, 31.3% lesser tubulointerstitial injury, although

Table 1
Identified differential metabolites based on GCtofMS metabolic fingerprint analysis.

Class	Rt/min[a]	Metabolites	*p*	Fold(M/C)[b]
Amino Acids	16.10	Hippurate	0.001076	11.79
	15.67	L-Ornithine	0.000782	−1.69
	7.09	L-Alpha-aminobutyric acid	5.62E−05	−2.06
	10.65	Alanine	0.003814	−1.41
	11.88	4-Hydroxy-L-proline	0.00476	−1.58
	12.82	Hypotaurinary	1.73E−06	−2.45
	11.80	D-Pyroglutamic acid	0.000155	−1.44
	11.81	L-Aspartic acid	0.000221	−1.40
	11.81	L-Methionine	0.002161	−1.33
	17.15	L-Lysine	0.008047	−1.45
	9.72	Serine	0.002659	−1.44
	10.06	Threonine	5.14E−05	−1.61
Other N-compounds	8.25	Urea	4.87E−05	3.49
	11.38	Nicotinamide	0.000147	−1.22
	11.97	Allantoin	5.68E−05	3.72
	19.66	Uric acid	0.000124	2.50
Carbohydrates	16.50	D-Fructose	0.001197	3.14
	19.31	N-Acetyl glucosamine	0.002639	1.46
	23.90	Maltose	0.000154	498.56
	16.57	Mannose	1.19E−05	7.43
	17.00	Glucose	0.000614	19.96
Di(Multi)carboxylic Acids	12.48	2-Hydroxyglutaric acid	7.54E−07	3.22
	6.50	Oxalic acid	0.001714	−1.75
	15.67	Citric acid	0.000855	2.14
	9.13	Succinic acid	6.35E−05	4.38
	9.63	Fumaric acid	1.87E−06	1.75
	11.40	Malic acid	1.51E−08	2.63
Fatty acids	21.17	Elaidic acid	1.45E−05	−2.08
	22.07	Arachidonic acid	0.003321	−1.28
Hydroxy Acids	8.03	4-Hydroxybutyric acid	5.42E−05	2.05
	5.69	2-Hydroxyacetic acid(Glycolic acid)	0.000775	−1.31
	9.47	2,3-Dihydroxybutanoic acid (4-Deoxythreonic acid)	1.21E−05	−3.08
	12.05	Threonic acid	0.000985	2.04
	5.46	Lactic acid	1.74E−06	2.75
Inorganic acid	8.54	Phosphate	0.002672	−1.16
Polyols	11.61	L-Threitol	0.000461	4.55
	14.29	L-(−)-Arabitol	0.000246	2.41
	17.28	D-Sorbitol	8.13E−06	16.75
	19.49	Myo-inositol	0.009698	−1.44

[a] The retention time (min) on GC/tofMS or UPLC/tofMS.
[b] The ratio of mean normalized peak intensity between model and control groups, where '+'and '−' represent increase and decrease in model group, respectively.

treatment with fosinopril did not alter levels of blood glucose and serum BUN and creatinine (Figs. 1 and 2).

3.2. Identification of metabolic alterations in renal cortex of diabetic rats with or without fosinopril treatment

In GC–TOF MS based metabolic fingerprint analyses, more than 600 variables with paired retention time and *m*/*z* were detected, among which about 120 metabolites were identified. To visualize the systemically metabolic alterations among different groups, the partial least square-discrimant analysis (PLSDA) model of dataset from all samples was applied in our study. As shown in the score plot of the established PLSDA model (Fig. 3A), the diabetic and control animals were completely isolated in first dimension by cut off value of 0, indicating that there are significant alterations in local metabolic status of rats with DKD. Fosinopril treatment group exhibited a certain degree of normalization towards control group, suggesting that diabetes associated metabolic disorders (based on GC–TOF MS analysis) could be improved by fosinopril treatment. As compared with the result of PLSDA model established using GC–TOF MS data, similar clustering status among three groups were observed in the score plots of PLSDA model from data acquired by electrospray (ES)+ and ES− mode in UPLC–TOF MS (Fig. 3B and C), which indicated that fosinopril treatment has similar recovery effect on metabolic fingerprint based on UPLC–TOF MS.

A number of differential metabolites between control and model groups were identified on the basis of GC–TOF MS and UPLC–TOF MS metabolomic analysis. They were classified according to their chemical structures and summarized in Tables 1 and 2, respectively. Exceptionally, hippurate and N-acetyl glucosamine were classified as amino acid and carbohydrate, respectively, according to the basic structure of their super class conjugates of basic structure. Taken together, lyso-glycerophosphocholines (lyso-GPCs), lyso-glycerophosphoethanolamines (lyso-GPEs), lyso-glycerophosphoinositols (lyso-GPIs) and almost all amino acids were significantly downregulated. In contrast, di(Multi)carboxylic acids, polyols, carbohydrates, acyl carnitines and glucuronides were significantly elevated. Limited by capability of our analytical platform, several isomers cannot be distinguished. In addition, it should be noticed that the baseline intensity (background) recorded by UPLC–TOF MS and GC–TOF MS are not comparable due to their different work principles. Since the fold change ratio of a metabolite was calculated from its mean relative intensity of each group recorded by individual analytical instrument, it is not surprised that the result of fold change of an identical metabolite detected by different instrument appeared to be discrepant to some degree. Besides glucose, lactic acid, N-acetyl glucosamine and other

Table 2
Identified differential metabolites based on LCtofMS metabolic fingerprint analyses.

Class	RT/min[a]	Quasi-molecular ion (m/z)[b]		Error (ppm)	Metabolites	Assignment based on	p	Fold (M/C)
		Observed	Theoretical					
Amino acids	0.60	124.0033	124.006839	−28.5	Taurine	+/−[c],AM[d],IP[e]	1.77E−05	−1.26
	1.25	178.0493	178.050418	−6.3	Hippurate	AM,IP,SM[f]	9.67E−07	4.34
Hydroxy acids	0.60	89.0227	89.023868	−13.1	Lactic acid/Hydroxypropionic acid/Glyceraldehyde	AM,IP	3.64E−07	1.99
Indole Derivatives	1.65	212.0011	212.001758	−3.1	Indoxyl sulfate	AM,IP,SM	0.000537	6.11
Pyridoxals	1.17	182.0454	182.045337	0.3	4-Pyridoxic acid	AM,IP,SM	1.07E−05	4.22
Carbohydrates	0.61	179.0557	179.05556	0.8	D-Glucose/D-Galactose/D-Mannose/D-Fructose/ Myoinositol/3-Deoxyarabinohexonic acid	AM,IP	4.6E−05	5.32
Fatty acids	10.99	279.2308	279.232409	−5.8	Linoleic acid/Bovinic acid/9E,11E-Octadecadienoic acid/10E,12Z-Octadecadienoic acid/Linoelaidic acid	AM,IP	0.008744	1.30
	13.04	307.265	307.26369	4.3	11,14-Eicosadienoic acid	AM,IP	0.003164	1.54
	11.86	305.2492	305.248065	3.7	8,11,14-Eicosatrienoic acid/5,8,11-Eicosatrienoic acid	AM,IP	0.005901	1.52
	11.30	329.2489	329.248065	2.5	Docosapentaenoic acid (22n-6)/ Clupanodonic acid/4,7,10,13,16-Docosapentaenoic acid	AM,IP	0.00818	1.41
	12.14	355.2645	355.26369	2.3	Tetracosahexaenoic acid	AM,IP	0.006771	1.67
Glucuronides	1.21	336.0722	336.071948	0.7	2,8-Dihydroxyquinoline-beta-D-glucuronide/ 3-Indole carboxylic acid glucuronide	+/−, AM,IP	0.001676	19.68
	1.31	340.107	340.103253	11.0	6-Hydroxy-5-methoxyindole glucuronide/ 5-Hydroxy-6-methoxyindole glucuronide	AM,IP	0.000389	9.91
	1.86	297.0974	297.09743	−0.1	2-Phenylethanol glucuronide	AM,IP	0.000142	27.04
	13.00	465.3038	465.303851	−0.1	Cholesterol sulfate	AM,IP	1.41E−05	−2.22
Steroids & Bile acids	3.43	407.2802	407.279742	1.1	Cholic acid/other isomers	+/−, AM,IP	9.38E−06	4.65
	2.96	464.3012	464.301227	−0.1	Glycocholic acid	AM,IP	0.005164	7.28
Lyso-GPE	7.94	478.2936	478.293353	0.5	LysoPE(18:1)	+/−, AM,IP, sCID[g]	0.007374	−1.26
	6.60	500.2778	500.277728	0.1	LysoPE(20:4)	+/−, AM,IP, sCID	0.002249	−1.44
Lyso-GPI	6.00	571.2899	571.288375	2.7	LysoPI(16:0)	AM,IP	0.000657	−1.59
Lyso-GPC	6.02	494.329	494.324658	8.8	LysoPC(16:1)	+/−, AM,IP, sCID	9.49E−07	−2.66
	6.35	544.3472	544.340345	12.6	LysoPC(20:4)	+/−, AM,IP, sCID	1.67E−06	−1.92
Acyl carnitines	1.45	246.1726	246.170529	8.4	2-Methylbutyroylcarnitine/ Isovalerylcarnitine/ Valerylcarnitine	AM,IP	0.009696	1.47
	6.68	424.3466	424.342694	9.2	Linoelaidyl carnitine/Linoleyl carnitine	AM,IP	0.000213	1.73
	7.47	400.346	400.342694	8.3	L-Palmitoylcarnitine	AM,IP	0.000486	1.34
	8.03	426.362	426.358319	8.6	Oleoylcarnitine/Vaccenyl carnitine/Elaidic carnitine/11Z-Octadecenylcarnitine	AM,IP	0.000335	1.39

[a] The retention time (min) on UPLC/tofMS
[b] Quasi-molecular ions (m/z) in this table have four species, including $[M+H]^+$ or $[M+NH_4]^+$ (ES+ mode) and $[M-H]^-$ or $[M+HCOO]^-$ (ES− mode).
[c] ES+ and ES− mode cross-assist analysis.
[d] Accurate mass.
[e] Isotopic pattern.
[f] Standard material.
[g] Source collision induced dissociation.

Table 3
Normalized differential metabolites in renal cortex of DKD model rats by fosinopril treatment.

Class	Metabolites	*p*	Fold (F/M)[a]
Based on GC/tofMS metabolic fingerprint analyses			
Amino acids	L-Alpha-aminobutyric acid	0.011668	1.56
	Threonine	0.038805	−1.14
	Hippurate	0.00529	−4.61
Di(Multi)carboxylic Acids	Malic acid	0.018845	−1.39
	2-Hydroxyglutaric acid	0.001413	−1.79
Hydroxy acids	2-Hydroxyacetic acid (Glycolic acid)	0.029426	1.19
	4-Hydroxybutyric acid	0.046969	−1.36
Polyols	L-Threitol	0.039386	−1.81
	L-(−)-Arabitol	0.017871	2.44
Carbohydrates	Mannose	0.038168	−1.93
	N-Acetyl glucosamine	3.52E-05	−1.81
	Maltose	0.045864	−2.14
Based on UPLC/tofMS metabolic fingerprint analyses			
Amino acids	Taurine	0.00068443	1.18
	Hippurate	0.00032286	−2.11
Fatty acids	Docosapentaenoic acid (22n-6)/Clupanodonic acid/4,7,10,13,16-Docosapentaenoic acid	0.0302717	−1.43
	Tetracosahexaenoic acid	0.03729837	−1.51
Glucuronides	2,8-Dihydroxyquinoline-beta-D-glucuronide/3-Indole carboxylic acid glucuronide	0.00479389	−5.94
	6-Hydroxy-5-methoxyindole glucuronide/5-Hydroxy-6-methoxyindole glucuronide	0.00532132	−3.14
	2-Phenylethanol glucuronide	0.0012848	−4.59
Lyso-GPC	LysoPC(20:4)	0.00963674	1.48
Acyl carnitines	2-Methylbutyroylcarnitine/Isovalerylcarnitine/Valerylcarnitine	0.02334845	−1.39

[a] The ratio of mean normalized peak intensity between fosinopril treatment and model group, where'+' and '−' represent increase and decrease in fosinopril treatment group, respectively.

expected metabolites, several metabolites with dramatic increase in model group were noticed in our result, including hippurate, indoxyl sulfate, 4-pyridoxic acid, 2-phenylethanol glucuronide, 2, 8-dihydroxyquinoline-beta-D-glucuronide/3-indole carboxylic acid glucuronide, 6-hydroxy-5-methoxyindole glucuronide/5-hydroxy-6-methoxyindole glucuronide, D-fructose D-sorbitol, maltose, allantoin, glycocholic acid cholic acid/other isomers et al. These intrarenal abnormal metabolites could be of importance for the development of DKD.

The comparisons of the levels of the identified differential metabolites in DKD were also performed between fosinopril treatment group and model group. The metabolites conforming to p (independent T test) <0.05 were listed in Table 3. Many differential metabolites exhibited significant recovery after administration of fosinopril. Of them, some significantly elevated metabolites within diabetic kidney, including hippurate, 2-phenylethanol glucuronide, 2, 8-dihydroxyquinoline-beta-D-glucuronide/3-indole carboxylic acid glucuronide, 6-hydroxy-5-methoxyindole glucuronide/5-hydroxy-6-methoxyindole glucuronide and N-acetyl glucosamine were reduced effectively, which suggested the potential mechanisms of fosinopril in treating DKD. The mean normalized peak intensities (relative contents) of some representative differential metabolites in control, model and fosinopril treatment group were further illustrated in column plots (Fig. 4A–C).

3.3. Correlations of identified differential metabolites in renal cortex of diabetic rats with urinary protein level and tubulointerstitial injury index

Correlations of identified differential metabolites in renal cortex of rats with biochemical and histopathological parameters were calculated to investigate the association between metabolic abnormalities and diabetic kidney injury. Part of these differential metabolites highly correlated with both 24 h urinary protein levels and tubulointerstitial injury index, and metabolites with both correlation coefficients more than 0.5 were summarized in Table 4. Among them, hippurate, 4-pyridoxic acid, N-acetyl glucosamine, 2-phenylethanol glucuronide, 2, 8-dihydroxyquinoline-beta-D-glucuronide/3-indole carboxylic acid glucuronide, 6-hydroxy-5-methoxyindole glucuronide/5-hydroxy-6-methoxyindole glucuronide showed again significant correlations with diabetic kidney injury including 24 h urinary protein levels and tubulointerstitial injury index (Table 4 and Fig. 5A–H).

3.4. Alterations of intrarenal organic toxins are associated with progressive diabetic kidney injury

In our identified abnormal metabolites, it has been noticed that several known uremic toxins [20], such as hippurate, indoxyl sulfate and 4-pyridoxic acid, were remarkably elevated in the kidney with diabetes and highly correlated with 24 h urinary protein levels and tubulointerstitial injury index (Table 4 and Fig. 4A and B). Increasing evidence shows that levels of serum uremic toxins predict progressive renal injury in patients with chronic kidney disease [21,22]. The ability of oral adsorbent AST-120 to prevent reduction of anionic sites and progressive renal injury such as urinary protein excretion and renal fibrosis confirmed the pathogenic importance of uremic toxins in chronic kidney disease [23–26]. The present study added new evidence that uremic toxins such as hippurate and indoxyl sulfate also significantly increased locally in the diabetic kidney and correlated with the severity of renal injury including 24-h proteinuria and tubulointerstitial damage. Normally, uremic toxins are mainly produced by liver and/or gastrointestinal flora metabolism [27], and eliminated primarily from

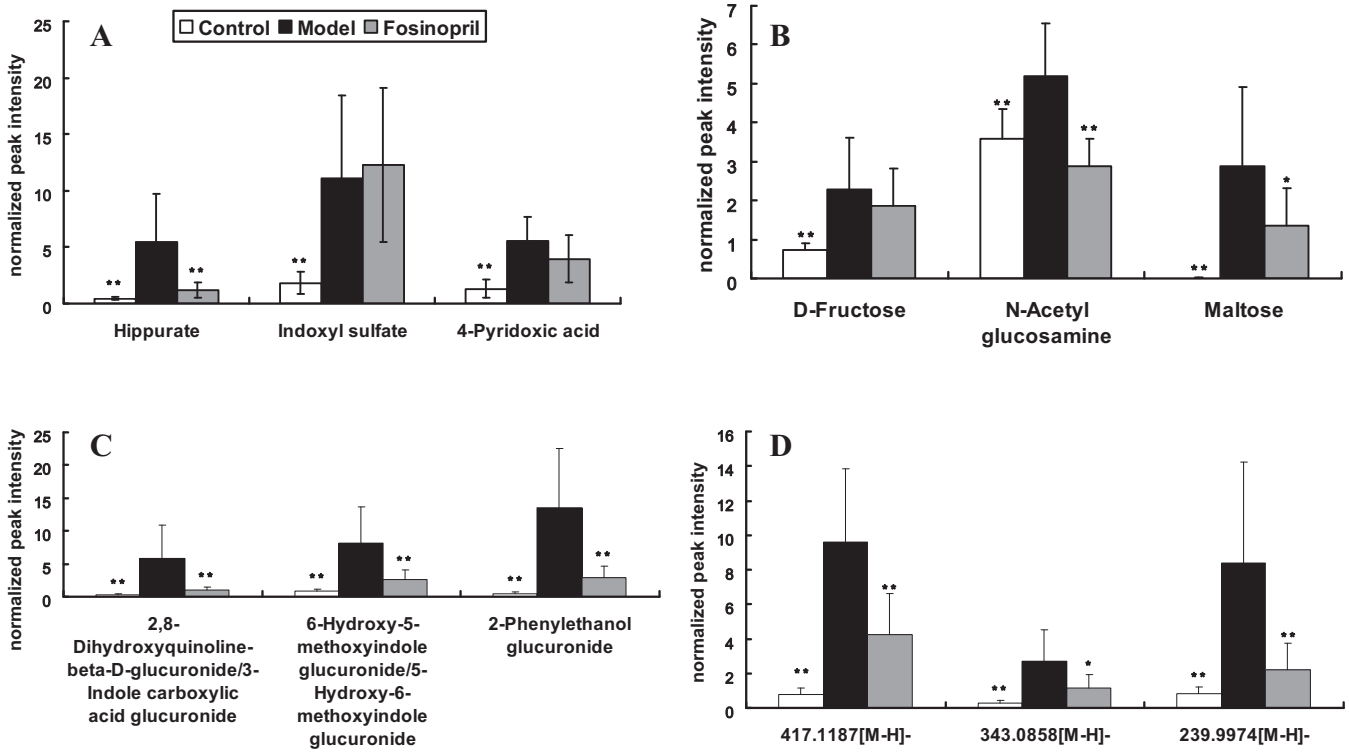

Fig. 4. The mean normalized peak intensities (relative contents) of several representative differential metabolites in perfused renal cortex of rats from control, model and fosinopril treatment group. The data are expressed as mean ± SD, $^{*}p < 0.05$, compared with model group, $^{**}p < 0.01$, compared with model group. A: Three known umeric toxins (hippurate, indoxyl sulfate and 4-pyridoxic acid); B: two carbohydrates (fructose and maltose) and N-acetyl glucosamine; C: three newly identified glucuronides (2-Phenylethanol glucuronide, 2,8-Dihydroxyquinoline-beta-D-glucuronide/3-Indole carboxylic acid glucuronide and 6-Hydroxy-5-methoxyindole glucuronide/5-Hydroxy-6-methoxyindole glucuronide) D: three important metabolites (detected from UPLC–TOF MS but unidentified) represented by accurate *m*/*z* of quasi-molecular ion.

plasma via active kidney tubular secretion [28]. Once the kidney becomes injured, elimination of hippurate and indoxyl sulfate is impaired, which results in higher levels of uremic toxins in plasma and may cause corresponding increase of uremic toxins in renal cells. Thus, theoretical degree of increase of uremic toxins in kidney should conform to that in blood. However, our results showed that intrarenal indoxyl sulfate and hippurate level in DKD model group increased by 5 and 10 times, respectively as compared with those in control group, while mean serum indoxyl sulfate level in spontaneously diabetic rats at 86 weeks increased only by about 50% compared with their baseline level at 21 weeks of age (from 0.19 mg/dl to 0.30 mg/dl) as reported by a previous study [24]. These experimental results suggested that the extent of increase of uremic toxins in kidney tissue of diabetic rats might be largely higher than that in serum. This obvious disagreement indicates that the increase in intrarenal uremic toxins is most likely to be the consequence of their accumulation when blood flowed through the diabetic kidney. Moreover, since active kidney tubular secretion is the primary elimination way for uremic toxins, we speculated that early tubular injury might be involved in the accumulation

Table 4
Correlations ($r > 0.5$) of differential metabolites in renal cortex of DKD model rats with both urinary protein level and tubulointerstitial injury index.

Metabolites	Urinary protein level		Tubulointerstitial injury index	
	r	*p*	*r*	*p*
2-Hydroxyglutaric acid	0.739	1.49804E−08	0.761	4.98219E−09
Allantoin	0.743	1.15051E−08	0.687	5.07825E−07
Citric acid	0.663	1.30266E−06	0.549	1.66822E−04
Hippurate	0.835	3.58081E−12	0.648	3.41770E−06
L-Threitol	0.751	6.70904E−09	0.618	1.30166E−05
Maltose	0.638	6.58833E−05	0.664	3.40151E−05
N-Acetyl glucosamine	0.692	2.8312E−07	0.524	3.71438E−04
Threonic acid	0.633	5.34887E−06	0.689	4.64666E−07
2,8-Dihydroxyquinoline-beta-D-Glucuronide/3-Indole carboxylic acid glucuronide	0.820	2.93182E−10	0.649	1.37957E−05
2-Phenylethanol glucuronide	0.725	8.47075E−08	0.616	2.30411E−05
4-Pyridoxic acid	0.680	7.27334E−07	0.749	1.77269E−08
6-Hydroxy-5-methoxyindole glucuronide/5-hydroxy-6-methoxyindole glucuronide	0.802	9.72237E−11	0.741	1.95489E−08
Cholesterol sulfate	−0.547	1.48661E−4	−0.723	6.48011E−08
Indoxyl sulfate	0.55	1.60930E−4	0.708	2.22672E−07
LysoPE (18:1)	−0.571	6.43707E−05	−0.629	8.03891E−06

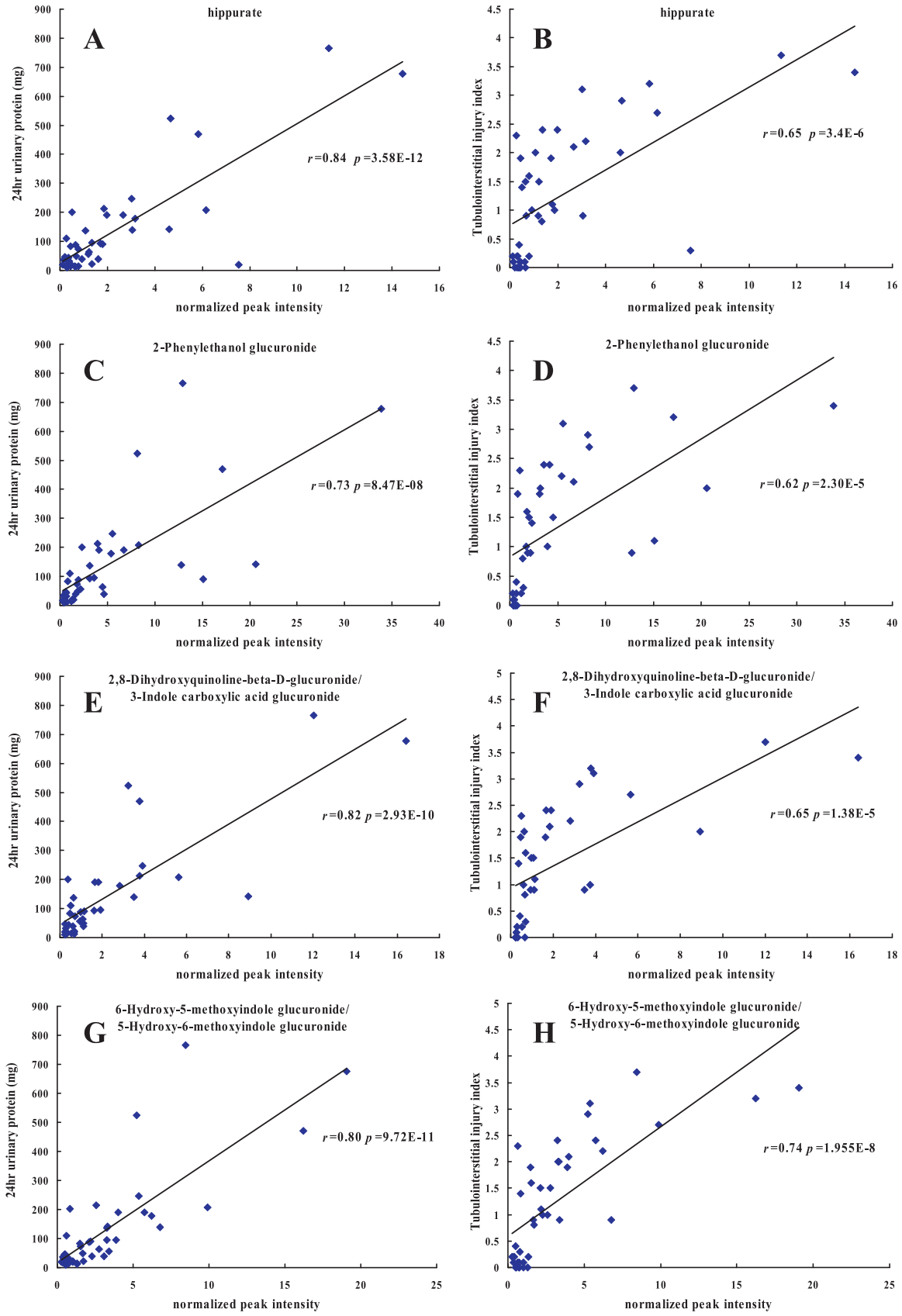

Fig. 5. Scatter plots showing correlations of several representative metabolites with 24 h urinary protein level (A, C, E, G, I, K, M) and tubularinterstitial injury index (B, D, F, H, J, L, N).

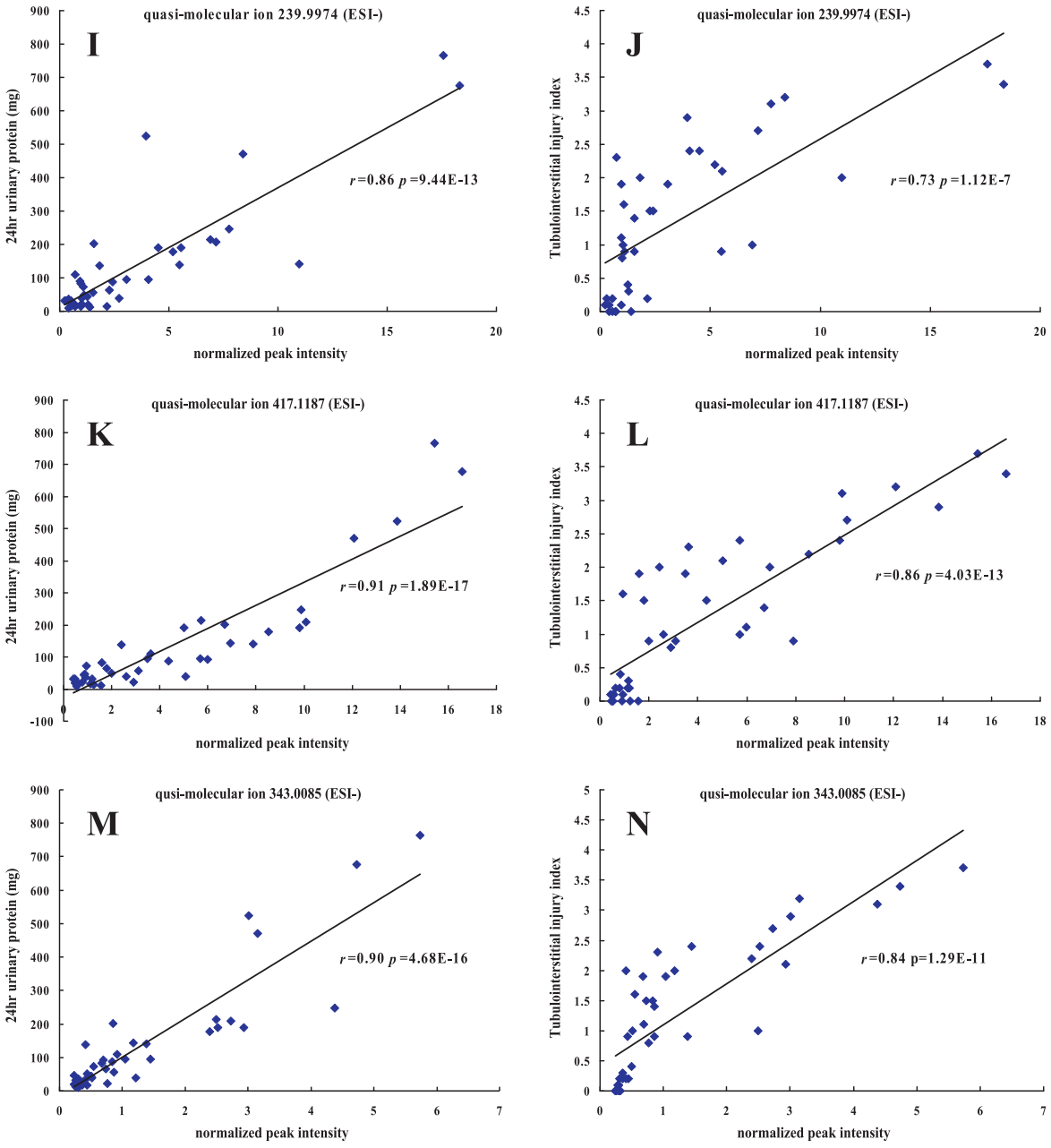

Fig. 5. (*Continued*).

of uremic toxins in kidney. Indeed, we had also observed tubulointerstitial injury and their correlation with the uremic toxins in our study, which moreover occurred when renal functions of rats remained normal. In addition, an evidence that indoxyl sulfate was found accumulated in the tubular cells with organic anion transporters (OAT)1 and/or OAT3 localized at the basolateral membrane by immunohistochemistry method in chronic renal failure (CRF) patients [29] also suggests that the accumulation of uremic toxins might just occur in kidney tubular cells. We found in this study that attenuation of diabetic renal injury with fosinopril treatment was associated with inhibition of intrarenal levels of hippurate. Results from this suggest that the renal protective effect of fosinopril on diabetes may be associated with inhibition of the accumulation of some uremic toxins. Thomas et al. reported that ACEI can increase the expression of tubular organic cation transporters (OCT) in experimental diabetes [30] and tubular organic ion clearance [31] in type 1 diabetes, which demonstrated that the protective effect of ACEI on diabetic tubular injury might influence the metabolic course of organic ion such as uremic toxins in kidney. Fosinopril, however, cannot normalized the elevated level of indoxyl sulfate in DKD groups, giving the hint that indoxyl sulfate may undergo alternative physiological course in kidney that could not influenced by fosinopril.

We also found that glucotoxicity-associated molecules such as sorbitol, fructose and N-acetyl glucosamine were also increased in the diabetic kidney and correlated with progressive renal injury. All of these metabolites are regarded as the components of the polyol and hexosaminic pathway and have been implicated in the pathogenesis of DKD [32,33]. The possible pathological mechanism of DKD concerned with polyol and hexosaminic pathway was illustrated in Fig. 6. Because glutamine:fructose-6-phosphate amidotransferase (GFAT) catalyzes the first and rate-limiting step in the formation of hexosamine products, this enzyme is the key regulator in this pathway. Increased glucose can not only increase the

Table 5
Statistical results of unidentified molecules potentially involved in the development of DKD.

RT/min	Observed quasi-molecular ion	*p* (M/C)	Fold (M/C)	*p* (F/M)	Fold (F/M)	Urinary protein level		Tubulointerstitial injury index	
						r	*p*	*r*	*p*
1.909	417.1187[M−H]⁻	1.67E−06	12.58	0.00205523	0.445525	0.862	9.4379E−13	0.733	1.11637E−07
1.963	343.0858[M−H]⁻	0.00035	9.10	0.02009706	0.426711	0.697	2.13458E−07	0.650	3.25129E−06
1.608	239.9974[M−H]⁻	0.000419	10.32	0.00326207	0.265078	0.791	9.56808E−09	0.698	3.19345E−06
1.1646	240.0035[M−H]⁻	0.000361	3.54	0.0009101	0.364313	0.824	1.15158E−11	0.816	4.39299E−11
1.1842	242.0091[M−H]⁻	0.000104	8.77	0.00306104	0.359785	0.803	9.70967E−11	0.750	1.08073E−08
1.7379	242.0122[M−H]⁻	4.84E−05	5.97	0.01130301	0.470617	0.912	1.89441E−17	0.858	4.03496E−13
1.9044	213.1122[M−H]⁻	8.06E−05	4.79	0.00734764	0.491341	0.901	4.68431E−16	0.835	1.09296E−11
2.0965	357.1025[M−H]⁻	3.16E−05	6.53	0.02376489	0.519681	0.733	2.22603E−08	0.796	3.05970E−10
2.2989	199.0069[M−H]⁻	0.000208	16.98	0.08711986	0.548346	0.767	3.21344E−09	0.823	4.02646E−11
2.4488	201.0204[M−H]⁻	2.55E−06	22.45	0.00487358	0.412111	0.777	1.43916E−09	0.849	2.35930E−12

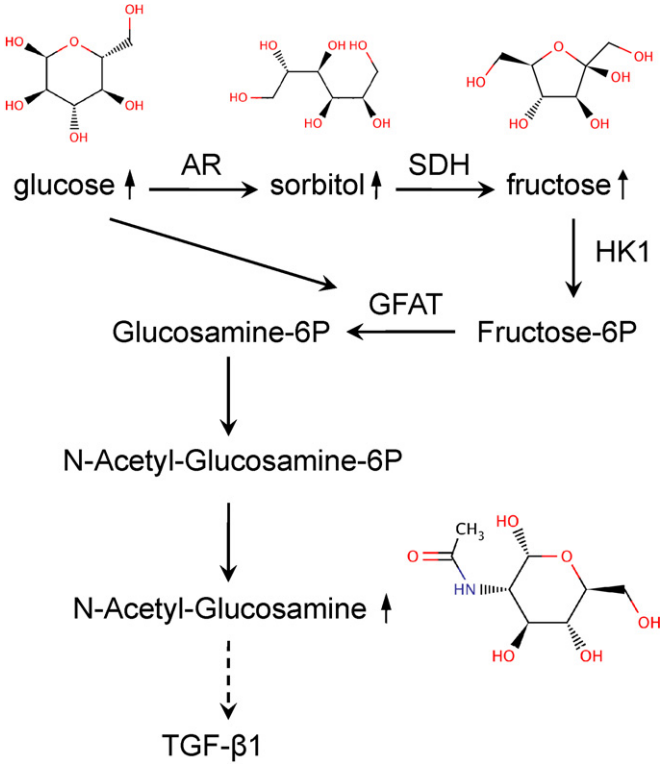

Fig. 6. The postulated pathological mechanism of DKD concerned with polyol and hexosaminic pathway. AR: aldose reductase; SDH: sorbitol dehydrogenase; HK1: Hexokinase 1; GFAT: glutamine:fructose-6-phosphate amidotransferase.

level of fructose-6P (the substrate of GFAT) by activating sorbitol metabolic pathway, but also stimulate the GFAT activity directly [34], thereby leading to the increased expression of glucosamine. Glucosamine has been reported to be able to stimulate transforming growth factor-β1 (TGF-β1, a well-known prosclerotic cytokine causally involved in DKD progression) transcription in cultured renal proximal tubular cells [33]. Our results also showed distinct correlation of N-acetyl glucosamine with tubulointerstitial injury and 24 h urinary protein, which further supported the involvement of hexosamine pathway in the development of DKD. Treatment with fosinopril did not reduce the increased sorbitol and fructose levels in rats with DKD, however, it contributed to the normalization of N-acetyl glucosamine. Moreover, it lowered remarkably the increased tubulointerstitial injury index in rats with DKD. Accordingly, we speculated that although fosinopril treatment failed to reduce the metabolic products in sorbitol pathway, it could attenuate the impairment of tubular epithelial cells by inhibiting the expression of GFAT and/or hexokinase 1(HK1) and their initiated hexosaminic pathway.

In the present study, we also found that three glucuronides (2, 8-dihydroxyquinoline-beta-D-glucuronide/3-indole carboxylic acid glucuronide, 6-hydroxy-5-methoxyindole glucuronide/5-hydroxy-6-methoxyindole glucuronide and 2-phenylethanol glucuronide) were markedly elevated in renal cortex of diabetic kidney and significantly correlated with 24 h urinary protein and tubulointerstitial injury. However, the relationship between glucuronides and DKD remains largely unknown. It has been shown that glucuronidation is able to assist the excretion of toxic substances, drugs or other substances [35]. Considering that glucuronides is a kind of formation of toxins elimination and excreted in the kidney, we conceived that they could play a similar role in the development of DKD as abovementioned uremic toxins. Therefore, these glucuronides could be significant for the prospective research of the effect of organic toxins on development of DKD.

3.5. A number of unidentified metabolites may be involved in the pathogenesis of diabetic kidney injury

A number of unidentified metabolites were also found significantly altered within the diabetic kidney as indicated by the accurate molecular weights of their observed quasi-molecular ions (Table 5 and Fig. 4D). Importantly, the increased levels of these unknown metabolites were correlated significantly with the diabetic kidney injury (Table 5 and Fig. 5I–N). Again, improved diabetic kidney injury by the treatment of fosinopril also attenuated the increase in these unidentified metabolites significantly (Table 5 and Fig. 4D). Identification of these new, previously unrecognized metabolites that are potentially associated with development of DKD is another significant finding in the present study. Although the functional importance of these unknown metabolites in the diabetic kidney remains unknown, they may warrant further investigations.

4. Conclusion

In this study, intrarenal metabolomics based on integrated GC–TOF MS and UPLC–TOF MS analytical platform was applied into the study of pathology of DKD as well as related pharmacological mechanisms of fosinopril. Multiple intrarenal metabolites are detected locally in the diabetic kidney and are correlated with progressive renal injury. Of them, an increase in intrarenal organic toxins including uremic toxins, glucuronides and glucotocixity – associated metabolites may be associated with the development of DKD. Fosinopril treatment can delay the development of DKD and block the increase of these toxic molecules in renal cortex of rats with DKD, which not only suggested new findings about

pharmacological effect of ACEIs on DKD but also further supported the association of organic toxins with the progression of DKD.

Acknowledgements

This work was supported by National Natural Scientific Foundation of China [grant number: 30973911, 81001488, 30801539], and China Postdoctoral Science Foundation [grant number: 20100480236]. We would like to thank Pan Lin for excellent technical assistance.

Appendix A. Supplementary data

Supplementary data associated with this article can be found, in the online version, at doi:10.1016/j.jpba.2011.11.010.

References

[1] G. Soldatos, M. Cooper, Diabetic nephropathy: important pathophysiologic mechanisms, Diabetes Res. Clin. Pract. 82 (2008) 75–79.
[2] J.D. Rippin, et al., Genetics of diabetic nephropathy, Best Pract. Res. Clin. Endocrinol. Metab. 15 (2001) 345–358.
[3] C.D. Cohen, et al., Improved elucidation of biological processes linked to diabetic nephropathy by single probe-based microarray data analysis, PLoS One 3 (2008) e2937.
[4] D. Choudhury, et al., Diabetic nephropathy—a multifaceted target of new therapies, Discov. Med. 10 (2010) 406–415.
[5] K.V. Lemley, When to initiate ACEI/ARB therapy in patients with type 1 and 2 diabetes, Pediatr. Nephrol. 25 (2010) 2021–2034.
[6] S.L. White, et al., Comparison of the prevalence and mortality risk of CKD in Australia using the CKD Epidemiology Collaboration (CKD-EPI) and Modification of Diet in Renal Disease (MDRD) Study GFR estimating equations: the AusDiab (Australian Diabetes, Obesity and Lifestyle) Study, Am. J. Kidney Dis. 55 (2010) 660–670.
[7] M. Buléon, et al., Pharmacological blockade of B2-kinin receptor reduces renal protective effect of angiotensin-converting enzyme inhibition in db/db mice model, Am. J. Physiol-Renal. 294 (2008) 1249–1256.
[8] E. Ripley, Complementary effects of angiotensin-converting enzyme inhibitors and angiotensin receptor blockers in slowing the progression of chronic kidney disease, Am. Heart J. 157 (2009) 7–16.
[9] Y. Bao, et al., Metabonomic variations in the drug-treated type 2 diabetes mellitus patients and healthy volunteers, J. Proteome Res. 8 (2009) 1623–1630.
[10] H. Li, et al., Pharmacometabonomic phenotyping reveals different responses to xenobiotic intervention in rats, J. Proteome Res. 6 (2007) 1364–1370.
[11] W.R. Wikoff, et al., Metabolomics identifies perturbations in human disorders of propionate metabolism, Clin. Chem. 53 (2007) 2076–2169.
[12] J. Zhang, et al., Metabonomics research of diabetic nephropathy and type 2 diabetes mellitus based on UPLC-oaTOF-MS system, Anal. Chim. Acta 650 (2009) 16–22.
[13] J.F. Xia, et al., Ultraviolet and tandem mass spectrometry for simultaneous quantification of 21 pivotal metabolites in plasma from patients with diabetic nephropathy, J. Chromatogr. B 877 (2009) 1930–1936.
[14] J.F. Xia, et al., Correlations of six related purine metabolites and diabetic nephropathy in Chinese type 2 diabetic patients, Clin. Biochem. 42 (2009) 215–220.
[15] H. Yuan, et al., Effects of cholesterol-tagged small interfering RNAs targeting 12/15-lipoxygenase on parameters of diabetic nephropathy in a mouse model of type 1 diabetes, Am. J. Physiol-Renal. 295 (2008) 605–617.
[16] M. Veniant, et al., Calcium blockade versus ACE inhibition in clipped and unclipped kidneys of 2K-1C rats, Kidney Int. 46 (1994) 421–429.
[17] H. Li, et al., Transcriptomic and metabonomic profiling of obesity-prone and obesity-resistant rats under high fat diet, J. Proteome Res. 7 (2008) 4775–4783.
[18] P. Jonsson, et al., A strategy for identifying differences in large series of metabolomic samples analyzed by GC/MS, Anal. Chem. 76 (2004) 1738–1745.
[19] P. Jonsson, et al., High-throughput data analysis for detecting and identifying differences between samples in GC/MS-based metabolomic analyses, Anal. Chem. 77 (2005) 5635–5642.
[20] E.P. Rhee, et al., Metabolite profiling identifies markers of uremia, J. Am. Soc. Nephrol. 21 (2010) 1041–1051.
[21] T. Niwa, Indoxyl sulfate is a nephro-vascular toxin, J. Ren. Nutr. 20 (2010) S2–S6.
[22] F.C. Barreto, et al., Serum indoxyl sulfate is associated with vascular disease and mortality in chronic kidney disease patients, Clin. J. Am. Soc. Nephrol. 4 (2009) 1551–1558.
[23] K. Okada, et al., Oral adsorbent prevents reduction of anionic sites of the glomerular basement membrane in diabetic nephropathy, Nephron Exp. Nephrol. 99 (2005) e56–e62.
[24] I. Aoyama, et al., Oral adsorbent AST-120 ameliorates interstitial fibrosis and transforming growth factor-β1 expression in spontaneously diabetic (OLETF) rats, Am. J. Nephrol. 20 (2000) 232–241.
[25] H. Shimizu, et al., Kremezin (AST-120) delays the progression of diabetic nephropathy in Japanese type 2 diabetic patients, Diabetes Care 28 (2005) 2590.
[26] S.H. Lee, et al., Effects of an oral adsorbent on oxidative stress and fibronectin expression in experimental diabetic nephropathy, Nephrol. Dial. Transplant. 25 (2010) 2134–2141.
[27] W.R. Wikoff, et al., Metabolomics analysis reveals large effects of gut microflora on mammalian blood metabolites, Proc. Natl. Acad. Sci. U. S. A. 106 (2009) 3073–3698.
[28] Y. Tsutsumi, et al., Renal disposition of a furan dicarboxylic acid and other uremic toxins in the rat, J. Pharmacol. Exp. Ther. 303 (2002) 880–887.
[29] K. Taki, et al., Accumulation of indoxyl sulfate in OAT1/3-positive tubular cells in kidneys of patients with chronic renal failure, J. Ren. Nutr. 16 (2006) 199–203.
[30] M.C. Thomas, et al., Reduced tubular cation transport in diabetes: prevented by ACE inhibition, Kidney Int. 63 (2003) 2152–2161.
[31] G. Mt, R. Ct, Increased tubular organic ion clearance following chronic ACE inhibition in patients with type 1 diabetes, Kidney Int. 67 (2005) 2494–2499.
[32] M. Dunlop, Aldose reductase and the role of the polyol pathway in diabetic nephropathy, Kidney Int. 58 (2000) 3–12.
[33] E.D. Schleicher, C. Weigert, Role of the hexosamine biosynthetic pathway in diabetic nephropathy, Kidney Int. 58 (2000) 13–18.
[34] M.C. Daniels, et al., Glutamine: fructose-6-phosphate amidotransferase activity in cultured human skeletal muscle cells: relationship to glucose disposal rate in control and non-insulin-dependent diabetes mellitus subjects and regulation by glucose and insulin, J. Clin. Invest. 97 (1996) 1235–1241.
[35] S.D. Salhanick, H.A. Salhanick, in, US Patent App. 20,080/188,439, 2007.

Journal of Pharmaceutical and Biomedical Analysis 60 (2012) 44–50

Contents lists available at SciVerse ScienceDirect

Journal of Pharmaceutical and Biomedical Analysis

journal homepage: www.elsevier.com/locate/jpba

Determination of protoberberine alkaloids in *Rhizoma Coptidis* by ERETIC ^{1}H NMR method

Pei-Lan Ding*, Li-Qin Chen, Yang Lu, Yong-Guo Li*

Department of Chemistry, Manufacturing, and Controls (CMC), Pharma Research & Early Development (pRED) China, F. Hoffmann-La Roche Ltd., Shanghai 201203, PR China

ARTICLE INFO

Article history:
Received 17 September 2011
Received in revised form 24 October 2011
Accepted 25 October 2011
Available online 4 November 2011

Keywords:
Electronic REference To access In vivo Concentrations (ERETIC)
Proton nuclear magnetic resonance (^{1}H NMR)
Protoberberine alkaloids
Rhizoma Coptidis
Quality assessment

ABSTRACT

An alternative quantification approach called ERETIC (Electronic REference To access In vivo Concentrations) utilizing electronic reference-based proton nuclear magnetic resonance (^{1}H NMR) spectroscopy techniques has been successfully introduced in our present study to simultaneously determine the contents of five major active protoberberine alkaloids (berberine, coptisine, jatrorrhizine, palmatine and epiberberine) in *Rhizoma Coptidis*, one of the most commonly used traditional Chinese medicines (TCM). The NMR experimental conditions including deuterated solvent, relaxation delay time, and ERETIC transmitter power level were optimized, and the developed method was validated in terms of precision, reproducibility, stability, accuracy, recovery, and limit of quantification (LOQ). The recoveries of the five tested alkaloids ranged between 89.94 and 97.72% for berberine, 90.87 and 100.05% for coptisine, 98.35 and 107.57% for jatrorrhizine, 95.37 and 101.26% for palmatine, and 93.18 and 98.00% for epiberberine, respectively, and LOQ was 0.1 mM for berberine. The high universality, accuracy, reproducibility, and efficiency of the ERETIC method demonstrated in this work suggest that this method could serve as a highly potential quantification alternative for quality assessment of TCM.

1. Introduction

Rhizoma Coptidis (Huang-Lian in Chinese), derived from the dried rhizome of *Coptis chinensis* Franch (Ranunculaceae), is one of the 50 fundamental traditional Chinese medicines (TCM) which has long been used to treat intestinal infections including acute gastroenteritis, cholera and bacillary dysentery, etc. [1]. Protoberberine alkaloids present in *Rhizoma Coptidis* have been reported to contribute to the biological activities of this species, which have demonstrated significant pharmacological activities such as antimicrobial activity against a variety of organisms including bacteria, viruses, fungi, protozoans, helminths and chlamydia, as well as anti-tumor activity against various carcinoma cell lines including liver cancer, tongue cancer, and colonic carcinoma etc. [2–6]. Thus the protoberberine alkaloids serve as the quality marker for *Rhizoma Coptidis* as well as its derived products. In Chinese Pharmacopoeia (CP) (2010 edition), berberine is the only alkaloid assigned as the quality marker for *Rhizoma Coptidis* [1]. However, since other alkaloids also contribute to the biological effects of this species [2], it is highly desirable to assess the quality of *Rhizoma Coptidis* by determining a wide range of protoberberine alkaloids including berberine, coptisine, jatrorrhizine, palmatine and epiberberine which make up of the five major active alkaloids for this crude drug [7].

Several quantitative methods mainly based on chromatographic techniques including TLC [8,9], H(U)PLC [7,10–12] and HPCE [13–17] have been employed to determine some of these protoberberine alkaloids in *Rhizoma Coptidis* and other herbal medicines. However, owing to the highly polar and basic properties, as well as highly structural similarity of these protoberberine alkaloids, the conventional chromatographic approaches could not always afford satisfactory results [7–16]. For instance, HPLC gives poor peak resolution and peak shape for these alkaloids, it requires long analysis time and needs unfavorable pH modifier which will potentially lead to column contamination and damage [7,10,11]. For HPCE, reproducibility or robustness is sometimes dissatisfactory because it is prone to be affected by slight variations in experimental conditions, and a well-chosen internal standard is required [13–16,18]. And what's more all the chromatographic methods require standard compounds and tedious procedures to construct calibration curves for quantitative analysis.

Nuclear magnetic resonance (NMR) spectroscopy is developing into a powerful tool for quantification because of the direct proportionality of signal intensity to the concentration of resonating nuclei [19]. The advantages of using NMR for quantitative analysis (qNMR) are manifold: it is rapid, straightforward, and non-invasive.

* Corresponding author. Tel.: +81 21 38954910x3310/3320; fax: +81 21 50790291.
E-mail addresses: penny.ding@roche.com, dingpeilan@yahoo.com.cn (P.-L. Ding), fred.li@roche.com (Y.-G. Li).

0731-7085/$ – see front matter © 2011 Elsevier B.V. All rights reserved.
doi:10.1016/j.jpba.2011.10.030

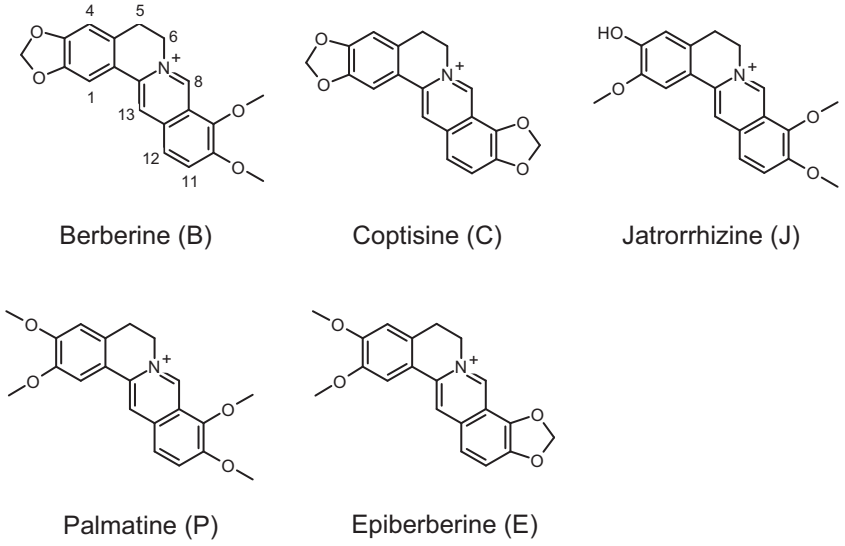

Fig. 1. Structures of the protoberberine alkaloids in *Rhizoma Coptidis*: berberine (B), coptisine (C), jatrorrhizine (J), palmatine (P), and epiberberine (E).

And most importantly, it enables detecting large numbers of components simultaneously just in a quick single measurement, and no standard compounds are needed for calibration curves preparation due to equal signal response factors, which significantly simplifies the analysis procedure. However, qNMR needs to be performed by spiking the sample with a known amount of appropriate chemical internal reference which has to meet many requirements in terms of solubility, stability, relaxation time, chemical shift, and chemical inertness toward the sample [20].

Recently, an alternative NMR quantification approach called ERETIC (Electronic REference To access In vivo Concentrations) has been introduced [21–23]. The main advantage of this technique is that it uses a calibrated electronic reference signal as an alternative to the chemical internal reference, which efficiently circumvents all the potential issues inherent to a chemical internal reference compound [24,25]. The electronic reference signal is generated as a pseudo-FID which possesses all of the characteristics of a real NMR signal [21]. The amplitude, linewidth and position (chemical shift) of this electronic signal are fully under control and freely set by the operator [20]. The ERETIC method is becoming a standard quantification technique, whose high precision, reproducibility and robustness have already been demonstrated for concentration measurements in synthetic chemistry [24], food chemistry [26–28], and metabolomics [21]. Nevertheless, to our knowledge, this method has not yet been reported to be utilized for quality assessment of TCM which tends to be a complex mixture presenting a daunting task for quantitative analysis.

The aim of our present study was to establish a fast, simple and reliable alternative quantification method in order to accommodate practical quality assessment needs for *Rhizoma Coptidis*, in which the aforementioned ERETIC approach has been employed to determine the contents of five major active protoberberine alkaloids (berberine, coptisine, jatrorrhizine, palmatine and epiberberine) in *Rhizoma Coptidis*. The effect of deuterated solvents on signal resolution was investigated, and the experimental parameters such as relaxation delay time and ERETIC transmitter power level were optimized. And the method was subsequently validated in terms of precision, reproducibility, stability, accuracy, recovery and limit of quantification (LOQ). As a result, the established method allows rapid and simultaneous determination of five protoberberine alkloids in five batches of *Rhizoma Coptidis* samples successfully.

2. Experimental

2.1. Rhizoma Coptidis samples

Five *Rhizoma Coptidis* samples were purchased from the local pharmaceutical stores in three provinces (Shanghai, Beijing, and Anhui) of PR China, and the species was verified as *C. chinensis* Franch by the authors.

2.2. Chemicals

The reference substances, berberine (>98%), jatrorrhizine (>98%), palmatine (>98%), and a mixture of coptisine and epiberberine (ratio ca 70%:30%) (structures shown in Fig. 1), were purchased from Tauto Biotech company (Shanghai, PR China). Methanol-d_4 (99.8%) and dimethyl sulfoxide-d_6 (99.9%) were purchased from Sigma–Aldrich (St Louis, MO, USA), acetone-d_6 (99.5%) and acetonitrile-d_3 (99.9%) were purchased from Beijing Chongxi High-Tech Incubator Co., Ltd. (Beijing, PR China). Hydrochloric acid (HCl) and methanol were of analytical reagent grade and purchased from Sinopharm company (Shanghai, PR China).

2.3. Preparation of stock solution and crude drug sample solutions

Stock solution: A stock solution of berberine (20 mM) was prepared in methanol-d_4. Analytical solutions of lower concentrations were prepared by appropriate dilution of the stock solution with methanol-d_4.

Sample solutions: Sample solutions were prepared according to the method described in CP [1], the *Rhizoma Coptidis* samples were crushed into powder, and about 200 mg of the pulverized crude drug passing through a 24 mesh sieve was weighed accurately in a 50 mL flask with stopper. Exactly 50.0 mL of methanol containing 0.1% HCl (v/v) was added and the flask was weighed again. After staying for 2 h, the mixture was subjected to ultrasonication at room temperature for 30 min, the solution was cooled to ambient temperature in order to remove the heat generated during ultrasonication, and then was made up to the original weight with methanol and mixed. An accurately measured aliquot (25.0 mL) of the successive filtrate was evaporated to dryness in vacuo, the residue was dissolved with 2.0 mL methanol-d_4 and filtered through a 0.22 μm membrane for NMR measurement. All samples

were prepared as described above and dissolved with methanol-d_4 for measurements.

2.4. NMR spectroscopy analysis

All spectra were recorded on a Bruker Avance 400 MHz (9.4 T) digital spectrometer (Bruker BioSpin, Falländen, Switzerland) operating at 400.11 MHz for proton (^{1}H) resonance frequency, equipped with a 5 mm I.D. broad band BBO probe permitting the observation of ^{1}H nuclei and the generation of the ERETIC signal, and using 5 mm sample tubes (5 mm diameter, 7 in length, 507-PP-7, Wilmad). Data acquisition and processing were carried out with Topspin 2.1 and ERETIC software (Bruker BioSpin, Falländen, Switzerland). The experimental temperature was controlled at 298 K.

The following acquisition parameters were applied: α (flip angle) = 30° (a 30° flip angle was used instead of a 90° angel in order to make sure the signals fully relax in a relatively shorter relaxation delay period), AQ (acquisition time) = 4.1 s, TD (size of fid) = 64k, NS (number of scan) = 32, SW (spectral width) = 8013 Hz, and $D1$ (relaxation delay) =15 s. Total experimental time for each run was 10 min. 90° pulse calibration was performed for each sample in order to ensure that a quantification experiment works properly. The relative standard deviation (RSD%) of 90° pulse among different samples including the calibration sample was less than 2%, so we supposed that the matrix in our study had little influence on the tank circuit quality factor Q of the probe head, and thus no studies on matrix effect were carried out.

The ERETIC reference signal was generated using one of the frequency channels of the spectrometer and was sent to the broad band (carbon) channel of the BBO probe during the acquisition of the NMR signal. The ERETIC signal consists of an exponentially decaying function that mimics the behavior of a decaying NMR signal. The characteristics of this exponential function were under the complete supervision of the user. In the present study, the ERETIC signal was positioned at – 2.00 ppm so that the electronic reference peak appeared in a region free of NMR proton resonances from the samples, the peak half width was set to 1.0 Hz to obtain a linewidth similar to the quantified NMR signals, and the ERETIC transmitter power level attenuation (PL25) of 40 dB was applied to keep the ERETIC signal intensity at the same order of the observed samples.

Data processing included zero filling to 128k prior to Fourier transformation (FT) and 0.7 Hz exponential line broadening. The spectra were subsequently manually phased, and the baseline was corrected by fitting with a 1st order polynomial curve.

Quantification by ERETIC method consists of two major steps [20,29]:

(1) Calibration step: the electronic reference signal (ERETIC) was calibrated against a standard solution with an exactly known concentration. In our study, a 10 mM solution of berberine standard with the H-13 signal at 8.73 ppm was used for calibration. The equivalent concentration of the electronic signal, [ERETIC], was determined by: $[\mathrm{ERETIC}] = (k_1 \times [\mathrm{REF}] \times A_{\mathrm{ERETIC}})/A_{\mathrm{REF}}$, where k_1 takes into account the number of protons per chemical group used for calibration, A_{ERETIC} and A_{REF} are the areas of the electronic signal and calibration peak respectively, and [REF] is the concentration of the calibration solution.

(2) Quantification step: the ERETIC signal was then used as a reference to determine the concentration of the analyte [COMP], by computing $[\mathrm{COMP}] = ([\mathrm{ERETIC}] \times A_{\mathrm{COMP}})/(k_2 \times A_{\mathrm{ERETIC}})$, where k_2 takes into account the number of protons per chemical group used to be quantified, and A_{COMP} is the peak area of the quantified chemical group. In our study, the H-13 resonance of each alkaloid was selected for quantification because it resonates in a specific region as a singlet with little interference.

All the experimental conditions and parameters for calibration and quantification analysis were equally set.

3. Results and discussion

In order to obtain adequate signal separation and qualified peak signals for the quantification of protoberberine alkaloids, in our study, the effect of deuterated solvents on signal resolution was investigated, the longitudinal relaxation times ($T1$) for the H-13 proton of each alkaloid were measured for relaxation delay time setting, and the ERETIC transmitter power level was optimized for the sake of generating an electronic internal reference signal with appropriate peak intensity.

3.1. Deuterated solvent selection

NMR quantification relies on the detection of resonance-specific signals, so it is essential to find out the proton resonating in a specific region without interference. In our study, H-13 of these five protoberberine alkaloids was selected for quantification because it

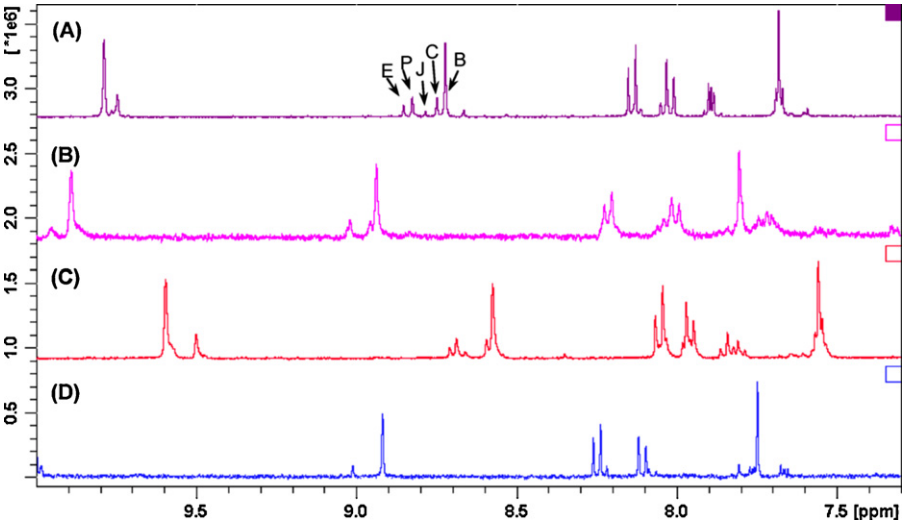

Fig. 2. Overlaid ^{1}H NMR spectra of the extract of *Rhizoma Coptidis* in methanol-d_4 (A), dimethyl sulfoxide-d_6 (B), acetone-d_6 (C), and acetonitrile-d_3 (D) with spectra range of 7.30–10.00 ppm (B: berberine, C: coptisine, J: jatrorrhizine, P: palmatine, E: epiberberine).

resonates as a singlet in a certain region between 8.5 and 9.0 ppm with least interference. However, the protoberberine alkaloids are structurally similar and their H-13 signals are easily to be interfered with each other if an inappropriate deuterated solvent is selected. So, the effect of different deuterated solvents on the separation of H-13 signals was evaluated in our present study, and four solvents methanol-d_4, dimethyl sulfoxide-d_6, acetone-d_6 and acetonitrile-d_3 were accordingly investigated. As a result, methanol-d_4 was found to be the optimal solvent as it gave a good separation of the H-13 peaks originating from berberine, coptisine, jatrorrhizine, palmatine and epiberberine (Fig. 2).

3.2. Longitudinal relaxation time (T1) measurement

Variability of $T1$ values of the quantified alkaloids might lead to unequal signal response factors (i.e., relationship between peak area and its corresponding molar concentration) in cases when relaxation delay ($D1$) is not sufficient. For quantitative purpose, a minimum $D1$ of $5T1_{longest}$ is required to ensure complete relaxation for all the quantified protons in order to obtain equal response factors in a single run. Thus the $T1$ values of the quantified proton H-13 of these five alkaloids need to be measured. In our study, the $T1$ values were determined by using an inversion recovery sequence with 12 inversion delays between the range of 1 ms–15 s (0.001, 0.01, 0.05, 0.1, 0.5, 1, 3, 5, 7, 9, 12, 15 s), and the data was computed by the $T1$ calculation software of the spectrometer. The $T1$ value calculated for the H-13 proton of each alkaloid with methanol-d_4 as solvent was: 1.04 s for berberine at a concentration of 10 mM, 1.06 s for coptisine at 1.17 mM, 899.2 ms for jatrorrhizine at 0.83 mM, 816.5 ms for palmatine at 0.83 mM, and 825.3 ms for epiberberine at 0.50 mM, the results indicated that the $T1$ values of H-13 proton for these five protoberberine alkaloids were of the same order. And it was also found that the $T1$ values were not affected significantly by the variations of sample concentrations ($T1 = 1.19 \pm 0.04$ s ($n = 6$) for berberine at the concentrations of 0.2, 0.5, 1.0, 2.0, 5.0, 10.0 mM) and medium pH values ($T1 = 1.09 \pm 0.12$ s ($n = 5$) for berberine solutions containing 0, 0.1, 0.5, 1.0 and 5.0% HCl (v/v)). Taking into account the $T1$ values measured, a relaxation delay time ($D1$) of 15 s was set to ensure full relaxation of all the quantified H-13 protons of these five protoberberine alkaloids.

3.3. ERETIC transmitter power optimization

In order to select a proper transmitter power to obtain an electronic reference signal (ERETIC) with intensity close to the testing samples, the effect of transmitter power level on the signal intensity was evaluated by recording the spectra under five different transmitter power level attenuations spanning 20 dB at an interval of every 5 dB (30, 35, 40, 45 and 50 dB), with three replicate measurements ($n = 3$) for each power level. The data of peak area versus transmitter power level attenuation was fit to an exponential function model, and as a result, the exponential decrease in ERETIC signal intensity with the ERETIC transmitter power level attenuation (dB) was observed, and the regression equation of the decrease was figured out as well (Fig. 3). Based on the result, an appropriate ERETIC transmitter power level attenuation of 40 dB was chosen to keep the ERETIC peak intensity at a close level of the observed sample signals.

3.4. Method validation

The ERETIC method was validated in terms of precision, reproducibility, stability, accuracy, recovery, and limit of quantification (LOQ).

Precision: the precision was assessed using berberine solution at three typical concentrations (1.0, 5.0, 10.0 mM) with five replicate measurements ($n = 5$) for each concentration, and the relative standard deviation (RSD%) was 1.57, 0.75 and 0.19% respectively.

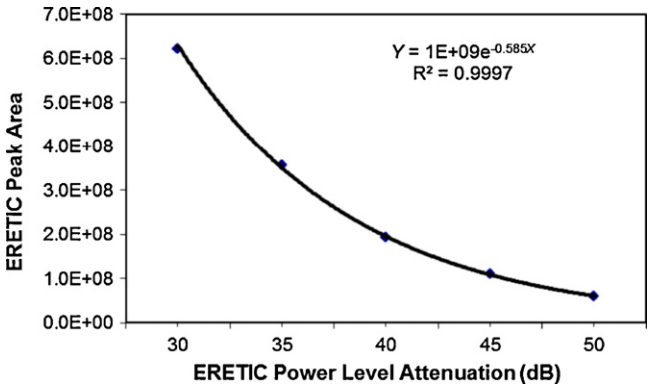

Fig. 3. A plot of the exponential regression relationship between the ERETIC signal intensity with the ERETIC transmitter power level attenuation.

Reproducibility: the reproducibility of the method was evaluated by running five replicate solutions ($n = 5$) for each *Rhizoma Coptidis* sample which were prepared independently in a single day, and the RSD% for all these five alkaloids in five samples ranged from 0.89% to 2.51% (Table 2).

Stability: the method stability was evaluated by analyzing the same standard mixture solution over a period of five days at an interval of every 12 h. Ten acquisitions were performed, and small variations with the RSD% ($n = 10$) of 0.49% for berberine, 1.43% for coptisine, 2.71% for jatrorrhizine, 1.22% for palmatine and 1.91% for epiberberine were observed respectively over this period (Fig. 4). So it demonstrated that the ERETIC method has a good stability and a weekly calibration is sufficient.

Accuracy: the accuracy of measurement system is the degree of agreement between the measured concentration and its true value, which is expressed as relative accuracy error (δ) and is calculated by $\delta = (|C_{measured} - C_{true}|/C_{true}) \times 100\%$, where $C_{measured}$ and C_{true} are the measured concentration and true concentration respectively. We assessed the system accuracy using eight concentration levels of berberine solution (0.1, 0.2, 0.5, 1.0, 2.0, 5.0, 10.0, 20.0 mM) over 2 orders of magnitude and each concentration in 10 replicates. The results showed an excellent agreement between the measured and theoretical concentrations with δ less than 3.00% over the tested concentration range ($n = 10$) (δ was 2.32, 2.94, 1.71, 0.72, 0.30, 0.09, 0.41 and 0.89% at the concentrations of 0.1, 0.2, 0.5, 1.0, 2.0, 5.0, 10.0 and 20.0 mM, respectively) (Fig. 5). And δ was even smaller ($\delta < 0.90\%$) if the concentration range was narrowed to 1–20 mM which represents the typical concentration range of the tested

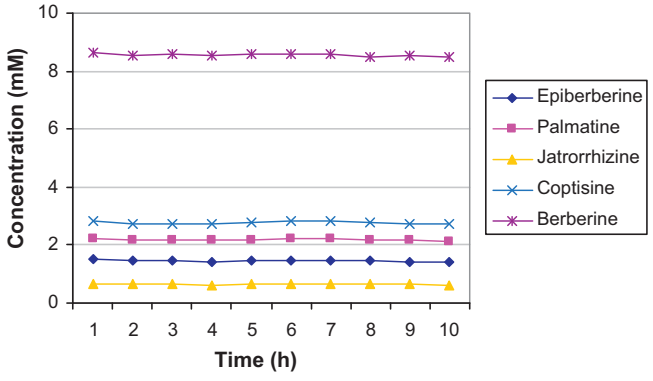

Fig. 4. Stability in time of the determination of the protoberberine alkaloid concentrations determined by the ERETIC method over a period of 108 h repeated every 12 h.

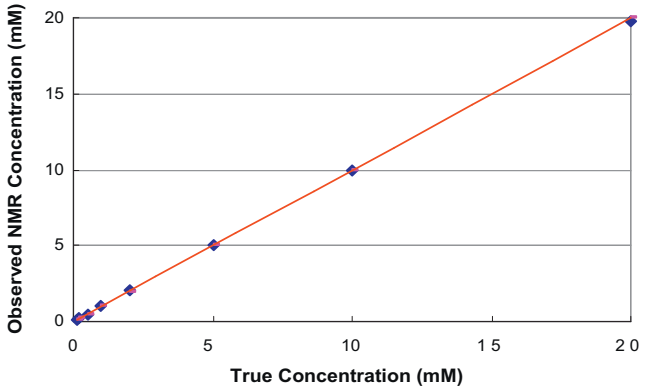

Fig. 5. Observed NMR concentrations vs true concentrations, relative accuracy error (δ) < 3.00% at the concentration range of 0.1–20.0 mM, and δ < 0.90% at the concentration range of 1.0–20.0 mM.

protoberberine alkaloids in the crude drug sample solutions. The correlation observed also illustrated the excellent linear relationship between the signal intensity and analyte concentration within the tested range.

Recovery: the extraction efficiency of the tested alkaloids from the herbal samples was evaluated in terms of recovery using standard addition method. Appropriate amounts of five reference alkaloids were added to an accurately weighed quantity of fine powder of *Rhizoma Coptidis*, and the mixture was extracted and analyzed using the proposed method. A control solution was prepared by extracting the appropriate amount of fine powder of *Rhizoma Coptidis* (to which no reference alkaloid was added) using exactly the same method. The recovery values were determined by comparing the concentrations of the five alkaloids in the spiked solution with those in the control solution. Five sets of recovery samples were analyzed with five replicate measurements for each sample. The results are given in Table 1, and the mean recoveries of the five alkaloids ranged between 94.15 and 104.32% with the RSD% less than 3.80% (n = 5).

LOQ: limit of quantification was 0.1 mM for berberine which was estimated at a signal-to-noise (S/N) ratio of 10 by recording a series of diluted berberine solution with known concentration.

All these results illustrated that the ERETIC method was precise, accurate, reproducible, stable and sensitive enough for quantification.

3.5. Determination of five protoberberine alkaloids in Rhizoma Coptidis

The developed ERETIC method has been applied for the determination of the contents of the five protoberberine alkaloids including berberine, coptisine, jatrorrhizine, palmatine and epiberberine in five different *Rhizoma Coptidis* samples. The singlet of H-13 was selected as a quantified peak for each alkaloid since it was quite well separated from the other peaks with almost no interference in the ^{1}H NMR spectrum.

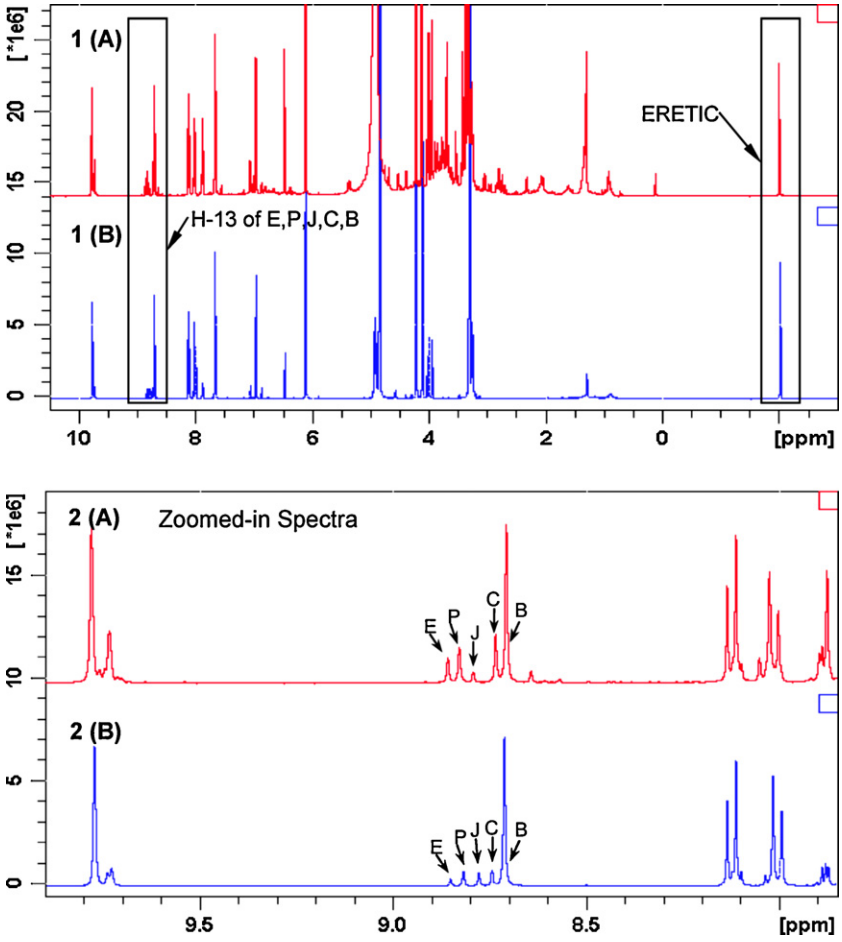

Fig. 6. Overlaid ^{1}H NMR spectra of the *Rhizoma Coptidis* extracts (A) and the reference standard mixture (B) in methanol-d_4 with the ERETIC signal generated at a position of – 2.00 ppm with a transmitter power level attenuation of 40 dB. (1) spectrum range – 3.00–10.50 ppm; (2) spectrum range 7.85–9.90 ppm (B: berberine, C: coptisine, J: jatrorrhizine, P: palmatine, E: epiberberine).

Table 1
Recovery of berberine, coptisine, jatrorrhizine, palmatine and epiberberine.

Sample	Berberine	Coptisine	Jatrorrhizine	Palmatine	Epiberberine
Recovery (%) #1	95.57	100.05	104.55	101.05	97.59
Recovery (%) #2	91.37	90.87	107.57	96.01	93.59
Recovery (%) #3	89.94	92.52	98.35	95.37	93.18
Recovery (%) #4	97.72	92.67	106.10	100.49	93.54
Recovery (%) #5	96.33	94.65	105.04	101.26	98.00
Mean Recovery (%)	94.18	94.15	104.32	98.84	95.18
RSD% (n = 5)	3.56	3.78	3.39	2.93	2.52

Table 2
The contents (mg/g) of berberine, coptisine, jatrorrhizine, palmatine and epiberberine in five *Rhizoma Coptidis* samples.

Sample	Berberine (mg/g)	RSD% (n = 5)	Coptisine (mg/g)	RSD% (n = 5)	Jatrorrhizine (mg/g)	RSD% (n = 5)	Palmatine (mg/g)	RSD% (n = 5)	Epiberberine (mg/g)	RSD% (n = 5)	Sum (mg/g)
HL #1	71.35	1.04	19.73	1.71	5.33	1.30	20.57	1.65	12.44	2.18	129.42
HL #2	58.47	1.91	20.65	1.28	5.21	0.89	15.68	2.31	11.32	0.95	111.33
HL #3	67.10	1.08	22.56	1.31	4.96	2.18	16.32	1.17	12.43	2.11	123.37
HL #4	64.80	2.51	19.38	2.28	4.98	1.81	17.31	2.02	11.05	1.81	117.52
HL #5	69.67	2.29	22.52	1.41	5.16	2.07	18.74	1.81	12.33	1.53	128.42

Fig. 6 showed the overlaid ^{1}H NMR spectra of the *Rhizoma Coptidis* extracts analyzed by the proposed method together with that of the standards mixture solution. The ERETIC signal was generated at a position of – 2.00 ppm with a transmitter power level attenuation of 40 dB. Signal assignment for the quantified protons (H-13 proton resonation) of each alkaloid was confirmed by spiking with the corresponding reference standard. The zoomed-in spectra within the region of 7.85–9.90 ppm showed clearly that the five protoberberine alkaloids were well separated. The contents of each individual protoberberine alkaloid determined in the five *Rhizoma Coptidis* samples have been summarized in Table 2 and shown in Fig. 7, each sample was measured in five replicates in order to obtain statistically significant result. As shown in Table 2, the crude drugs generally contained these five selected protoberberine alkaloids, and the contents were very high. The content ranged from 58.47 to 71.35 mg/g for berberine, 19.38 to 22.56 mg/g for coptisine, 4.96 to 5.33 mg/g for jatrorrhizine, 15.68 to 20.57 mg/g for palmatine, and 11.05 to 12.44 mg/g for epiberberine, respectively, and the total content of these five alkaloids was 111.33–129.42 mg/g. It was also found that the variations of the alkaloid contents in different samples were small, indicating the qualities of these five crude drug samples were relatively close. Among the five detected alkaloids, berberine was the most dominant one in *Rhizoma Coptidis*, the contents of coptisine and palmatine were of a close level, then epiberberine followed after, and jatrorrhizine was always present in a lowest content. The present results were consistent with those reported previously [7,17].

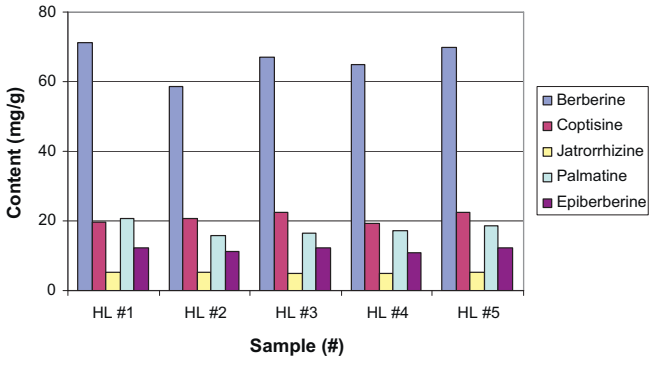

Fig. 7. The contents (mg/g) of berberine, coptisine, jatrorrhizine, palmatine and epiberberine in five *Rhizoma Coptidis* samples.

4. Conclusions

An alternative quantification method called ERETIC utilizing electronic reference-based ^{1}H NMR has been established to quantify the contents of five protoberberine alkaloids in *Rhizoma Coptidis*. To our knowledge, this is the first time the ERETIC method has been applied to quality assessment of TCM, and the results obtained in our present study illustrated the adaptation and effectiveness of this technique for TCM quality control.

The proposed ERETIC method was demonstrated to be simple, rapid, efficient, and reliable with many advantages over the reported conventional quantitative methods: (1) the performance of the ERETIC approach is excellent, it provides high precision, accuracy, reproducibility, and sufficient sensitivity. And the robustness should be emphasized since the method is less prone to operator's error; (2) the ERETIC method (including qNMR) does not require quantitative reference substances for calibration curves preparation. And it enables detecting large numbers of components simultaneously in a single measurement and has definite capability to identify unknown compounds in complex mixture. So the ERETIC method dramatically simplifies sample preparation procedure and shorten sample analysis time, and is of great value when no reference substances are available; (3) unlike conventional qNMR method, the ERETIC method utilizes an electronic reference instead of a chemical internal reference which gets rid of all the drawbacks raised by the latter. The approach is flexible because the ERETIC signal (frequency, linewidth, amplitude) could be freely set, and the quantitative nuclei could be easily extended to other nuclei such as ^{19}F (fluorine), ^{31}P (phosphorous), and ^{13}C (carbon), etc. All these aforementioned features make the ERETIC method an attractive alternative to both chromatographic and conventional qNMR techniques in routine quality assessment and quantification work, especially in situations where multiply components are needed to be quantified and in cases when no reference standards are available. It needs to be mentioned that in situations when complicated samples are analyzed, especially for biological samples with high ionic strength, the effect of matrix on the tank circuit quality factor Q of probe head is absolutely necessary to be taken into careful consideration [30].

Acknowledgement

The authors would like to thank Dr. Lu Shan from Bruker BioSpin Corp. (Beijing, PR China) for his invaluable suggestions and technical supports of this research.

References

[1] State Pharmacopoeia Commission of PRC, Pharmacopoeia of the People's Republic of China, vol. I, Chemical Industry Press, Beijing, 2010, pp. 285.
[2] K.J. Hsu, Chinese Traditional Medicine, Chinese Pharmaceutical Science and Technology Publication Company, Beijing, 1996.
[3] X.M. Ding, Y.M. Ning, Progress in pharmacological studies of *Rhizoma Coptidis*, Int. J. Trad. Chin. Med. 33 (2011) 184–186.
[4] N. Wang, Y.B. Feng, M.F. Zhu, C.M. Tsang, K. Man, Y. Tong, S.W. Tsao, Berberine induces autophagic cell death and mitochondrial apoptosis in liver cancer cells: the cellular mechanism, J. Cell. Biochem. 111 (2010) 1426–1436.
[5] W.H. Hsu, Y.S. Hsieh, H.C. Kuo, C.Y. Teng, H.I. Huang, C.J. Wang, S.F. Yang, Y.S. Liou, W.H. Kuo, Berberine suppresses in vitro migration and invasion of human SCC-4 tongue squamous cancer cells through the inhibitions of FAK, IKK, NF-jB, u-PA and MMP-2 and -9, Canc. Lett. 279 (2009) 155–162.
[6] W.H. Hsu, Y.S. Hsieh, H.C. Kuo, C.Y. Teng, H.I. Huang, C.J. Wang, S.F. Yang, Y.S. Liou, W.H. Kuo, Berberine induces apoptosis in SW620 human colonic carcinoma cells through generation of reactive oxygen species and activation of JNK/p38 MAPK and FasL, Arch. Toxicol. 81 (2007) 719–728.
[7] B.X. Zhang, F. Peng, W.Z. Luo, C.H. Wang, Z.J. Luo, Y. Yang, Determination of the content of six alkaloids in Coptidis Rhizoma from different areas, Chin. J. Mod. Appl. Pharm. 28 (2011) 128–133.
[8] F.J. Liu, D.M. Sun, J.H. Lu, A.L. Xu, Determination of alkaloid from combination of *Rhizoma Coptidis* and Fructus Evodiae by TLCS, Chin. Trad. Patent Med. 32 (2010) 75–79.
[9] Z.C. Ge, J.M. Zhou, Determination of berberine, palmatine and jatrorrhizine in Coptis and its preparations by micellar thin layer chromatographic scanning method, Chin. J. Anal. Chem. 32 (2004) 99–101.
[10] C. Sun, H.Z. Liu, Application of non-ionic surfactant in the microwave-assisted extraction of alkaloids from *Rhizoma Coptidis*, Anal. Chim. Acta 612 (2008) 160–164.
[11] S.J. Zhang, M.Y. Wang, C.H. Wang, Preparative separation and purification of alkaloids from *Rhizoma Coptidis* by high-speed counter-current chromatography, Sep. Purif. Technol. 76 (2011) 428–431.
[12] W.J. Kong, Y.L. Zhao, X.H. Xiao, J.B. Wang, H.B. Li, Z.L. Li, C. Jin, Y. Liu, Spectrum-effect relationships between ultra performance liquid chromatography fingerprints and anti-bacterial activities of *Rhizoma Coptidis*, Anal. Chim. Acta 634 (2009) 279–285.
[13] S.G. Ji, Y.F. Chai, G.Q. Zhang, Y.T. Wu, D.S. Liang, Z.M. Xu, Determination of berberine in *Rhizoma Coptidis* and its preparations by non-aqueous capillary electrophoresis, Biomed. Chromatogr. 13 (1999) 439–441.
[14] P.H. Wei, G.B. Li, L.R. Chen, Y.Q. Wei, J.R. Yuan, Influence of extracting solvent on the content of alkaloids in the extract of *Coptidis Rhizoma*-Phellodendri Cortex by capillary electrophoresis, Chin. J. Anal. Chem. 31 (2003) 569–572.
[15] S.W. Sun, H.M. Tseng, Sensitivity improvement on detection of Coptidis alkaloids by sweeping in capillary electrophoresis, J. Pharm. Biomed. Anal. 37 (2005) 39–45.
[16] Q. Liu, Y.J. Liu, Y.Q. Li, S.Z. Yao, Nonaqueous capillary electrophoresis coupled with laser-induced native fluorescence detection for the analysis of berberine, palmatine, and jatrorrhizine in Chinese herbal medicines, J. Sep. Sci. 29 (2006) 1268–1274.
[17] J.H. Chen, H.Q. Zhao, X.R. Wang, F.S. Lee, H.H. Yang, L. Zheng, Analysis of major alkaloids in *Rhizoma Coptidis* by capillary electrophoresis-electrospray-time of flight mass spectrometry with different background electrolytes, Electrophoresis 29 (2008) 2135–2147.
[18] Z.M. Wen, J.L. Zhang, L.S. Xu, Application of HPCE to the analysis of traditional herbal drugs, Chin. Trad. Herb. Drugs 31 (2000) 141–144.
[19] A. Abragam, The Principles of Nuclear Magnetism, Oxford University Press, New York, 1961.
[20] A. Olivier, Eretic Software Operation & User Guide, Version 002, Bruker Biospin SA, Wissembourg, 2006, pp. 5.
[21] L. Barantin, A. LePape, S. Akoka, A new method for absolute quantitation of MRS metabolites, Magn. Reson. Med. 38 (1997) 179–182.
[22] A. Cazor, C. Deborde, A. Moing, D. Rolin, H. This, Sucrose, glucose, and fructose extraction in aqueous carrot root extracts prepared at different temperatures by means of direct NMR measurements, J. Agric. Food Chem. 54 (2006) 4681–4686.
[23] C. Deborde, M. Maucourt, P. Baldet, S. Bernillon, B. Biais, G. Talon, C. Ferrand, D. Jacob, H. Ferry-Dumazet, A. de Daruvar, D. Rolin, A. Moing, Proton NMR quantitative profiling for quality assessment of greenhouse-grown tomato fruit, Metabolomics 5 (2009) 183–198.
[24] V. Rizzo, V. Pinciroli, Quantitative NMR in synthetic and combinatorial chemistry, J. Pharm. Biomed. Anal. 38 (2005) 851–857.
[25] S. Akoka, M. Trierweiler, Improvement of the ERETIC method by digital synthesis of the signal and additional of a broadband antenna inside the NMR probe, Instrum. Sci. Technol. 30 (2002) 21–29.
[26] J.E.A. Rodrigues, G.L. Erny, A.S. Barros, V.I. Esteves, T. Brandao, A.A. Ferreira, E. Cabrita, A.M. Gil, Quantification of organic acids in beer by nuclear magnetic resonance (NMR)-based methods, Anal. Chim. Acta 674 (2010) 166–175.
[27] V. Molinier, B. Fenet, J. Fitremann, A. Bouchu, Y. Queneau, Concentration measurements of sucrose and sugar surfactants solutions by using the ^{1}H NMR ERETIC method, Carbohydrate Res. 341 (2006) 1890–1895.
[28] F. Ziarelli, S. Caldarelli, Solid-state NMR as an analytical tool: quantitative aspects, Solid State Nucl. Magn. Reson. 29 (2006) 214–218.
[29] S. Akoka, L. Barantin, M. Trierweiler, Concentration measurement by proton NMR using the ERETIC method, Anal. Chem. 71 (1999) 2554–2557.
[30] F. Ziarelli, S. Viel, S. Caldarelli, D.N. Sobieski, M.P. Augustine, General implementation of the ERETIC^{TM} method for pulsed field gradient probe heads, J. Magn. Reson. 194 (2008) 307–312.

Journal of Pharmaceutical and Biomedical Analysis 60 (2012) 51–58

Contents lists available at SciVerse ScienceDirect

Journal of Pharmaceutical and Biomedical Analysis

journal homepage: www.elsevier.com/locate/jpba

Optimization and validation of liquid chromatography and headspace-gas chromatography based methods for the quantitative determination of capsaicinoids, salicylic acid, glycol monosalicylate, methyl salicylate, ethyl salicylate, camphor and l-menthol in a topical formulation

Jochen Pauwels [1], Ward D'Autry [1], Larissa Van den Bossche, Cédric Dewever, Michel Forier, Stephanie Vandenwaeyenberg, Kris Wolfs, Jos Hoogmartens, Ann Van Schepdael, Erwin Adams *

Laboratory for Pharmaceutical Analysis, Faculty of Pharmaceutical Sciences, Katholieke Universiteit Leuven, O&N 2, PO Box 923, Herestraat 49, B-3000 Leuven, Belgium

ARTICLE INFO

Article history:
Received 6 July 2011
Received in revised form 18 October 2011
Accepted 21 October 2011
Available online 25 October 2011

Keywords:
Liquid chromatography
Gas chromatography
Headspace sampling
Topical formulation

ABSTRACT

Capsaicinoids, salicylic acid, methyl and ethyl salicylate, glycol monosalicylate, camphor and l-menthol are widely used in topical formulations to relieve local pain. For each separate compound or simple mixtures, quantitative analysis methods are reported. However, for a mixture containing all above mentioned active compounds, no assay methods were found. Due to the differing physicochemical characteristics, two methods were developed and optimized simultaneously. The non-volatile capsaicinoids, salicylic acid and glycol monosalicylate were analyzed with liquid chromatography following liquid–liquid extraction, whereas the volatile compounds were analyzed with static headspace-gas chromatography. For the latter method, liquid paraffin was selected as compatible dilution solvent. The optimized methods were validated in terms of specificity, linearity, accuracy and precision in a range of 80% to 120% of the expected concentrations. For both methods, peaks were well separated without interference of other compounds. Linear relationships were demonstrated with R^2 values higher than 0.996 for all compounds. Accuracy was assessed by performing replicate recovery experiments with spiked blank samples. Mean recovery values were all between 98% and 102%. Precision was checked at three levels: system repeatability, method precision and intermediate precision. Both methods were found to be acceptably precise at all three levels. Finally, the method was successfully applied to the analysis of some real samples (cutaneous sticks).

1. Introduction

Capsaicin (CP), salicylic acid (SA) and related esters, camphor and l-menthol are frequently used in topical formulations to treat various sources of pain including arthritis, twists and inflammation. CP is widely known as the principal ingredient of several hot pepper species and self-defense repellents [1,2]. Related pharmacologically active CP substances also found in *Capsicum* species include dihydrocapsaicin (DHCP) and nordihydrocapsaicin (NDHCP). Capsaicinoids are often added to pharmaceuticals in the form of *Capsicum* oleoresins. Pharmacological mechanisms of capsaicinoids have been extensively reviewed [3]. SA, a naturally occurring compound in the bark of *Salix alba*, was formerly used as an anti-inflammatory and antipyretic agent, but for these purposes is now replaced by acetylsalicylic acid [4]. Salicylate esters like methyl salicylate (MeS), ethyl salicylate (ES) and glycol monosalicylate (GMS) are commercially synthesized by esterification of SA with methanol, ethanol and ethylene glycol, respectively. Beside the pleasant odor, salicylate esters are used in topical formulations as pain relieving adjuvants owing to their rubefacient properties [5]. Camphor and l-menthol both have a terpene skeleton and are naturally occurring compounds with a characteristic, minty odor. Both substances are also used in topical formulations for their analgesic properties. Moreover, it was recently discovered that the pain relieving mechanisms for both components are similar to those of CP [6,7].

Various analysis methods exist for the determination of naturally occurring capsaicinoids. Apart from established chromatographic techniques such as gas chromatography (GC), thin layer chromatography (TLC) and liquid chromatography (LC), more recent (hyphenated) analytical methods include solid phase micro extraction–gas chromatography–mass spectrometry (SPME–GC–MS) [8] and liquid chromatography–time-of-flight MS

* Corresponding author. Tel.: +32 16 323444; fax: +32 16 323448.
E-mail address: erwin.adams@pharm.kuleuven.be (E. Adams).
[1] These authors contributed equally to this work.

0731-7085/$ – see front matter © 2011 Elsevier B.V. All rights reserved.
doi:10.1016/j.jpba.2011.10.024

[9]. A micellar electrokinetic capillary chromatography method was reported by Laskaridou–Monnerville [10]. Different extraction procedures for separating capsaicinoids from their matrix were recently compared by Jeon and Lee [11]. A liquid–liquid extraction using methanol was found to provide better results over acetonitrile extraction and solid-phase extraction. The European Pharmacopoeia (Ph. Eur.) prescribes an LC method for the determination of capsaicinoids in bulk products and *Capsicum* oleoresins. For the determination of CP and DHCP in a pharmaceutical formulation, an LC method following liquid–liquid extraction (LLE) was developed by Kaale et al. [12]. For the determination of SA in cosmetic and pharmaceutical preparations, LC methods have been developed [13,14]. SA can be quantitatively determined employing optical methods such as ultraviolet (UV), Fourier transform infrared (FT-IR) and FT-Raman spectroscopy [15–17]. Because of the volatility of MeS and ES, it is not surprising that these compounds are generally determined with GC. Few reports can be found about the determination of salicylate esters in pharmaceutical products [18,19]. For the analysis of camphor and l-menthol, GC has been the method of choice due to their low UV absorbance and high volatility. Several studies dealing with the analysis of camphor and/or l-menthol in topical formulations were performed [20,21]. Recent sample enrichment techniques such as SPME have been used for the determination of l-menthol in blood samples [22–24].

The aim of this study was to develop and validate an analytical assay method to quantify capsaicinoids, SA, GMS, MeS, ES, camphor and l-menthol in a solid ointment (fatty stick). Hitherto, no reports were found dealing with the quantification of all these compounds in one topical formulation. Taking into account the diverse physicochemical properties of the involved compounds, the assay was divided into a separate LC–UV and static headspace (sHS)–GC with flame ionization detection (FID) method. The non-volatile capsaicinoids, SA and GMS were analyzed with LC, whereas the more volatile substances (i.e. MeS, ES, camphor and l-menthol) were determined with sHS-GC-FID. With sHS, only the gas phase portion of a heated, closed vial containing the sample is analyzed, avoiding non-volatile matrix compounds being injected onto the column. The principles of HS–GC are well explained in the reference work of Kolb and Ettre [25]. Finally, the method was applied to real samples.

2. Experimental

2.1. Reagents and samples

LC grade methanol and phosphoric acid were obtained from VWR (Haasrode, Belgium). LC–MS grade methanol and formic acid were obtained from Biosolve LTD (Valkenswaard, The Netherlands). Analytical grade *n*-hexane was from Chemlab NV (Zedelgem, Belgium). Highly liquid paraffin and SA were obtained from Merck (Darmstadt, Germany). GMS was from API Corporation (Osaka, Japan), ES from Synapharm (Liège, Belgium), MeS from Aako (Leusden, The Netherlands), camphor from Düllberg Konzentra (Hamburg, Germany), l-menthol from IMCD (Mechelen, Belgium) and *Capsicum* oleoresin (containing 8% m/m of capsaicinoids, henceforth expressed as capsaicin) from Inga Pharmaceuticals (Mumbai, India). Capsaicin (≥95%) and dihydrocapsaicin (approximately 90%) were from Sigma–Aldrich (St. Louis, MO, USA). The cutaneous stick, available on the Belgian market, contains the following active ingredients: MeS 26.47 mg/g, ES 17.64 mg/g, GMS 8.82 mg/g, SA 8.82, camphor 4.41 mg/g, l-menthol 55.14 mg/g and *Capsicum* oleoresin 15.44 mg/g; and excipients: emulsifying cetostearyl alcohol, oleyl oleate, paraffin and vaselinum album. Water was purified with a Milli-Q® Gradient system (Millipore, Milford, MA, USA).

2.2. Liquid chromatography

Three components of the formulation were quantitatively determined with LC equipped with UV-detection: SA, GMS and CP. The liquid–liquid extraction procedure and LC method were based on a previously in-house developed analysis method for CP in a topical formulation [12].

2.2.1. Sample preparation: liquid–liquid extraction

An amount of 1500 g of stick was dissolved in 20.0 ml of *n*-hexane. The compounds of interest were extracted with a methanol–water (60:40, v/v) mixture. First, the organic and aqueous phases were stirred with a magnetic stirrer. In order to rapidly separate the phases, the mixture was centrifuged using a Jouan B4i centrifuge (Newport Pagnell, UK) at 2880 × *g* for 2 min. Extraction was carried out in quadruplicate (two times with 15.0 ml methanol–water [60:40, v/v] followed by two times with 10.0 ml methanol–water [60:40, v/v]). The aqueous phases were collected for analysis. The combined aqueous phases were further diluted to 50.0 ml with methanol–water (60:40, v/v). According to the labeled concentrations and supposing 100% extraction efficiency, the concentrations in the sample solution of SA and GMS were 0.265 mg/ml, and 0.037 mg/ml of CP. These concentrations were considered as the 100% level throughout the study.

2.2.2. Preparation of reference solutions

A reference stock solution was prepared for each compound as follows: 26.50 mg of SA or GMS and 18.50 mg of CP reference substance was weighed and dissolved in 10.0 ml of methanol–water (60:40, v/v). The stock solutions were labeled S1, S2 and S3, respectively. The reference solution for quantification was prepared by mixing and diluting 1.0 ml of both S1 and S2 and 200 μl of S3 with methanol–water (60:40, v/v) to a total volume of 10.0 ml. For identification of the DHCP peak, a DHCP reference solution was prepared by dissolving about 1 mg of DHCP in 25.0 ml of methanol–water (60:40, v/v).

2.2.3. Chromatographic system and conditions

A Dionex (Sunnyvale, CA, USA) LC system consisting of an LPG-3400A pump, a WPS-3000 SL autosampler, an SOR-100 degasser and a UVD-340U detector was used with accompanying Chromeleon 6.80 software. The analytes were separated on a Thermoquest (Runcorn, UK) Hypersil BDS C18 column (250 × 4.6 mm) with a particle size of 5 μm. The column was thermostatted at 30 °C. Gradient elution was applied as follows: mobile phase A was a mixture of methanol–water–phosphoric acid 1 M (47:43:10, v/v) while mobile phase B was a mixture of the same components but in a different ratio (67:23:10, v/v). The gradient elution program was as follows: 0–12 min: 0% B; 12–13 min: 0 → 60% B; 13–30 min: 60 → 70% B; 30–40 min: 70 → 80% B; 40–50 min: 0% B. The injection volume was 100 μl and the flow rate 1 ml/min. The wavelength of the UV-detector was set at 280 nm.

2.3. Capsaicinoid identification by liquid chromatography–mass spectrometry

A Thermo Finnigan (San Jose, CA, USA) LCQ ion trap mass spectrometer, equipped with an electrospray ionization source (ESI), was used for the identity confirmation of NDHCP. The MS was operated in the positive ion mode and tuned with CP reference substance, dissolved in methanol–H_2O (60:40, v/v) at a concentration of 0.05 mg/ml. Injection into the MS system was performed by direct infusion as follows: the CP reference solution coming from a built-in syringe pump at a flow rate of 10 μl/min was mixed with the mobile phase (formic acid (0.1%, m/v) in a mixture of methanol–water (50:50, v/v)) through a T-piece. The temperature

of the heated capillary was set at 250 °C. Nitrogen was used as sheath and auxiliary gas. Helium was used as the damping and collision gas at a pressure of 0.1 Pa. Nitrogen and helium were obtained from Air Liquide (Liège, Belgium). All parameters were kept constant during subsequent MS analysis of CP and the unknown.

The unknown peak, which was expected to contain NDHCP, was manually collected with the LC-method described above and injected into a desalting system consisting of a TSP (San Jose, CA, USA) Spectra System 1000XR operated at a flow rate of 200 μl/min. An XTerra®column (250 mm × 2.1 mm, 5 μm) from Waters (Milford, MA, USA) was used. Two mobile phases were utilized: mobile phase A consisting of formic acid (0.1%, m/v) in water and mobile phase B consisting of formic acid (0.1%, m/v) in methanol. First, mobile phase A was pumped to remove salts from the column. Second, the proportion of mobile phase B was increased to 60% in order to elute the unknown from the column towards the MS system. Salt elution as well as the unknown was monitored with a TSP Spectra 100 UV detector.

2.4. Static headspace-gas chromatography

Four compounds of the formulation were quantitatively analyzed with sHS-GC: camphor, l-menthol, MeS and ES.

2.4.1. Sample preparation and sample vials

A sample solution was prepared by dissolving 2000 g of stick in 18,000 g of liquid paraffin in a glass stoppered conical flask. Mixing was accelerated by heating the solution at 55 °C for 10 min. Headspace vials were filled with 1500 g of sample solution. Liquid paraffin was added to obtain a total weight of 3000 g in the vial. According to the drug label, the amounts of camphor, l-menthol, MeS and ES in the sample vials were 0.66 mg, 8.27 mg, 3.97 mg and 2.65 mg, respectively. These amounts were considered as 100% concentration levels throughout the study.

2.4.2. Preparation of blank stick and blank solution

To mimic the sample matrix, a stick was prepared without camphor, l-menthol, MeS and ES. A blank solution was made by mixing 2000 g of blank stick with 18,000 g of liquid paraffin, similar to the sample solution.

2.4.3. Preparation of reference solution

Appropriate amounts of camphor (22.05 mg), l-menthol (275.70 mg), MeS (132.35 mg) and ES (88.20 mg) were weighed into a glass stoppered conical flask. After the powders were dissolved in the salicylate liquids, liquid paraffin was added up to a total weight of 50,000 g. Headspace vials were filled with 1500 g of reference solution and 1500 g of blank solution.

2.4.4. Chromatographic system and conditions

For static headspace sampling, a Perkin–Elmer (Waltham, MA, USA) Turbomatrix 40 HS autosampler was used. Headspace vials (22 ml) and high-temperature resistant silicone/PTFE caps were obtained from FilterService (Eupen, Belgium). Vials were thermostatted at 90 °C for 60 min. Needle and transfer line temperature were kept at 180 °C and 190 °C, respectively, to avoid carry-over. Following thermostatting, vials were pressurized to 150 kPa for 1.5 min. Finally, gas phase was injected for 0.04 min. The gas chromatograph used was a Delsi (Suresnes, France) DN200 equipped with an FID. The analytes of interest were separated on an AT™-Aquawax-DA column (30 m × 0.53 mm × 0.5 μm), purchased from Alltech (Lokeren, Belgium). Injector and detector temperatures were 200 °C and 250 °C, respectively. As carrier gas, helium 5.6 was used at a flow rate of 4.0 ml/min. The applied temperature program was as follows: first an initial temperature of 100 °C was set for 1 min, then the temperature was raised to 180 °C at a rate of 4 °C/min. The final temperature was held for 10 min.

2.5. Validation

Both the LC and sHS-GC method were validated according to the guidelines for assay methods of the International Conference on Harmonisation of Technical Requirements for Registration of Pharmaceuticals for Human Use (ICH) [26].

2.5.1. Specificity

For both methods, vials with blank sample solution were spiked with each reference compound separately to assess the retention times. Blank chromatograms were recorded to check for interfering matrix peaks. Finally, chromatograms of test solutions were reviewed for critical peak separations. Whenever appropriate, chromatographic resolution was calculated.

2.5.2. Linearity

With the LC method, linearity was investigated at 50%, 75%, 100%, 125% and 150% of the sample concentration. Reference solutions were prepared in the same manner as described in Section 2.2.2. Each concentration level was analyzed in triplicate. With the sHS-GC method, linearity was investigated at concentration levels of 25%, 50%, 75%, 100%, 125% and 150%. A reference solution containing camphor, l-menthol, MeS and ES was prepared in the same manner as mentioned in Section 2.4.3. In the vials, the required amounts of reference solution were weighed together with 1500 g of blank solution. Liquid paraffin was added to attain a total weight of 3000 g in all vials. Each concentration level was analyzed in quadruplicate.

2.5.3. Accuracy

For both methods, accuracy was established across the specified range at three concentration levels. The developed analytical procedures were applied to three self-made sticks containing all investigated analytes at concentration levels of 80%, 100% and 120%, respectively. Analyte recoveries were calculated by comparing the obtained analyte peak areas of the self-made sticks with the corresponding peak areas of the 100% reference solution. Six determinations (two per spiking level) were performed with the LC method, whereas nine determinations (three per spiking level) were performed with the sHS-GC method.

2.5.4. Precision

Precision of the methods was investigated at three levels: system repeatability, method precision and intermediate precision.

2.5.4.1. System repeatability. System repeatability was assessed by injecting each quantity level of the linearity investigation in triplicate (LC) or quadruplicate (sHS-GC). With LC, repeated injections were from the same vial while for sHS-GC, multiple vials were used, as the equilibrated gas phase of a vial can only be injected once.

2.5.4.2. Method precision. The method precision was calculated as the relative standard deviation of repeated accuracy determinations (LC: $n = 6$; sHS-GC: $n = 9$).

2.5.4.3. Intermediate precision. To evaluate intermediate precision, the complete analytical procedure was applied to one sample batch by 2 different analysts on 2 different days. A Student's *t*-test was applied to compare the mean values of both groups [27]. An *F* test was used to assess variance equivalence [27]; variances were grouped if not significantly different. A 95% confidence level was adopted throughout.

2.5.5. Matrix effect

For the sHS-GC method, the effect of the matrix was verified by analyzing two groups, each consisting of four reference vials. In addition to 1500 g of reference solution, one group contained 1500 g of blank solution, whereas the other group contained 1500 g of pure liquid paraffin. An *F*-test was used to test variance equivalence and a Student's *t*-test was applied to compare the mean values of both groups (see above).

2.6. Assay procedure applied to real samples

For each sample batch, two independent sample and reference solutions were prepared as described for the respective analysis methods (see Sections 2.2 and 2.4). Solutions were analyzed in triplicate with LC and in quadruplicate with sHS-GC. As a final result, the mean contents of the two independent determinations were calculated.

3. Results and discussion

3.1. Method optimization

3.1.1. Liquid–liquid extraction–liquid chromatography

Compared to the initial procedure of Kaale et al. [12], the ratio methanol–water of the extraction solvent was changed from 80:20 to 60:40, v/v, to improve the peak shape. Four extractions instead of three were necessary to obtain complete yields for the capsaicinoids. The feasibility of analyzing camphor, MeS and ES with the same LLE-LC method was investigated. Although all those compounds were separated on the LC column, none of them could be fully extracted from the cutaneous stick. Moreover, camphor exhibited very weak UV absorbance. Therefore, it was decided to determine these compounds with sHS-GC, together with l-menthol. As regards the mobile phase used with LC, the small acetonitrile content was omitted as it was not critical for the separation. Acetic acid was replaced by phosphoric acid to improve the separation between GMS and SA. Finally, a gradient elution program was applied to improve the peak shape of DHCP and to shorten analysis time. LC reference and sample solutions were found to be stable for at least 48 h when stored in a closed container at room temperature.

3.1.2. Static headspace-gas chromatography

Commonly used solvents for sHS-GC in pharmaceutical analysis such as water, *N*,*N*-dimethylformamide or *N*,*N*-dimethyl sulfoxide could not be used because the formulation is not soluble in these solvents. Liquid paraffin was selected as suitable alternative owing to miscibility with the sample and low vapor pressure. Headspace parameters were set to values yielding complete equilibration in the vial, repeatable injections and good peak shapes. Needle and transferline temperatures were set to high values to avoid carry-over. GC reference and sample solutions were found to be stable for at least 48 h when stored in a closed container at room temperature.

3.2. Unknown capsaicinoid identification with LC–MS

In both the LC chromatograms of the reference and sample solution, the peak with a retention time of 26.6 min was suspected to be NDHCP (see Fig. 1). Identity confirmation is essential as the peak area of NDHCP needs to be taken into account for calculation of the content [28]. Due to the lack of NDHCP reference substance, the peak was identified using LC–MS. The CP reference solution used for tuning was further investigated by MS/MS. The MS settings were those of the method reported by Schweiggert et al. [29].

ESI analysis of capsaicin resulted in a protonated molecule $[M+H]^+$ at m/z 306.0. MS/MS investigation of the precursor ion gave product ions with m/z 137.2, 170.1 and 182.1. The unknown was characterised by comparison of its fragmentation pattern with that of capsaicin. ESI analysis of the unknown resulted in a protonated molecule $[M+H]^+$ at m/z 294.0. MS/MS investigation of the precursor ion gave product ions with m/z 137.2, 158.2 and 170.1. The obtained mass spectra and literature derived [29,30] fragmentation patterns of CP reference and NDHCP are shown in Fig. 2. The unknown was confirmed to be NDHCP.

3.3. Validation

3.3.1. Specificity

Representative chromatograms of the test solution for both methods are shown in Fig. 1. With the LC method, all three compounds of interest were well separated. Retention times for GMS, SA, NDHCP, CP and DHCP were 8.0 min, 9.6 min, 26.6 min, 28.1 min and 36.9 min, respectively. Critical peak separations are those between GMS and SA and between NDHCP and CP, with resolutions (calculated according to Ph. Eur.) of 2.9 and 2.7, respectively. Other active compounds or excipients did not interfere with the analytes of interest. The four compounds determined with sHS-GC were also well separated. The retention times of camphor, l-menthol, MeS and ES were 8.6 min, 10.9 min, 14.7 min and 15.4 min, respectively. There were no critical peak separations. Furthermore, the dilution solvent liquid paraffin did not give rise to interfering solvent or matrix peaks.

3.3.2. Matrix effect

A test for detection of matrix effect in sHS-GC was carried out (see Section 2.5.5). First, an *F*-test was applied to assess equivalence of the variances. For none of the compounds, a significant difference between variances was found. Consequently, variances were pooled for the Student's *t*-test. A Student's *t*-test was applied to check for statistically significant differences between the two groups of obtained peak areas. The results are shown in Table 1. A significant matrix effect was detected for camphor and l-menthol, whereas no matrix effect was seen for MeS and ES. Hence, for all validation and assay procedures blank solution was added to the vials containing reference solution to mimic the sample matrix.

3.3.3. Linearity

Both methods showed a good linear relationship for all compounds over their respective ranges, defined in Section 2.5.2. Equations and regression data as requested by ICH are presented in Table 2. Determination coefficients were >0.996 for all analytes investigated.

3.3.4. Accuracy

Recovery results obtained for all compounds are shown in Table 3. For the sHS-GC method, the complete accuracy procedure was repeated thrice, while for the LC method this was only done in duplicate because of better system repeatability (see Section 3.3.5.1 below). According to the European Pharmacopoeia method for the analysis of *Capsicum* oleoresins, the sum of the peak areas of CP, DHCP and NDHCP was taken into account [28]. For all compounds, mean recovery values were between 98% and 102%. LC and sHS-GC single recovery values ranged from 97.7% to 103.0%, and from 96.0% to 108.0%, respectively.

3.3.5. Precision

3.3.5.1. System repeatability. Relative standard deviations (RSD %) of the obtained peak areas for each compound at all concentration

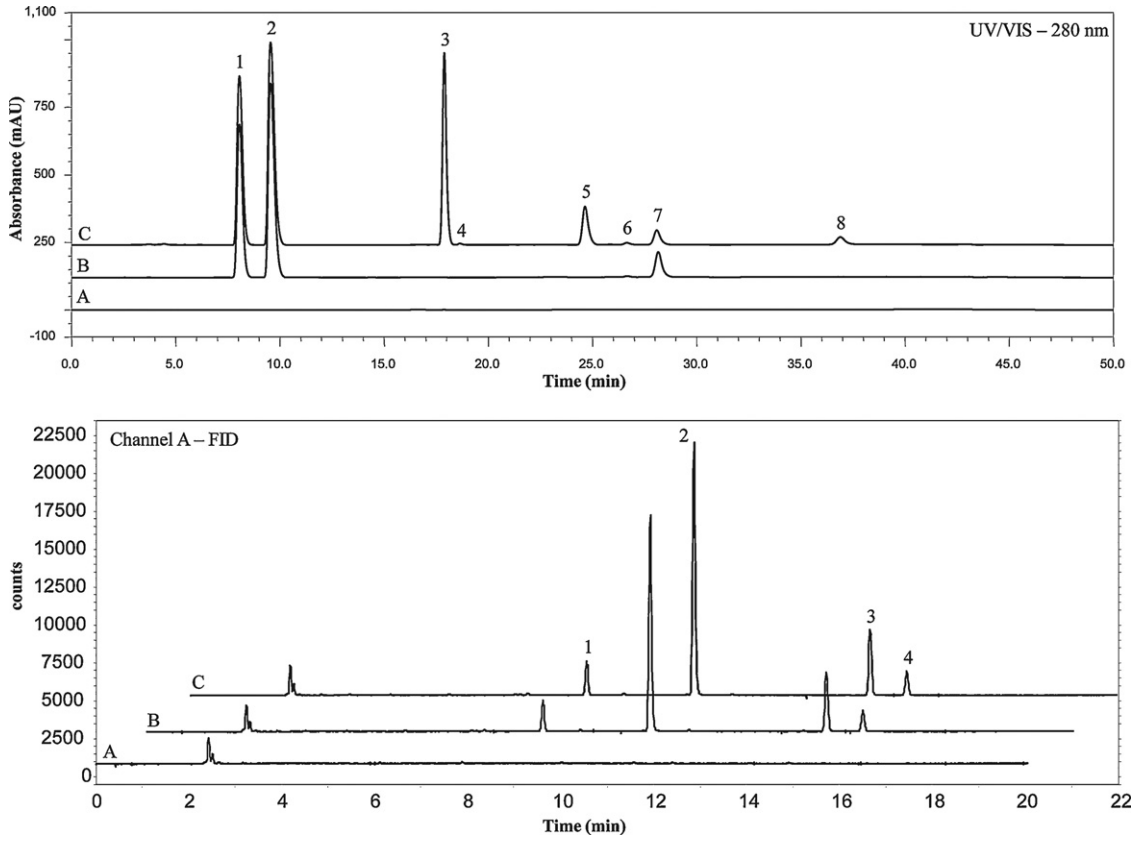

Fig. 1. Representative chromatograms of LC (top) and sHS-GC (bottom). A: blank solution; B: reference solution used for quantification; C: sample solution. Peak identification in LC: (1) glycol monosalicylate, (2) salicylic acid, (3) methyl salicylate, (4) camphor, (5) ethyl salicylate, (6) nordihydrocapsaicin, (7) capsaicin, (8) dihydrocapsaicin. Peak identification in sHS-GC: (1) camphor, (2) l-menthol, (3) methyl salicylate, (4) ethyl salicylate.

levels are reported in Table 4. For the compounds determined with LC, all RSD values were ≤1.5%, whereas for the compounds determined with sHS-GC, all RSD values were ≤5.3%. These values meet the generally accepted criteria for the respective techniques.

3.3.5.2. Method precision. Method precision was evaluated by calculating the RSD of the obtained recovery values for accuracy (Table 2). For the LC method, RSD values of the six determinations were 1.5% for SA, 1.5% for GMS and 1.8% for CP. With

Table 1
Test for matrix effect with the sHS-GC method. Group 1 vials contained matrix while Group 2 vials were without matrix.

	Camphor		l-Menthol		MeS		ES	
	Group 1	Group 2	Group 1	Group 2	Group 1	Group 2	Group 1	Group 2
Mean peak area[a]	26,100	24,876	214,738	206,392	62,834	63,189	23,404	23,716
s	285.4	223.4	2534.9	1472.4	659.6	1726.7	247.4	361.6
s^2	81,445	49,925	6.43E+06	2.17E+06	435,053	2.98E+06	61,189	130,738
$F(s_a^2/s_b^2; a>b)$	1.63		2.96		6.85		2.14	
$F_{critical}$	9.23		9.23		9.23		9.23	
df	6		6		6		6	
$t_{calculated}$	6.75		5.69		0.38		1.42	
$t_{critical}$[b]	2.45		2.45		2.45		2.45	

s, standard deviation; s^2, variance; df, degrees of freedom.
[a] $n=4$.
[b] 95% Confidence level.

Table 2
Regression analysis for all compounds.

	SA	GMS	CP	Camphor	l-Menthol	MeS	ES
R^2	0.9998	0.9997	0.9966	0.9999	0.9992	0.9983	0.9974
Slope[a]	2.43 ± 0.07	1.70 ± 0.06	0.31 ± 0.03	165.3 ± 2.70	1481 ± 58.2	406.6 ± 23.3	158.5 ± 11.1
Intercept[a]	8.25 ± 7.4	5.19 ± 6.0	2.25 ± 3.4	−462.2 ± 263	−2569 ± 5662	−535.9 ± 2268	−806.6 ± 1085
RSS[b]	8.85	5.91	1.90	4.15E+04	1.92E+07	3.08E+06	7.04E+05
$S_{y,x}$[c]	1.72	1.40	0.80	102	2190	878	420

[a] Mean ± 95% confidence interval.
[b] Residual sum of squares.
[c] Standard error of regression.

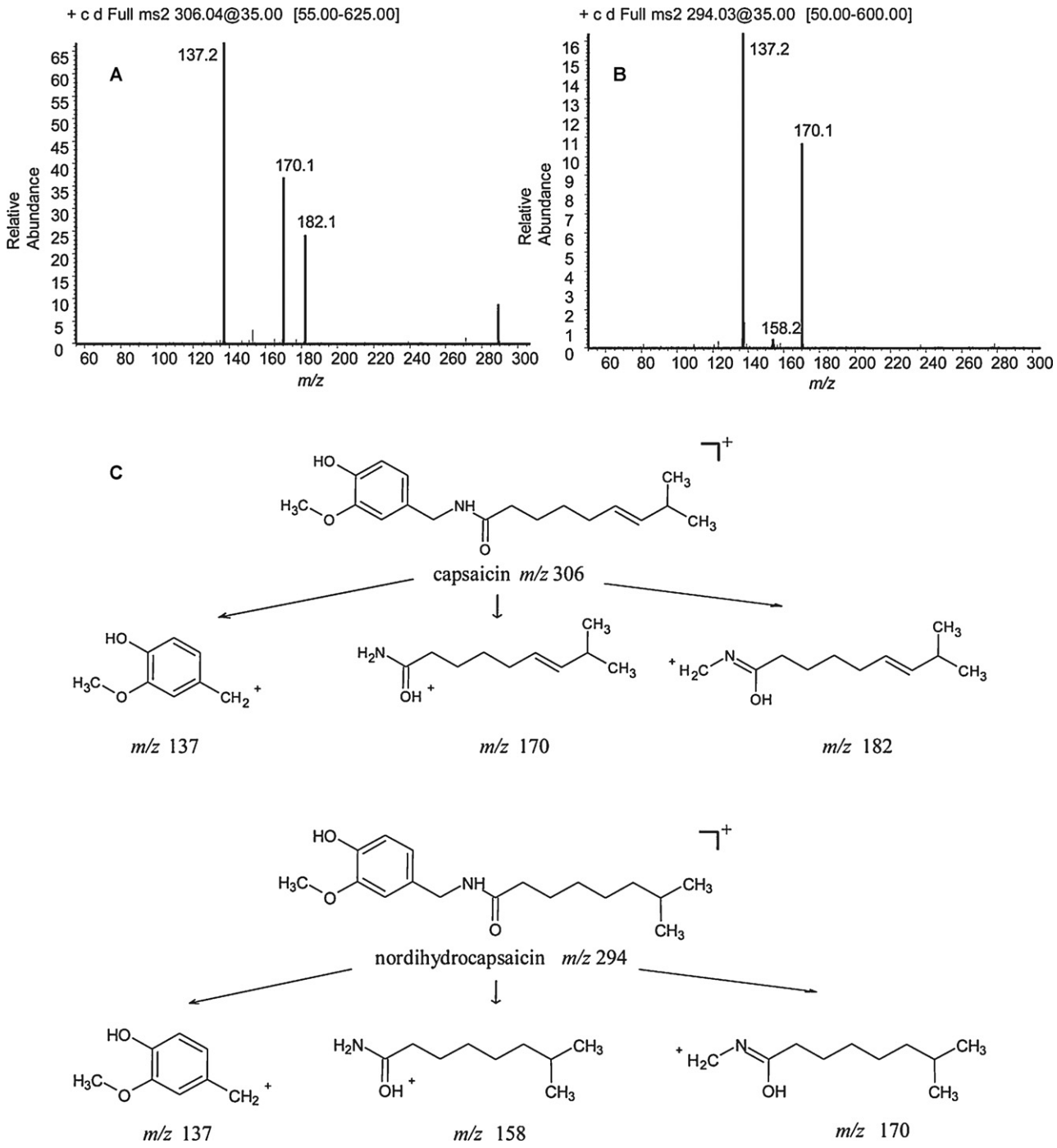

Fig. 2. Identity confirmation of nordihydrocapsaicin with LC–MS/MS. A: Mass spectrum of capsaicin reference substance. B: Mass spectrum of the unknown. C: proposed fragmentation pattern of capsaicin and nordihydrocapsaicin [29,30].

the sHS-GC method, RSD values of the nine determinations were 3.0% for camphor, 3.2% for l-menthol, 2.7% for MeS and 2.3% for ES.

3.3.5.3. Intermediate precision. A complete assay procedure, including duplicate sample preparation, was carried out by two different analysts on two different days. The results are shown in Table 5. A significant difference between variances was found for GMS and SA, so no pooling was done for the *t*-test for these compounds. A Student's *t*-test was applied on both groups of results to check for significant differences of the mean values. No significant differences of the means were found at the 95% confidence level except for CP (99.5% confidence) and camphor (99.8% confidence).

3.4. Application of the method

Three different batches of the formulation were analyzed according to the described assay method (Section 2.6). Table 6 summarizes the content of each compound with respect to the labeled concentrations and the respective standard deviation values. All contents were within the desired range of 90% to 110%. This range is acceptable as certain (volatile) active compounds are somewhat overdosed to compensate for their possible loss during

Table 3
Recovery results for each compound. Results are expressed as % recovery with respect to the known spiked amount.

Quantity level	GMS	SA	CP	Camphor	l-Menthol	MeS	ES
80%	98.6	98.1	99.0	98.2	100.0	98.0	99.9
	102.5	101.9	102.3	102.3	104.6	101.5	105.5
				106.4	108.0	106.3	101.5
100%	102.2	101.4	100.8	99.6	101.7	100.6	101.5
	103.0	102.1	101.0	98.6	100.0	97.9	100.7
				101.2	99.9	102.4	97.7
120%	101.7	101.1	98.2	96.0	97.7	97.8	99.8
	101.6	100.9	97.7	98.4	99.1	99.5	103.0
				99.2	98.9	100.8	98.9
Mean	101.6	100.9	99.8	100.0	101.1	100.5	100.9
RSD[a] (%)	1.5	1.5	1.8	3.0	3.2	2.7	2.3

[a] $n = 6$ for LC and $n = 9$ for sHS-GC.

Table 4
System repeatability results expressed as relative standard deviations (RSD %) of the peak areas obtained with replicate injections at each concentration level of the linearity investigation.

Quantity level	SA	GMS	CP	Camphor	l-Menthol	MeS	ES
25%	–	–	–	2.4	1.6	1.5	2.6
50%	0.2	0.3	0.2	1.9	1.6	2.4	4.9
75%	0.2	0.1	0.1	2.0	2.4	3.1	5.3
100%	0.5	0.6	0.5	3.1	3.1	3.4	3.9
125%	1.5	1.5	1.5	1.7	2.6	2.0	4.4
150%	1.0	1.0	1.0	1.4	1.3	3.5	1.4

Table 5
Intermediate precision. The mean values are the final contents with respect to the labeled concentrations of each compound found by analyst A and B, respectively ($n = 6$ for LC and $n = 8$ for sHS-GC).

	GMS		SA		CP		Camphor		l-Menthol		MeS		ES	
	A	B	A	B	A	B	A	B	A	B	A	B	A	B
Mean (%)	99.8	100.8	96.6	96.6	96.1	93.8	113.4	108.8	106.1	105.6	108.5	110.1	111.6	113.0
s (%)	0.39	1.04	0.38	1.33	1.40	1.02	2.70	2.60	1.43	2.14	1.79	2.60	1.85	2.79
s^2	0.15	1.09	0.14	1.78	1.95	1.04	7.29	6.75	2.05	4.58	3.19	6.77	3.44	7.77
$F(s_a^2/s_b^2; a>b)$	7.22		12.53		1.87		1.08		2.23		2.13		2.26	
$F_{critical}$	7.15		7.15		7.15		4.99		4.99		4.99		4.99	
df	6		6		10		14		14		14		14	
$t_{calculated}$	2.20		0.00		3.36		3.46		0.60		1.45		1.14	
$t_{critical}$	2.45[a]		2.45[a]		3.58[b]		3.79[c]		2.15[a]		2.15[a]		2.15[a]	

s, standard deviation; s^2, variance; df, degrees of freedom.
[a] 95% confidence level.
[b] 99.5% confidence level.
[c] 99.8% confidence level.

Table 6
Method application on three different batches of the topical formulation. The reported values are mean % contents with respect to the labeled concentrations together with the standard deviations.

Batch	GMS	SA	CP	Camphor	l-Menthol	MeS	ES
1	104.0 ± 0.1	100.3 ± 0.2	101.7 ± 0.8	100.9 ± 0.7	99.4 ± 0.8	103.0 ± 0.7	106.7 ± 0.8
2	101.6 ± 0.8	98.9 ± 0.6	96.5 ± 2.2	109.0 ± 1.5	107.5 ± 1.0	105.1 ± 4.1	109.5 ± 2.7
3	102.5 ± 0.1	99.2 ± 0.4	93.6 ± 0.4	99.8 ± 2.3	103.4 ± 2.9	93.2 ± 3.3	101.0 ± 3.9

the manufacturing process which involves heating of the mixture of ingredients.

4. Conclusion

An LC and an sHS-GC method for the assay of all active compounds in a cutaneous stick were successfully optimized and validated. All compounds were well separated with no interference of matrix peaks. The methods showed acceptable linearity, precision and accuracy. Although two methods need to be employed, there are several advantages. First, complex extraction procedures to recover all analytes with acceptable yield are avoided. Second, alternative detection methods for camphor and l-menthol are not necessary. Finally, the use of sHS sampling with liquid paraffin as dilution matrix implies very little sample preparation, barely increasing total analysis time when carried out in parallel with LC.

References

[1] R. Gamse, A. Wax, R.E. Zigmond, S.E. Leeman, Immunoreactive substance-P in sympathetic-ganglia - distribution and sensitivity towards capsaicin, Neuroscience 6 (1981) 437–441.
[2] A.A. Gbolade, O.R. Omobuwajo, R.O. Soremekun, Evaluation of the quality of Nigerian chillies for pharmaceutical formulations, J. Pharm. Biomed. Anal. 15 (1997) 545–548.
[3] A. Patapoutian, S. Tate, C.J. Woolf, Transient receptor potential channels: targeting pain at the source, Nat. Rev. Drug Discovery 8 (2009) 55–68.
[4] P.A. Mackowiak, Brief history of antipyretic therapy, Clin. Infect. Dis. 31 (2000) S154–S156.

[5] L. Mason, R.A. Moore, J.E. Edwards, H.J. McQuay, S. Derry, P.J. Wiffen, Systematic review of topical rubefacients containing salicylates for the treatment of acute and chronic pain, Br. Med. J. 328 (2004) 995–997.
[6] H.X. Xu, N.T. Blair, D.E. Clapham, Camphor activates and strongly desensitizes the transient receptor potential vanilloid subtype 1 channel in a vanilloid-independent mechanism, J. Neurosci. 25 (2005) 8924–8937.
[7] Y. Karashima, N. Damann, J. Prenen, K. Talavera, A. Segal, T. Voets, B. Nilius, Bimodal action of menthol on the transient receptor potential channel TRPA1, J. Neurosci. 27 (2007) 9874–9884.
[8] A. Pena-Alvarez, E. Ramirez-Maya, L.A. Alvarado-Suarez, Analysis of capsaicin and dihydrocapsaicin in peppers and pepper sauces by solid phase microextraction–gas chromatography–mass spectrometry, J. Chromatogr. A 1216 (2009) 2843–2847.
[9] A. Garces-Claver, M.S. Arnedo-Andres, J. Abadia, R. Gil-Ortega, A. Alvarez-Fernandez, Determination of capsaicin and dihydrocapsaicin in Capsicum fruits by liquid chromatography-electrospray/time-of-flight mass spectrometry, J. Agric. Food Chem. 54 (2006) 9303–9311.
[10] A. Laskaridou-Monnerville, Determination of capsaicin and dihydrocapsaicin my micellar electrokinetic capillary chromatography and its application to various species of Capsicum, Solanaceae, J. Chromatogr. A 838 (1999) 293–302.
[11] G. Jeon, J. Lee, Comparison of extraction procedures for the determination of capsaicinoids in peppers, Food Sci. Biotechnol. 18 (2009) 1515–1518.
[12] E. Kaale, A. Van Schepdael, E. Roets, J. Hoogmartens, Determination of capsaicinoids in topical cream by liquid–liquid extraction and liquid chromatography, J. Pharm. Biomed. Anal. 30 (2002) 1331–1337.
[13] E. Mikami, T. Goto, T. Ohno, H. Matsumoto, M. Nishida, Simultaneous analysis of dehydroacetic acid, benzoic acid, sorbic acid and salicylic acid in cosmetic products by solid-phase extraction and high performance liquid chromatography, J. Pharm. Biomed. Anal. 28 (2002) 261–267.
[14] M.S. Shou, W.A. Galinada, Y.C. Wei, Q.L. Tang, R.J. Markovich, A.M. Rustum, Development and validation of a stability-indicating HPLC method for simultaneous determination of salicylic acid, betamethasone dipropionate in their related compounds in Diprosalic lotion (R), J. Pharm. Biomed. Anal. 50 (2009) 356–361.
[15] T.R.M. De Beer, W.G. Baeyens, Y. Vander Heyden, J.P. Remon, C. Vervaet, F. Verpoort, Influence of particle size on the quantitative determination of salicylic acid in a pharmaceutical ointment using FT-Raman spectroscopy, Eur. J. Pharm. Sci. 30 (2007) 229–235.
[16] B.W. Glombitza, P.C. Schmidt, Comparison of 3 new spectrophotometric methods for simultaneous determination of aspirin and salicylic acid in tablets without separation of pharmaceutical excipients, J. Pharm. Sci. 83 (1994) 751–757.
[17] M.R. Sohrabi, M. Davallo, F. Tadayyon, F. Nabipoor, A. Khamneifar, Simultaneous determination of acetyl salicylic acid and acetaminophen in acetaminophen-caffeine-aspirin (ACA) tablets by FT-IR/ATR spectrometry with multivariate calibration data treatment, Asian J. Chem. 17 (2005) 541–547.
[18] H.S.I. Tan, P.A. Kemper, P.E. Padron, Gas–liquid-chromatographic assay of mixtures of camphor, menthol, and methyl salicylate in ointments, J. Chromatogr. 238 (1982) 241–246.
[19] S.K. Pant, P.N. Gupta, K.M. Thomas, B.K. Maitin, C.L. Jain, Simultaneous determination of camphor, menthol, methyl salicylate, and thymol in analgesic ointments by gas–liquid-chromatography, LC–GC 8 (1990) 322–325.
[20] J.P. Sapio, K. Sethachutkul, J.E. Moody, Simultaneous GLC-determination of methyl salicylate and menthol in a topical analgesic formulation, J. Pharm. Sci. 68 (1979) 506–508.
[21] Y. Sitaramaraju, A. Van Hul, K. Wolfs, A. Van Schepdael, J. Hoogmartens, E. Adams, Static headspace gas chromatography of (semi-)volatile drugs in pharmaceuticals for topical use, J. Pharm. Biomed. Anal. 47 (2008) 834–840.
[22] M. Spichiger, R.C. Muhlbauer, R. Brenneisen, Determination of menthol in plasma and urine of rats and humans by headspace solid phase microextraction and gas chromatography-mass spectrometry, J. Chromatogr. B 799 (2004) 111–117.
[23] K. Schulz, M. Bertau, K. Schlenz, S. Malt, J. Dressler, D.W. Lachenmeier, Headspace solid-phase microextraction-gas chromatography–mass spectrometry determination of the characteristic flavourings menthone, isomenthone, neomenthol and menthol in serum samples with and without enzymatic cleavage to validate post-offence alcohol drinking claims, Anal. Chim. Acta 646 (2009) 128–140.
[24] M. Ligor, B. Buszewski, Determination of menthol and menthone in food and pharmaceutical products by solid-phase microextraction-gas chromatography, J. Chromatogr. A 847 (1999) 161–169.
[25] B. Kolb, L.S. Ettre, Static Headspace - Gas Chromatography: Theory and Practice, 2nd ed., Wiley-VCH, Weinheim, 1997.
[26] International Conference on Harmonisation of Technical Requirements for Registration of Pharmaceuticals for Human Use: Q2(R1): Validation of Analytical Procedures: Text and Methodology, Geneva, 1994.
[27] D.C. Harris, Quantitative Chemical Analysis, 7th ed., W.H. Freeman and Company, New York, 2007.
[28] Monograph 2336: capsicum oleoresin, in: European Pharmacopoeia, 6th ed., European Department for the Quality of Medicines, Strasbourg, 2010, pp. 1405–1406.
[29] U. Schweiggert, R. Carle, A. Schieber, Characterization of major and minor capsaicinoids and related compounds in chili pods (Capsicum frutescens L.) by high-performance liquid chromatography/atmospheric pressure chemical ionization mass spectrometry, Anal. Chim. Acta 557 (2006) 236–244.
[30] F. Beaudry, P. Vachon, Quantitative determination of capsaicin, a transient receptor potential channel vanilloid 1 agonist, by liquid chromatography quadrupole ion trap mass spectrometry: evaluation of in vitro metabolic stability, Biomed. Chromatogr. 23 (2009) 204–211.

Journal of Pharmaceutical and Biomedical Analysis 60 (2012) 59–64

Contents lists available at SciVerse ScienceDirect

Journal of Pharmaceutical and Biomedical Analysis

journal homepage: www.elsevier.com/locate/jpba

Enhancing sensitivity and precision on NIR reflectance determination of an API at low concentration: Application to an hormonal preparation

J. Arruabarrena, J. Coello, S. Maspoch*

Departament de Química, Unitat de Química Analítica, Universitat Autònoma de Barcelona, E-08193 Bellaterra, Barcelona, Spain

ARTICLE INFO

Article history:
Received 19 May 2011
Received in revised form 21 October 2011
Accepted 24 October 2011
Available online 29 October 2011

Keywords:
NIR reflectance
Precision
Scattering
Hormone
Sensitivity

ABSTRACT

The use of a mixed calibration sample set (intact production tablets and powdered doped samples used to enlarge calibration range) is a usual procedure for the NIR reflectance determination of the API content of a pharmaceutical solid preparation. However, the high difference in scattering properties and the intrinsic low sensitivity of NIR make difficult the achievement of a good precision when API is at a low mass proportion (≈1%, w/w). The compression of the calibration powdered samples has been studied as a very simple procedure to enhance the sensitivity of NIR reflectance measurements and, consequently, to improve precision. Different pretreatments (SNV, 1D, 2D and their combinations) have been applied to reduce the spectral difference between powdered and compressed samples. Although none eliminates completely this difference, the combined pretreatment SNV + 2D has proved to be the one with a better performance. Results obtained by using both calibration sample sets (powdered and compacted) in the quantification of estradiol valerate (VE, 2 mg/tablet, ≈1.6%, w/w) and medroxyprogesterone (MPA, 10 mg, ≈8%, w/w) in intact tablets of the hormonal preparation show that a slight but significant improvement in precision is obtained when using compacted samples for calibration. A HPLC procedure was developed to be used as reference method.

1. Introduction

Near-Infrared Spectroscopy (NIRS) has become an essential technique on the process quality assurance of many industries, especially on pharmaceutical [1]. NIR spectroscopy has several advantages over classical analytical techniques: there is no residue generation, a very important fact in green chemistry era; any sample presentation is allowed [2,3], the result of the analysis can be obtained immediately (live control of a process can be performed, not only final product control) [4], it is a versatile technique that can be used to analyze many different sample forms (gels, powdered, tablets, ...), it can be used for the determination of both physical and chemical parameters [5,6], it is a fast and non-destructive technique, etc. Nevertheless, it is clear that its popularity as analytical tool in the pharmaceutical industry comes from the possibility of analyzing solid samples, powdered or intact tablets, just measuring their reflectance spectra or, in a less extent, the transmission ones.

There is not a global accepted theory describing the radiation absorption of a scattering material. The best known approach is the so called, Kubelka–Munck (K–M) function; Eq. (1). Recently, several authors have suggested new approaches [7] although the final equations are very similar and only the interpretation of the terms used changes slightly.

$$f(R) = \frac{1 - R_\infty}{2R_\infty} = \frac{K}{S} \quad (1)$$

In K–M function, the reflectance of an "infinite thick sample" (R_∞), i.e. the reflectance of a sample where transmittance can be neglected and considered null, is related to the ratio between two fundamental optical properties expressed as the absorption (K) and scattering (S) coefficients. Because of the practical and theoretical limitations of K–M approach [8] most analysts prefer to use a purely experimental approach, translating to reflectance the classical Beer–Lambert–Bourget's law; Eq. (2).

$$A_{\text{apparent},\lambda} = \log\frac{1}{R} = \log\frac{1}{R_{\text{sample}}/R_{\text{ref}}} = a_\lambda \cdot f \cdot c = k \cdot c \quad (2)$$

where the relative reflectance (R) is the ratio of the absolute reflectance of the sample (R_{sample}) and the reflectance of the reference (R_{ref}); a_λ is the term associated with the chemical information; f is the optical pathlength and c is the concentration. The expression can be summarized to $A_{\text{apparent},\lambda} = kC$, assuming the pathlength to be constant for different samples. However, this fact is almost never completely true since it depends, in a complex way, on the physical properties of the samples (refraction index, ratio between

* Corresponding author. Tel.: +34 935811011; fax: +34 935812379.
E-mail address: santiago.maspoch@uab.es (S. Maspoch).

0731-7085/$ – see front matter © 2011 Elsevier B.V. All rights reserved.
doi:10.1016/j.jpba.2011.10.026

wavelength and particle size, compressing degree, sample surface, particle distribution...). Hence, small changes in the proportional constant k, have to be expected from sample to sample. These changes are usually referred as "changes in scattering" and are mainly visualized as a spectral baseline shift or drift. If the scattering can be considered constant for different samples, the apparent absorbance ($\log 1/R$) can be linearly related to the concentration of the analyte. Since it is rather difficult in practice, several spectral pretreatments (derivatives, Standard Normal Variate...) are usually applied to reduce these variations [9] and improve the calibration/prediction performances.

A stable calibration model requires to be developed on a wide range of the independent variable (i.e. concentration range of the analyte). This is a very serious problem in many industrial applications and especially in pharmaceutical analysis, where samples have a very narrow concentration interval around the nominal value due to their very reproducible production.

It is clear that the best procedure to prepare calibration samples with the physical properties of the commercial ones would be to produce the calibration samples exactly as the commercial are prepared (i.e. in the production or at least in a pilot plant). However, this procedure is very expensive and has only been exceptionally used [10]. A classical approach is the preparation of calibration samples in the analytical laboratory mixing the ingredients (active pharmaceutical ingredient [API] and excipients) in different proportions. In order to introduce the physical characteristics and the variability of the commercial preparation into the calibration model, several tablets from different production batches are included in the calibration set, just producing a mixed sample set (powdered samples to extend concentration range plus tablets to introduce production variability) [11]. A slightly different approach is to grind some production tablets and to over and under-dose by adding a known amount of API or a mixture of excipients, following a prefixed design to reduce collinearity. Since the powder from ground tablets still retains some of the production physical properties, this approach produces a calibration set much more similar to the production samples that the previous one [12]. However, as production samples have been employed, a reference method to quantify the actual content of API must be used.

NIRS sensitivity is not very high and the precise quantification of an API content at a mass proportion of about 1% (w/w) can be troublesome [13,14]. In these cases, the selection and preparation of samples must be carried out following a very precise methodology and the traditional ways do not seem to be the best ones to achieve the required sensitivity and precision. A reasonably approach is to reduce the noise in the calibration sample set minimizing the scattering differences between samples.

A powdered sample presents a higher scattering than a compressed one [15]. This is a problem in quantifying low content tablets, because the "effective pathlength" is smaller and consequently the sensitivity decreases.

The aim of this work is to report a NIR reflectance procedure to quantify the API content in a commercial hormone preparation (Perifem) which contains two APIs: medroxyprogesterone acetate (MPA) (at a mass proportion of aprox. 8%, w/w) and estradiol valerate (VE) (at a mass proportion of aprox. 1.6%, w/w). Since we know, these analytes have not been previously determined by a NIR procedure.

Two procedures to prepare the calibration sample set are assayed and compared. The first one is the above described mixed procedure of over- under-dosed powdered samples with intact commercial tablets. In a second one, these powdered samples are compressed by using a typical laboratory press to produce what is named "compressed calibration samples". Also several spectral pretreatments commonly used to reduce scattering are assayed and the results compared.

2. Materials and methods

2.1. Instruments and software

Near infrared spectra were recorded on a NIRSystems 5000 spectrophotometer (FOSS, NIRSystems, MN, USA) equipped with a Rapid-Content Analyzer (RCA) module. HPLC reference method was performed by using an Agilent 1100 (Santa Clara, CA, USA), coupled to a G1315B DAD detector (λ = 280 nm) and a 25 cm long, 4.6 mm internal diameter SymmetryShield RP18 column. UV–Vis spectra of pure active compounds were acquired on a Hewlett-Packard (Waldbrom, Germany) 8453A spectrophotometer. A Turbula T2C shaker mixer from WAB (Basel, Switzerland) was used for blending doped samples. Laboratory compressed tablets were prepared on a Perkin-Elmer 15.001 (Waltham, MA, USA) press, with a cross-section of 132.7 mm^2. Multivariate models were built up with the aid of Unscrambler X (Trondheim, Norway).

2.2. Production samples

Perifem® (Organon, Barcelona, Spain) samples from three different batches were directly purchased in different pharmaceutical stores. Each box contains a total of 21 uncoated pills, 11 of them colored in white and 10 in blue. Label claim for APIs are 2 mg of estradiol valerate (VE) in white pills and 2 mg of VE and 10 mg of medroxyprogesterone acetate (MPA) in the blue ones, which represents a mass proportion of approximately 1.6% and 8%, respectively. Corn starch and lactose monohydrate are used in both cases as major excipients together with other minor excipients.

2.3. Laboratory samples

Under and over dosing of powdered production samples was used to enlarge the APIs concentration range from 75% to the 125% of the nominal concentration. In order to minimize the correlation between APIs and excipients, three different mixtures of the two major excipients were prepared (3:1, 1:1, 1:3, w/w). Three different samples were prepared at each concentration level (75, 88, 112 and 125% (w/w) of the nominal value) with each excipient mixture. Since blue pills contain two active compounds, the calibration sample set was prepared independently to each one, maintaining the second API at the nominal value. Other seven samples with different concentrations inside the calibration range were also prepared to be used as validation samples (in each calibration set).

The shaking time needed to reach sample homogenization was studied. Known amounts of powdered production samples and lactose monohydrate were introduced into the turbula shaker and were shaken for a total time of 40 min; an NIR spectrum was recorded every 5 min and the root mean squared difference between successive spectra was computed. The minimum was reached between 20 and 25 min. Hence, a shaking time of 22 min was established for the preparation of all laboratory samples.

2.4. NIR procedure

The goal was to record the spectrum of the same sample in two different solid presentations: compressed and powdered. Hence, powdered production samples were mixed with active compounds and/or excipients to over and under dose the samples following the design described above. After homogenization, every sample was poured into a 10 mm internal diameter glass Petri plate and the NIR spectrum acquired. Immediately, 300 mg of the powdered mixture was compressed to 739 MPa and the NIR spectrum of the tablet recorded. Previously, the amount of powder necessary to ensure that the thickness of compressed tablet was enough to avoid light transmission had been evaluated and estimated to be

Table 1
Effect of the spectral pretreatment in the difference between powdered and compressed spectra, computed according to Eq. (2). b_i refers to the differences between powdered and compressed spectra of a sample. B_m is a measure of instrumental reproducibility.

	Abs	SNV	1D[a]	2D[b]	2D + SNV[c]	SNV + 2D[b]
b_1	583.5	59.8	58.5	56.9	24.4	22.4
b_2	1184.9	60.9	57.1	79.0	41.1	31.9
b_3	173.0	74.0	60.1	87.2	31.0	35.7
b_4	160.7	69.2	61.4	111.3	55.6	45.0
b_5	638.1	31.1	117.5	79.2	20.2	32.0
B_m	0.4	4.5	25.9	6.2	10.5	6.2

Wavelengths removed from calculation (see text).
[a] 1314 nm and 1432 nm.
[b] 1314, 1432 and 1528 nm.
[c] 1164, 1314, 1460 and 1528 nm.

around 250 mg. Given the press diameter, 2.5 mm thick tablets were produced. Measurements were made on diffuse reflectance mode, using the RCA module. The spectrum of each sample, in the 1100–2500 nm range, was recorded three times as the average of 32 automatic scans; the powder was removed between each recording and the tablet rotated. The average spectrum was computed and used in following calculations.

Following the same procedure, the spectra of 37 production intact tablets (20 white and 17 blue) were acquired and the APIs content determined by HPLC. These spectra were split up in calibration and validation sets. For that purpose a PCA was computed and calibration samples selected in order to cover the maximum of variability.

2.5. HPLC reference method

The reference method was developed from a previous work [16] just changing acetonitrile by methanol and increasing the proportion of organic solvent in the mobile phase to obtain acceptable retention times. The final chromatographic conditions were: (a) NH_4NO_3 (pH 5.7 ± 0.1; 0.07 M)–MeOH (10:90, v/v) mobile phase. (b) An elution temperature of 25 °C (the column was introduced into thermostatized chamber). (c) λ = 280 nm. (d) 20 μL injection volume. Under these conditions MPA's retention time was 3.2 min and VE's retention time was 7.4 min. All solutions were filtered through a nylon membrane (0.45 mm).

2.6. Quantification

Six different calibration models were developed, one for each active compound, kind of tablet and sample presentation. PLS1 algorithm, constructed by leave-one-out cross-validation procedure was used in all cases. For each wavelength range, the number of latent factors was chosen as the lowest producing a Standard Error of Calibration (SEC) close to 1% of the average analyte concentration (value chosen as an approximate value of the precision of the reference values) and a slope and intercept of the found vs reference plot close to one and zero, respectively.

3. Results and discussion

The very different scattering properties of the intact production samples and the powdered doped samples used to enlarge the calibration range is one of the inherent problems involved in using a mixed calibration sample set. That can be overcome by powdering the commercial product, but reduces considerably the sampling throughout and makes difficult its application in quality control of production batches. A method, to be really applicable, must analyze the samples with the minimum pretreatment, and ideally without any. Taken this into account, mixed (intact production-powdered dosed samples) were already proposed some years ago [12,17]. However, when the API contribution to the sample spectra is low, because of a low content or a low absorptivity, and since the sensitivity of NIR is not very high, a precise determination may become troublesome. In order to increase the precision, we have evaluated different spectral pretreatments to find which one better reduces the scattering differences between powdered and compressed samples; also, we have studied the effect of compressing powdered calibration samples with a usual press that can be found in many laboratories. The underlying hypothesis is that the compression of calibration samples would decrease the scattering differences between production and calibration samples and that this should drive to a slight increase of the effective optical path. As a result, an enhancing of precision should be expected.

3.1. Effect of spectral pretreatments

To evaluate the capability of different pretreatments to remove the spectral differences due to the physical presentation (i.e. the scattering properties), several production samples were powdered, the NIR spectrum of the powder was acquired, then compressed and finally the NIR spectra of the samples were acquired again. Hence, the spectra of the "same" (understood as same chemical composition) sample in the two different physical forms were obtained. That procedure was repeated five times.

The first parameter used to evaluate similarity between spectra was the correlation coefficient, but the correlation was very high in all cases. Furthermore, this parameter measures the similarity between spectral profiles, but does not reflect "quantitative" information between spectra with the same profile but different intensity. This quantitative information was obtained from the sum of the squared relative differences at every wavelength Eq. (3), which is used to compute the b value of each sample. In order to have a target value to be used as a comparative reference of the lowest value that can be expected after each pretreatment, a similar parameter was computed, B_m (according to Eq. (4)) just comparing the differences in spectra for the same sample in different days. In fact, B_m was computed as the mean value of five production samples. These samples were stored in a desiccator before and between spectral acquisitions to prevent alterations of spectra due to humidity absorption. The results showed (Table 1) that any pretreatment made the spectra of powdered and compressed samples exactly identical and that SNV + 2D is the pretreatment that minimizes the differences, although 2D + SNV performed in a very similar way. It must be noted that derivatives transform some signal values to near 0, which can have a wicked effect on the quotient. Consequently, some wavelength (as indicated in Table 1) should be taken out. It was surprising that the B_m value for SNV spectra was higher than the B_m for the raw data. This can be explained by the presence of broad spectral ranges with signal values near 0. In those intervals, quotient's values $((X_{\text{day 1}}^{\text{production}} - X_{\text{day 2}}^{\text{production}})/X_{\text{day 1}}^{\text{production}})$ were clearly higher than average. Since it is an artifact produced by the

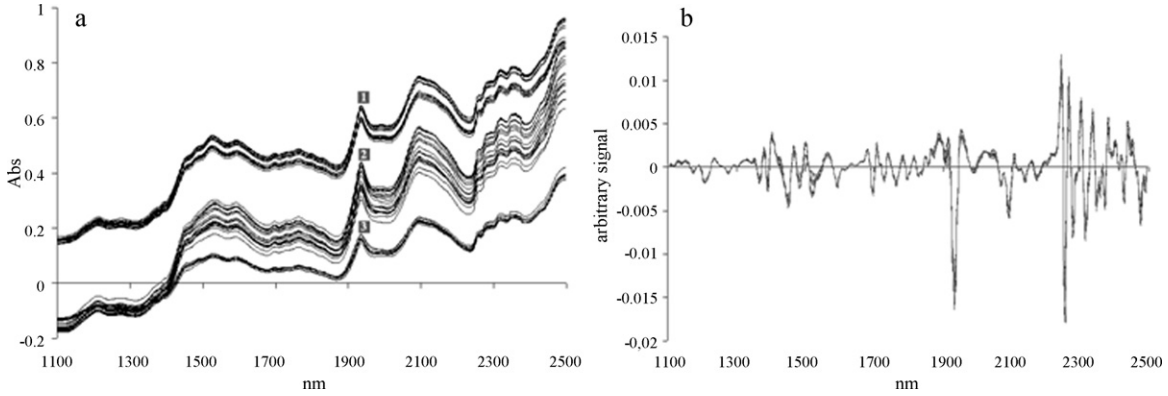

Fig. 1. (a) Raw spectra of production (1), powdered (2) and compressed (3) samples. (b) The same spectra after SNV + 2D.

treatment itself, those bands were not removed. Other artifacts produced by SNV, non linearity and band variability shift, have been already reported [18,19]. In the case of derivatives, only individual wavelengths had exaggerated values of the quotient, so their effect was suppressed just taking those wavelengths out of calculation, as indicated in Table 1.

$$b_m = \sqrt{\sum_{l=1}^{n} \left(\frac{X_l^{\text{compressed}} - X_l^{\text{powdered}}}{X_l^{\text{powdered}}} \right)^2} \quad (3)$$

$$B_m = \sqrt{\sum_{\lambda=1}^{n} \left(\frac{X_{\text{day 1}}^{\text{production}} - X_{\text{day 2}}^{\text{production}}}{X_{\text{day 1}}^{\text{production}}} \right)^2} \quad (4)$$

where $X^{\text{compacted}}$ is the signal of the compacted sample at each wavelength and X^{powdered} refers to the same parameter in powdered samples. Fig. 1 shows (a) the raw spectra of white tablets' samples from production, compressed and powdered, and (b) the same spectra after the above mentioned SNV + 2D pretreatment. The differences in scattering properties are clearly observed in the raw spectra. Production samples show a small but significant difference between two groups of spectra, corresponding to different production batches. That difference can be attributed to a different compaction pressure [20]. Spectra of laboratory compacted samples are practically parallel to the spectra of production samples, and also this difference can be attributed to the differences in press pressure. Powdered samples show a higher dispersion and a change in the spectral slope, produced for the very different scattering properties. On the other hand, it must be pointed out that although SNV + 2D is the pretreatment that minimizes differences between spectra, some significant differences are found towards water absorption bands (1440 and 1940 nm). Even though spectra were recorded as soon as possible, the whole process (milling, doping, homogenization, spectra recording, compressing, ...) needed several hours; it seems clear than during that time the sample absorbed some humidity from the laboratory environment, just introducing a sort of "artificial" differentiation between samples. Due to that, the spectral wavelength ranges of 1400–1500 and 1900–2000 nm were deleted in some of the subsequent calculations.

3.2. Compressing effect

The relationship between compaction pressure and scattering properties of pharmaceutical samples has been studied by different authors [21,22]. It has been proved that increasing pressure, reduces the sample scattering and consequently, increases the effective pathlength or, expressing the same concept in other words, the analyzed effective mass of the sample increases. A practical consequence of this (assuming the validity of Eq. (2)) should be an increase of sensitivity. In order to prove this hypothesis, some production samples were grinded; NIR spectra of the powders were recorded, the samples were compressed and their NIR spectra were acquired again. Hence, the spectrum of exactly the same sample was acquired in both physical presentations. To remove the effect of the different "slope", in order to enable the visual evaluation of overlapped spectra, the 2nd derivative of both spectra was computed. Absolute value of both spectra was plotted overlapped (Fig. 2). As can be seen, the signal is greater for compressed samples all along the spectra in a systematical way. A comparison between peak maxima of both, compressed and powdered samples in Fig. 2, shows that the increment of intensity is independent of wavelength, so it can be attributed to an increase of effective optical path length of 2.0 ± 0.1. Similar results were found in all assayed samples.

3.3. API determination

Quantitative models have been developed using SNV + 2D as spectral pretreatment. Several wavelength ranges were assayed, namely: the whole spectra, the whole spectra removing water bands (each one or both), and the short range 1100–1300 nm. Although the latter could be considered too narrow, it must be pointed out that both APIs show a characteristic band in that region, whereas the absorption bands of excipients are less intense in this region than at longer wavelengths. In order to illustrate this fact,

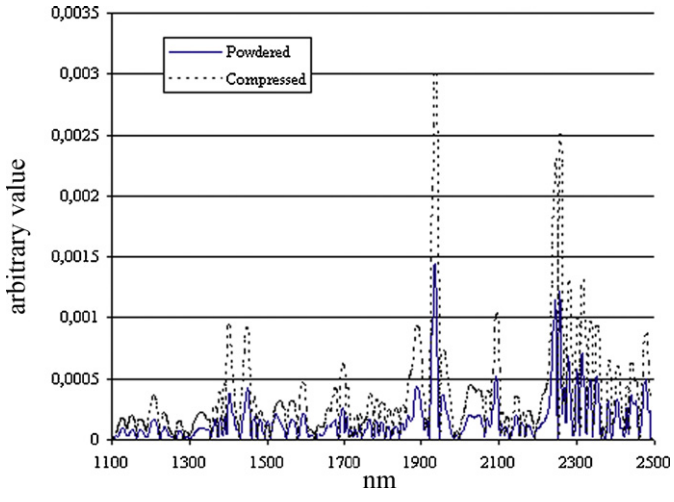

Fig. 2. Absolute values of 2D spectra of a powdered and compressed blue tablet.

Table 2
Figures of merit found with the best models for the determination of VE in white tablets using powdered and compressed samples. The wavelength range for compressed samples calibration model was from 1100 to 1300. For powdered samples spectral range was 1100–1400, 1500–1900 and 2000–2450 nm.

	Compressed		Powdered	
	Cal	Pred	Cal	Pred
PLS factors	6		6	
Number of samples	21	13	21	16
Slope	0.99 ± 0.03	1.04 ± 0.08	0.99 ± 0.02	0.91 ± 0.10
Intercept (mg/100 mg)	0.02 ± 0.04	−0.07 ± 0.14	0.02 ± 0.04	0.14 ± 0.15
SEC/SEP (mg/100 mg)	0.027	0.042	0.025	0.056

Table 3
Figures of merit found with the best models for the determination of VE in blue tablets using powdered and compressed samples. In all cases, the spectral range was 1100–1400, 1500–1900 and 2000–2450 nm.

	Compressed		Powdered	
	Cal	Pred	Cal	Pred
PLS factors	5		5	
Number of samples	18	13	18	13
Slope	0.97 ± 0.04	0.93 ± 0.10	0.94 ± 0.06	0.98 ± 0.10
Intercept (mg/100 mg)	0.05 ± 0.07	0.09 ± 0.16	0.09 ± 0.09	0.03 ± 0.25
SEC/SEP (mg/100 mg)	0.042	0.039	0.055	0.062

Table 4
Figures of merit found with the best models for the determination of MPA in blue tablets using powdered and compressed samples. In all cases, the spectral range was 1100–1400, 1500–1900 and 2000–2450 nm.

	Compressed		Powdered	
	Cal	Pred	Cal	Pred
PLS factors	3		3	
Number of samples	17	16	19	16
Slope	1.00 ± 0.01	1.01 ± 0.03	0.98 ± 0.03	1.10 ± 0.09
Intercept (mg/100 mg)	0.03 ± 0.10	0.08 ± 0.28	0.12 ± 0.24	−0.84 ± 0.72
SEC/SEP (mg/100 mg)	0.101	0.097	0.204	0.260

a binary sample spectrum (API and major excipient) was computed, assuming an equivalence between the concentration and absorbance ratio, pre-treated with SNV followed by 2D. VE concentration was fixed at its nominal value (1.6%) and major excipients (98.4%); the ratio between the area (sum of absolute intensities) for API and for the sample at 200 nm intervals was computed (Fig. 3). Even though it can be just considered a rough estimation, it clearly shows that the participation of API to the total sample absorbance is higher between 1100 and 1300 nm.

Figures of merit of the developed calibration models are shown in Tables 2–4. To simplify, only results for the best calibration models are shown, although it must be pointed out that in some cases rather similar results were found by using different wavelength ranges with no statistically significant differences between them.

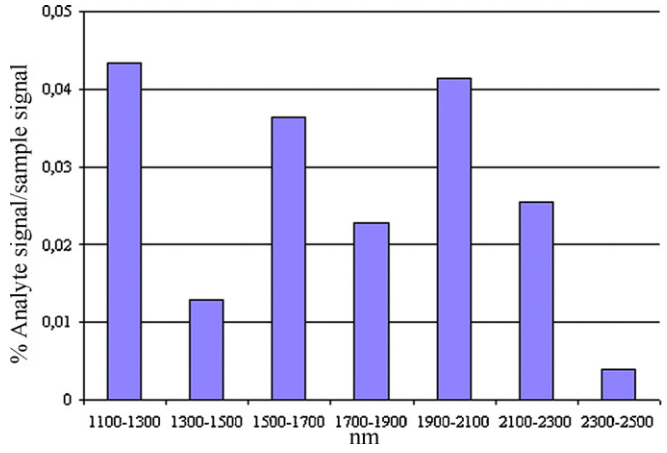

Fig. 3. Relative spectral contribution of VE (at nominal concentration) on a major excipient matrix.

It must be pointed out that reasonably good models can be obtained in all cases and that VE needs 5-6 factors to be modeled, while MPA needs only 3. That difference can be clearly attributed to the difference in concentration between both APIs. However, the most relevant fact extracted from these tables is that best precision (lower SEP values, narrower confidence interval for intercept and slope) is always reached using compressed calibration samples. This is coherent with the situation described above: an expected higher sensitivity to the models built with compressed doped samples, what drives to a lower dispersion of the prediction values.

Tables 5–6 show the results obtained for the production samples of the prediction set. No significant difference between NIR and HPLC values were obtained (paired *t* test)

Table 5
Determination of VE in individual commercial white samples. Nominal value: 2 mg VE/tablet. All results expressed in mg VE/tablet.

Mass (mg)	HPLC	NIR	Δ^a
119.3	1.91	1.98	0.07
118.7	1.89	1.91	0.02
118.8	1.91	1.87	−0.04
118.8	1.90	1.96	0.06
119.7	1.91	1.88	−0.03
119.6	1.93	1.89	−0.04
120.1	1.91	1.88	−0.03
120.8	1.91	1.93	0.02
120.9	1.91	1.91	0.00
		t_{exp}	0.23
		mean	0.00
		sd	0.04

[a] NIR mass – HPLC mass.
t_{crit}: 2.31; $\alpha = 0.05$; $n = 9$.

Table 6
Determination of MPA in individual commercial blue samples. Nominal values: 2 mg VE and 10 mg MPA/tablet. All results expressed in mg API/tablet.

Mass (mg)	HPLC	NIR	Δ[a]
VE			
117.0	1.84	1.87	0.03
117.9	1.85	1.87	0.02
117.5	1.86	1.84	−0.02
119.8	1.91	1.88	−0.03
117.7	1.88	1.83	−0.05
118.0	1.89	1.87	−0.02
119.7	1.92	1.89	−0.03
119.2	1.93	1.91	−0.02
		t_{exp}	0.30
		Mean	−0.01
		sd	0.03
MPA			
117.0	9.36	9.30	−0.06
117.9	9.43	9.34	−0.09
117.5	9.44	9.50	−0.06
119.8	9.66	9.72	0.06
117.7	9.51	9.51	0.00
118.0	9.48	9.37	−0.11
119.7	9.73	9.66	−0.07
119.2	9.74	9.85	0.11
		t_{exp}	0.41
		Mean	−0.03
		sd	0.08

[a] NIR mass − HPLC mass.
t_{crit}: 2.36; $\alpha = 0.05$; $n = 8$.

4. Conclusions

Although no pretreatment was found to be able to completely remove the spectral differences between powdered and compressed samples, SNV followed by 2D has been demonstrated to be the spectral pretreatment that better minimizes them.

In the whole wavelength range, the spectrum of a compressed sample shows higher band intensities than that of a powdered one. This is consistent with the reduction of light scattering and, consequently, the increase of the effective path length and the mass fraction measured in compressed samples. As expected, compression makes the spectra of calibration samples more similar to those in production and increases effectively the sensitivity, improving the precision in the determination of both APIs.

It has also been demonstrated that hormones can be determined in intact tablet by near infrared diffuse reflectance spectroscopy with an accuracy and precision comparable to a standard HPLC procedure.

Acknowledgements

The authors are grateful to Spain's Ministry of Science and Innovation (MICINN) for funding this research within the framework of Project CTQ2007-62528.

References

[1] J. Luypaert, D.L. Massart, Y. Vander Heyden, Near-infrared spectroscopy applications in pharmaceutical analysis, Talanta 72 (2007) 865–883.
[2] M. Andersson, O. Svensson, S. Folestad, M. Josefson, K. Wahlund, NIR spectroscopy on moving solids using a scanning grating spectrometer-impact on multivariate process analysis, Chemom. Intell. Lab. Syst. 75 (2005) 1–11.
[3] M. Fuentes, I. Gonzalez-Martin, J.M. Hernandez-Hierro, C. Hidalgo, B. Govaerts, J. Etchevers, K.D. Sayre, L. Dendooven, The natural abundance of 13C with different agricultural management by NIRS with fibre optic probe technology, Talanta 79 (2009) 32–37.
[4] A. Peinado, J. Hammond, A. Scott, Development, validation and transfer of a Near Infrared method to determine in-line the end point of a fluidised drying process for commercial production batches of an approved oral solid dose pharmaceutical product, J. Pharm. Biomed. Anal. 54 (2011) 13–20.
[5] R. Zornoza, C. Guerrero, J. Mataix-Solera, K.M. Scow, V. Arcenegui, J. Mataix-Beneyto, Near infrared spectroscopy for determination of various physical, chemical and biochemical properties in Mediterranean soils, Soil Biol. Biochem. 40 (2008) 1923–1930.
[6] H. Wu, M.A. Khan, Quality-by-Design (QbD): an integrated process analytical technology (PAT) approach for real-time monitoring and mapping the state of a pharmaceutical coprecipitation process, J. Pharm. Sci. 99 (2010) 1516–1534.
[7] D.J. Dahm, K.D. Dahm, Representative layer theory for diffuse reflectance, Appl. Spectrosc. 53 (1999) 647–654.
[8] D.A. Burns, E.W. Ciurczak, Handbook of Near-Infrared Analysis, 2nd ed., Marcel Dekker, New York, 2001.
[9] D. Sun, Infrared Spectroscopy for Food Quality Analysis and Control, 1st ed., Academic Press, Salt Lake City, 2009.
[10] N.W. Broad, R.D. Jee, A.C. Moffat, M.R. Smith, Application of transmission near-infrared spectroscopy to uniformity of content testing of intact steroid tablets, Analyst (Cambridge, U.K.) 126 (2001) 2207–2211.
[11] M. Blanco, M. Bautista, M. Alcala, Preparing calibration sets for use in pharmaceutical analysis by NIR spectroscopy, J. Pharm. Sci. 97 (2007) 1236–1245.
[12] M. Blanco, J. Coello, H. Iturriaga, S. Maspoch, N. Pou, Influence of the procedure used to prepare the calibration sample set on the performance of near infrared spectroscopy in quantitative pharmaceutical analyses, Analyst (Cambridge, U.K.) 126 (2001) 1129–1134.
[13] P. Chalus, Y. Roggo, S. Walter, M. Ulmschneider, Near-infrared determination of active substance content in intact low-dosage tablets, Talanta 66 (2005) 1294–1302.
[14] E. Ziemons, J. Mantanus, P. Lebrun, E. Rozet, B. Evrard, P. Hubert, Acetaminophen determination in low-dose pharmaceutical syrup by NIR spectroscopy, J. Pharm. Biomed. Anal. 53 (2010) 510–516.
[15] M. Blanco, A. Peguero, Influence of physical factors on the accuracy of calibration models for NIR spectroscopy, J. Pharm. Biomed. Anal. 52 (2010) 59–65.
[16] A. Segall, F. Hormaechea, M. Vitale, V. Perez, M.T. Pizzorno, Development and validation of a reversed-phase liquid chromatographic method for analysis of estradiol valerate and medroxyprogesterone acetate in a tablet formulation, J. Pharm. Biomed. Anal. 19 (1999) 803–808.
[17] M. Blanco, M. Bautista, M. Alcala, API determination by NIR spectroscopy across pharmaceutical production process, AAPS PharmSciTech 9 (2008) 1130–1135.
[18] T. Fearn, C. Riccioli, A. Garrido-Varo, J.E. Guerrero-Ginel, On the geometry of SNV and MSC, Chemom. Intell. Lab. Syst. 96 (2009) 22–26.
[19] T. Fearn, Interaction between Standard Normal Variate and derivatives, NIR News 19 (2008) 16–17.
[20] M. Blanco, M. Alcala, Content uniformity and tablet hardness testing of intact pharmaceutical tablets by near infrared spectroscopy, Anal. Chim. Acta 557 (2006) 353–359.
[21] M. Otsuka, H. Tanabe, K. Osaki, K. Otsuka, Y. Ozaki, Chemoinformetrical evaluation of dissolution property of indomethacin tablets by near-infrared spectroscopy, J. Pharm. Sci. 96 (2007) 788–801.
[22] W. Kessler, D. Oelkrug, R. Kessler, Using scattering and absorption spectra as MCR-hard model constraints for diffuse reflectance measurements of tablets, Anal. Chim. Acta 642 (2009) 127–134.

Journal of Pharmaceutical and Biomedical Analysis 60 (2012) 65–70

Contents lists available at SciVerse ScienceDirect

Journal of Pharmaceutical and Biomedical Analysis

journal homepage: www.elsevier.com/locate/jpba

Structural and energetic aspects of a new bupropion hydrochloride polymorph

Elisabetta Maccaroni[a,*], Luciana Malpezzi[a], Antonino Famulari[a], Norberto Masciocchi[b]

[a] Department of Chemistry, Materials and Chemical Engineering "G. Natta", Politecnico di Milano, Via Mancinelli 7, I-20131 Milano, Italy
[b] Dipartimento di Scienze Chimiche e Ambientali, Università dell'Insubria, Via Valleggio 11, I-22100 Como, Italy

ARTICLE INFO

Article history:
Received 28 July 2011
Received in revised form 24 October 2011
Accepted 31 October 2011
Available online 6 November 2011

Keywords:
X-ray powder diffraction
Structure solution
Polymorphism
Thermal analysis
Solid state quantum mechanics calculations

ABSTRACT

Crystalline bupropion hydrochloride [(±)1-(3-chlorophenyl)-2-[(1,1-dimethylethyl)amino]-1-propanone hydrochloride], recently characterized as form **1,** was found to undergo, upon storage at RT within months, a solid–solid conversion to a new polymorphic form, hereafter named form **2,** containing a markedly different molecular conformer in the solid state. This new form, available only as a polycrystalline material, has been fully characterized using structural X-ray powder diffraction methods, coupled to thermoanalytical analyses. The relative stability of the two crystalline phases (forms **1** and **2**) was compared by quantum mechanics calculations including density functional methods specific for solid state molecular systems. Bupropion hydrochloride form **2** crystallizes in the orthorhombic space group *Pbca* with $Z=8$, $a=27.2853(5)$ Å, $b=8.7184(3)$ Å, $c=12.0422(3)$ Å, $V=2864.7(1)$ Å^3, as centrosymmetric dimers, thanks to the presence of N–H...Cl interactions, and μ_2-bridging chloride ions, each connected to two protonated amine moieties.

1. Introduction

In the recent past, crystal polymorphism has pervaded the field of solid state organic chemistry and, particularly, drug development and formulation, from basic science to industrial process control, up to patent litigation and infringing issues. The reason for such a blooming comes from the well-established knowledge that different polymorphs can have markedly different physico-chemical properties (hence different therapeutic activities, tabletting and formulation difficulties, shelf lives, etc.). In the particular case where a spontaneous, or poorly controlled, phase transition from a polymorphic form to another one occurs during the production stage and/or during prolonged storage, the phase purity of the active pharmaceutical ingredient (APIs) at the final distribution and marketing stages, cannot be safely controlled, with evident health (and economic) risks [1].

The thermodynamic behaviour of different polymorphs can be described as enantiotropic or monotropic, depending on topology of their P/T and ΔH, ΔG/T phase diagrams, addressing their stability ranges. If they can undergo a reversible solid–solid transformation at a transition point below the (real or virtual) melting point of both forms, they are defined as enantiotropically related. If one polymorph is always stable below the melting point of both crystal forms, the two polymorphs are defined monotropically related. In this case, the transition point lies above the melting points of both polymorphs and it is a virtual transition point [1,2]. Needless to say, much more complex phase diagram and transition behaviour can be found if the number of polymorphs exceeds two.

Conventional experimental methods employed to assess, at constant pressure, the relative thermal stability of polymorphs are thermoanalytical analyses (DSC/TGA) or variable temperature X-ray powder diffraction (TXRPD). These techniques, which can be occasionally biased by kinetic effects, typically provide only approximate temperature values of the thermal events but, under normal circumstances, clearly indicate the stability order of the different crystal phases. However, independent experimental – for example by slurrying a mixture of polymorphs in weakly solving solvents – or computational evidence – by numerical simulations, based on quanto-mechanical methods at different levels of approximation – can be gathered. Other common rules of thumb can be used, such as the Ostwald rules of stages [3], but, since several exceptions exist, [4,5] none of these methods can be considered *per se* definitive. For an instructive example of a misleading interpretation derived from thermo-diffractometric/calorimetric analysis *only*, see the case study of Atovaquone, an API used in the malaria treatment [6]. Accordingly, only a coherent set of experiments and of numerical simulations can strengthen the correct knowledge of the *true* polymorphic stability order.

The structural characterization of bupropion hydrochloride (see Scheme 1), an API used for smoke cessation, recently appeared in the literature [7]. Upon prolonged storage at ambient conditions, microcrystalline powders of this widely marketed material (now called polymorph **1**) were found to undergo a phase transition generating a new crystal phase, hereafter named polymorphic form **2**,

* Corresponding author. Tel.: +39 02 2399 3022; fax: +39 02 2399 3180.
E-mail address: elisabetta.maccaroni@chem.polimi.it (E. Maccaroni).

0731-7085/$ – see front matter © 2011 Elsevier B.V. All rights reserved.
doi:10.1016/j.jpba.2011.10.031

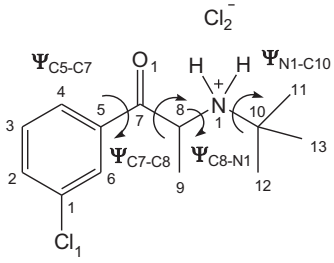

Scheme 1. The molecular scheme, atomic numbering and labeling of the freed torsion angles of the title compound.

which, to our knowledge, has never been reported in the scientific and patent literature.

These findings prompted us to tackle the complete characterization of the new polymorphic form of bupropion hydrochloride (form **2**), and to compare it with the already known form **1**. As anticipated, and in the absence of crystalline samples of suitable size and quality for conventional diffraction analysis, we extensively used structural X-ray powder diffraction (XRPD) methods to address the crystallochemical features of these phases, and thermal analyses to investigate their thermal behaviour. In addition, the potential energy surface (PES) pertaining to the interconversion of isolated cation moieties of form **1** and form **2** (gas phase approximation) was estimated; finally, quantum mechanics calculations, aiming at evaluating lattice binding energies of the two polymorphs/conformers by solid state density functional methods were carried out.

2. Experimental

2.1. Materials

Bupropion hydrochloride form **2** was obtained on leaving form **1** at ambient temperature for about one year, in a storage experiment. After solving the crystal structure of form **2**, the quantitative determination of the residual form **1** was performed by whole-pattern profile fitting (quantitative Rietveld method), which indicated a small (8 weight %) contamination of **1** in **2**.

2.2. Methods

2.2.1. Thermal analysis

Differential scanning calorimetric analyses were performed on a Perkin Elmer DSC 8500 at scanning rate of 10 °C min^{-1}, in the 50–280 °C temperature range. The sensor and the sample were maintained under a nitrogen purge during the whole experiment (flow rate: 20 ml min^{-1}). The calibration was done with metallic indium. Each sample, accurately weighted, was heated in crimped aluminium pan. The transition temperatures were determined by the onset method, *i.e.* taking the temperature value measured at the crossing point between the baseline and the tangent segment taken at the lower inflection point of the endothermic peak.

Thermogravimetric analysis was performed on a TA Q600 SDT instrument operated on *ca.* 9.2 mg of sample at scanning rate of 10 °C min^{-1} and under a flux of N_2 as purge gas, in the 30–400 °C temperature range.

2.2.2. X-ray powder diffraction analysis

Bupropion hydrochloride form **2** was gently ground in an agate mortar, and then deposited in the hollow of a 0.2 mm deep aluminium sample holder, equipped with a quartz monocrystal zero background plate (supplied by *The Gem Dugout*, State College, PA). Diffraction data were collected in the 5–105° 2θ range, sampling with a 0.02° step scan, on a θ:θ vertical scan Bruker AXS D8 Advance diffractometer, equipped with a linear Lynxeye position sensitive detector, set at 300 mm from the sample (Ni-filtered Cu-K$\alpha_{1,2}$ radiation). Peak search and profile fitting allowed the location of the most prominent, low angle peaks, which, after elimination of those of the minor contaminant (polymorph **1**), were later used in the indexing process by the TOPAS-R software; approximate lattice parameters of a primitive orthorhombic cell were determined to be a = 27.27 Å, b = 8.71 Å and c = 12.03 Å, with a figure of merit of GOF(20) = 47.2. Systematic absences conditions suggested *Pbca* as the probable space group, later confirmed by successful structure solution and refinement. Density considerations indicated Z = 8, thus limiting the structure solution process of phase **2** to the individuation of the centre of mass location, orientation and conformational freedom of a unique (N-protonated) bupropion molecular cation and the location of a freely floating chloride anion. The initial molecular model of the protonated bupropion fragment, identical to that employed in the crystal structure determination of form **1** [7], was used as a fixed rigid body (flexible at a few torsional angles – see Scheme 1), fed to the TOPAS-R program by Cartesian (absolute) atomic coordinates. Real space structure modelling by the simulated annealing algorithm coupled to Monte Carlo-search allowed the definition of a suitable model, later refined by the Rietveld method. Conversely, the complete model already determined for form **1** was used to take into account its small contribution to the total powder diffraction trace of the biphasic (impure) sample, allowing a minor relaxation of its lattice parameters, partially influenced by the presence of unavoidable experimental aberrations and sample displacement/transparency effects. Structure solution and final refinements were carried out by TOPAS-R software, also used in the quantitative evaluation of the relative phase amounts in the biphasic samples. The background contribution was modelled by a polynomial fit (fourth order Chebyshev model); atomic scattering factors for neutral atoms were taken from the internal library of TOPAS-R. Preferred orientation corrections, in the March–Dollase formulation, were applied on the [1 0 0] pole, with final magnitude r = 0.737(2). Anisotropic peak broadening, by the spherical harmonics approach, has been tested, but lead only to a marginally lower agreement factors and was, therefore, abandoned. Fig. 1 shows the final Rietveld refinement plot, in which the most prominent discrepancies (peaks near 13 and 18°), present also in the structureless Le Bail refinement, are probably due to the incomplete correction for axial effects, likely due to sample transparency. The use of a capillary (transmission) mode may only partially overcome this experimental problem, and, therefore, was not tested. Fractional atomic coordinates have been deposited as CIF file within the Cambridge Crystallographic Database as publication No. CCDC 831486. For the multiphase diffraction dataset, overall agreement factors are: R_p = 0.071, R_{wp} = 0.101. 2θ range 10–105°.

Crystal data of form **1**: $C_{13}H_{19}NOCl_2$, f.w. = 276.21 g mol^{-1}, 298 K, λ (Å) = 1.5418, monoclinic space group $P2_1/c$, a = 14.326(2) Å, b = 8.753(2) Å, c = 11.885(3) Å, β = 78.07(2)°, V = 1458.2(5) Å^3, Z = 4, ρ_{calc}, 1.281 g cm^{-3}, μ (CuKα) = 3.89 mm^{-1}, R_{Bragg} = 0.077.

Crystal data of form **2**: $C_{13}H_{19}NOCl_2$, f.w. = 276.21 g mol^{-1}, 298 K, λ (Å) = 1.5418, orthorhombic space group *Pbca*, a = 27.2853(5) Å, b = 8.7184(3) Å, c = 12.0422(3) Å, V = 2864.7(1) Å^3, Z = 8, ρ_{calc}, 1.281 g cm^{-3}, μ (CuKα) = 3.96 mm^{-1}, R_{Bragg} = 0.056.

2.2.3. Computational details

Quantum mechanics calculations have been performed to compare the energy of bupropion cation conformers with potential Energy Surface (PES) scan in the gas phase approximation and the packing efficiency of the crystalline forms **1** and **2** (under periodical boundary conditions calculations). In particular, density functional theory (DFT) calculations in the *local density approximation* (LDA), coupled with the Perdew–Wang (PWC) functional [8], have been adopted as implemented in the DMol^3 software [9] in order to deal

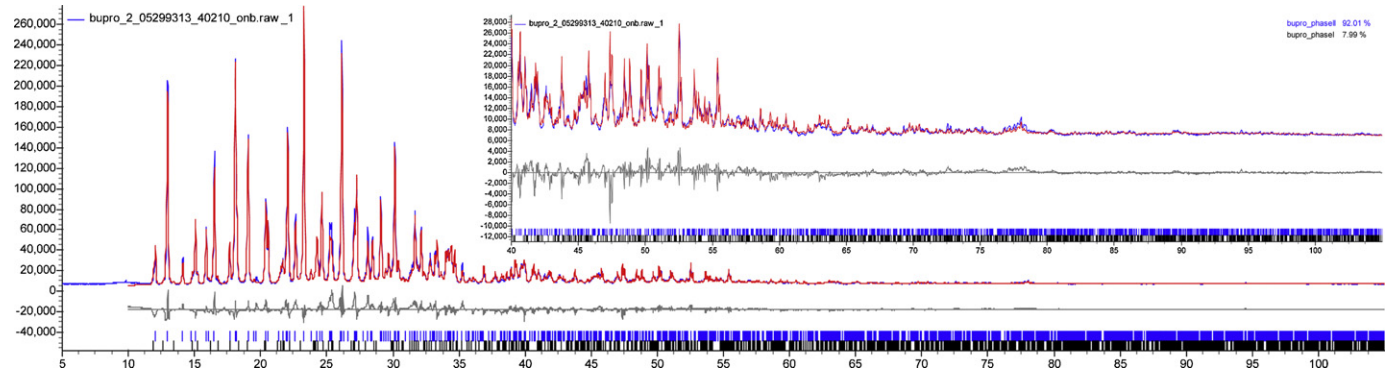

Fig. 1. Final Rietveld refinement plot for a mixture of bupropion hydrochloride form **1** (8%) and form **2** (92%), with peak markers and difference plot ($y_{obs} - y_{calc}$) at the bottom. Blue: observed data (y_{obs}); red: calculated data (y_{calc}). The insert shows the high angle region ($2\theta > 40^\circ$) in a magnified scale (9×). (For interpretation of the references to color in this figure legend, the reader is referred to the web version of the article.)

with both gas phase and solid state systems. In this way, lattice binding energies and PES scans were evaluated at the same level of the theory and with the same code. Lattice binding energy (LBE), *i.e.* is the minimum amount of energy necessary to completely separate one mole of a solid ionic compound in its corresponding ions in the gaseous state, was calculated assuming fixed experimental atomic coordinates and cell parameters. Numerical basis functions centred on the atoms were used for all the calculations. Double zeta quality sets were chosen: namely DN, DND and DNP basis sets, the latter also including polarization functions on all the involved atoms. The results showed that the addition of polarization functions only on non-H atoms (PWC/DND calculations) is of particular importance. The same scheme of calculation presented in this work was recently used for the study of crystalline phases of thiophene based oligomers and polymers showing a good accordance between estimated geometries, sublimation energies and available experimental findings [10].

3. Results and discussion

3.1. Thermal properties

The DSC trace recorded for bupropion hydrochloride form **2** (see Fig. 2) shows a small endothermic broad peak at T_{onset} of *ca.* 220 °C, with $\Delta H = 0.78\ kJ\ mol^{-1}$, attributed to a solid–solid phase transition to form **1**. The occurrence of the solid–solid phase transition was further proved by heating form **2** in an oven at 190 °C for 20 min, leaving the sample between two watch glasses to avoid sample mass loss owing to its tendency toward sublimation. A complete conversion to form **1** was observed by XRPD. An endothermic transition from form **2** to form **1** suggests that the two phases are enantiotropically related, with **2** being the most stable polymorph at low temperature, as also witnessed by the slow, but spontaneous transformation occurred, at r.t. within months, of pristine form **1,** described above. Such an interpretation is also strengthened by the

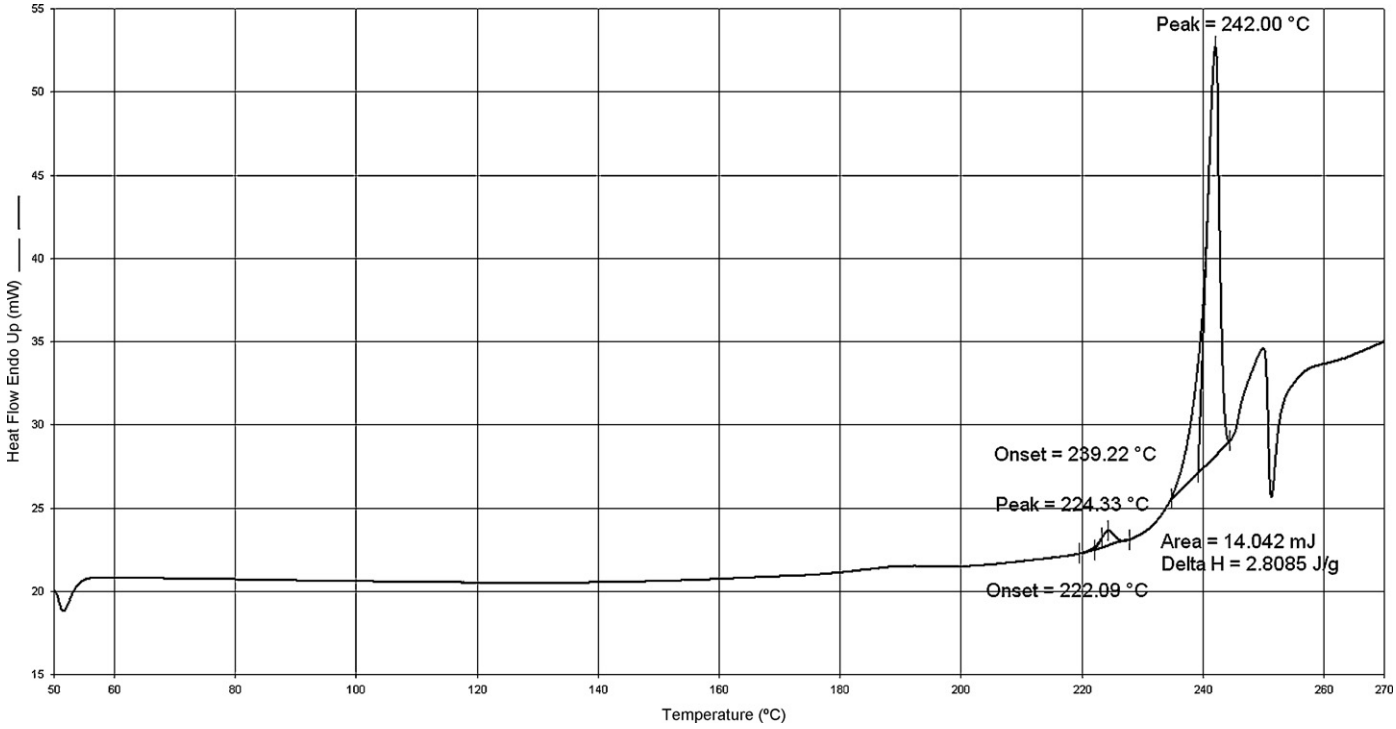

Fig. 2. DSC trace of bupropion hydrochloride form **2** measured at a scanning speed of 10 °C min^{-1}.

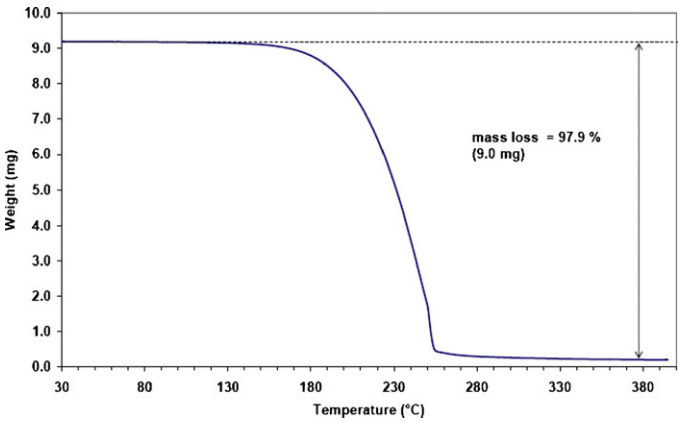

Fig. 3. TGA trace of bupropion hydrochloride form **2** measured at a scanning speed of 10 °C min^{-1}.

comparison of the r.t. molar volumes, larger in **1** than in **2** (365 vs. 358 Å^3, respectively).

At higher temperatures, a sharp and intense endothermic peak at T_{onset} of *ca.* 239 °C, corresponding to sample sublimation is observed. Direct calorimetric measurements cannot give reliable sublimation enthalpy values since it is difficult to ensure the equilibrium between the solid and gas phase. For this reason, the sublimation enthalpy could not be correctly measured and its value was not reported [11]. That sublimation occurs was indeed proved by the TGA analysis, where a nearly complete weight loss above 240 °C was observed (Fig. 3). On the basis of these observations, we can foresee that melting of form **1** can occur only at pressures above 1 atm, and that "virtual" melting (at ambient pressure) of form **2**, must fall above 220 °C. *Inter alia*, this evidence somewhat contradicts our previous report on the thermal event observed near 240 °C for form **1**, which, on the basis of these new observations, should be then interpreted as sublimation, rather than melting [7].

3.2. Crystal and molecular structures of bupropion hydrochloride in form **2**

Powder diffraction methods from laboratory data on moderately complex materials do not allow the refinement of the structural models by the IAM (Independent atom model) technique, thus limiting the quality of the geometrical information which can be retrieved there from. Accordingly, refinement of intramolecular distances and angles degrees of freedom was not allowed, leaving a meaningful discussion only to torsion angles and intermolecular contacts with the heaviest scatterer (here, the chlorine ions). This choice well agrees with the known (relative) rigidity of bond distances and angles values (of the organic type), at least if compared to the variability (and the energetics) of the torsion angles about C–C and C–N single bonds. Under this premises, only conformational differences between the different (protonated) bupropion molecules in the different hydrochloride phases (forms **1**, **2**) can be safely discussed. They were found to depend mainly on the meta-chlorophenyl group orientation with respect to the carbonyl group (see Fig. 4): in form **2**, the chloro- and the carbonyl groups point in opposite directions (*anti* conformation), while in form **1** they are aligned in *syn* fashion. The complete conformation of the two polymorphs is quantitatively addressed by the set of torsion angle values reported in Table 1. Three of the four torsion angles are very similar, while a significant difference is observed for the torsion angle Ψ_{C5-C7}, responsible of the different orientation of the chloro substituent with respect to the carbonyl group.

Table 1
Selection of the relevant conformational parameters of the bupropion hydrochloride, form **1** and form **2** (for sake of comparison, R enantiomers, from centrosymmetric crystal structures, have been arbitrarily chosen).

Torsion angle		Form **1**	Form **2**
C6–C5–C7–O1 (°)	Ψ_{C5-C7}	27.5(2)	−165.3(3)
C5–C7–C8–N1 (°)	Ψ_{C7-C8}	−148.2(1)	−151.3(2)
C7–C8–N1–C10 (°)	Ψ_{C8-N1}	79.9(3)	85.1(4)
C8–N1–C10–C11 (°)	Ψ_{N1-C10}	179.0(3)	−168.8(4)[a]

[a] In form **2** the C13 atom of the *t*-butyl residue has been used.

As for bupropion hydrochloride form **1**, crystals of form **2** are based upon an ionic arrangement of protonated bupropion cations and chloride anions. In all phases, protonation occurs at the most basic site, the N1 atom, which, therefore, becomes tetrahedrically bound to two carbon atoms and two hydrogen atoms. In both forms, two bridging chlorine ions connect the protonated amine moieties of two different molecules through a total of four hydrogen bonds involving the two hydrogen atoms of each amine group. This arrangement results in the formation of dimeric moieties. A schematic drawing of the molecular packing of form **2** is depicted in

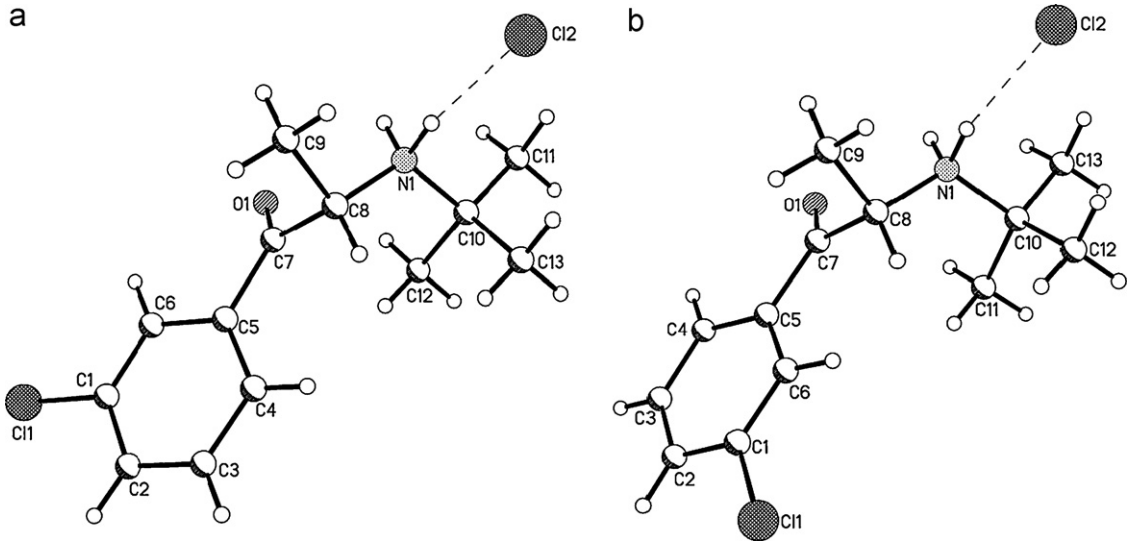

Fig. 4. Schematic drawing of the molecular conformations of bupropion hydrochloride form **1** (a) and form **2** (b). Intermolecular hydrogen bonds are shown with fragmented lines. The O1 and Cl1 atoms point in the same direction in (a) while in opposite direction in (b).

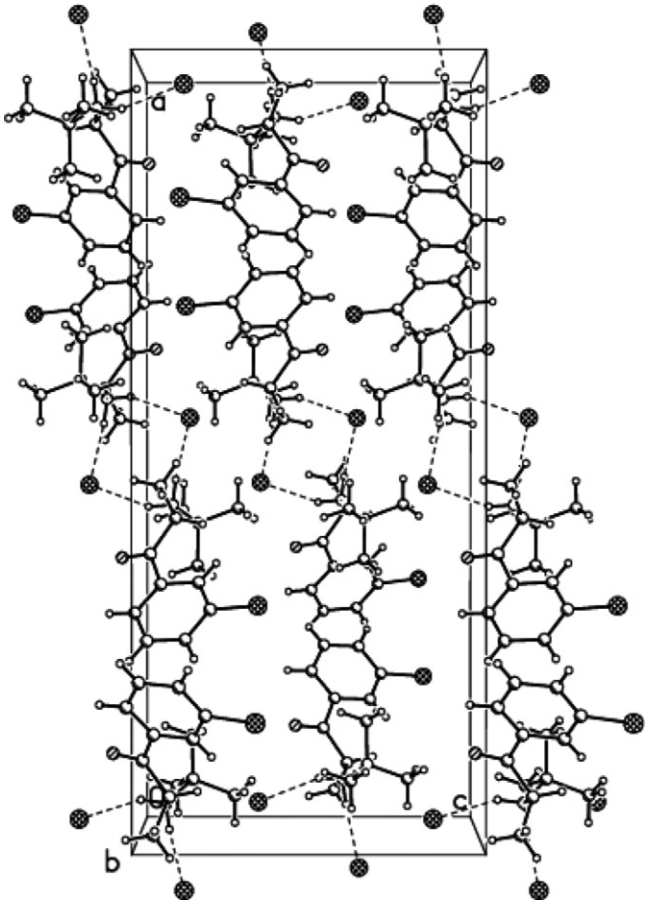

Fig. 5. Crystal packing of bupropion hydrochloride form **2** viewed down *b*. As evidenced by fragmented lines, molecules are bridged through intermolecular hydrogen bonds of the N–H. . .Cl type.

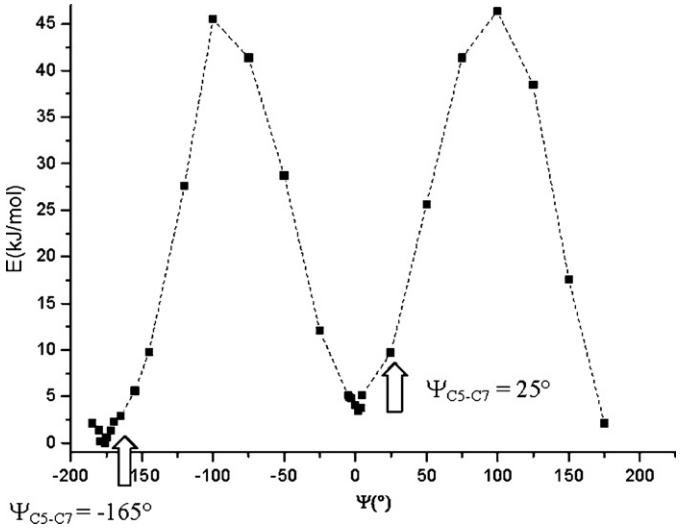

Fig. 6. Cation PES scan around the torsion angle Ψ_{C5-C7} calculated at the DFT PWC/DNP level. Horizontal axis, degrees. Vertical axis, kJ mol^{-1}. The arrows indicate the experimentally observed conformers in forms **2** (left) and **1** (right).

Fig. 5. Interestingly, this form is isomorphous with a recent report [12] on the crystal structure of polymorph form IV of bupropion hydrobromide.

Worthy of note, even if polymorphic forms **1** and **2** crystallize in different systems and space groups, the analysis of the main packing features allow to derive the following features: (i) the **b** parameter is nearly identical in the two phases, and it is related to the stacking of molecular "dimers", located, in both phases, about crystallographic inversion centres. Accordingly, the same 2_1/c symmetry operations are present in the monoclinic (**1**) and orthorhombic (**2**) crystals; (ii) also the **c** axis is similar, although to a lesser extent than for what has been observed for **b**; (iii) at variance, the **a** axis in **2** is nearly twice that found in **1**. Also, the β angle is different: *ca.* 78° in **1**, and rigorously 90° in **2**. These observations suggest therefore somewhat similar packing features, hidden in the nature of the translational components along the **a** direction: what was originally a simple lattice vector in **1**, becomes, in **2**, a glide plane normal to **c**, with **a/2** translational shift (thus implying a significant molecular reorganization, even if the centre of masses of the molecular dimers are nearly preserved).

3.3. Quantum mechanics DFT calculations

DFT calculations (see Section 2.2.3) were carried out to establish the energetic barrier involved in the rotation around the torsion angle Ψ_{C5-C7} (see Scheme 1) within the cation moiety, which heavily affects the conformational energy of the system.

DFT PWC/DN, PWC/DND and PWC/DNP calculations showed similar results. The scan of cation PES calculated at the DFT PWC/DNP level is reported in Fig. 6. For a free molecule *in gas phase*, the energetic barrier was assessed varying the Ψ_{C5-C7} torsion angle in 30° steps over the whole 360° range (several extra steps, 1° each, are reported in vicinity of the minimal energy conformers). It can be observed that, for the experimentally determined cation conformation of form **2** ($\Psi_{C5-C7} = -165°$), a lower energy has been calculated of about 6.8 kJ mol^{-1} with respect to that corresponding to conformation of form **1** ($\Psi_{C5-C7} = 25°$). Neglecting (as a very crude approximation) crystal packing and ionic contributions *necessarily* present in the solid, this result is consistent with the higher stability of molecular conformation found in the form **2**.

In addition, the conformation of the cation in form **2** is very close to the absolute minimum calculated (Ψ_{C5-C7} lying in the deep basin near −176°, see Fig. 6) with a marginal energy penalty of only 2.9 kJ mol^{-1}. On the contrary, the experimental conformation of the cation in form **1** ($\Psi_{C5-C7} = 25°$) is close to a relative minimum calculated (with Ψ_{C5-C7} close to 2°) with a slightly higher energy penalty (6.2 kJ mol^{-1}). The energetic barrier showed by the calculated PES is about 45 kJ mol^{-1}, thus demonstrating the possibility of interconversion of *gaseous* conformers even at ambient temperature conditions. At variance, bupropion molecules are not expected to easily rotate in the crystal lattice of form **1**, generating the most stable conformer within form **2**, since variation of the intermolecular contacts upon molecular movement (even if allowing cooperation of other degrees of freedom) would highly increase the packing energy. Of course, a highly cooperative rearrangement of all molecules of **1** (within sizable crystal domains) cannot be excluded, but, in our opinion (and in the absence of ancillary computational or experimental evidence), this process, *at ambient temperature*, should be energetically unfavourable. Thus, recrystallization of form **2** from solid **1**, at room temperature, can be explained only by invoking surface seeding or the intermediacy of ambient moisture granting enhanced molecular mobility. An intuitive, though crude, explanation for the higher stability of polymorph **2**, may be addressed by the relative disposition of the C=O and C–Cl dipolar moments, *anti*-(parallel) in **2**, and *syn*-organized in **1**.

In order to rationalize the X-ray experimental findings we further estimate the lattice binding energies (LBEs) of the system, at the same levels of the theory used for the scan of the PES. LBEs were calculated assuming experimental frozen geometries. The gas

phase cation–anion pair interaction energy is stronger in form **1**, than in form **2**, by less than 10 kJ mol^{-1} (506.3 vs. 496.0 kJ mol^{-1}, DFT PWC/DNP calculations). At variance, in the crystalline phase, the LBE stabilization of an ion pair with respect to gas phase state is comparable for form **1** and form **2** (230.1 vs. 228.9 kJ mol^{-1}). Thus, for the reaction bupropion$H^+_{(g)}$ + $Cl^-_{(g)}$ = [bupropionH]$Cl_{(s)}$, ΔE = −736.4 and −724.9 kJ mol^{-1} (for forms **1** and **2**, respectively), making the ratio of solid phase and gas phase ion pair interaction energies only marginally higher in the latter case (1.461, form **2** vs. 1.454, form **1**). We can thus conclude that crystals of form **1** and form **2** possess very similar packing energies, and that the lower enthalpy value of form **2**, vs. form **1**, must be safely attributed to the lower conformational energy of the bupropionH^+ cation.

4. Conclusions

The new polymorphic form **2** of bupropion hydrochloride was structurally and thermodynamically characterized using a combination of different techniques. Interconversion between the different crystalline phases was assessed by thermal analysis (DSC/TGA). Form **1** spontaneously converts into form **2** on prolonged storage at room temperature (about one year). Differently, form **2** can be transformed back into form **1** by heating it slightly above *ca.* 220 °C.

The complete structural characterization of form **2** was achieved by structural powder diffraction methods, developed by us [13] and others [14] in the recent past. The refined models show that both structures are formed by a dimeric arrangement of the molecules held together by four hydrogen bonds of the N–H. . .Cl type. Quantum mechanical calculations in the gas phase and in the solid state were employed to address the different contributions, of intra- and intermolecular origin, contributing to the stabilization energy. These results, coupled to geometrical analysis of the packing environments, suggest that transformation of form **1** into form **2** upon prolonged storage may occur *only* through surface-or moisture-mediated processes.

Acknowledgements

We thank Dr. C. Pellegatta (Solmag S.p.A., Garbagnate Milanese (MI), Italy) for having provided bupropion hydrochloride samples. We are also indebted to the reviewers for valuable suggestions.

References

[1] R. Hilfiker, F. Blatter, M. von Raumer, in: Rolf Hilfiker (Ed.), Relevance of Solid-State Properties for Pharmaceutical Products in Polymorphism in the Pharmaceutical Industry, Wiley-VCH Verlag GmbH &Co. KGaA, 2006.
[2] J. Bernstein, Polymorphism in Molecular Crystals, Clarendon Press, Oxford, 2002.
[3] W. Ostwald, Studien über die Bildung und Umwandlung fester Körper, Z. Physikal. Chem. 22 (1897) 289–330.
[4] G. Di Profio, A. Caridi, R. Caliandro, A. Guagliardi, E. Curcio, E. Drioli, Fine dosage of antisolvent in the crystallization of L-Histidine: effect on polymorphism, Cryst. Growth Des. 10 (2010) 449–455.
[5] P.J. Skrdla, Observation of oscillatory behaviour during the dissolution of a pharmaceutical compound and evidence for the existence of an inverse Ostwald rule, Phys. Chem. Chem. Phys. 12 (2010) 3788–3798.
[6] (a) L. Malpezzi, C. Fuganti, E. Maccaroni, N. Masciocchi, Thermal and structural characterization of two polymorphs of Atovaquone and of its chloro derivative, J. Therm. Anal. Calorim. 102 (1) (2010) 203–210;
(b) R. Ceolin, I. Rietveld, Phenomenology of polymorphism and topological pressure–temperature diagrams. Description of the phase relationship involving Atovaquone polymorphs I and III, J. Therm. Anal. Calorim. 102 (1) (2010) 357–360.
[7] E. Maccaroni, L. Malpezzi, N. Masciocchi, Structures from powders: bupropion hydrochloride, J. Pharm. Biomed. Anal. 50 (2009) 257–261.
[8] J.P. Perdew, Y. Wang, Accurate and simple analytic representation of the electron-gas correlation energy, Phys. Rev. B 45 (1992) 13244–13249.
[9] (a) B. Delley, From molecules to solids with the DMol^3 approach, J. Chem. Phys. 113 (2000) 7756;
(b) Materials Studio and DMOL^3 are Accelrys Inc. products (see www.accelrys.com).
[10] A. Famulari, G. Raos, R. Po, S.V. Meille A solid state density functional study of crystalline alkylthiophene oligomers and polymers. Unpublished results.
[11] A. Gavezzotti, Molecular aggregation, in: Structure Analysis and Molecular Simulation of Crystals and Liquids, IUCr, Oxford University Press, Inc., New York, 2007, pp. 190–193.
[12] J. Du, C. Wu, H. Xiang, Y. Zhang, 2010, CN101811975, CAS 34841-39-9.
[13] N. Masciocchi, S. Galli, A. Sironi, X-ray powder diffraction characterization of polymeric metal diazolates, Comm. Inorg. Chem. 26 (2005) 1–37.
[14] W.I.F. David, K. Shankland, L.B. Mc Cusker, Ch. Baerlocher (Eds.), Structure Determination from Powder Diffraction Data, Oxford University Press, Oxford, UK, 2006.

Journal of Pharmaceutical and Biomedical Analysis 60 (2012) 71–79

Contents lists available at SciVerse ScienceDirect

Journal of Pharmaceutical and Biomedical Analysis

journal homepage: www.elsevier.com/locate/jpba

Rapid characterization of caged xanthones in the resin of *Garcinia hanburyi* using multiple mass spectrometric scanning modes: The importance of biosynthetic knowledge based prediction

Jing Yang[a,b], Li Ding[a,b,*], Linlin Hu[a,b], Shaohong Jin[c,**], Wenyuan Liu[a,b], Qidong You[d], Qinglong Guo[d]

[a] *Department of Pharmaceutical Analysis, China Pharmaceutical University, 24 Tongjiaxiang, Nanjing 210009, China*
[b] *Key Laboratory of Drug Quality Control and Pharmacovigilance, China Pharmaceutical University, 24 Tongjiaxiang, Nanjing 210009, China*
[c] *National Institution for the Control of Pharmaceutical and Biological Products, Beijing 100050, China*
[d] *Jiangsu Key Laboratory of Carcinogenesis and Intervention, China Pharmaceutical University, 24 Tongjiaxiang, Nanjing 210009, China*

ARTICLE INFO

Article history:
Received 3 July 2011
Received in revised form 28 October 2011
Accepted 29 October 2011
Available online 6 November 2011

Keywords:
Caged xanthones
Garcinia hanburyi
Biosynthetic knowledge
Mass spectrometry

ABSTRACT

Although the anticancer activities of the resin of *Garcinia hanburyi* have been well demonstrated, the chemical composition of this medicinal plant is still not fully understood. In this study, a highly effective qualitative method was developed for rapidly profiling the target and non-target caged xanthones in the resin of *G. hanburyi*. This method mainly involves three steps as follows: (1) prediction of the possible unknown caged xanthones in the resin of *G. hanburyi* according to the structure characters of the known ones and some well established biosynthetic knowledge; (2) structure classification according to the diagnostic fragment ions (DFIs) of the known caged *Garcinia* xanthones; (3) detection and characterization of the target and non-target caged xanthones in the resin of *G. hanburyi* using multiple mass spectrometric (MS) scanning modes. By use of such procedures, mass spectrometric data can be used for confirming the rationally predicted chemical structure rather than sophisticated and time-consumed *de novo* structure elucidation of a completely unknown component. Finally, a total of 34 caged xanthones including 18 likely new ones from the resin of *G. hanburyi* were rapidly detected and characterized within one working day.

1. Introduction

During the past few decades, inspired by the unusual chemical skeleton and remarkable bioactivity of caged xanthones derived mainly from the resin of *Garcinia hanburyi*, scientists from various fields have shown increasing interest in these promising natural products, gambogic acid being the best representative [1]. A lot of biological studies have revealed that these caged xanthones, characterized by a unique 4-oxa-tricyclo[4.3.1.$0^{3,7}$]dec-2-one scaffold, have potent inhibitory effects on several experimental tumors both *in vitro* and *in vivo* [2].

Although the anticancer activities of the resin of *G. hanburyi* are well recognized, the chemical profile of this plant extract is still not fully understood. Recently, Xu et al. [3] developed an ultra-performance liquid chromatography–quadrupole time-of-flight mass spectrometry method for analysis of 15 caged *Garcinia* xanthones, including two likely new ones. Guo et al. [4] identified 14 caged *Garcinia* xanthones using traditional phytochemistry methodology. To provide a more integrated chemical profile of the resin of *G. hanburyi*, this study was dedicated to developing a more effective qualitative method. However, rapid and reliable identification of complex chemical components in herbal medicines of interest remains a challenge, despite recent advances in analytical techniques. Hopefully, coincident with the accelerating increase of achievement in plant metabolic pathway engineering studies has been a growing appreciation of the biosynthetic knowledge of natural products or secondary metabolites [5]. Using this knowledge, a lot of unknown chemical components from the herbal medicines might be predicted based on the chemical structure of known component and then be monitored and characterized by modern analytical techniques especially liquid chromatography–mass spectrometry (LC–MS). This idea is analogous to the biotransformation knowledge based drug metabolites identification, which has been well recognized and successfully applied to many drug

* Corresponding author at: Department of Pharmaceutical Analysis, China Pharmaceutical University, 24 Tongjiaxiang, Nanjing 210009, China.
Tel.: +86 25 83271289; fax: +86 25 83271289.
** Corresponding author. Tel: +86 010 67095258; fax: +86 010 67095258.
E-mail addresses: dinglidl@hotmail.com, dinglihg@sina.com (L. Ding), shaohongjin@gmail.com (S. Jin).

0731-7085/$ – see front matter © 2011 Elsevier B.V. All rights reserved.
doi:10.1016/j.jpba.2011.10.035

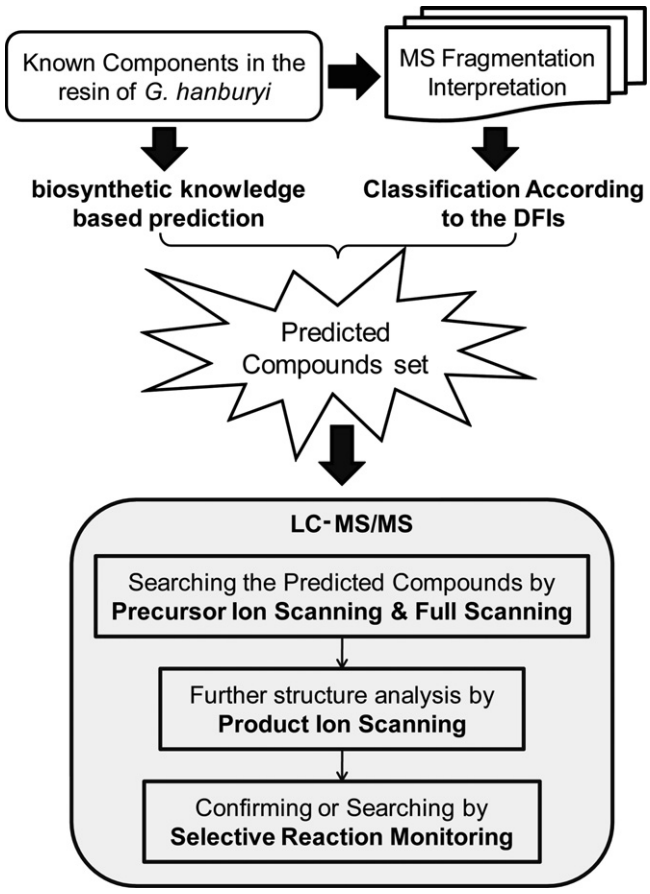

Fig. 1. The scheme of the proposed method for rapid discovery and characterization of caged xanthones in the resin of *G. hanburyi* (*Note*: DFIs, diagnostic fragment ions).

metabolites studies [6–8]. Conceivably, the biosynthetic knowledge based predictive strategy may also be applied for natural product discovery.

Therefore, the main purpose of this study is to meld the LC–MS/MS technique and some well established biosynthetic knowledge to rapidly profile the caged xanthones in the resin of *G. hanburyi*. This protocol mainly involves three steps as follows: (1) prediction of the possible unknown caged xanthones in the resin of *G. hanburyi* according to the structure characters of the known ones and some well established biosynthetic knowledge; (2) structure classification according to the diagnostic fragment ions (DFIs) of the known caged *Garcinia* xanthones; (3) detection and characterization of the target and non-target caged xanthones in the resin of *G. hanburyi* using multiple mass spectrometric (MS) scanning modes. By using this protocol (Fig. 1), a total of 34 caged xanthones, including 18 likely new ones, were originally detected and rapidly characterized in the resin of *G. hanburyi*.

2. Experimental

2.1. Chemicals and reagents

The dried resin powder of *G. hanburyi* was authenticated by *prof.* Feng Feng, Department of Natural Medicinal Chemistry, China Pharmaceutical University. The reference standards of forbesione, desoxygaudichaudione A, desoxymorellin, gambogenic acid and gambogic acid were kindly provided by *prof.* Feng Feng as well. HPLC grade acetonitrile and acetic acid were obtained from Tedia (Fairfield, OH, USA). Ammonium acetate was analytical grade and was obtained from Sinopharm Chemical Reagent Co, Ltd. (SCRC) (Shanghai, China). Deionized water was purified using a Milli-Q system (Millipore, Milford, MA, USA).

2.2. Instrumentation and LC–MS/MS conditions

The HPLC was performed using a Finnigan Surveyor LC Pump with an autosampler (Thermo Finnigan, San Jose, CA, USA). Isocratic chromatographic separation was performed on a Luna C18 column (150 mm × 2.0 mm i.d., 3.0 μm, Phenomenex, Torrance, CA, USA) with a security C18 guard column (4 mm × 2.0 mm i.d., Phenomenex); the mobile phase was composed of acetonitrile and 10 mM ammonium acetate in water (75:25, v/v), at a flow rate of 0.25 mL/min. The column temperature was maintained at 35 °C. Sample injection volume was 5 μL.

A TSQ Quantum Discovery MAX triple-quadrupole mass spectrometer (Thermo Finnigan), equipped with an ESI source, was used. Multiple mass spectrometric scanning modes including precursor ion scanning (PrecIS), full scanning (FS), product ion scanning (PIS), and selected reaction monitoring (SRM) were conducted for the qualitative analysis.

In negative ion mode, the spray voltage was set to −3.0 kV, and the capillary temperature was maintained at 320 °C. Nitrogen was used as the sheath gas (25 Arb) ion Sweep Gas (10 Arb) and auxiliary gas (5 Arb) for nebulization. The collision energy in the in-source dissociation mode was set at 7 eV. For collision-induced dissociation (CID), argon was used as the collision gas at a pressure of 1.5 mTorr and the collision energy was set at 40 or 50 eV.

In positive ion mode, the spray voltage was set to 4.0 kV, and the capillary temperature was maintained at 320 °C. Nitrogen was used as the sheath gas (30 Arb), ion Sweep Gas (10 Arb) and auxiliary gas (10 Arb) for nebulization. The collision energy in the in-source dissociation mode was set at 7 eV. For collision-induced dissociation (CID), argon was used as the collision gas at a pressure of 1.0 mTorr and the collision energy was set at 20 eV.

Both Q1 and Q3 peak widths were set at 0.7 Th. Analytical data were acquired using Xcalibur 2.0.7 software (Thermo Finnigan).

2.3. Sample preparation

The accurately weighed powder of dry resin of *G. hanburyi* (4.0 mg) was suspended in 5 mL acetonitrile, ultrasonically extracted for 30 min, and then cooled at room temperature. The solution was centrifuged at 15,000 rpm for 10 min. The supernatants (3 mL) were diluted with 1 mL water and filtered with 0.22 μm filtration membrane, and then transferred to an autosampler vial for LC–MS/MS analysis.

3. Results and discussion

3.1. Biosynthetic knowledge guided prediction of the possible unknown caged xanthones in the resin of G. hanburyi

The continuous investigation on *G. hanburyi* led to a series of reports of caged xanthones with potent anti-tumor activities [3,9–11]. Of interest, the side chain on the caged ring of these known xanthones mainly has four different types including prenyl unit, hydroxyl prenyl unit, formyl prenyl unit and carboxyl prenyl unit. In view of that change to the oxidation state of a molecule is one of the most frequent procedures as a natural product is synthesized or modified [12], it is appropriate to presume that the known caged xanthones containing carboxyl prenyl unit, such as gambogic acid and gambogenic acid, are the end products of successive bio-oxidation procedures (Fig. 2A). Moreover, this hypothesis is also understandable from chemical aspect, because the activation energy for allylic hydroxylation is relatively low. In principle, all of the known caged xanthones are derivable from these biosynthetic

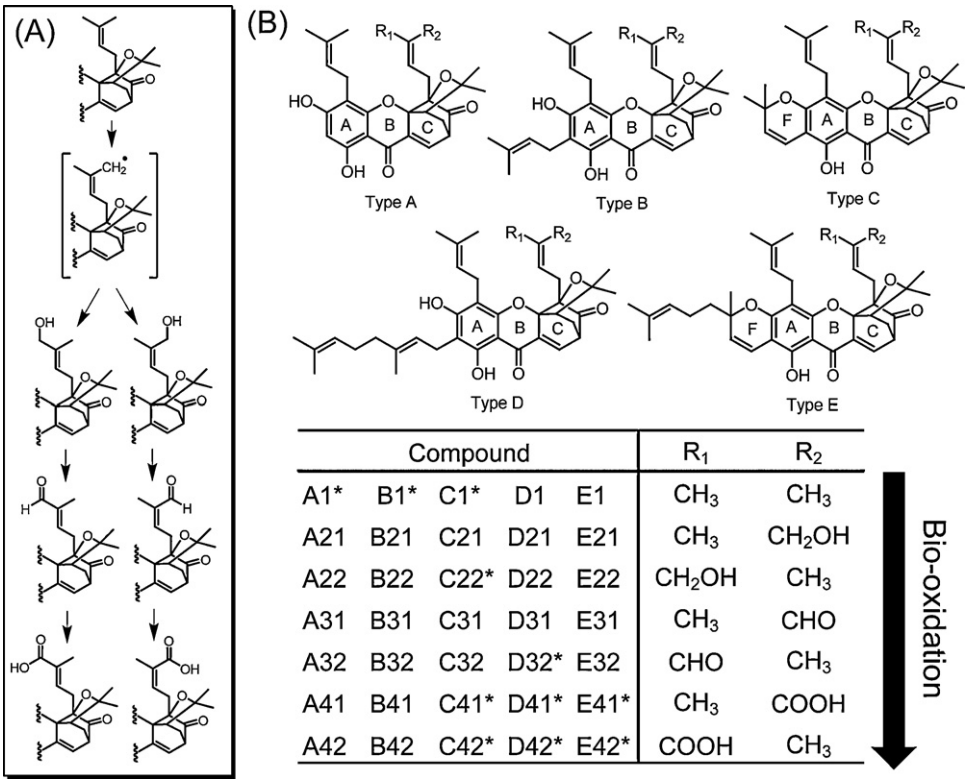

Compound					R_1	R_2
A1*	B1*	C1*	D1	E1	CH_3	CH_3
A21	B21	C21	D21	E21	CH_3	CH_2OH
A22	B22	C22*	D22	E22	CH_2OH	CH_3
A31	B31	C31	D31	E31	CH_3	CHO
A32	B32	C32	D32*	E32	CHO	CH_3
A41	B41	C41*	D41*	E41*	CH_3	COOH
A42	B42	C42*	D42*	E42*	COOH	CH_3

Fig. 2. The plausible biosynthetic pathway of caged xanthones in the resin of *G. hanburyi* (A) and the predictive compounds set (B). The compounds marked with asterisks refer to the known caged xanthones in the resin of *G. hanburyi*.

procedures. In addition, once mono-hydroxylation or successive bio-oxidation take place on the prenyl unit, a pair of *trans*, *cis*-isomers will be formed (Fig. 2A). Taken together, if a caged xanthone containing carboxyl prenyl unit has already been found in the resin of *G. hanburyi*, its analogs with different oxidation state may also exist, including its conformation isomer, one containing the original prenyl unit, two isomers containing hydroxyl prenyl unit, and two isomers containing formyl prenyl unit. In other word, at least six compounds containing the same chemical skeleton can be derived from one known caged *Garcinia* xanthone. According to this idea and the major known caged xanthones from the resin of *G. hanburyi*, a total of 35 caged xanthones including 11 known ones related to the bio-oxidation procedures were hypothetically predicted (Fig. 2B).

3.2. Diagnostic fragmentation ions (DFIs) of caged xanthones for structure classification

In general, compounds with a similar chemical skeleton are subjected to the similar mass spectrometric (MS) fragmentation pathways and thereby generate the so-called DFIs. The DFI can be used as a signature of a class of compounds with a similar chemical skeleton, so it is of value in structure identification of the target and non-target compounds from plant extracts [13–15]. To obtain the DFIs of caged xanthones from the resin of *G. hanburyi*, the reference standards of forbesione, desoxygaudichaudione A, desoxymorellin, gambogenic acid and gambogic acid were subjected to the MS and MS^2 analyses.

In positive ion mode, the major product ions of $[M+H]^+$ of all these caged xanthone are distinct (data not shown), although they undergo a similar fragmentation pattern. This finding was also supported by observations of Zhou et al. [3]. It is probably because that the most of the major product ions of these caged xanthones retain the structure information of the alteration to these compounds. Hence, no major product ions could be chosen as DFIs for a class of caged xanthones.

In negative ion mode, the deprotonated molecular ions $[M-H]^-$ of these reference standards undergo a major fragmentation pathway (Fig. 3). Initially, they undergo Retro-Diels–Alder (RDA) rearrangement to form intermediate A, and the latter will rapidly give the intermediate B by elimination of 2,2-dimethyl-2H-oxete (84 Da) through a series of charge and proton transferring processes. The intermediate B will lose the prenyl chain on caged ring or the substituted ones immediately and give the main characterized fragment ions of these 5 caged xanthones at *m*/*z* 325, 393, 391, 461 and 459 respectively (Fig. 3). The characteristic fragmentation of prenyl groups was also supported by observations of other groups [16,17]. Because each of these ions does not retain the structure information of the alteration to the C-ring prenyl chain, they can therefore be used as the DFIs for structure classification. Accordingly, the compounds shown in Fig. 2 were classified in five chemical structure types (A–E).

3.3. Rapid detection and characterization of caged xanthones in the resin of G. hanburyi

The precursor ion scanning (PrecIS) experiment using DFIs is an ideal means to start in the structure elucidation of non-target substances by determining if they contain an unaltered portion of the parent molecule or an expected alteration [18]. Accordingly, the PrecIS experiments using the aforementioned DFIs as the fixing product ions were first performed to screen the type A–E compounds depicted in Fig. 2, respectively. As shown in Fig. 4, a total of 14 known and 17 likely unknown components were detected. It is noteworthy that a cross-talk effect was found in the channel B with the DFI at *m*/*z* 393, because the type D compounds can also be fragmentized to give the same ion (Fig. 3D). By comparing the MS data in both positive and negative ionization modes and

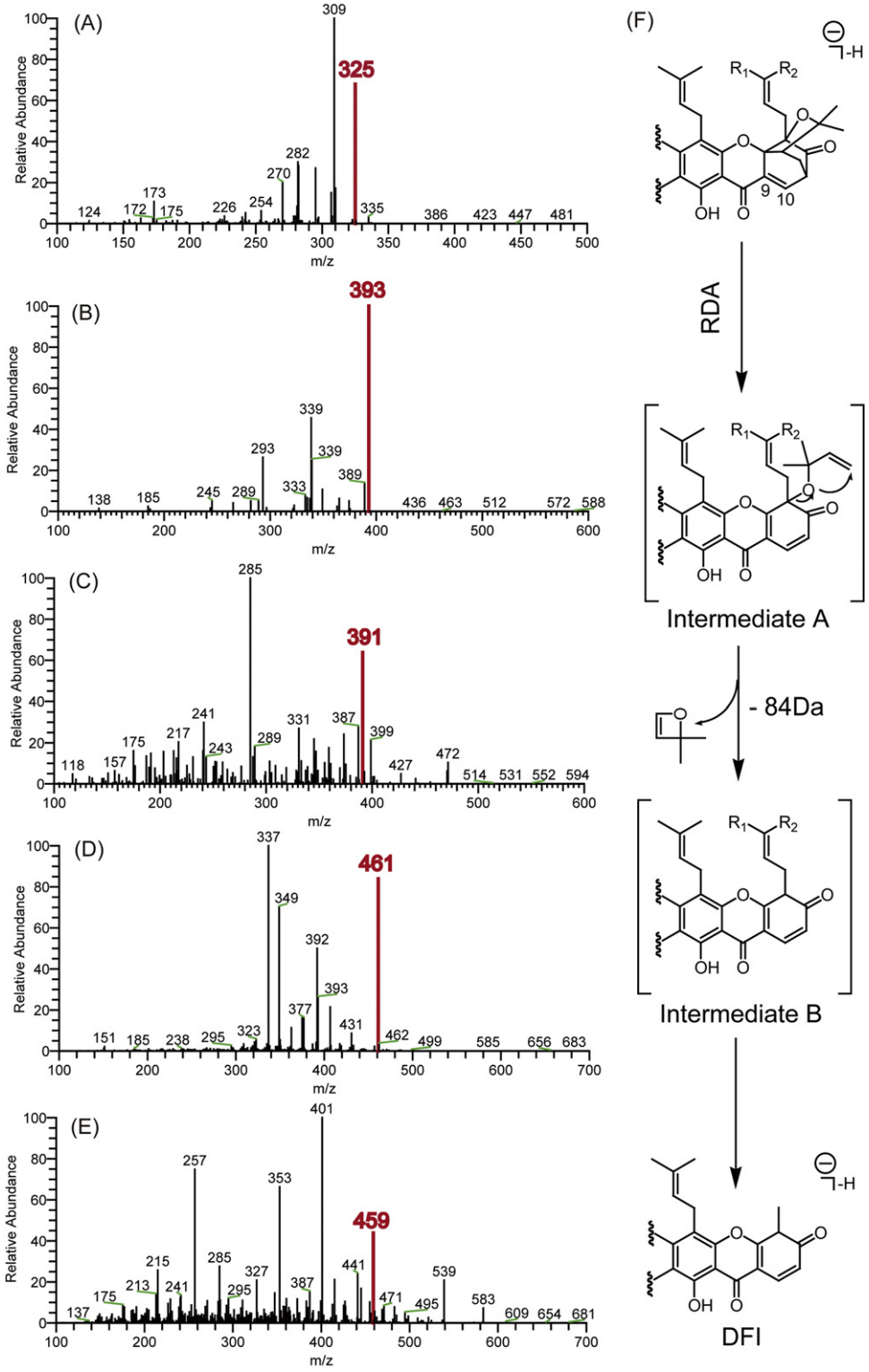

Fig. 3. Product ion scanning spectra of the reference standards of forbesione (A), desoxygaudichaudione A (B), desoxymorellin (C), gambogenic acid (D) and gambogic acid (E), and the proposed formation process of diagnostic fragment ions (DFIs) for caged xanthones from the resin of *G. hanburyi* in negative ion mode (F).

the retention times with those of the reference standards and/or the data in the literatures [3,19–21], the 14 known compounds were readily identified as forbesione (A1), desoxygaudichaudione A (B1), morellic acid (C41), isomorellic acid (C42), isogambogenin (D32), gambogenic acid (D41), isogambogenic acid (D42), S/R-gambogic acid (E41/E42), S/R-isogambogic acid (E43/E44), S-30-hydroxygambogic acid (E51) and R-30-hydroxyisogambogic acid (E52) and a minor known caged xanthone, hanburin (F1), respectively. The *trans*- and *cis*-isomers were differentiated by the McLafferty rearrangement fragment ions in positive ionization mode according to the protocol proposed by Zhou et al. [3]. Meanwhile, the elution order of the geometric isomers of the caged xanthone in the reverse phase HPLC experiments is generally the *trans* before the *cis* [3,21]. Among the left 17 likely unknown

Table 1
List of the caged xanthones identified in *G. hanburyi* by LC–(+/−) ESI-MS/MS.

No.	t_r (min)	$[M-H]^-$	Major fragment ions of $[M-H]^-$	$[M+H]^+$	Major fragment ions of $[M+H]^+$	Identification
A1	4.5	463	335, **325**, 310, 309(100), 295	465	437, 381(100), 313, 299, 285	Forbesione[S, R]
A41	4.9	493	365, 355(100), 340, **325**, 311	495	495, 467, 411(100), 439	Forbesionic acid
A42	4.7	493	365, 355(100), 340, **325**, 311	495	495, 467, 411(100), 439, 343, 329, 315	Isoforbesionic acid
B1	14.3	531	**393**(100), 377, 363, 349, 323	533	533, 507, 477(100), 459, 449, 431, 393	Desoxygaudichaudione A[S, R]
B21	7.5	547	**393**(100), 377, 363, 337,	549	549, 507, 489, 479, 493(100), 475, 465, 457, 409	Gaudichaudionol
B22	5.7	547	**393**(100), 377, 363, 337,	549	549, 507, 489, 479, 493(100), 475, 465, 457, 409	Isogaudichaudionol
$B2^{NP}$	21.3	547	463, 407, **393**(100), 377, 363, 337, 323	549	549, 507, 489, 479, 493(100), 465, 409	Epoxylgaudichaudione A
B31	7.8	545	**393**(100), 389, 379, 377, 363, 349, 337	547	547, 519, 491(100), 479, 463, 445, 427, 415	Gaudichaudione A
B32	7.5	545	**393**(100), 389, 379, 377, 363, 349, 337	547	547, 519, 491(100), 479, 463, 445, 427, 415, 393	Isogaudichaudione A
B41	8.0	561	517, **393**, 389, 377(100)	563	563, 535, 517, 507(100), 495, 489, 479, 461, 443, 421, 399	Gaudichaudionic acid
B42	5.3	561	517, 473, **393**(100), 389, 377, 349	563	563, 535, 517, 507(100), 495, 489, 479, 461, 443, 421, 399, 393	Isogaudichaudionic acid
C1	28.5	ND	NA	531	531, 503(100), 475, 447, 463, 429, 407, 419, 393, 351, 287	Desoxymorellin[S, R]
C21	9.7	ND	NA	547	547, 529, 511, 501, 491, 473, 461(100), 443, 433, 405	Morellinol
C22	9.0	ND	NA	547	547, 529, 511, 501, 491, 473, 461(100), 443, 433, 405	Isomorellinol[R]
C31	13.5	543	499, **391**(100), 363, 347, 285	545	545, 517, 499, 489, 477, 461, 421(100), 375	Morellin
C32	12.9	543	**391**(100), 373	545	545, 517, 499, 489, 477, 461, 421(100), 379, 375	Isomorellin
C41	8.1	559	515, 471, 427, **391**, 363, 347, 285(100)	561	561, 505(100), 477, 459, 419	Morellic acid[S, R]
C42	7.4	559	**391**(100), 373	561	561, 505(100), 477, 459, 419, 379	Isomorellic acid[S, R]
D1	44.4	599	**461**, 407, 392, 375, 363, 349, 337(100), 323	601	601, 573, 477(100), 459, 449, 431, 393, 367	Desoxygambogenin
D21	15.1	615	**461**, 407, 393, 392, 375, 363, 349, 337(100)	617	617, 589, 561, 533, 493(100), 465, 447, 409	Gambogeninol
D22	14.5	615	**461**, 407, 393, 392, 375, 363, 349, 337(100)	617	617, 589, 561, 533, 493(100), 465, 461, 447, 409	Isogambogeninol
D31	22.2	613	**461**, 407, 392, 375, 363, 349, 337(100), 323, 309	615	615, 587, 559, 531, 491(100), 463, 435, 367	Gambogenin
D32	20.4	613	**461**, 407, 392, 375, 363, 349, 337(100), 323, 309	615	615, 587, 559, 531, 491(100), 463, 435, 367	Isogambogenin[R]
D41	13.3	629	585, **461**, 407, 393, 392, 375, 363, 349, 337(100), 323, 309	631	631, 603, 575, 547, 529, 507(100), 479, 461, 443	Gambogenic acid[S, R]
D42	11.2	629	585, **461**, 407, 393, 392, 375, 363, 349, 337(100), 323, 309	631	631, 603, 575, 547, 529, 507(100), 479, 461, 443	Isogambogenic acid[R]
D^{NP}	8.2	631	**461**(100), 392	633	633, 615, 605, 587, 549, 509(100), 491, 481, 473, 425	Dihydrodesoxygambogenin
E41	23.2	627	583, 539, **459**, 445, 415, 401(100), 353, 285, 257	629	629, 601, 573(100), 561, 545, 527, 487, 355, 299	S-gambogic acid[S, R]
E42	22.3	627	583, 539, **459**, 445, 415, 401(100), 353, 285, 257	629	629, 601, 573(100), 561, 545, 527, 487, 355, 299	R-gambogic acid[S, R]
E43	19.8	627	**459**(100), 390	629	629, 601, 573(100), 561, 545, 527, 487, 447, 355, 299	S-isogambogic acid[R]
E44	17.2	627	**459**(100), 390	629	629, 601, 573(100), 561, 545, 527, 487, 447, 355, 299	R-isogambogic acid[R]
E51	9.6	643	599, 581, 555(100), 537, 493, **459**, 431, 353, 285, 257	645	645, 627, 599, 589(100), 571, 559, 543, 503	S-30-Hydroxygambogic acid[R]
E52	9.2	643	599, 581, 555(100), 537, 493, **459**, 431, 353, 285, 257	645	645, 627, 599, 589(100), 571, 559, 543, 503	R-30-Hydroxygambogic acid[R]
E^{NP}	18.2	631	587, 573, 545, 485, **459**(100), 419, 391	633	633, 605, 587, 577(100), 549, 521, 491, 355	Tetrahydrogambogic acid
F1	12.8	531	**393**(100), 377, 363, 349, 323	533	533, 507, 477(100), 459, 449, 431, 393	Hanburin[R]

Notes: t_r, retention time; the DFIs in negative ion mode were shown in bold font; ND, not detected; NA, not analyzed; NP, not predicted; *S*, with standard; *R*, with data in references.

components, 14 ones hit the predicted compounds set (Fig. 2) according to the deprotonated molecular ions $[M-H]^-$ in the extracted mass spectra and chromatographic behavior, which were preliminarily identified as forbesionic acid (A41), isoforbesionic acid (A42), gaudichaudionol (B21), isogaudichaudionol (B22), gaudichaudione A (B31), isogaudichaudione A (B32), gaudichaudionic acid (B41), isogaudichaudionic acid (B42), morellin (C31), isomorellin (C32), desoxygambogenin (D1), gambogeninol (D21),

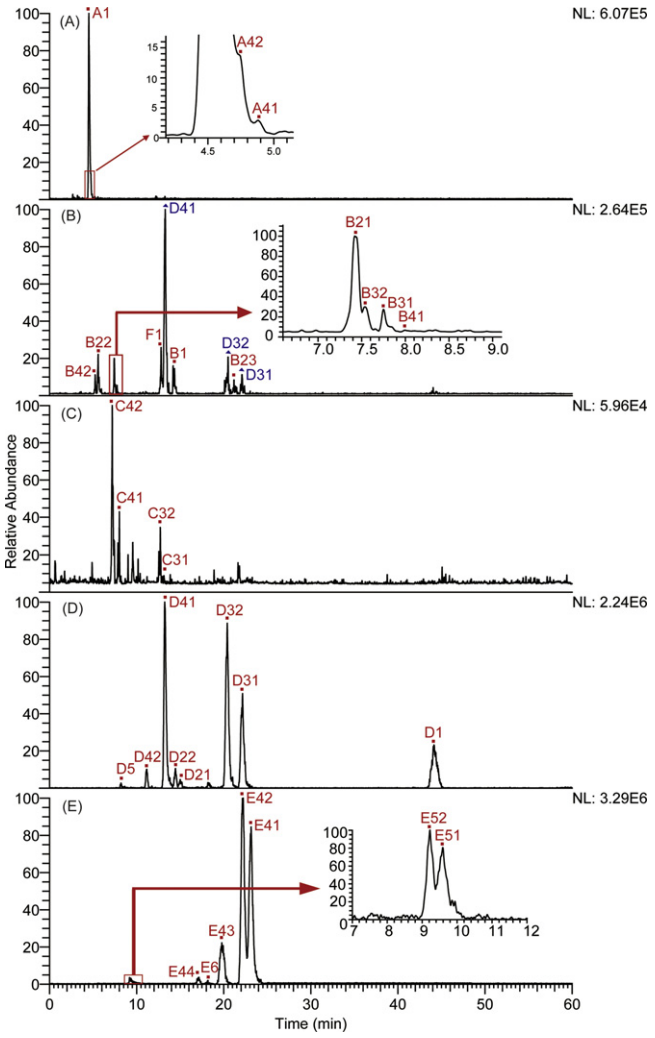

Fig. 4. Total ion chromatograms of the resin of *G. hanburyi* obtained from the precursor ion scanning experiments in negative ion mode using the fixed product ions at *m*/*z* 325 (A), 393 (B), 391 (C), 461 (D) and 459 (E), respectively.

isogambogeninol (D22), gambogenin (D31), respectively (Table 1). However, two target caged xanthones, desoxymorellin (C1) and morellinol (C21), and 11 non-target ones in the predicted compound set failed to be detected in the PrecIS experiments, it was probable because of the limitations of the analytical capacity of this mode [8].

Next, both the negative ion full scanning and the positive ion full scanning modes were performed for the further screening tests. In addition to the detected components by the PrecIS experiments, three new but weak peaks were detected in the positive ion full scanning mode to give the predominate ions at *m*/*z* 531, 547, 547 respectively, which could be preliminarily assigned as the protonated molecular ions $[M+H]^+$ of desoxymorellin (C1), morellinol (C21) and isomorellinol (C22), respectively.

To further confirm the structures of the detected target and non-target components, the product ion scanning (PIS) experiments were conducted to give more structure information. Table 1 lists the major fragment ions of deprotonated/protonated molecular ions of these components formed in the (+/−) ESI source. As expected, the components classified in the same type generated almost the same major fragment ions in negative ion mode. These major fragmentation patterns include: (1) RDA rearrangement, which occurs at the double bond in the C ring for all the components and occurs mainly at the double bond in at the B ring for type C and E compounds [22]; (2) loss of side chain in the A ring (for types B and D) or F ring (for types C and E); (3) neutral loss of the small molecules such as CO_2, CO and H_2O (Fig. 5). This result further demonstrated the accuracy of structure classification. However, the negative ion MS^2 spectra the caged xanthones could not provide adequate structure information about the alteration to the C-ring side chain of these xanthones. By contrast, most of the major product ions of the caged xanthones retain these structure information in positive ion mode (Fig. 6). It is probably because that the protonated molecular ions of these compounds may give the relative stable intermediate B (Fig. 3) [3]. Accordingly, the positive ion MS^2 spectra of the detected caged *Garcinia* xanthones were used principally to further confirm their chemical structures. Finally, all of the major fragment ions in the (+/−) ESI-MS^2 spectra can be properly assigned for the preliminarily characterized components.

Furthermore, the SRM experiments were also performed to screen the undetected components in the predictive compounds set by setting the possible transitions of the deprotonated molecular ions of these components to their corresponding DFIs. Some new but weak chromatographic peaks could be detected in the transition channels of *m*/*z* 479 → 325, *m*/*z* 613 → 459 which referred to the A21/22 and E21/22 (data not shown). However, their chemical structure cannot be confirmed because of the lack of MS^2 data, and further study is needed.

To sum up, a total of 34 components including 16 known caged xanthones and 15 likely new ones in the resin of *G. hanburyi* were rapidly detected using multiple mass spectrometric scanning modes, and their chemical structures were confirmed by reference standards and/or (+/−) ESI-MS^2 data as well as chromatographic behaviors.

3.4. Identification of the non-target components out of the proposed predictive compounds set

Three non-target components being failed by hitting the proposed predictive compounds set were detected in the PrecIS experiments (Fig. 4). According to their corresponding detection channels (Table 1), they could be easily classified and were denoted as B23, D5 and E6 respectively. The PrecIS spectra of these components exhibited the deprotonated molecular ions at *m*/*z* 547, 631 and 631 respectively. The mass shifts of 16 Da, 32 Da and 4 Da compared with B1, D1 and E1 respectively implied mono-oxidation, di-oxidation and di-reduction of the latter molecules respectively.

The B23 peak has the similar (+/−) ESI-MS^2 spectra to those of the B21/22 (Table 1). However, the retention of the former on the C18 column was much stronger than that of the latter two compounds (Fig. 4B). This finding tentatively suggested that the B23 might be the epoxidation product of B1 (desoxygaudichaudione A) and that the epoxidation most likely took place on the C-ring prenyl chain.

The D5 peak exhibited the similar fragmentation pathway to all the type D compounds to give the major characteristic fragment ions at *m*/*z* 549, 509, 425 in positive ion mode. Combined with the relative weak retention on the C18 column, D5 could be tentatively characterized as dihydrodesoxygambogenin.

The E6 peak showed the similar fragmentation pathway to the E41/42 to give some major characteristic fragment ions at *m*/*z* 587 ($-CO_2$) and 459 (DFI of type E) in negative ion mode and at *m*/*z* 577, 549, 491 in positive ion mode. Thus, E6 could be tentatively identified as the tetrahydrogambogic acid, and the reduction occurred most likely in the caged ring.

Of note, although these 3 likely new caged xanthones did not hit the proposed predictive compounds set, their structure analysis could also be guided by the biosynthetic knowledge.

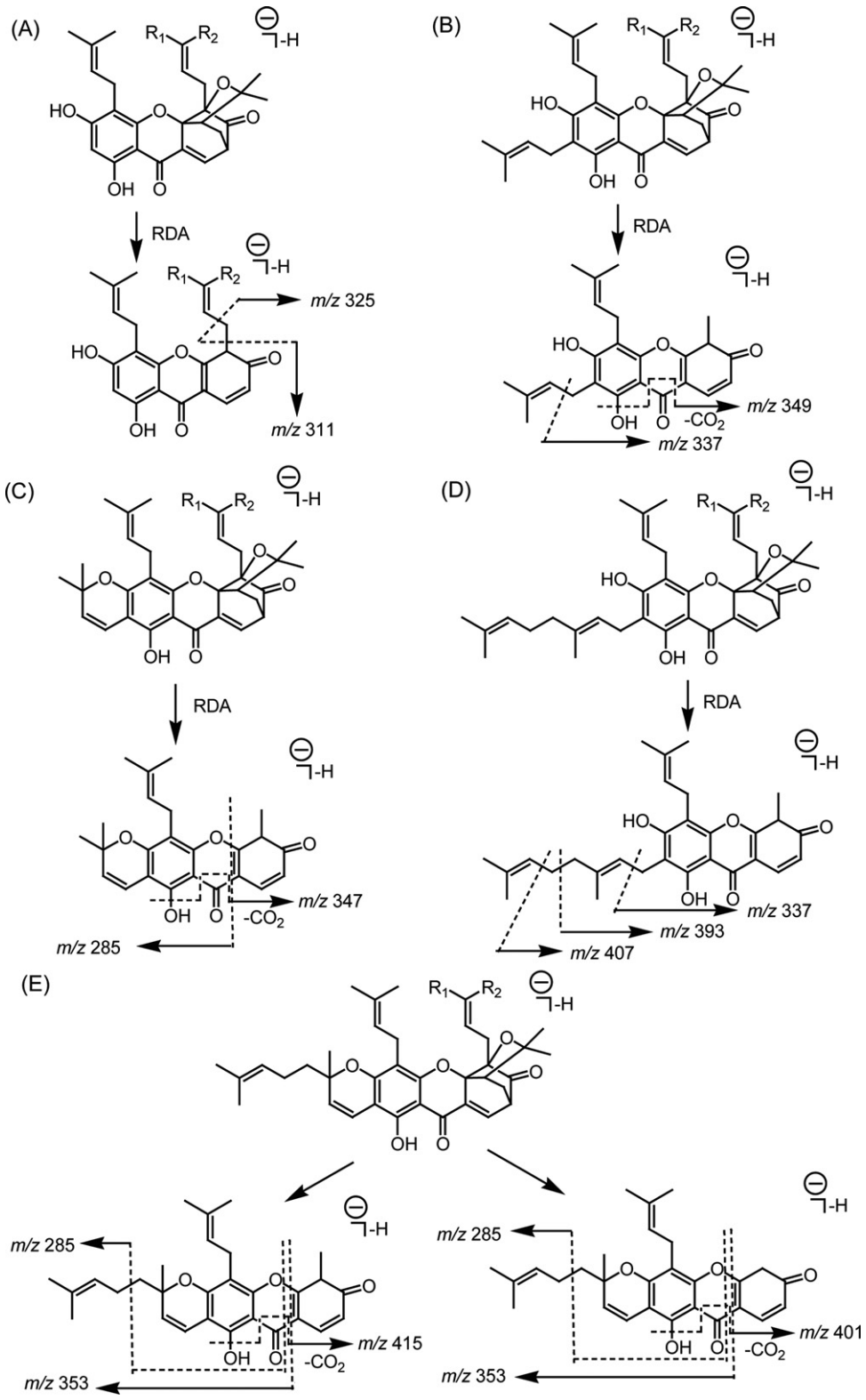

Fig. 5. Proposed fragmentation pathways of caged xanthones from the resin of *G. hanburyi* in negative ion mode.

3.5. The importance of biosynthetic knowledge based prediction in nature products discovery

During the past few decades, biosynthetic knowledge and methods have greatly promoted the development of phytochemistry research. As a result, the plausible chemical origins of known natural products could be well predicted by this knowledge [23,24]. Furthermore, many biosynthesis or bio-modification patterns on the specific sites or groups of some natural products could also be well rationally predicted. In this study, the knowledge of the changes to the oxidation state of a molecule, one of the most frequent biosynthetic procedures, was used to predict the possible

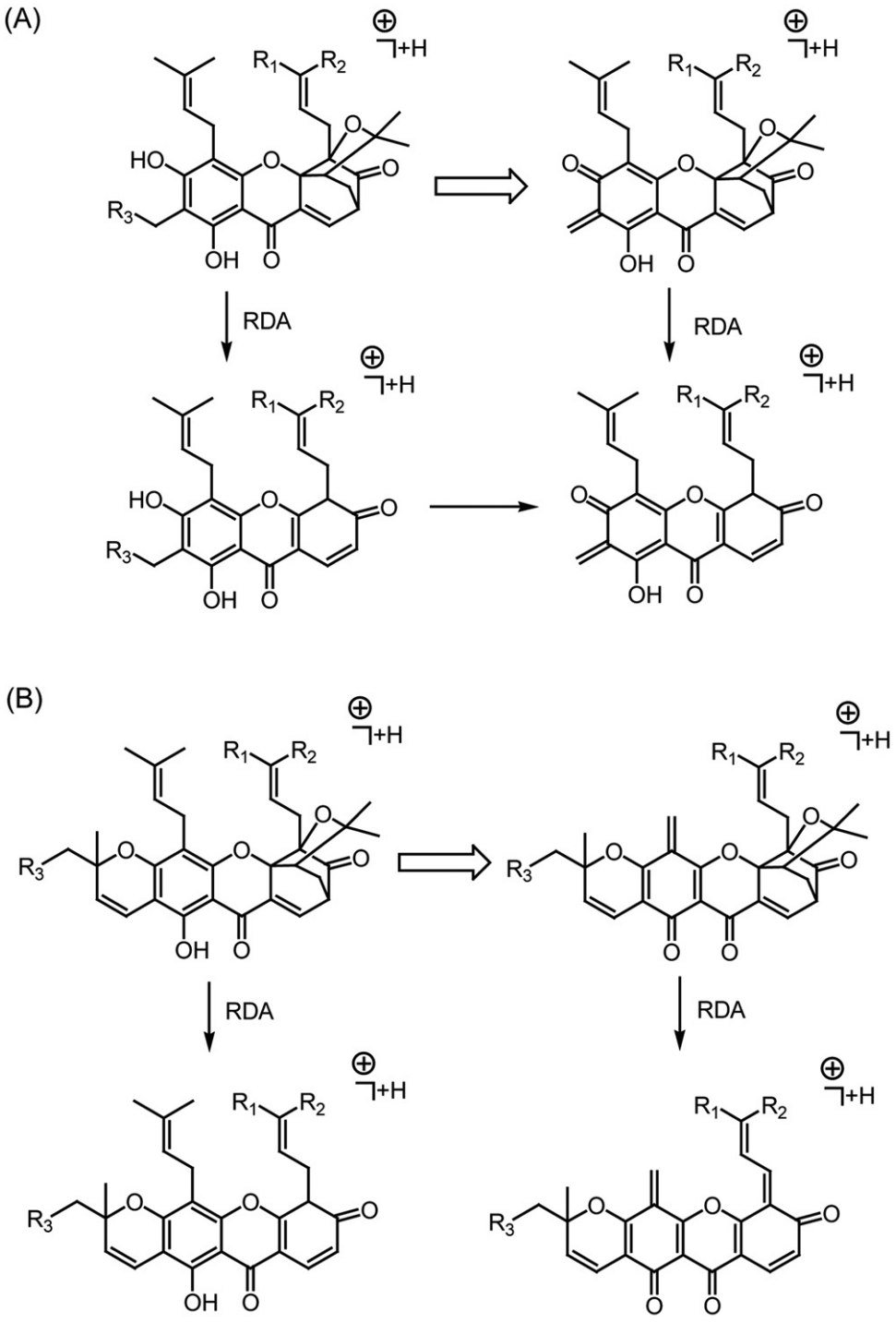

Fig. 6. Proposed fragmentation pathways of caged xanthones from the resin of *G. hanburyi* in positive ion mode.

non-target caged xanthones in the resin of *G. hanburyi*. In addition, there are many other biosynthetic procedures that can be also used for structure prediction, such as methylation and acetylation on the hydroxyl and phenolic hydroxyl groups [25,26], esterification [27], cyclization via nucleophilic attack [28], etc. Moreover, many bioactive natural products such as ginsenoside and flavonoid glycosides contain one or more sugar units in their structure, and an understanding of biosynthetic pathways also allows rational connecting links of sugar units to be established [12]. However, the non-target natural product with a novel chemical skeleton can hardly be predicted according to the current biosynthetic knowledge, it is mainly because that the formation of these structures generally undergoes some unusual chemical and enzymatic procedures. Nevertheless, the present study first demonstrated that a combination of biosynthetic knowledge guided prediction and advanced LC–MS/MS technique is a promising protocol for rapid profiling natural products, whereas it will require more proof-of-concept studies in the future. This protocol allows MS data to be used for confirmatory analysis of the rationally predicted chemical structure rather than the sophisticated and time-consumed *de novo* structure elucidation of a completely unknown component, thus boosting the efficiency of MS analysis.

4. Conclusions

In this study, a highly effective qualitative method (Fig. 1) was developed for rapidly profiling the target and non-target caged xanthones in the resin of *G. hanburyi*. Collectively, a total of 34 caged xanthones including 18 likely new ones from the resin of *G. hanburyi* were rapidly detected and characterized within one working day. More generally, this study demonstrated that a combination of biosynthetic knowledge guided prediction and advanced LC–MS/MS technique could serve as a valuable tool in natural products discovery.

Acknowledgements

This work was financially supported by the National Natural Science Foundation of China (Grant No. 81072609), and the authors would like to thank *prof.* Feng Feng, China Pharmaceutical University, for kindly providing us the reference standards and thank *prof.* Boyang Yu, *prof.* Zhunjian Zhang, and *prof.* Jianping Zhou, China Pharmaceutical University, for their helpful advises and discussions.

References

[1] Q.B. Han, H.X. Xu, Caged *Garcinia* xanthones: development since 1937, Curr. Med. Chem. 16 (2009) 3775–3796.
[2] Q.L. Guo, Q.D. You, Z.Q. Wu, S.T. Yuan, L. Zhao, General gambogic acids inhibited growth of human hepatoma SMMC-7721 cells in vitro and in nude mice, Acta Pharmacol. Sin. 25 (2004) 769–774.
[3] Y. Zhou, X. Liu, J. Yang, Q.B. Han, J.Z. Song, S.L. Li, C.F. Qiao, L.S. Ding, H.X. Xu, Analysis of caged xanthones from the resin of *Garcinia hanburyi* using ultra-performance liquid chromatography/electrospray ionization quadrupole time-of-flight tandem mass spectrometry, Anal. Chim. Acta 629 (2008) 104–118.
[4] S.J. Tao, S.H. Guan, W. Wang, Z.Q. Lu, G.T. Chen, N. Sha, Q.X. Yue, X. Liu, D.A. Guo, Cytotoxic polyprenylated xanthones from the resin of *Garcinia hanburyi*, J. Nat. Prod. 72 (2009) 117–124.
[5] S.B. Zotchev, Biosynthesis of natural products applied to drug discovery, Curr. Top. Med. Chem. 8 (2008) 616–617.
[6] Y. Wang, X. Chen, Q. Li, D. Zhong, Metabolite identification of arbidol in human urine by the study of CID fragmentation pathways using HPLC coupled with ion trap mass spectrometry, J. Mass Spectrom. 43 (2008) 1099–1109.
[7] J. Yang, L. Ding, S. Jin, X. Liu, W. Liu, Z. Wang, Identification and quantitative determination of a major circulating metabolite of gambogic acid in human, J. Chromatogr. B: Anal. Technol. Biomed. Life Sci. 878 (2010) 659–666.
[8] N.J. Clarke, D. Rindgen, W.A. Korfmacher, K.A. Cox, Systematic LC/MS metabolite identification in drug discovery, Anal. Chem. 73 (2001) 430A–439A.
[9] Q.B. Han, Y. Zhou, C. Feng, G. Xu, S.X. Huang, S.L. Li, C.F. Qiao, J.Z. Song, D.C. Chang, K.Q. Luo, H.X. Xu, Bioassay guided discovery of apoptosis inducers from gamboge by high-speed counter-current chromatography and high-pressure liquid chromatography/electrospray ionization quadrupole time-of-flight mass spectrometry, J. Chromatogr. B: Anal. Technol. Biomed. Life Sci. 877 (2009) 401–407.
[10] Q. Han, L. Yang, Y. Liu, Y. Wang, C. Qiao, J. Song, L. Xu, D. Yang, S. Chen, H. Xu, Gambogic acid and epigambogic acid, C-2 epimers with novel anticancer effects from *Garcinia hanburyi*, Planta Med. 72 (2006) 281–284.
[11] Q.B. Han, J.Z. Song, C.F. Qiao, L. Wong, H.X. Xu, Preparative separation of gambogic acid and its C-2 epimer using recycling high-speed counter-current chromatography, J. Chromatogr. A 1127 (2006) 298–301.
[12] P.M. Dewick, Medicinal Natural Products: A Biosynthetic Approach, 2nd ed., John Wiley & Sons, Ltd., Chichester, 2002.
[13] R. Li, Y. Zhou, Z. Wu, L. Ding, ESI-QqTOF-MS/MS and APCI-IT-MS/MS analysis of steroid saponins from the rhizomes of *Dioscorea panthaica*, J. Mass Spectrom. 41 (2006) 1–22.
[14] J. Liu, X. Yang, J. He, M. Xia, L. Xu, S. Yang, Structure analysis of triterpene saponins in *Polygala tenuifolia* by electrospray ionization ion trap multiple-stage mass spectrometry, J. Mass Spectrom. 42 (2007) 861–873.
[15] B. Portet, N. Fabre, R. Rozenberg, J.L. Habib-Jiwan, C. Moulis, J. Quetin-Leclercq, Analysis of minor flavonoids in *Piper hostmannianum* var. berbicense using liquid chromatography coupled with atmospheric pressure chemical ionization mass spectrometry, J. Chromatogr. A 1210 (2008) 45–54.
[16] R. Simons, J.P. Vincken, M.C. Bohin, T.F. Kuijpers, M.A. Verbruggen, H. Gruppen, Identification of prenylated pterocarpans and other isoflavonoids in *Rhizopus* spp. elicited soya bean seedlings by electrospray ionisation mass spectrometry, Rapid Commun. Mass Spectrom. 25 (2011) 55–65.
[17] C.T. da Costa, J.J. Dalluge, M.J. Welch, B. Coxon, S.A. Margolis, D. Horton, Characterization of prenylated xanthones and flavanones by liquid chromatography/atmospheric pressure chemical ionization mass spectrometry, J. Mass Spectrom. 35 (2000) 540–549.
[18] A.H. Iglesias, L.F. Santos, F.C. Gozzo, Identification of cross-linked peptides by high-resolution precursor ion scan, Anal. Chem. 82 (2010) 909–916.
[19] J. Asano, K. Chiba, M. Tada, T. Yoshii, Cytotoxic xanthones from *Garcinia hanburyi*, Phytochemistry 41 (1996) 815–820.
[20] F. Feng, W.Y. Liu, Y.S. Chen, Q.L. Guo, Q.D. You, Five novel prenylated xanthones from Resina Garciniae, J. Asian Nat. Prod. Res. 9 (2007) 735–741.
[21] S.L. Li, J.Z. Song, Q.B. Han, C.F. Qiao, H.X. Xu, Improved high-performance liquid chromatographic method for simultaneous determination of 12 cytotoxic caged xanthones in gamboges, a potential anticancer resin from *Garcinia hanburyi*, Biomed. Chromatogr. 22 (2008) 637–644.
[22] J. Yang, L. Ding, L.L. Hu, S.H. Jin, W.Y. Liu, Z.Z. Wang, W. Xiao, Q.D. You, Q.L. Guo, Comparison of electron capture—atmospheric pressure chemical ionization and electrospray ionization for the analysis of gambogic acid and its main circulating metabolite in dog plasma, Eur. J. Mass Spectrom. (Chichester, England) 16 (2010) 605–617.
[23] P.M. Dewick, The biosynthesis of C5–C25 terpenoid compounds, Nat. Prod. Rep. 19 (2002) 181–222.
[24] P.M. Dewick, Biosynthesis of rotenoids and coumestans, Hoppe Seylers Z. Physiol. Chem. 353 (1972) 132–133.
[25] C. Zheng, H. Hao, X. Wang, X. Wu, G. Wang, G. Sang, Y. Liang, L. Xie, C. Xia, X. Yao, Diagnostic fragment-ion-based extension strategy for rapid screening and identification of serial components of homologous families contained in traditional Chinese medicine prescription using high-resolution LC–ESI-IT-TOF/MS: Shengmai injection as an example, J. Mass Spectrom. 44 (2009) 230–244.
[26] J. Luo, J.S. Wang, X.B. Wang, J.G. Luo, L.Y. Kong, Chuktabularins E-T, 16-norphragmalin limonoids from *Chukrasia tabularis* var. velutina, J. Nat. Prod. 73 (2010) 835–843.
[27] R.M. Van Wagoner, M. Satake, A.J. Bourdelais, D.G. Baden, J.L. Wright, Absolute configuration of brevisamide and brevisin: confirmation of a universal biosynthetic process for *Karenia brevis* polyethers, J. Nat. Prod. 73 (2010) 1177–1179.
[28] R.B. Williams, J.F. Hu, K.M. Olson, V.L. Norman, M.G. Goering, M. O'Neil-Johnson, G.R. Eldridge, C.M. Starks, Antibiotic indole sesquiterpene alkaloid from Greenwayodendron suaveolens with a new natural product framework, J. Nat. Prod. 73 (2010) 1008–1011.

Journal of Pharmaceutical and Biomedical Analysis 60 (2012) 80–85

Contents lists available at SciVerse ScienceDirect

Journal of Pharmaceutical and Biomedical Analysis

journal homepage: www.elsevier.com/locate/jpba

Short communication

Simultaneous analysis method for polar and non-polar ginsenosides in red ginseng by reversed-phase HPLC-PAD

Sa-Im Lee[a], Ha-Jeong Kwon[b], Yong-Moon Lee[c], Je-Hyun Lee[d], Seon-Pyo Hong[a,*]

[a] Department of Oriental Pharmaceutical Sciences, Kyung Hee East-West Pharmaceutical Research Institute, College of Pharmacy, Kyung Hee University, Hoegi-dong, Dongdaemoon-gu, Seoul 130-701, South Korea
[b] Department of Preventive and Social Dentistry, College of Dentistry, Kyung Hee University, Hoegi-dong, Dongdaemoon-gu, Seoul 130-701, South Korea
[c] College of Pharmacy, CBITRC, Chungbuk National University, Chongju 361-763, South Korea
[d] Department of Korean Medicine, Dongguk University, Geongju 780-714, South Korea

ARTICLE INFO

Article history:
Received 19 May 2011
Accepted 18 August 2011
Available online 25 August 2011

Keywords:
Column temperature
Ginsenosides
Pulsed amperometric detection
Red ginseng
Simultaneous determination

ABSTRACT

The paper describes the development of a simultaneous determination method for polar and non-polar ginsenosides in red ginseng with a reversed-phase high-performance liquid chromatography-pulsed amperometric detection method. This method could be applied directly without any pretreatment steps and enabled the performance of highly sensitive analysis within 1 h. The detection ($S/N = 3$) and quantification ($S/N = 10$) limits for the ginsenosides ranged 0.02–0.10 ng and 0.1–0.3 ng, respectively. The linear regression coefficients ranged 0.9975–0.9998. Intra- and inter-day precisions were <9.91%. The mean recoveries ranged 98.08–103.06%. The total amount of ginsenosides in the hairy root of red ginseng was higher than that in the main root.

1. Introduction

Ginseng, the root of *Panax ginseng*, is widely used in Chinese traditional medicine and contains diverse polar ginsenosides (triterpene saponins) as active ingredients. Red ginseng is generated from ginseng through an additional steaming and drying step. During the steaming process, some of the polar ginsenosides are transformed into non-polar ginsenosides by hydrolysis of the sugar moieties. Consequently, non-polar ginsenosides are newly produced from polar ginsenosides and exist only in red ginseng. As such, the name provided by the Korean Pharmacopoeia (IX) for red ginseng (Ginseng Radix Rubra) is different from that for ginseng (Ginseng Radix Alba).

Polar and non-polar ginsenosides have diverse biologically beneficial activities, such as neuroprotective (G-Rb_1, G-Rd, G-Rg_1, G-Rg_2, G-Rg_3) [1–4], anti-cancer (G-Rb_2, G-Rg_3, G-Rh_2) [5–8], cardio-protective (G-Rb_3) [9], anti-diabetic (G-Rc) [10], anti-nociception (G-Rf) [11], anti-oxidant (G-Re, G-Rg_3, G-Rh_1, G-Rh_2) [12–15], vasodilating (G-Rg_3) [16], and hepatoprotective effects (G-Rg_3, G-Rh_2) [17]. Red ginseng contains typical non-polar ginsenosides such as ginsenoside Rg_2 (G-Rg_2), G-Rg_3, G-Rh_1, and G-Rh_2, as well as polar ginsenosides such as G-Rb_1, G-Rb_2, G-Rb_3, G-Rc, G-Rd, G-Rf, G-Rg_1, and G-Re [18,19]. The chemical structures of these various ginsenosides are shown in Fig. 1.

The separation of ginsenosides on various functional columns was unsuccessful because of the significant difference in polarity between polar and non-polar ginsenosides. Therefore, analytical methods for ginsenosides have mainly been developed specifically for polar [20–23] or non-polar ginsenosides [24]. HPLC-evaporate light scattering detection (HPLC-ELSD) is a general method for detecting both polar and non-polar ginsenosides [25]. However, it could not be used to detect the small quantity of non-polar ginsenosides in red ginseng because of its limited detectability (0.3 μg for G-Rg_2, 0.3 μg for G-Rh_1, 0.1 μg for G-Rh_2). Charged aerosol detection (CAD) method introduced as an alternative to ELSD, had better sensitivity, wider dynamic range, ease of use, and constancy of response factors than ELSD method [26]. And there was enzyme-linked immunosorbent assay (ELISA) method as a way to detect ginsenosides [27,28]. However, they could not also solve the problem, such as limited detectability for non-polar ginsenosides. A sensitive and quantitative method to simultaneously identify polar and non-polar ginsenosides in red ginseng is therefore needed.

Pulsed amperometric detection (PAD) is an electrochemical detection method that measures the positive potential produced by carbohydrate oxidation on a gold electrode, allowing the direct detection of carbohydrates at low pico-mol levels [29]. High-performance anion-exchange chromatography-pulsed amperometric detection (HPAEC-PAD) has been used to quantify carbohydrates in plant resources [30–32] because of its strong

* Corresponding author. Tel.: +82 2 961 9207; fax: +82 2 966 3885.
E-mail address: seonhong@khu.ac.kr (S.-P. Hong).

0731-7085/$ – see front matter © 2011 Elsevier B.V. All rights reserved.
doi:10.1016/j.jpba.2011.08.030

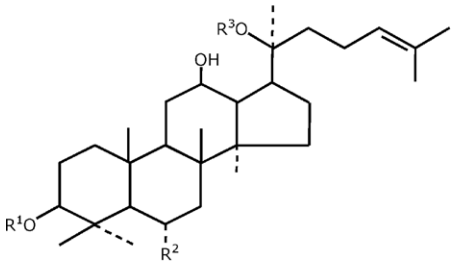

20(S)-protopanaxadiol type
R^2=H

	R^1	R^3
Rb_1	-Glc^2-Glc	-Glc^6-Glc
Rb_2	-Glc^2-Glc	-Glc^6-Ara(p)
Rb_3	-Glc^2-Glc	-Glc^6-Xyl
Rc	-Glc^2-Glc	-Glc^6-Ara(f)
Rd	-Glc^2-Glc	-Glc
Rg_3	-Glc^2-Glc	-H
Rh_2	-Glc	-H

20(S)-protopanaxatriol type
R^1= -H, R^2= -O-R^4

	R^3	R^4
Re	-Glc	-Glc^2-Rha
Rf	-H	-Glc^2-Glc
Rg_1	-Glc	-Glc
Rg_2	-H	-Glc^2-Rha
Rh_1	-H	-Glc

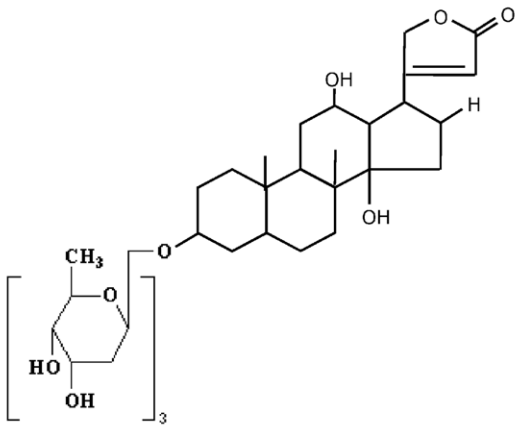

Digoxin

Fig. 1. Chemical structures of ginsenosides and digoxin (I.S.).

anion-exchange properties that efficiently separate carbohydrates. However, HPAEC-PAD has rarely been applied to the analysis of glycosides because of the difficulty in separating glycosides from sugars on an anion exchange column.

We have developed two different reversed-phase methods of HPLC-PAD (RP-HPLC-PAD) for polar [33] or non-polar ginsenosides [24]. However, simultaneous separation of the polar and non-polar ginsenosides remains difficult. Such separations result in a chromatogram with various problems, such as severely overlapping ginsenoside peaks and long analysis times when changes in the eluent compositions or gradient system are applied. The present study describes a simultaneous determination method for polar and non-polar ginsenosides in red ginseng through the optimization of several analytical conditions. This new method could be applied directly without pretreatment or extraction steps and enabled highly sensitive analysis within 1 h.

2. Experimental

2.1. Materials

Crude drugs were purchased from the *Kyungdong* Market (Seoul, South Korea) in accordance with the standards stipulated in Korea Pharmacopoeia (VIII). The main roots of 6-year-old red ginseng (MR-6) and the hairy roots of 6-year-old red ginseng (HR-6) were purchased from a local drug store. HPLC-grade acetonitrile and 50% sodium hydroxide were purchased from Fisher Scientific (Fairlawn, NJ, USA). All other reagents and solvents used were of guaranteed or analytical grade.

G-Rg_3, G-Rh_2, G-Rg_2, G-Rh_1, G-Rb_2, G-Rb_3, and G-R_f were purchased from ChromaDex (Santa Ana, CA, USA). G-Rb_1, G-Rc, G-Rd, G-Re, and G-Rg_1 were purchased from Wako (Tokyo, Japan). Digoxin was purchased from Toronto Research Chemicals (Toronto, Canada). A Millipore membrane filter (type HA, pore size 0.45 μm) was used for solvent filtration. All samples were filtered through disposable syringe filters (Hydrophobic PTFE, pore size 0.20 μm, Advantec MFS, Tokyo, Japan) before injection. Standard solutions, sample solutions, and mobile phase were prepared using 18 MΩ purified water produced by an Automatic Aquarius AW-1001 water purification system (Top Trading, Seoul, South Korea).

2.2. Apparatus and high-performance liquid chromatography

A PAD system from the ICS-3000 series Dionex (Sunnyvale, CA, USA) was equipped with an Au-Flowcell containing a gold working electrode and a solvent-compatible cell containing an Ag/AgCl reference electrode. The gold electrode was cleaned by rubbing the surface twice a week with the pink eraser (Dionex P/N. 049721) provided in the polishing kit. HPLC equipment, consisting of a Model Nanospace SI-2/3201 pump and a 3004 column oven, was purchased from Shiseido (Tokyo, Japan). The Nanospace SI-2/3201 pump has a metal-free head made of polyetheretherketone (PEEK) resin, which resists aggressive chemicals such as alkaline solutions.

Chromatographic separation was performed using a Kinetex C-18 column (100 mm × 2.1 mm I.D.; 2.6 μm, Phenomenex, Torrance CA) or a Unison UK-C-18 column (150 mm × 2.0 mm I.D.; 3 μm, Imtakt, Kyoto, Japan). The potential waveform was as follows: E1 = −0.2 V (from 0.00 to 0.04 s); E2 = 0 V (from 0.05 to 0.21 s); E3 = +0.22 V (from 0.22 to 0.46 s); E4 = 0 V (from 0.47 to 0.56 s); E5 = −2 V (from 0.57 to 0.58 s); and E6 = +0.6 V (0.59 s). The mobile phase consisted of 10% (v/v) acetonitrile (solvent A) and 85% (v/v) acetonitrile (solvent B).

When the Kinetex C-18 column was used, the following ratios of solvent A:B were employed: linear gradient elution (87:13–85:15) (0–10 min), linear gradient elution (85:15–83:17) (10–16 min), linear gradient elution (83:17–78:22) (16–18 min), isocratic elution (78:22) (18–30 min), linear gradient elution (78:22–75:25) (30–33 min), linear gradient elution (75:25–50:50) (33–55 min), and linear gradient elution (50:50–33:67) (55–63 min). The column was then washed with 100% solvent B for 10 min. The flow rate was 0.2 mL/min and the column temperature was 30, 45, or 60 °C.

When the Unison C-18 column was used, the following ratios of solvent A:B were employed: isocratic elution (85.3:14.7) (0–24 min), linear gradient elution (85.3:14.7–73.3:26.7) (24–25 min), linear gradient elution (73.3:26.7–72:28) (25–34 min), linear gradient elution (72:28–71.3:28.7) (34–35 min), isocratic elution (71.3:28.7) (35–37 min), linear gradient elution (71.3:28.7–70:30) (37–39 min), linear gradient elution (70:30–47:53) (39–49 min), linear gradient elution (47:53–33:67) (49–59 min), and linear gradient elution (33:67–30:70) (59–63 min). The column was then washed with 100% solvent B for 10 min. The flow rate was 0.2 mL/min and the column temperature was 30, 45, or 60 °C.

A post-column delivery system of 200 mM sodium hydroxide at a flow rate of 0.8 mL/min was added to the RP-HPLC-PAD system. The mobile phase was made through being degassed by vacuum filtration after the mixture of water with acetonitrile on a daily basis, followed by sonication for 20 min before use. Data were collected on a computer running the Chromeleon client program supplied by Dionex. The injection volume was 10 μL.

2.3. Standard preparation

Stock solutions were prepared by dissolving 1 mg of each standard (G-Rb_1, G-Rb_2, G-Rb_3, G-Rc, G-Rd, G-R_f, G-Re, G-Rg_1, G-Rg_2, G-Rg_3, G-Rh_1, and G-Rh_2) in 1 mL of 50% (v/v) acetonitrile/water in an Eppendorf tube. Each stock solution was diluted with water to create six calibration points (1, 5, 10, 20, 25, and 50 μg/mL) for the preparation of the calibration curves. The concentration of digoxin, the internal standard (I.S.), was 50 μg/mL for all analytes.

2.4. Sample preparation

One gram of red ginseng sample powder was added to 100 mL of methanol and then extracted under reflux for 1 h before being filtered. The MR-6 extract (110.5 mg) and the HR-6 extract (216.5 mg) were obtained by lyophilizating the filtrate. Ten milligrams each of red ginseng extract and digoxin (I.S.) (equivalent to 100 μg) were dissolved in 2 mL of 50% (v/v) acetonitrile/water. Each red ginseng extract solution was filtered through a MFS 13 disposable syringe before injection.

2.5. Method validation

Linear calibration curves were made at least ten times for each reference compound. The regression equation used was $y = ax + b$, where y and x are the ratio of the peak area (analytes/I.S.) and sample concentration, respectively. Repeatability was evaluated by performing intra- and inter-day ($n = 5$) assays. Recovery tests of 12 polar- and non-polar ginsenosides were performed by adding known amounts of each standard (50, 100, and 250 ng) to the MR-6 samples. Three injections of each sample were performed to measure recovery.

3. Results and discussion

3.1. Optimization of the RP-HPLC-PAD system

The RP-HPLC-PAD system was composed as follows. A mixture of acetonitrile and water was used in the gradient eluent system. Under this condition, 12 compounds of polar- and non-polar ginsenosides were clearly separated on the C-18 column. The eluent carrying each separated ginsenoside was mixed with sodium hydroxide (NaOH) solution in a T-shaped mixer before entering the PAD.

The detection of sugar moieties using PAD has great potential for selective ginsenoside monitoring, which requires sensing of the redox of sugar residues. PAD detection was highly responsive to ginsenoside in the NaOH alkaline condition. The optimal column, post-column reagent, and PAD waveform conditions were described previously [24,33]. Because large volumes of acetonitrile reduce PAD detectability, we used a 2.1-mm-diameter C-18 column (length, 100 mm) at a flow rate of 0.2 mL/min to reduce the acetonitrile volume in the mobile phase. To obtain high sensitivity, the concentration and flow rate of the post-column eluent were adjusted to 200 mM NaOH and 0.8 mL/min, respectively. Of the three different types of PAD waveforms (triple-, quadruple-, and six-potential), the highly sensitive six-potential waveform was used.

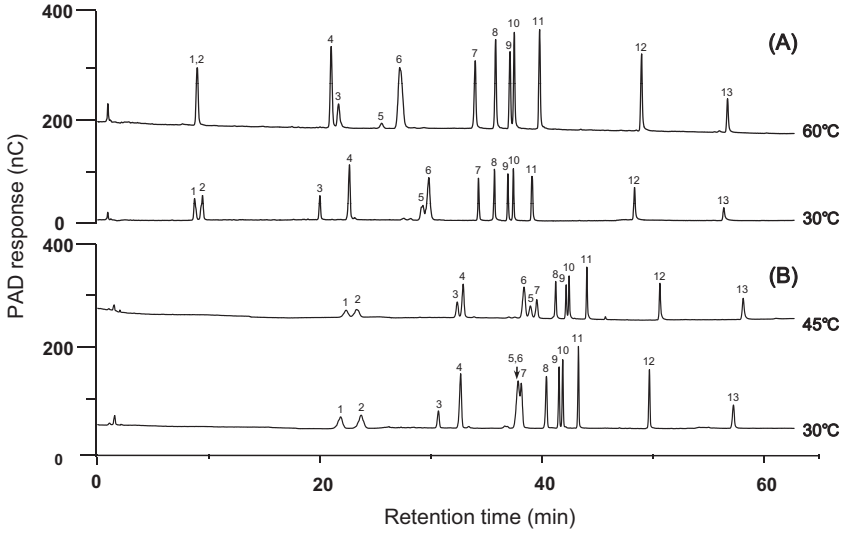

Fig. 2. Standard chromatograms of ginsenosides by Kinetex C-18 column (A) and Unison UK-C-18 column (B). Peaks: 1, G-Rg_1; 2, G-Re; 3, digoxin (I.S.); 4, G-Rf; 5, G-Rh_1; 6, G-Rg_2; 7, G-Rb_1; 8, G-Rc; 9, G-Rb_2; 10, G-Rb_3; 11, G-Rd; 12, G-Rg_3; 13, G-Rh_2. Injected amount: 500 ng for each ginsenoside.

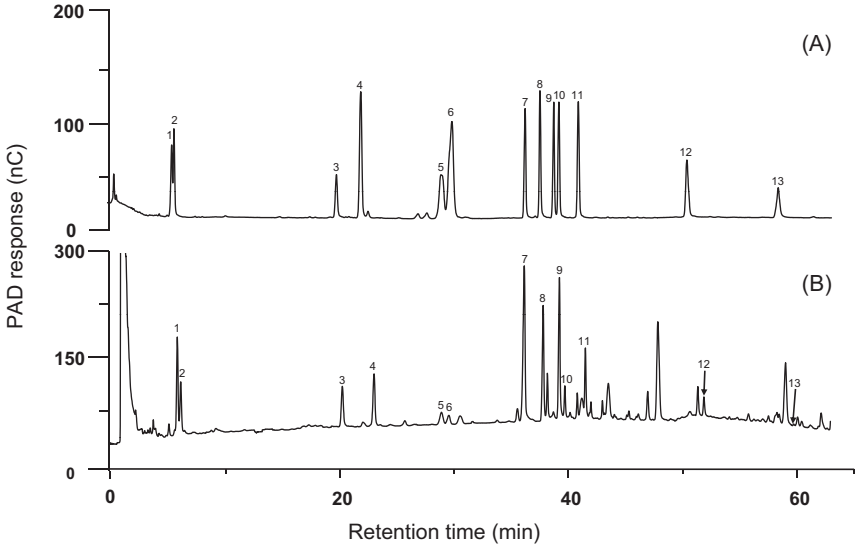

Fig. 3. Chromatograms for standard ginsenosides (A) and the main root of 6-year-old red ginseng (B) at 30 °C. Peaks: 1, G-Rg_1; 2, G-Re; 3, digoxin (I.S.); 4, G-Rf; 5, G-Rh_1; 6, G-Rg_2; 7, G-Rb_1; 8, G-Rc; 9, G-Rb_2; 10, G-Rb_3; 11, G-Rd; 12, G-Rg_3; 13, G-Rh_2. Injected volume: 10 μL.

3.2. Ginsenoside separation patterns according to column type and temperature

Fig. 2 shows the separation patterns for 12 ginsenosides, standards, and digoxin according to the type of column used (A, Kinetex C-18; B, Unison UK C-18) and the column temperature (30–60 °C).

In the Kinetex C-18 column (Fig. 2A), the resolution between G-Rg_1 (peak 1) and G-Re (peak 2) was highest at 1.90 at 30 °C, but decreased with increasing column temperature (1.20 at 45 °C, 0 at 60 °C). The retention time of G-Rf (peak 4) was relatively stable regardless of the column temperature. Notably, the internal standard digoxin (peak 3) eluted later than G-Rf (peak 4) at 60 °C. The resolution between G-Rh_1 (peak 5) and G-Rg_2 (peak 6) was increased at high temperature, while the resolution between G-Rb_2 (peak 9) and G-Rb_3 (peak 10) was increased at low temperature. The other ginsenosides were completely separated regardless of the column temperature. The pump pressure was increased at low column temperatures, which frustrated attempts to operate the HPLC at temperatures <30 °C.

In the Unison UK C-18 column (Fig. 2B), the resolution between G-Rg_1 (peak 1) and G-Re (peak 2) was better at low temperature than at high temperature (resolutions of 2.30, 1.15, and 0 at 30 °C, 45 °C, and 60 °C, respectively). The resolution between digoxin (peak 3) and G-Rf (peak 4) was greatly improved at low temperature, whereas the two peaks moved closer together as the column temperature increased until they overlapped at 60 °C. G-Rh_1 (peak 5), G-Rg_2 (peak 6), and G-Rb_1 (peak 7) overlapped at 30 °C and became separated at 45 °C. At 45 °C, G-Rg_2 (peak 6) was eluted faster than G-Rh_1 (peak 5). The resolution between G-Rb_2 (peak 9) and G-Rb_3 (peak 10) was 1.81, with a higher resolution at 30 °C. The other ginsenosides were well separated.

From the tolerable column pressure and the good separation for all analytes, we selected the Kinetex C-18 column at 30 °C as our optimum analytical condition. Fig. 3 shows the chromatograms for standard ginsenosides and red ginseng analyzed under the optimum condition.

3.3. Analysis of ginsenosides

The analytical method was validated with respect to the linearity, limits of detection (LOD), limits of quantification (LOQ), precision, accuracy, and recovery. The linearity of detection for each analyte was examined using 6 different standard solutions (1, 5, 10, 20, 25, and 50 μg/mL). A calibration curve was constructed by performing linear regression of the peak area ratio (analyte/internal standard) *vs.* analyte concentration. The equations and linear ranges are listed in Table 1. The correlation coefficients ranged 0.9975–0.9998. The LODs ($S/N = 3$) and LOQs ($S/N = 10$) obtained

Table 1
Linear range, linear equation, correlation coefficient, limits of detection (LOD) and limits of quantitation (LOQ) for ginsenosides.

Ginsenoside	Linear range (μg/mL)	Linear equation[a]	r^2	PAD		ELSD[b]	
				LOD (ng)	LOQ (ng)	LOD (ng)	LOQ (ng)
Rg_1	0.02–50	$y = 0.0236x + 0.0379$	0.9992	0.07	0.20	200	400
Re	0.02–50	$y = 0.0409x + 0.0798$	0.9991	0.07	0.20	250	450
Rf	0.01–50	$y = 0.0487x + 0.1806$	0.9995	0.02	0.10	300	600
Rb_1	0.02–50	$y = 0.0453x + 0.1168$	0.9991	0.05	0.20	150	300
Rc	0.01–50	$y = 0.0207x + 0.0321$	0.9984	0.02	0.10	150	300
Rb_2	0.01–50	$y = 0.0454x + 0.0392$	0.9975	0.02	0.10	150	300
Rb_3	0.01–50	$y = 0.0277x + 0.0177$	0.9977	0.02	0.10	200	450
Rd	0.01–50	$y = 0.0425x + 0.0190$	0.9998	0.03	0.10	200	450
Rh_1	0.02–50	$y = 0.0309x + 0.0173$	0.9992	0.05	0.20	300	800
Rg_2	0.03–50	$y = 0.0264x + 0.0282$	0.9993	0.10	0.30	300	800
Rg_3	0.02–50	$y = 0.0691x - 0.1821$	0.9981	0.05	0.20	75	125
Rh_2	0.03–50	$y = 0.0489x - 0.1728$	0.9985	0.10	0.30	100	150

[a] y = peak area ratio (analyte/IS); x = theoretical concentration.
[b] Data from *J. Pharm. Biomed. Anal.* 2007, 45, 164–170.

Table 2
Intra- and inter-day ($n = 5$), recovery ($n = 3$) validations for determining ginsenoside contents in the main root of 6-year-old red ginseng.

Ginsenoside	Intra-day precision		Inter-day precision		Recovery	
	Content (mg/g)	RSD (%)	Content (mg/g)	RSD (%)	Mean recovery (%)	RSD (%)
Rg_1	1.56 ± 0.07	4.16	1.56 ± 0.09	5.63	98.08 ± 6.49	6.62
Re	0.85 ± 0.02	2.01	0.83 ± 0.01	1.27	98.64 ± 5.31	5.38
Rf	0.37 ± 0.01	2.43	0.37 ± 0.01	1.92	101.51 ± 5.41	5.33
Rb_1	2.87 ± 0.25	8.68	2.87 ± 0.20	6.67	102.18 ± 2.54	2.49
Rc	1.71 ± 0.14	7.95	1.70 ± 0.07	4.37	100.33 ± 3.84	3.83
Rb_2	1.24 ± 0.01	0.89	1.24 ± 0.05	4.34	98.63 ± 6.21	6.30
Rb_3	0.20 ± 0.02	7.46	0.20 ± 0.01	4.23	100.44 ± 4.63	4.61
Rd	0.83 ± 0.04	5.09	0.83 ± 0.06	7.03	100.54 ± 4.16	4.14
Rh_1	0.18 ± 0.01	4.49	0.18 ± 0.01	6.58	103.06 ± 3.85	3.73
Rg_2	0.07 ± 0.01	8.45	0.07 ± 0.01	8.81	101.26 ± 4.65	4.60
Rg_3	0.34 ± 0.03	9.55	0.33 ± 0.03	9.86	98.22 ± 3.55	3.62
Rh_2	0.03 ± 0.00	9.91	0.03 ± 0.00	8.73	102.08 ± 4.03	3.95

Recovery (%) = (observed amount − original amount)/spiked amount × 100.

for each standard ginsenoside were 0.02–0.10 and 0.10–0.30 ng, respectively. Significantly, PAD showed 1000–15,000 times higher sensitivity in detecting ginsenosides than the reported ELSD detection [25].

3.4. Analysis of ginsenosides in red ginseng

To validate our method, we analyzed the reproducibility and recovery of 12 ginsenosides in the main roots of 6-year-old red ginseng (Table 2). The intra- and inter-day precisions (RSDs) were 0.89–9.91% and 1.27–9.86%, respectively. The recoveries of ginsenosides were evaluated by adding 500 μL of a ginsenoside mixture (5, 10, or 25 μg each) to 500 μL of each sample and then injecting 10 μL of mixed solutions (50, 100, or 250 ng each) into the HPLC system. The mean recoveries and RSD ranges for ginsenosides were 98.08–103.06% and 2.49–6.62%, respectively (Table 2). Therefore our method showed good precision and accuracy.

3.5. Applications

We determined the polar and non-polar ginsenosides contained in the main roots (MR-6) or hairy roots (HR-6) of 6-year-old red ginseng (Table 3). Total contents of ginsenosides contained in MR-6 and HR-6 were 10.21 and 45.65 mg/g, respectively. The contents of polar ginsenosides in MR-6 and HR-6 were as follows, respectively: Rg_1, 1.56 and 2.96 mg/g; Re, 0.83 and 7.39 mg/g; Rf, 0.37 and 1.14 mg/g; Rb_1, 2.87 and 12.64 mg/g; Rc, 1.70 and 10.47 mg/g; Rb_2, 1.24 and 4.46 mg/g, Rb_3, 0.20 and 1.29 mg/g; Rd, 0.83 and 3.09 mg/g. The HR-6 contained 4.5 times more total ginsenosides, as well as 1.9–8.9 times more polar ginsenosides, than MR-6. Specifically, 8.9, 6.2, and 6.5 times more G-Re, G-Rc, and G-Rb_3 were seen in HR-6 than in MR-6. The contents of non-polar ginsenosides in MR-6 and HR-6 were as follows, respectively: Rh_1, 0.18 and 0.28 mg/g; Rg_2, 0.07 and 0.76 mg/g; Rg_3, 0.33 and 1.13 mg/g; Rh_2, 0.03 and 0.03 mg/g. HR-6 contained 10.8, 3.4, and 1.6 times more G-Rg_2, G-Rg_3, and G-Rh_1, respectively, than MR-6, while G-Rh_2 appeared in similar levels in HR-6 and MR-6. The percentage of total ginsenosides that were non-polar was 6.0% and 4.8% for MR-6 and HR-6, respectively. In red ginseng, MR-6 has been generally known to be more useful than HR-6 as a material of oriental medicinal preparation, but we thought that HR-6 might be more effective than MR-6, because we confirmed that HR-6 had more polar and non-polar ginsenosides through our experiment.

Table 3
Ginsenoside content of the main root (MR-6) and hairy root (HR-6) of 6-year-old red ginseng as detected by PAD ($n = 4$).

Ginsenoside	Main root		Hairy root	
	Content (mg/g)	RSD (%)	Content (mg/g)	RSD (%)
Rg_1	1.56 ± 0.09	5.63	2.96 ± 0.08	2.73
Re	0.83 ± 0.01	1.27	7.39 ± 0.57	7.75
Rf	0.37 ± 0.01	1.92	1.14 ± 0.05	4.54
Rb_1	2.87 ± 0.20	6.67	12.64 ± 0.89	7.04
Rc	1.70 ± 0.07	4.37	10.47 ± 0.26	2.45
Rb_2	1.24 ± 0.05	4.34	4.46 ± 0.40	8.87
Rb_3	0.20 ± 0.01	4.23	1.29 ± 0.05	3.73
Rd	0.83 ± 0.06	7.03	3.09 ± 0.18	5.91
Rh_1	0.18 ± 0.01	6.58	0.28 ± 0.01	4.91
Rg_2	0.07 ± 0.01	8.81	0.76 ± 0.06	8.34
Rg_3	0.33 ± 0.03	9.86	1.13 ± 0.09	7.78
Rh_2	0.03 ± 0.00	8.73	0.03 ± 0.00	5.25
Total	10.21 ± 0.52	5.10	45.65 ± 2.64	5.77

4. Conclusion

We developed a method to simultaneously detect polar and non-polar ginsenosides in red ginseng using the RP-HPLC-PAD method. The polar and non-polar ginsenosides were well separated by a water-acetonitrile gradient elution system on the Kinetex C-18 column at a column temperature of 30 °C. Our method could be applied directly without any pretreatment steps and had a high selectivity, high sensitivity, and good reproducibility. This method will likely serve as a useful tool in the quality control of red ginseng.

Acknowledgement

This study was supported by a Korea Research Foundation (KRF) grant funded by the Korea government (MEST) (No. 2011-0003260).

References

[1] B. Liao, H. Newmark, R. Zhou, Neuroprotective effects of ginseng total saponin and ginsenosides Rb_1 and Rg_1 on spinal cord neurons *in vitro*, Exp. Neurol. 173 (2002) 224–234.
[2] R. Ye, N. Li, J. Han, X. Kong, R. Cao, Z. Raoand, G. Zhao, Neuroprotective effects of ginsenoside Rd against oxygen–glucose deprivation in cultured hippocampal neurons, Neurosci. Res. 64 (2009) 306–310.
[3] N. Li, B. Liu, D.E. Dluzen, Y. Jin, Protective effects of ginsenoside Rg_2 against glutamate-induced neurotoxicity in PC12 cells, J. Ethnopharmacol. 111 (2007) 458–463.
[4] J. Tian, F. Fu, M. Geng, Y. Jiang, J. Yang, W. Jiang, C. Wang, K. Liu, Neuroprotective effect of 20(S)-ginsenoside Rg on cerebral ischemia in rats, Neurosci. Lett. 374 (2005) 92–97.
[5] K.S. Kang, B.C. Kang, B.J. Lee, J.H. Che, G.X. Li, J.E. Trosko, Y.S. Lee, Preventive effect of epicatechin and ginsenoside Rb_2 on the inhibition of gap junctional intercellular communication by TPA and H_2O_2, Cancer Lett. 152 (2000) 97–106.
[6] P.Y. Yue, D.Y. Wong, P.K. Wu, P.Y. Leung, N.K. Mak, H.W. Yeung, L. Liu, Z. Cai, Z.H. Jiang, T.P. Fan, R.N. Wong, The angiosuppressive effects of 20(R)-ginsenoside Rg_3, Biochem. Pharmacol. 72 (2006) 437–445.

[7] X. Luo, C.Z. Wang, J. Chen, W.X. Song, J. Luo, N. Tang, B.C. He, Q. Kang, Y. Wang, W. Du, T.C. He, C.S. Yuan, Characterization of gene expression regulated by American ginseng and ginsenoside Rg_3 in human colorectal cancer cells, Int. J. Oncol. 32 (2008) 975–983.
[8] T. Ota, M. Maeda, S. Odashima, J. Ninomiya-Tsuji, M. Tatsuka, G_1 phase-specific suppression of the Cdk2 activity by ginsenoside Rh_2 in cultured murine cells, Life Sci. 60 (1997) PL39–PL44.
[9] T. Wang, X. Yu, S. Qu, H. Xu, B. Han, D. Sui, Effect of ginsenoside Rb_3 on myocardial injury and heart function impairment induced by isoproterenol in rats, Eur. J. Pharmacol. 636 (2010) 121–125.
[10] M.S. Lee, J.T. Hwang, S.H. Kim, S. Yoon, M.S. Kim, H.J. Yang, D.Y. Kwon, Ginsenoside Rc, an active component of *Panax ginseng*, stimulates glucose uptake in C2C12 myotubes through an AMPK-dependent mechanism, J. Ethnopharmacol. 127 (2010) 771–776.
[11] J.S. Mogil, Y.H. Shin, E.W. McCleskey, S.C. Kim, S.Y. Nah, Ginsenoside Rf, a trace component of ginseng root, produces antinociception in mice, Brain Res. 792 (1998) 218–228.
[12] J.T. Xie, Z.H. Shao, T.L.V. Hoek, W.T. Chang, J. Li, S. Mehendale, C.Z. Wang, C.W. Hsu, L.B. Becker, J.J. Yin, C.S. Yuan, Antioxidant effects of ginsenoside Re in cardiomyocytes, Eur. J. Pharmacol. 532 (2006) 201–207.
[13] K.S. Kang, H.Y. Kim, N. Yamabe, J.H. Park, T. Yokozawa, Preventive effect of 20(S)-ginsenoside Rg_3 against lipopolysaccharide-induced hepatic and renal injury in rats, Free Radic. Res. 41 (2007) 1181–1188.
[14] Y.C. Park, C.H. Lee, H.S. Kang, K.W. Kim, H.T. Chung, H.D. Kim, Ginsenoside-Rh_1 and Rh_2 inhibit the induction of nitric oxide synthesis in murine peritoneal macrophages, Biochem. Mol. Biol. Int. 40 (1996) 751–757.
[15] K.S. Kang, H.Y. Kim, N. Yamabe, T. Yokozawa, Stereospecificity in hydroxyl radical scavenging activities of four ginsenosides produced by heat processing, Bioorg. Med. Chem. Lett. 16 (2006) 5028–5031.
[16] N.D. Kim, E.M. Kim, K.W. Kang, M.K. Cho, S.Y. Choi, S.G. Kim, Ginsenoside Rg_3 inhibits phenylephrine-induced vascular contraction through induction of nitric oxide synthase, Br. J. Pharmacol. 140 (2003) 661–670.
[17] H.U. Lee, E.A. Bae, M.J. Han, D.H. Kim, Hepatoprotective effect of 20(S)-ginsenosides Rg_3 and its metabolite 20(S)-ginsenoside Rh_2 on tert-butyl hydroperoxide-induced liver injury, Biol. Pharm. Bull. 28 (2005) 1992–1994.
[18] I. Kitagawa, M. Yoshikawa, M. Yoshihara, T. Hayashi, T. Taniyama, Chemical studies on crude drug procession. I. On the constituents of ginseng radix rubura (I), Yakugaku Zasshi 103 (1983) 612–622.
[19] I. Kitagawa, T. Taniyama, H. Shibuya, T. Noda, M. Yoshikawa, Chemical studies on crude drug processing. V. On the constituents of ginseng radix rubra (2): comparison of the constituents of white ginseng and red ginseng prepared from the same *Panax ginseng* root, Yakugaku Zasshi 107 (1987) 495–505.
[20] X. Wang, T. Sakuma, E. Asafu-Adjaye, G.K. Shiu, Determination of ginsenosides in plant extracts from *Panax ginseng* and *Panax quinquefolius* L. by LC/MS/MS, Anal. Chem. 71 (1999) 1579–1584.
[21] M. Bonfill, I. Casals, J. Palazon, A. Mallol, C. Morales, Improved high performance liquid chromatographic determination of ginsenosides in *Panax ginseng*-based pharmaceuticals using a diol column, Biomed. Chromatogr. 16 (2002) 68–72.
[22] L. Li, J.L. Zhang, Y.X. Sheng, D.A. Guo, Q. Wang, H.Z. Gou, Simultaneous quantification of six major active saponins of Panax notoginseng by high-performance liquid chromatography-UV method, J. Pharm. Biomed. Anal. 38 (2005) 45–51.
[23] J. Guan, C.M. Lai, S.P. Li, A rapid method for the simultaneous determination of 11 saponins in Panax notoginseng using ultra performance liquid chromatography, J. Pharm. Biomed. Anal. 44 (2007) 996–1000.
[24] H.J. Kwon, J.S. Jeong, H.J. Sim, Y.M. Lee, Y.S. Kim, S.P. Hong, Sensitive high-performance liquid chromatography method of non-polar ginsenosides by alkaline-enhanced pulsed amperometric detection, J. Chromatogr. A 1216 (2009) 4445–4450.
[25] S.N. Kim, Y.W. Ha, H. Shin, S.H. Son, S.J. Wu, Y.S. Kim, Simultaneous quantification of 14 ginsenosides in *Panax ginseng* C.A. Meyer (Korean red ginseng) by HPLC-ELSD and its application to quality control, J. Pharm. Biomed. Anal. 45 (2007) 164–170.
[26] C.C. Bai, S.Y. Han, X.Y. Chai, Y. Jiang, P. Li, P.F. Tu, Sensitive determination of saponins in radix etrhizoma notoginseng by charged aerosol detector coupled with HPLC, J. Liquid Chromatogr. Relat. Technol. 32 (2009) 242–260.
[27] W. Putalun, N. Fukuda, H. Tanaka, Y. Shoyama, A one-step immunochromatographic assay for detecting ginsenosides Rb_1 and Rg_1, Anal. Bioanal. Chem. 378 (2004) 1338–1341.
[28] B. Sritularak, O. Morinaga, C.S. Yuan, Y. Shoyama, H. Tanaka, Quantitative analysis of ginsenosides Rb_1, Rg_1, and Re in American ginseng berry and flower samples by ELISA using monoclonal antibodies, J. Nat. Med. 63 (2009) 360–363.
[29] J.S. Jeong, H.R. Yoon, S.P. Hong, Development of a new diagnostic method for galactosemia by high-performance anion-exchange chromatography with pulsed amperometric detection, J. Chromatogr. A 1140 (2007) 157–162.
[30] T.R.I. Cataldi, G. Margiotta, L. Iasi, B.D. Chio, C. Xiloyannis, S.A. Bufo, Determination of sugar compounds in olive plant extracts by anion-exchange chromatography with pulsed amperometric detection, Anal. Chem. 72 (2000) 3902–3907.
[31] K. Schutz, E. Muks, R. Carle, A. Schieber, Separation and quantification of inulin in selected artichoke (*Cynara scolymus* L.) cultivars and dandelion (Taraxacum officinale WEB. ex WIGG.) roots by high-performance anion exchange chromatography with pulsed amperometric detection, Biomed. Chromatogr. 20 (2006) 1295–1303.
[32] C. L'homme, J.L. Peschet, A. Puigserver, A. Biagini, Evaluation of fructans in various fresh and stewed fruits by high-performance anion-exchange chromatography with pulsed amperometric detection, J. Chromatogr. A 920 (2001) 291–297.
[33] H.J. Kwon, J.S. Jeong, Y.M. Lee, S.P. Hong, A reversed-phase high-performance liquid chromatography method with pulsed amperometric detection for the determination of glycosides, J. Chromatogr. A 1185 (2008) 251–257.

Journal of Pharmaceutical and Biomedical Analysis 60 (2012) 86–90

Contents lists available at SciVerse ScienceDirect

Journal of Pharmaceutical and Biomedical Analysis

journal homepage: www.elsevier.com/locate/jpba

Short communication

Quantification of potential impurities by a stability indicating UV-HPLC method in niacinamide active pharmaceutical ingredient

Saji Thomas*, Amber Bharti, Kalsang Tharpa, Ashutosh Agarwal

Jubilant Life Sciences Ltd., Analytical Research Department R&D Centre, C-26, Sector-59, Noida, Uttar Pradesh 201301, India

ARTICLE INFO

Article history:
Received 29 August 2011
Received in revised form 28 October 2011
Accepted 29 October 2011
Available online 6 November 2011

Keywords:
Niacinamide
Impurity
Forced degradation
Validation

ABSTRACT

A sensitive, stability indicating reverse phase UV-HPLC method has been developed for the quantitative determination of potential impurities of niacinamide active pharmaceutical ingredient. Efficient chromatographic separation was achieved on C18 stationary phase in isocratic mode using simple mobile phase. Forced degradation study confirmed that the newly developed method was specific and selective to the degradation products. Major degradation of the drug substance was found to occur under oxidative stress conditions to form niacinamide *N*-oxide. The method was validated according to ICH guidelines with respect to specificity, precision, linearity and accuracy. Regression analysis showed correlation coefficient value greater than 0.999 for niacinamide and its six impurities. Detection limit of impurities was in the range of 0.003–0.005% indicating the high sensitivity of the newly developed method. Accuracy of the method was established based on the recovery obtained between 93.3% and 113.3% for all impurities.

1. Introduction

Niacinamide (nicotinamide or nicotinic acid amide) is chemically known as pyridine-3-carboxamide was first isolated from horse erythrocytes in 1935. It is a form of vitamin B_3, and its deficiency and adverse effects are well documented [1]. Both niacinamide and niacin are converted into NAD and NADP, in vivo [2]. Niacinamide inhibits ADP-ribosyl transferring enzymes modulating immune cell function and cell [3].

There are quite a number of reports on a simultaneous assay determination of niacinamide and niacin in samples such as food and multi-vitamin tablets by LC-UV [4–7]; and stability indicating LC-UV method for the determination of niacinamide in the presence of riboflavin, pyridoxine and thiamine is also reported [8]. Current United States Pharmacopoeia [9] and European Pharmacopoeia [10] employ assay procedures without concerning the related substance of niacinamide. There is no report on chromatographic separation of related substances (process or stressed) in niacinamide partly because niacinamide is classified as food additive rather than pharmaceutical agent thereby its formal safety evaluation remained less important. The concern is that since niacinamide is given in high doses, its purity needs to be scrutinized. Therefore it was felt necessary to develop an accurate, specific and stability indicating method for the determination of potential impurities of niacinamide. The present ICH drug stability test guideline [11] suggests that stress studies should be carried out on a drug substance to establish its inherent stability characteristics, leading to separation of degradation impurities and hence supporting the suitability of the proposed analytical procedure, which must be fully validated [12].

The present work deals with method development, method validation and forced degradation study of niacinamide. Niacinamide is commercially manufactured by the catalytic hydrolysis of 3-cyanopyridine. Therefore, the positional isomers of 3-cyanopyridine and undesired hydrolyzed products were considered as potential impurities for method development. To the best of our knowledge, this is the first report on identification of stress related impurities of niacinamide and method for quantitative determination of process related impurities.

2. Experimental

2.1. Materials and reagents

Sample of niacinamide API and standards of niacin, isonicotinic acid, niacinamide-*N*-oxide, isonicotinamide, picolinamide and 3-cyanopyridine were obtained from Chemical Research and Development Department, Jubilant Life Sciences Limited (Noida, India). Deionized water was prepared using a Milli-Q plus water purification system from Millipore (Bedford, MA, USA). HPLC grade acetonitrile, analytical reagent grade of ammonium acetate, acetic

* Corresponding author. Tel.: +91 120 4362210; fax: +91 120 2580033.
E-mail address: saji_thomas@jubl.com (S. Thomas).

0731-7085/$ – see front matter © 2011 Elsevier B.V. All rights reserved.
doi:10.1016/j.jpba.2011.10.033

acid, sodium hydroxide, hydrogen peroxide and hydrochloric acid were purchased from Merck India Limited (Mumbai, India).

2.2. High performance liquid chromatography

Samples were analyzed on Waters alliance 2690 separation module equipped with 2487 UV detector and 2996 PDA detector for stability study (Waters Corporation, Milford, MA, USA) using an Inertsil ODS 3V (250 mm × 4.6 mm, 5.0 μm, GL Sciences Inc., Tokyo, Japan). The mobile phase consisted of 20 mM ammonium acetate adjusted to pH 5.00 ± 0.05 with acetic acid–acetonitrile (970:30, v/v). Mobile phase was used as diluent for sample preparation. The injection volume was 10 μL (1.50 mg/mL sample concentration) and the wavelength of detector was set to 254 nm. The column was maintained at 30 °C throughout the analysis.

2.3. Sample preparation for forced degradation studies

About 55 mg each of niacinamide sample were weighed into four different 20 mL volumetric flasks and labeled them as A, B, C and D. Two milliliters each of 1 N hydrochloric acid, 1 N sodium hydroxide and Milli-Q water (pH 7.01), and 5 mL of 1% (v/v) hydrogen peroxide were added in volumetric flask A, B, C and D, respectively. Volumetric flasks A, B and C were kept in a water bath at 80 °C for 3 h and volumetric flask D at room temperature for 3 h. The excess of acid or base in volumetric flask A and B were neutralized and made up to the volume with diluent. Corresponding blank solutions were prepared following the sample procedure without niacinamide sample. Thermal degradation was done at 105° C for 24 h on solid sample. Photolytic degradation was performed by keeping 500 mg of each sample in two separate loss on drying (LOD) bottles in a photo stability chamber model TP 0000090G (Thermo Lab equipments Pvt. Ltd., Mumbai, India). One bottle was covered with lid and then with aluminum foil (dark control) whereas another bottle (photolytic exposed sample) was covered with lid to get a minimum exposure of 1.2 million lux hours for light and 200 Wh/m^2 for ultraviolet region. A 1.50 mg/mL sample was prepared for thermal degradation and photolytic degradation samples.

3. Results and discussion

3.1. HPLC method development

Initially niacinamide sample was analyzed by pharmacopoeial methods [9,10] and found that most of the impurities were co-eluting with the main peak. The main objective of the method development was to achieve efficient separation of impurities listed in Table 1. Using the literature report, the niacin pK_a of 4.81 [13] and niacinamide pK_a of 3.35 [14], formed the basis of choices over the pH of the mobile phase. At pH 5.00, the protonation of amide moiety of niacinamide, Imp-3 and Imp-4 is suppressed and the carboxylate ion of Imp-1 and Imp-2 predominates. Therefore, both Imp-1 and Imp-2 elute earlier on the hydrophobic column (C18) with less protonated or relatively more non-polar compounds such as niacinamide, Imp-3 and Imp-4 eluting later. Finally after conducting serious of experiments for method development, and routine optimization experiments, using an Intersil ODS 3V C-18 column with ammonium acetate buffer at pH adjusted to 5.00 ± 0.05 with acetic acid, in combination with 3% acetonitrile, yielded optimum resolution under isocratic condition (Fig. 1A).

3.2. Forced degradation studies and identification of major degradants

Niacinamide molecule was found to be susceptible to acid, base and oxidative conditions. In oxidative degradation condition, significant degradation was observed and the impurity formed at RRT 0.42 was identified as niacinamide *N*-oxide. In acidic and alkaline conditions niacin was the major degradant. Chromatograms of forced degradation study have been depicted in Fig. 1B. Degradation studies and peak purity test results derived from PDA detector confirmed that the spectral purity of niacinamide peak was homogenous thus confirmed the stability indicating power of the newly developed method.

4. Method validation

Validation study was carried out for the analysis of Imp-A, Imp-1, Imp-2, Imp-3, Imp-4 and Imp-5. The system suitability and selectivity were checked by injecting 1.50 mg/mL of niacinamide solution containing 0.15% of all impurities (Fig. 1A). Method validation results are summarized in Table 2.

4.1. Accuracy and precision

Accuracy of the method was evaluated in triplicate at three concentration levels, i.e. QL, 0.015% and 0.226% of the analyte concentration (1.5 mg/mL). The percentage of recovery for each impurity was calculated at each level and found in the range of 88.89–113.33% (Table 2). The precision of the related substances method was checked by injecting six individual preparations of (1.5 mg/mL) niacinamide spiked with 0.15% of each impurity. Percentage RSD for peak areas of each impurity was calculated (Table 2). Precision was also determined by performing the same procedures on a different day (inter-day precision).

4.2. Sensitivity

The sensitivity was determined by establishing the detection limit (DL) and quantitation limit (QL) for all the impurities by injecting a series of dilute solutions with known concentration. The DL and QL for Imp-1, Imp-2, Imp-3, Imp-4, Imp-5 and Imp-A were about 0.005% and 0.015%, respectively indicating high sensitivity of the method.

4.3. Linearity and range

Linearity was established between ranges of QL to 0.225% of the analyte concentration (1.50 mg/mL) using least squares method. The correlation coefficient obtained was not less than 0.999 for all impurities. Standard deviation of peak area was significantly low and %RSD was below 4.1%.

4.4. Robustness and ruggedness

Close observation of analysis results of the deliberately changed in chromatographic conditions (flow rate, pH, mobile phase composition and column temperature) revealed that the resolution between niacinamide and Imp-3 was greater than 2.0, illustrating the robustness of the method. The intermediate precision (ruggedness) of the method was also evaluated by a different analyst and different instrument in the same laboratory with %RSD areas of each impurity within 4.0.

4.5. Solution stability

The solution stability of niacinamide and its related substances was established by spiked and unspiked sample solution in tightly capped HPLC vials at 30 °C in auto sampler. Content of each impurity was determined after every 4 h against freshly prepared standard

Table 1
Niacinamide and potential impurities.

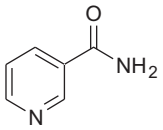

Niacinamide

Sl. no.	Name	Structure	Mol. wt.	Code	Origin
1	Isonicotinic acid	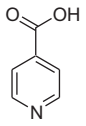	123.03	Imp-1	Process impurity
2	Niacin	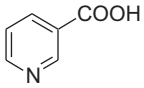	123.03	Imp-2	Process and degradation impurity
3	Isonicotinamide	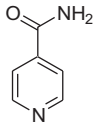	122.05	Imp-3	Process impurity (positional isomer)
4	Picolinamide	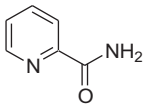	122.05	Imp-4	Process impurity (positional isomer)
5	3-Cyanopyridine	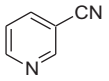	104.04	Imp-5	Process impurity (starting material)
6	Niacinamide *N*-oxide	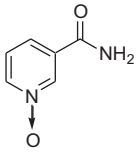	138.04	Imp-A	Oxidative degradation impurity

Table 2
System suitability, response factor, DL, QL, linearity, precision and accuracy.

Parameter	Imp-1	Imp-A	Imp-2	Imp-3	Niacinamide	Imp-4	Imp-5
System suitability							
RT	4.04	4.56	5.03	9.98	11.02	24.90	26.87
RRT	0.37	0.41	0.46	0.91	1.00	2.26	2.46
R_s	–	2.80	2.47	18.85	3.06	24.97	2.54
N	7487	10304	10428	15735	15647	17583	18370
T	1.11	1.11	1.08	1.01	1.07	1.04	1.01
Linearity (μg/mL)	15.0–226	9.00–226	15.0–226	15.0–226	15.0–226	15.0–226	15.0–226
r	0.9999	0.9994	0.9996	0.9992	0.9995	0.9990	0.9984
Slope	183,784	635,629	219,994	151,863	202,434	229,253	182,407
Confidence interval of slope[a]	±2002.9	±12957.7	±1783.9	±1427.6	±1777.4	±2757.8	±1968.8
Intercept	274	−613	−468	126	140	296	419
Detection limit	0.005%	0.003%	0.005%	0.005%	0.005%	0.005%	0.005%
Quantitation limit	0.015%	0.009%	0.015%	0.015%	0.015%	0.015%	0.015%
Precision %RSD ($n = 6$)	1.75	4.01	1.66	0.94	2.95	3.88	1.29
Accuracy at QL level ($n = 3$)							
Amount added (%)	0.015	0.009	0.015	0.015	0.015	0.015	0.015
Amount recovered (%)	0.014	0.008	0.017	0.015	0.014	0.014	0.015
% Recovery	93.33	88.89	113.33	100.00	93.33	93.33	100.00
Accuracy at 100% level ($n = 3$)							
Amount added (%)	0.151	0.150	0.149	0.149	0.151	0.150	0.150
Amount recovered (%)	0.150	0.147	0.158	0.157	0.149	0.148	0.149
% Recovery	99.34	98.00	106.04	105.37	98.68	98.67	99.33
Accuracy at 150% level ($n = 3$)							
Amount added (%)	0.226	0.225	0.227	0.224	0.226	0.227	0.225
Amount recovered (%)	0.224	0.224	0.240	0.232	0.222	0.221	0.220
% Recovery	99.12	99.56	105.73	103.57	98.23	97.36	97.78

n, number of determinations; RT, retention time; RRT, relative retention time; R_s, USP resolution; *N*, number of theoretical plates; *T*, USP tailing factor; *r*, correlation coefficient.
[a] At 95% confidence level.

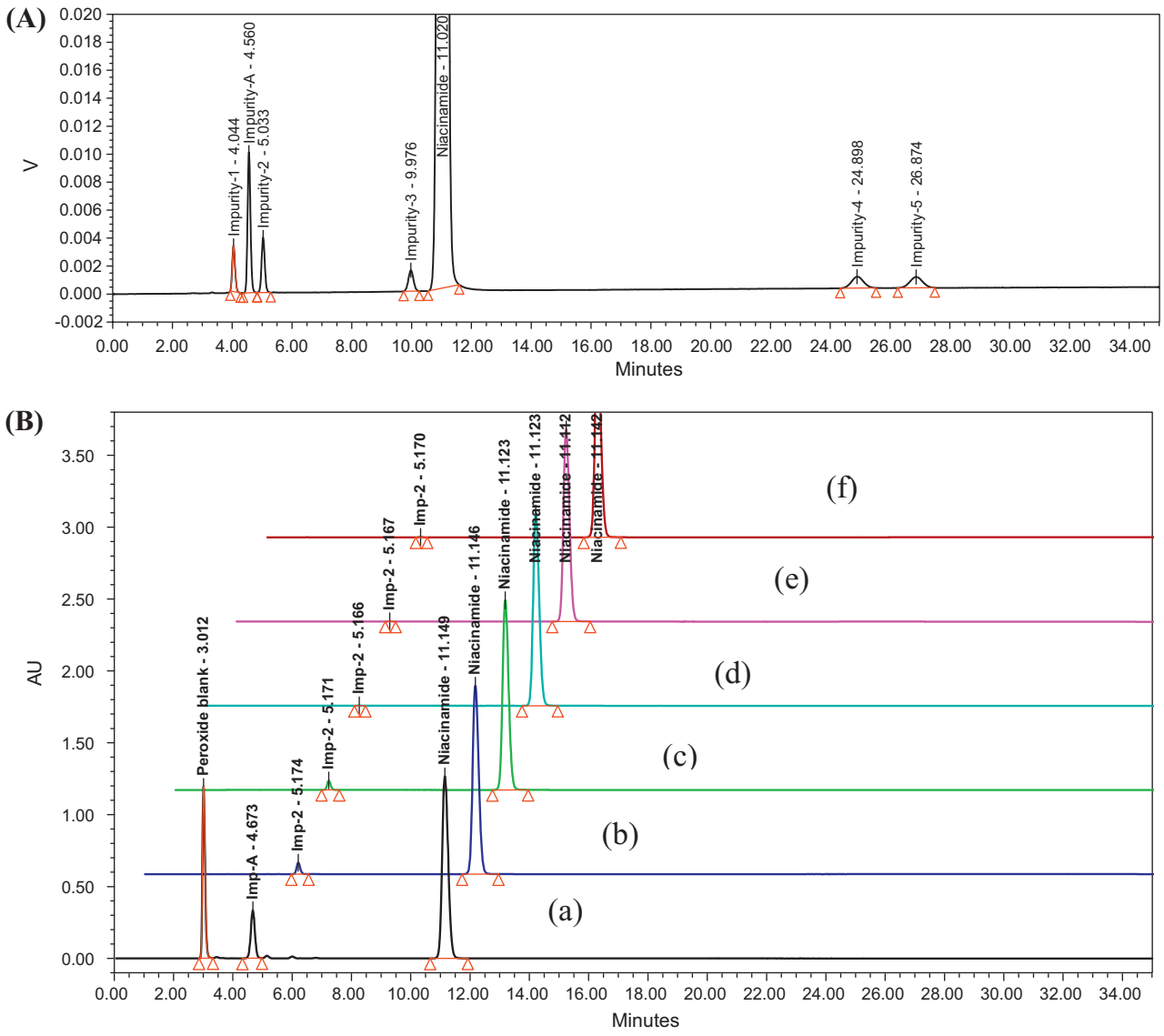

Fig. 1. (A) Chromatogram of niacinamide spiked with impurities and (B) chromatogram of niacinamide under stress conditions: (a) oxidative degradation, (b) acid hydrolysis, (c) base hydrolysis, (d) aqueous hydrolysis, (e) thermal degradation, and (f) photolytic degradation.

solution. The solution stability experiments data confirmed that sample solutions were stable up to 24 h.

5. Conclusions

The newly developed RP-LC method for quantitative determination of niacinamide and related substances was found to be sensitive, precise, accurate, specific and stability indicating. The major oxidative degradant was identified as niacinamide *N*-oxide. This newly developed method has been validated as per regulatory requirements and can be used for routine and stability studies for the quantitative determination of potential impurities in niacinamide drug substance.

Acknowledgements

The authors are thankful to the management of Jubilant Life Sciences Limited for providing necessary facilities. Authors would like to thank Mr. Sanjeev Shandilya, Dr. Hawaldar Maurya for their co-operation in carrying out this work.

References

[1] S.C. Sweetman (Ed.), Martindale—The Complete Drug Reference, 36th ed., Pharmaceutical Press, London, 2011, pp. 2117–2120.
[2] P. Jaconello, Niacin versus niacinamide, CMAJ 147 (1992) 990b.
[3] H. Kolb, V. Burkart, Nicotinamide in type 1 diabetes, Diabetes Care 22 (1999) B16–B20.
[4] M.C. Walker, B.E. Carpenter, E.L. Cooper, Simultaneous determination of niacinamide, pyridoxine, riboflavin, and thiamine in multivitamin products by high-pressure liquid chromatography, J. Pharm. Sci. 70 (1981) 99–101.
[5] R.L. Kirchmeier, R.P. Upton, Simultaneous determination of niacin, niacinamide, pyridoxine, thiamine, and riboflavin in multivitamin blends by ion-pair high-pressure liquid chromatography, J. Pharm. Sci. 67 (1978) 1444–1446.
[6] R.D. Kirchhoefer, I.I. Niacin, Identification of isonicotinic acid in niacin by liquid chromatography with diode array detection, J. AOAC Int. 77 (1994) 587–590.
[7] H. Takashi, M. Yukimasa, A. Nobumi, S. Yamamoto, Y. Oji, Simultaneous determination of niacin and niacinamide in meats by high-performance liquid chromatography, J. Chromatogr. 457 (1988) 403–408.
[8] S. Thomas, R. Kumar, A. Sharma, R. Issarani, B.D. Nagori, Stability-indicating HPLC method for determination of vitamins B_1, B_2, B_3 and B_6 in pharmaceutical liquid dosage form, Indian J. Chem. Technol. 15 (2008) 598–603.

[9] The United States Pharmacopoeia 34-NF29, National Formulary 19, Rockville, USP Convention, USA, 2011, p. 3651.
[10] European Pharmacopoeia, 2011, p. 2567.
[11] International Conference on Harmonization Q1A (R2) IFMPA, Geneva, 2003.
[12] International Conference on Harmonization of Technical Requirements for Registration of Pharmaceuticals for Human Use S ICH Harmonized Tripartite Guideline Validation of Analytical Procedures: Text and Methodology Q2(R1), November, 2005.
[13] Kirk–Othmer Encyclopedia of Chemical Technology, Pyridine and Pyridine Derivatives, vol. 21, 4th ed., John Wiley and Sons, 1998, pp. 1–36.
[14] http://www.drugs.com/mmx/niacinamide.html.

Journal of Pharmaceutical and Biomedical Analysis 60 (2012) 91

Contents lists available at SciVerse ScienceDirect

Journal of Pharmaceutical and Biomedical Analysis

journal homepage: www.elsevier.com/locate/jpba

Letter to the Editor

Inaccurate data cannot be used as standards in pharmaceutical and biomedical analysis

Keywords:
Quinolizidine alkaloids
Lupinus species
Pharmaceutical and biomedical analysis

The paper "Determination of quinolizidine alkaloids in different *Lupinus* species by NACE using UV and MS detection" (M. Ganzera, A. Krüger, M. Wink), published by the Journal of Pharmaceutical and Biomedical Analysis (53:1231–1235) is in general interesting and relevant as the development of quinolizidine alkaloid analysis continues to present a challenge to scientists [1–6]. As the authors state, lupin species have potential in food and organic feed production (low-alkaloid cultivars) and in industrial applications (rich-alkaloid cultivars) [7–10,12], and therefore objective measurement and the control of alkaloids are of extreme importance. However, the article contains some inaccuracy.

There is a contradiction between the data in Fig. 3 (p. 1233) and Table 2 (p. 1235) in the case of *Lupinus polyphyllus*. Comparison of standard peaks in Fig. 3 with the peaks of *Lupinus albus* and *L. polyphyllus* leads to the conclusion that the lupanine content and amount of *L. polyphyllus* is considerably higher as in *L. albus* as the peaks are on different scale. When good quantitative and qualitative standards are used, it is possible to provide electropherograms on the same scale as the peaks as evidence, if they are from the same research series. Moreover, angustifoline content is also higher in the standard and in *L. albus*. The content of hydroxylupanine is higher in *L. polyphyllus* than in *L. albus* but lower than in the standard. In contrast, in Table 2 in the case of *L. polyphyllus* the content of lupanine is stated to be less than in *L. albus* and the content of 13-α-hydroxylupanine to be more than 3.5 times that in *L. albus*. Angustifoline high content in *L. polyphyllus* is a mistake as angustifoline is not an alkaloid typically found for *L. polyphyllus*, which is a perennial species. Angustifoline is an alkaloid typically occurring in annual lupins, especially *Lupinus angustifolius*. The alkaloids typical to *L. polyphyllus* belong to the lupanine group, while the content of the angustifoline group of alkaloids does not exceed 2.1% of the total alkaloid content in this species and the content of the sparteine group of alkaloids in *L. polyphyllus* does not exceed 0.7% of the total alkaloid content [9,10,11]. The authors state in the abstract that "the quantitative results were in good agreement with literature data". In the light of above-mentioned facts it is impossible to accept this statement and accept the data concerning *L. polyphyllus* in this paper. What are the possible sources of this inaccuracy? One possibility is that the samples were not of *L. polyphyllus* but of *L. angustifolius* (both species have blue flowers). The alkaloid profile given for *L. polyphyllus* fits almost perfectly with that of *L. angustifolius* (!), although the content is too high. Alternatively, the source of the error lies in the identification of standards substituting lupanine for angustifoline and vice versa. In this case, the total alkaloid content of *L. polyphyllus* mentioned in Table 2 is acceptable as in this species is equal to 1.74X, where X is a content of lupanine [9,10,11]. However, because of its changeable and oxidative character, lupanine is not the best quantitative and qualitative standard.

References

[1] T. Aniszewski, Alkaloids – Secrets of Life. Alkaloid Chemistry, Biological Significance, Application and Ecological Role, Elsevier, Amsterdam, Oxford, 2007, 316 pp.
[2] W. Wysocka, A. Przybył, Alkaloids from *Lupinus albus* and *Lupinus angustifolius* L.: an efficient method of extraction, Sci. Leg. 1 (1994) 37–50.
[3] T. Aniszewski, The biological basis of quinolizidine alkaloids, Sci. Leg. 1 (1994) 1–24.
[4] T. Aniszewski, From iodine to enzyme: a critical review of chemical and biological methods of lupine alkaloids analysis, Sci. Leg. 1 (1994) 25–36.
[5] T. Aniszewski, Perennial stability of total alkaloid content in alkaloid-poor Washington lupin (*Lupinus polyphyllus* Lindl.), J. Sci. Food Agric. 76 (1998) 195–199.
[6] T. Aniszewski, QAs (+) and QAs(−) plants in Fabaceae populations, in: E. Spalding, M. Thomashow, S.P. Long, J. Balley-Serres, A.S.N. Reddy, A.M. Jones, B. Kunkel (Eds.), Plant Biology, American Society of Plant Biologists, Seattle, Washington, 2005, p. 231.
[7] T. Aniszewski, The alkaloid-rich and alkaloid-poor Washington lupine (*Lupinus polyphyllus* Lindl.) as a potential industrial crop, Ind. Crops Prod. 1 (1993) 147–157.
[8] T. Aniszewski, Nutritive quality of the alkaloid-poor Washington lupine (*Lupinus polyphyllus* Lindl. Var. SF/TA) as a potential protein crop, J. Sci. Food Agric. 61 (1993) 409–421.
[9] T. Aniszewski, Lupine: a potential crop in Finland, Studies on the ecology, productivity and quality of *Lupinus* spp., PhD thesis summary, University of Joensuu, Public. Sci. 29 (1993) 1–50.
[10] T. Aniszewski, Lupine: a potential crop in Finland, Studies on the ecology, productivity and quality of *Lupinus* spp., PhD thesis, Joensuu University Press, Joensuu, 1993, 148 pp.
[11] T. Aniszewski, A theoretical formula for the determination of total alkaloid content of quinolizidine alkaloifs of *Lupinus polyphyllus* Lindl, Sci. Leg. 1 (1994) 111–116.
[12] T. Aniszewski, D. Ciesiołka, K. Gulewicz, Equilibrium between basic nitrogen compounds in lupin seeds with differentiated alkaloid content, Phytochemistry 57 (2001) 43–50.

Tadeusz Aniszewski*
Research and Teaching Laboratory of Applied Botany, Biological Interactions and Ecological Engineering. Department of Biology, University of Eastern Finland, Joensuu Campus, P.O. Box 111, 80101 Joensuu, Finland

*Tel.: +358 132513581/3573;
fax: +358 132513590.
E-mail address: Tadeusz.Aniszewski@uef.fi

17 May 2011

10 October 2011

21 October 2011
Available online 25 October 2011

DOI of original article: 10.1016/j.jpba.2011.10.027.

doi:10.1016/j.jpba.2011.10.025

Journal of Pharmaceutical and Biomedical Analysis 60 (2012) 92–97

Contents lists available at SciVerse ScienceDirect

Journal of Pharmaceutical and Biomedical Analysis

journal homepage: www.elsevier.com/locate/jpba

Comparisons of different regressions tools in measurement of antioxidant activity in green tea using near infrared spectroscopy

Quansheng Chen[a,*], Zhiming Guo[a,b], Jiewen Zhao[a], Qin Ouyang[a]

[a] School of Food & Biological Engineering, Jiangsu University, 301 Xuefu Road, Zhenjiang 212013, PR China
[b] National Engineering Research Center for Information Technologies in Agriculture, Beijing 100097, PR China

ARTICLE INFO

Article history:
Received 30 May 2011
Received in revised form 18 October 2011
Accepted 18 October 2011
Available online 25 October 2011

Keywords:
Near infrared (NIR) spectroscopy
Regression tool
Measurement
Tea
Antioxidant activity

ABSTRACT

To rapidly and efficiently measure antioxidant activity (AA) in green tea, near infrared (NIR) spectroscopy was employed with the help of a regression tool in this work. Three different linear and nonlinear regressions tools (i.e. partial least squares (PLS), back propagation artificial neural network (BP-ANN), and support vector machine regression (SVMR)), were systemically studied and compared in developing the model. The model was optimized by a leave-one-out cross-validation, and its performance was tested according to root mean square error of prediction (*RMSEP*) and correlation coefficient (R_p) in the prediction set. Experimental results showed that the performance of SVMR model was superior to the others, and the optimum results of the SVMR model were achieved as follow: *RMSEP* = 0.02161 and R_p = 0.9691 in the prediction set. The overall results sufficiently demonstrate that the spectroscopy coupled with the SVMR regression tool has the potential to measure AA in green tea.

1. Introduction

A free radical is an atom, molecule, or compound that is highly unstable. As a result, free radicals are very reactive as they attempt to pair up with other molecules, atoms, or even individual electrons to create a stable compound. To achieve a more stable state, free radicals can "steal" a hydrogen atom from another molecule, bind to another molecule, or interact in various ways with other free radicals [1]. Free radical action has been implicated in certain chronic and ageing diseases such as cancer, heart disease, stroke, rheumatoid arthritis, cataracts and Alzheimer's disease. Increasing evidence is highlighting that antioxidants may be able to protect the body against the destructive effects of free radicals. Antioxidants neutralize free radicals by donating one of their own electrons and ending the electron-"stealing" reaction. Although donating an electron, the antioxidant nutrients themselves would not become free radicals, because they are relatively stable form. They act as scavengers to prevent cell and tissue damage that could lead to some diseases [2,3].

Tea (*Camellia sinensis* L.) is one of the most popular beverages consumed across the world, which is of great interest due to its beneficial medicinal properties [4]. Increasing evidences show that some specific substances in green tea have antioxidant activity (AA); among these specific substances, flavonoids in green tea are the main source of AA in green tea. Preliminary researches have indicated that flavonoids in green tea are linked with a reduction in the risk of cardiovascular disease, chronic gastritis, and cancer [5,6]. Antioxidants in green tea are the phenolic compounds that can delay or inhibit the oxidation of lipids or other molecules by inhibiting the initiation or propagation of oxidizing chain reactions. AA in green tea is mainly due to the redox properties from phenolic compounds, which can play an important role in adsorbing and neutralizing free radicals, quenching singlet and triplet oxygen, or decomposing peroxides [7]. Green tea is rich in phenolic compounds; moreover, typically 93% of total phenolic compounds are flavonoids. The types and amounts of flavonoids presented in green tea would differ dependent on the tea plant's species, growing environment, processing, manufacturing and infusion preparation [8,9]. AA is often used to evaluate the medical functions in green tea; besides, AA is also an important indicator in evaluating the quality of green tea, and linked with the price of green tea product in the market. Therefore, a simple, rapid and accurate method, to detect antioxidant activity in green tea, is urgently needed for tea quality monitoring in the tea industry and as well as quality control agencies.

Nowadays, numerous classical assays are employed to measure the antioxidant activity in the plant such as scavenging activity of DPPH (1,1-diphenyl-2-picrylhydrazyl) free radical, oxygen radical absorbance capacity (ORAC), and trolox equivalent antioxidant capacity (TEAC) [10–15]. However, these assays mentioned above belong to wet-chemical analysis, and include multi-steps such as sample preprocessing, crude materials extraction,

* Corresponding author. Tel.: +86 511 88780174; fax: +86 511 88780201.
E-mail address: q.s.chen@hotmail.com (Q. Chen).

0731-7085/$ – see front matter © 2011 Elsevier B.V. All rights reserved.
doi:10.1016/j.jpba.2011.10.020

chemical-reagent preparation and instrumental analysis. Therefore, they are time consuming and difficult to handle. Near infrared (NIR) spectroscopy has been proved to be a fast, simple, nondestructive and chemical-free analytical tool, and it can act as a replacement of chemical analysis. Currently, NIR spectroscopy has been widely used in many sectors such as agricultural sector [16], petrochemical sector [17] and pharmaceutical sector [18]. In 1999, Schulz, et al. attempted to simultaneously measure the contents of alkaloids and phenolic substances in green tea using NIR spectroscopy [19]. Recently, Chen, et al. attempted to measure the contents of caffeine and total polyphenol in green tea using NIR spectroscopy [20,21]. These studies show that NIR spectroscopy has a high potential in measurement of active compositions in green tea. However, the most commonly used multivariate calibrations are linear approaches, such as partial least-squares (PLS) and principle component regression (PCR). Green tea is the natural product, and there includes numerous complicated flavonoids that contain a great quantity of hydrogenous bonds (i.e. C–H, O–H, S–H, and N–H). NIR spectroscopy is based on overtones and combinations of fundamental vibrations from the hydrogenous bonds. These overtone and combination bands in the NIR region are typically very broad, leading to complex spectra; it could be difficult to assign specific features to specific chemical components. Thus, the correlation between the NIR spectra and AA in green tea would incline to nonlinearity. And the linear regression tools alone may not provide a complete solution to the regression problem in this work. Therefore, it is necessary that different linear and nonlinear tools should be attempted, and that is the aim of the present work.

The objective of this study was to explore the potential that NIR spectroscopy could be used to measure AA in green tea; besides, we systematically studied the applications of different linear and nonlinear regression tools on the quantitative analysis of NIR spectroscopy. In this work, three different regression tools – partial least squares (PLS), back propagation artificial neural network (BP-ANN), and support vector regression (SVMR), were used to develop the models, and the optimal model was selected from the three models.

2. Materials and methods

2.1. Sample preparation

A large selection of green tea harvested within 4 months and from different geographical areas was collected. The chemical compositions of samples differed according to their species, cultivation conditions such as weather, moisture, latitude, season, and manufacturing. Experiments were done under the controllable conditions. Before spectra acquisitions, the whole green tea leaves were ground for 10 s by a small electric coffee mill (Huanya, HY-02, Beijing, China). After this procedure, the powders were sieved with a mesh width of 500 μm and this sieved powder was used for spectra acquisition and wet-chemical analysis.

2.2. Spectra acquisition

In this experiment, spectra acquisition was based on a diffuse reflectance mode, and each sample was measured using an Antaris™ II Method Development Sampling (MDS) system (Thermo Fisher Scientific Inc., Madison, WI, USA). Spectra were recorded between 10,000 cm^{-1} and 4000 cm^{-1} at 4 cm^{-1} resolution by co-adding 32 scans using an integrating sphere. The reflectance values (R) were converted into the absorbance values (A) using the formula $A = \log(1/R)$. Spectra were measured by 1.928 cm^{-1} interval, and thus, there were 3112 variables in each spectrum. The standard sample accessory holder was used for spectra acquisitions. The sample accessory holder was sample cup specifically designed by Thermo Fisher Scientific. For each sample, 10 ± 0.1 g powders were filled into the sample cup according to a standard procedure. Each sample was collected once every rotating the cup 120° angle; thus, each sample was collected 3 times. The average of the 3 spectra was used for the next analysis.

2.3. Reference measurement

Reference measurement of antioxidant activity (AA) in green tea is the classical wet-chemical analysis in this work. Here, AA in green tea was measured by the DPPH (1,1-diphenyl-2-picrylhydrazyl) free radical scavenging activity assay, and it is the well known and frequently employed method proposed by Khalaf with slight modification [11]. DPPH is a stable free radical due to its spare electron delocalization including the whole molecule. The delocalization causes a deep violet color with the band (λ) at 517 nm. When a solution of DPPH is mixed with a substrate acting as a hydrogen atom donor, a stable non-radical from of DPPH is obtained with simultaneous color change from violet to pale yellow.

In the reference measurement, the experiment procedures were briefly introduced as follows: first of all, DPPH (0.04 mg/mL), as a standard, was prepared in ethanol for the next use; then, green tea materials (3 g) were infused with 500 mL distill water for 40 min in the dark; next, the extracted tea infusion (2 mL) was mixed with 2 mL DPPH (0.04 mg/mL, 2 mL) in a test tube; finally, the mixed solution was kept in dark for 30 min and optical density was measured at 517 nm by the UV-1600 spectrometer (Rayleigh Co., Beijing, China). Methanol (2 mL) with DPPH solution (0.04 mg/mL, 2 mL) was used as blank. To determine the antioxidant activity from the sample, two optical densities (i.e. A_0 and A_i) were recorded, and the scavenging activity (SA) from DPPH free radical was calculated using Eq. (1):

$$\mathrm{SA} = 1 - \frac{A_0 - A_i}{A_0} \quad (1)$$

where A_0 is the optical density of the blank, and A_i is the optical density of sample. In the experiment, 1,1-diphenyl-2-picryl-*h*ydrazyl (DPPH) was obtained from Sigma–Aldrich Co., St. Louis, USA. All other chemicals used were of analytical grade.

2.4. Spectra preprocessing

Fig. 1a presents the raw spectra of the samples. All samples, in this work, were tea powders, and their particle sizes were significantly different, which resulted in the light scatter. Raw spectra acquired from NIR spectrometer contained background information and noises beside sample information. The spectra should be preprocessed before the model calibration, in order to achieve a reliable, accurate and stable model. Compared with other spectra preprocessing tools, standard normal variate (SNV), multiplicative scatter correction (MSC), and min/max normalization (MIN/MAX) have better performance in the correction of scatter light [22]. Therefore, SNV, MSC, and MIN/MAX were attempted in this work.

First of all, SNV is used to remove slope variation, and to correct scatter light effects. Each spectrum was first centered individually, and then scaled by the standard deviation calculated from the individual spectrum. The spectra by SNV preprocessing are presented in Fig. 1b. MSC spectra preprocessing separates additive and multiplicative effects on measurement by linear fitting each individual spectrum to a reference spectrum that is usually an average. It is an important procedure for the correction of scatter light on the basis of different particle sizes. The spectra by MSC preprocessing are presented in Fig. 1c. Finally, MIN/MAX normalization was used to transform the data into a desired range by subtracting the minimum value from each individual spectrum and then

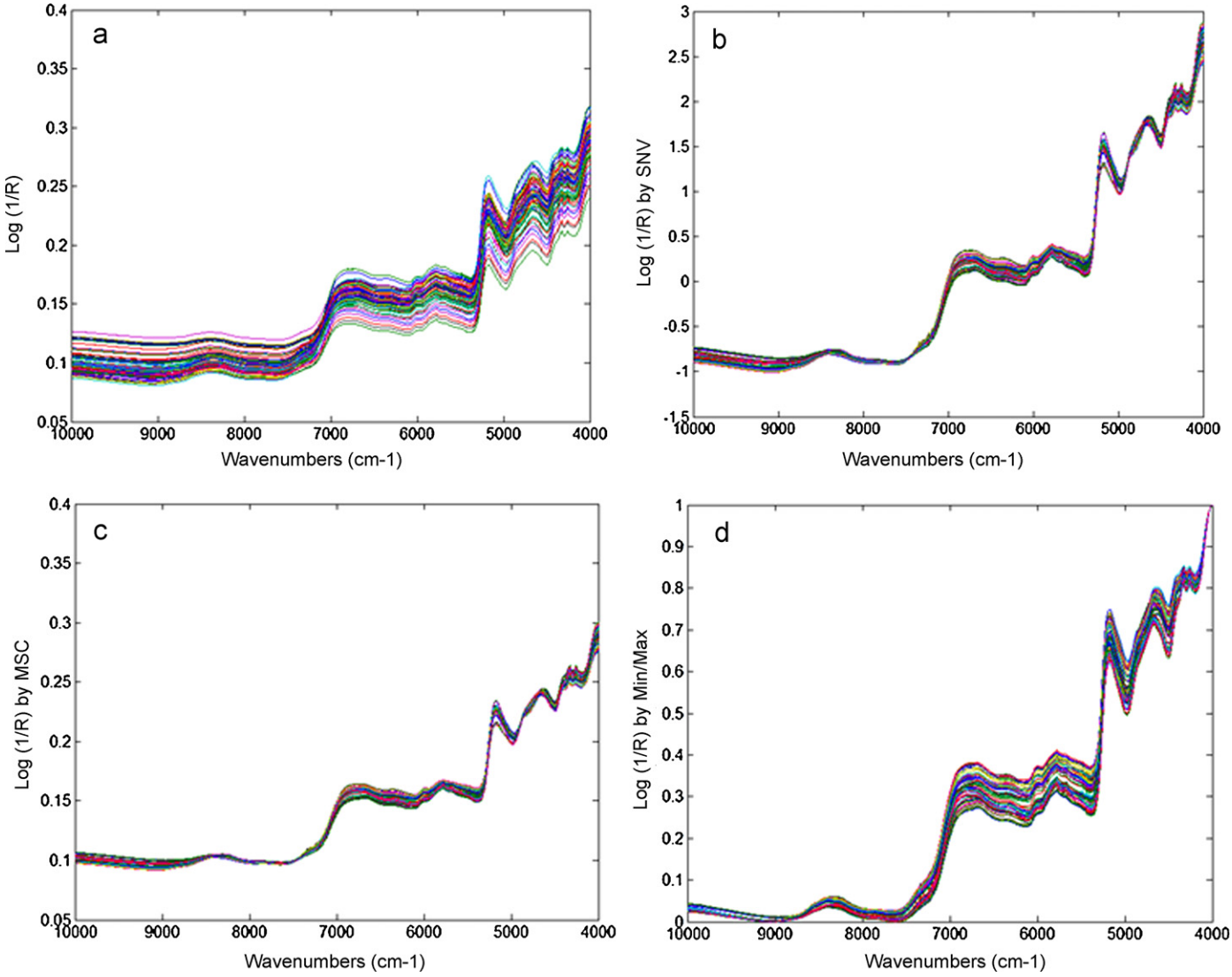

Fig. 1. Raw spectra (a), spectra by SNV (b), spectra by MSC (c), and spectra by MIN/MAX (d) from tea samples.

dividing the range from this spectrum [22]. The spectra by MIN/MAX preprocessing are presented in Fig. 1d.

2.5. Software

All algorithms were implemented in Matlab V7.0 (Mathworks Co., USA). Results Software (Antaris II System, Thermo Electron Co., USA) was used for spectra acquisition. SVMR program was implemented by LS-SVM Matlab codes, which were downloaded free of charge from http://www.esat.kuleuven.ac.be/sista/lssvmlab/.

3. Results and discussion

3.1. Calibration of models

In this work, 110 samples were divided into 2 subsets. One was called the calibration set in which all samples were used for calibrating model; the other was called the prediction set in which all samples were used to test the performance of the model. To achieve a robust model, selecting sample was important for calibrating model and done as follows: first, all samples were sorted according to their *y*-values (the value of reference measurement); then, according to division of 3/2 for calibration/prediction spectra, 2 samples of every 5 samples were selected into the prediction set. So, the calibration set contains 66 samples; the prediction set contains 44 samples. As shown in Table 1, the range of *y*-value in the calibration set covers its range in the prediction set. And the distributions of *y*-values are close in the calibration and prediction sets.

Calibrating model, with the help of a regression tool, was used to establish a model between reference measurement and NIR spectra in the calibration set. Optimizing model was done by a leave-one-out cross-validation. The optimum model was determined according to the first local minimum value of root mean square error cross-validation (*RMSECV*). The performance of the final PLS model was tested according to the value of root mean square error of prediction (*RMSEP*) and the correlation coefficient (R_p) in prediction set. In this work, the performance of the model

Table 1
Reference measurement results in the calibration and prediction sets.

Subsets	No. of samples	Ranges	Mean	Standard deviation
Calibration set	66	0.442–0.806	0.703	0.0827
Prediction set	44	0.446–0.801	0.701	0.0848

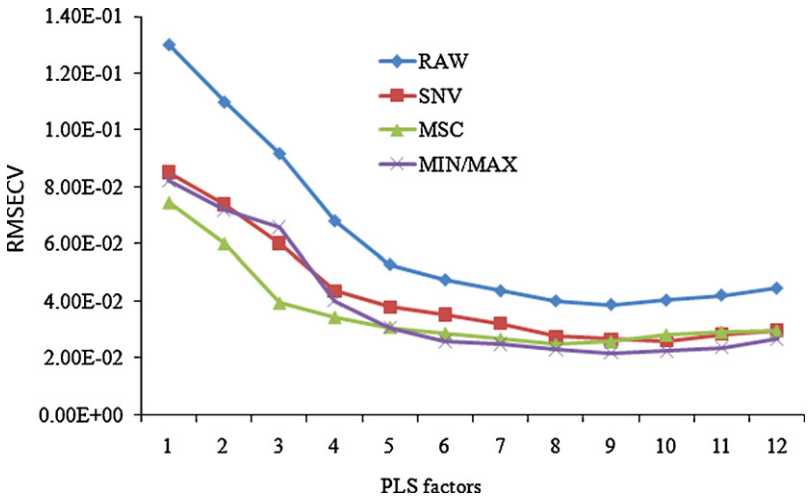

Fig. 2. *RMSECV* value with different PLS factors and spectra preprocessing methods.

refers to its prediction accuracy and robustness, and usually, a good model means a higher R_p and a lower value of *RMSEP* in the prediction set.

3.2. Results of PLS model

Partial least square (PLS) is one of the most classical multivariate regression tools. Generally, the number of PLS factors and the spectra preprocessing are two critical factors in calibrating model. In this work, the number of PLS factors and the spectral preprocessing were optimized by a leave-one-sample-out cross-validation, and were determined according to the first local minimum of *RMSECV*. Fig. 2 shows multiple lines graphs of the values of *RMSECV*, which are plotted with respect to the number of PLS factors and defined lines in term of spectral preprocessing. As shown in Fig. 2, both spectral preprocessing and PLS factors have significant effect on the performance of PLS model. For spectral preprocessing, MIN/MAX is a little better than others. For PLS factors, the values of *RMSECV* decline with the increment of PLS factors, and the values of *RMSECV* decline sharply in the beginning, but slowly decline when more PLS factors are included; thus, the first local minimum of *RMSECV* occurs when 6 PLS factors are included. So the optimum PLS model was achieved when 6 PLS factors and MIN/MAX spectra preprocessing were included in this work.

3.3. Results of BP-ANN model

Back propagation artificial neural network (BP-ANN) is a powerful data-modeling tool to capture and represent complex correlation between inputs and outputs. The output expresses the resemblance that an object corresponds with a training pattern. Along with every process of a training pattern and adjustment of the weight factors, the difference between the desired value and calculated network output, defined as the network output error, will gradually become less and less until it meets the desired value. An epoch is one cycle through all training patterns. In this work, 3 layers (input layer, hidden layer and output layer) of BP-ANN were arranged. Principal components (PCs) extracted by principal component (PCA) were used for the input of BP-ANN, and the number of PCs was also optimized according to cross-validation. The output of BP-ANN was AA in green tea; the number of hidden nodes were optimized by 'trial and error', and optimum of the number of hidden nodes was determined according to the minimum mean square error (MSE) value [23]. Both learning rate and momentum were set the default values, and scale function was set 'tanh' function. The permitted regression error was set 0.01, and the maximum iterative epoch was set 2000 times. The optimum BP-ANN model can be achieved when 3 PCs and 8 nodes in the hidden layers were included; thus, the optimum network architecture was obtained with the 3-8-1 topological architecture. Fig. 3 is the scatter plot between reference measurements and NIR predicted results. Fig. 3a shows the results in the calibration set, and Fig. 3b shows its results in the prediction set.

3.4. Results of SVMR model

Support vector machine (SVM) is typically adopted to describe classification problems [24]. However, with the help of ε-insensitive loss function, SVM has been extended to solve the nonlinear regression problems, and thus a regression version of SVM is also called support vector machine regression (SVMR). SVMR can map the complex and nonlinear data into a higher dimensional feature space, where the nonlinear problem could be solved by a linear tool. Mapping data into a higher dimensional space is often implemented through a kernel function [25]. In general, SVMR has 3 classical kernel functions: polynomial, radial basic function (RBF), and sigmoid. Kernel functions have a great influence on the performance of SVMR model. Among three kernel functions, RBF is simpler and faster to compute in contrast to the others. Gaussian kernel function is often the best choice where prior experience is lacking [26]. Thus, RBF, as the kernel function, was adopted in this work.

To obtain a good performance, some parameters in SVMR model had to be optimized by cross-validation. These parameters include: (1) Regularization parameter (γ), it determines the balance between minimizing the training error and minimizing model complexity; (2) Kernel parameter (σ^2), it is the bandwidth of the RBF-kernel function. The initial values of two parameters were pre-given, and parameter optimization was based on the two pre-given initial values. In SVMR, the cost value was used to optimize SMV model and the optimum SVMR model was achieved according to the minimum of cost value.

Fig. 4 shows a contour map according to different cost values that are indicated by different colors. The optimum parameters of γ and σ^2 were determined according to two steps grid-search. In the first step, a larger step length in 10×10 grids represented as "·" was performed and the optimum region was determined according to cross-validation. Subsequently, a much smaller step length in 10×10 grids as "×" was performed and the optimum parameters were determined from the above optimum region. Eventually,

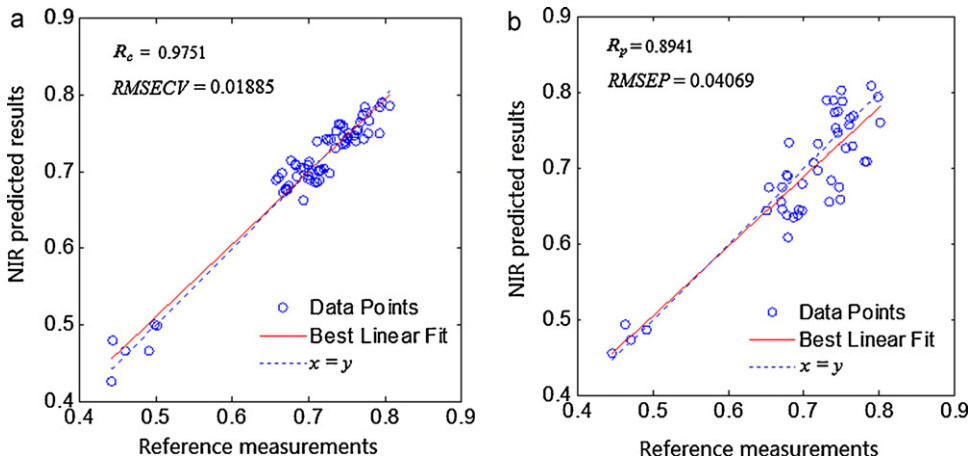

Fig. 3. Scatter plot between reference measurements and NIR predicted results by BP-ANN model in the calibration set (a) and the prediction set (b).

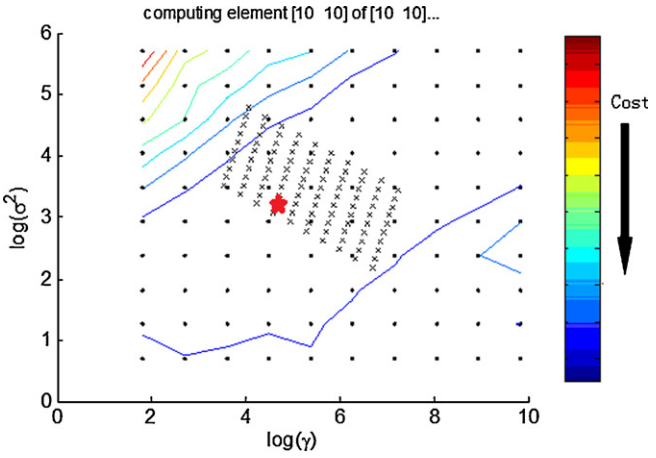

Fig. 4. Contour map of the optimization the parameters γ and σ^2 by the leave-one-sample-out cross-validation.

the optimum combination of two parameters was determined according to the minimum of cost value that can be found in the contour map. According to two steps grid-search, the optimum combination of two parameters were obtained, which was marked by the asterisk in Fig. 4. After two parameters of SVMR model were determined, the number of PCs was also optimized by cross-validation, and the optimum number of PCs was also determined according to the minimum value of *RMSECV*. Results showed that the optimum SVMR model was achieved when 3 PCs were included. Fig. 5a shows the results in the calibration set; Fig. 5b shows the results in the prediction set.

Table 2
Comparison of results from PLS, BP-ANN and SVMR models.

Methods	PCs	Calibration set		Prediction set	
		R_c	*RMSECV*	R_p	*RMSEP*
PLS	6	0.9621	0.02467	0.9568	0.024319
BP-ANN	3	0.9751	0.01885	0.8941	0.04069
SVMR	3	0.9813	0.01720	0.9691	0.02161

4. Discussion

To get a good performance in measurement of AA in green tea using NIR spectroscopy, we systematically studied the regression tools and parameter optimization that had to be gone through in developing the regression model. Table 2 shows the results from PLS, BP-ANN, and LS-SVM approaches used in this study.

First of all, SVMR model was compared with PLS model. SVMR is a universal nonlinear regression tool; while PLS is a linear regression tool. AA in green tea is depended on the capacity of scavenging the free radicals by flavonoids. Tea is a natural product including a large number of complicated flavonoids, and these flavonoids contain a great quantity of hydrogenous

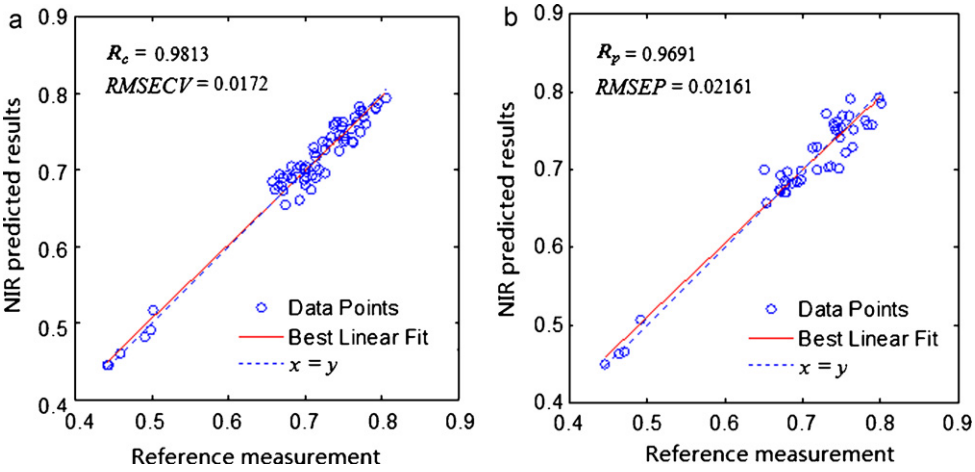

Fig. 5. Scatter plot between reference measurements and NIR predicted results by SVRM model in the calibration set (a) and the prediction set (b).

bonds (i.e. C–H, O–H, S–H, N–H, etc.). NIR spectroscopy is based on overtones and combinations of fundamental vibrations from the hydrogenous bonds. These overtone and combination bands in the NIR region are typically very broad, leading to complex spectra; it could be difficult to assign specific features to specific chemical components. Thus, the correlation between the NIR spectra and AA in green tea could incline to nonlinearity. Linear regression tools may not provide a complete solution to such nonlinear cases in this work. In fact, the nonlinear correlation was also diagnosed by the approach of augmented partial residual plots (APaRP) [27]. A quantitative numerical tool (run test) was employed to calculate the degree of nonlinearity based on APaRP approach, and the value of $|z|$ was 2.894, which exceeded the critical value ($|z| = 1.96$); thus, a nonlinearity conclusion is credible in this work, and also, the conclusion that SVMR model is superior to PLS model is reasonable.

Secondly, SVMR model was compared with BP-ANN model. BP-ANN is a traditional nonlinear regression tool based on the empirical risk minimization (ERM) principle. It easily suffers difficulty with the generalization of model. For example, the "best" model by training would result in the worse predictive results, and it means that this model has a weak generalization. SVMR is based on the structural risk minimization (SRM) principle that is superior to the ERM principle in intelligent machine learning. SRM minimizes an upper bound on the expected risk, as opposed to ERM that minimizes the error on the training data [28], and is superior to the ERM principle in that. In summary, SVMR not only has advantages as a nonlinear tool, but also yields excellent generalization, so the LS-SVM model results in a better performance in contrast to the BP-ANN model.

Finally, the numbers of PCs from BP-ANN model (3 PCs) and SVM model (3 PCs) are fewer than that from PLS model (6 PLS factors). It shows that nonlinear is simpler than linear model in the structure of model. In this work, the top 3 PCs can explain the majority of total variances; while, the later PCs have very few contributes in variance explanation. Nonlinear tool has a strong capacity of self-learning and can ignore these minor PCs by self-adjusting weights.

5. Conclusion

The overall results sufficiently demonstrate that NIR spectroscopy with the help of a regression tool can be successfully used in measurement of AA in green tea. Three different regression tools (PLS, BP-ANN, and SVMR) were compared in their ability to develop a regression model. Among the 3 models, the performance of SVMR model was the best. We can infer that NIR spectroscopy coupled with the SVMR tool may have a potential in measurement of AA in other natural products.

Acknowledgements

This work has been supported financially by the National Natural & Science Foundation of China (30800666), the Natural & Science Foundation of Jiangsu Province (BK2009216), the Granted Special Grade of the Financial Support from China Postdoctoral Science Foundation (201003559), and the Project Funded by the Priority Academic Program Development of Jiangsu Higher Education Institutions.

References

[1] D. Wu, A.I. Cederbaum, Alcohol, oxidative stress, and free radical damage, Alcohol Res. Health 27 (2003) 277–284.
[2] M. Martinez-Cayuela, Oxygen free radicals and human disease, Biochimie 77 (1995) 147–161.
[3] C.E. Cross, B. Halliwell, E.T. Borish, W.A. Pryor, B.N. Ames, R.L. Saul, J.M. McCord, D. Harman, Oxygen radicals and human disease, Ann. Intern. Med. 107 (1987) 526–545.
[4] C.S. Yang, P. Maliakal, X. Meng, Inhibition of carcinogenesis by tea, Annu. Rev. Pharmacol. Toxicol. 42 (2002) 25–54.
[5] K. Nakachi, S. Matsuyama, S. Miyake, M. Suganuma, K. Imai, Preventive effects of drinking green tea on cancer and cardiovascular disease: epidemiological evidence for multiple targeting prevention, Biofactors 13 (2000) 49–54.
[6] V.W. Setiawan, Z.F. Zhang, G.P. Yu, Q.Y. Lu, Y.L. Li, M.L. Lu, M.R. Wang, C.H. Guo, S.Z. Yu, R.C. Kurtz, C.C. Hsieh, Protective effect of green tea on the risks of chronic gastritis and stomach cancer, Int. J. Cancer 92 (2001) 600–604.
[7] W. Zheng, S.Y. Wang, Antioxidant activity and phenolic compounds in selected herbs, J. Agric. Food Chem. 49 (2001) 5165–5170.
[8] C. Astill, M.R. Birch, C. Dacombe, P.G. Humphrey, P.T. Martin, Factors affecting the caffeine and polyphenol contents of black and green tea infusions, J. Agric. Food Chem. 49 (2001) 5340–5347.
[9] C. Lakenbrink, S. Lapczynski, B. Maiwald, U.H. Engelhardt, Flavonoids and other polyphenols in consumer brews of tea and other caffeinated beverages, J. Agric. Food Chem. 48 (2000) 2848–2852.
[10] K.M. Gillespie, J.M. Chae, E.A. Ainsworth, Rapid measurement of total antioxidant capacity in plants, Nat. Protoc. 2 (2007) 867–870.
[11] N.A. Khalaf, A.K. Shakya, A. Al-Othman, Z. El-Agbar, H. Farah, Antioxidant activity of some common plants, Turk. J. Biol. 32 (2008) 51–55.
[12] S. Milardovic, D. Ivekovic, B.S. Grabaric, A novel amperometric method for antioxidant activity determination using DPPH free radical, Bioelectrochemistry 68 (2006) 175–180.
[13] C.L. Peng, S.W. Chen, Z.F. Lin, G.Z. Lin, Detection of antioxidative capacity in plants by scavenging organic free radical DPPH, Prog. Biochem. Biophys. 27 (2000) 658–661.
[14] R. Re, N. Pellegrini, A. Proteggente, A. Pannala, M. Yang, C. Rice-Evans, Antioxidant activity applying an improved ABTS radical cation decolorization assay, Free Radic. Biol. Med. 26 (1999) 1231–1237.
[15] D. Koracevic, G. Koracevic, V. Djordjevic, S. Andrejevic, V. Cosic, Method for the measurement of antioxidant activity in human fluids, J. Clin. Pathol. 54 (2001) 356–361.
[16] C.J. Clark, V.A. McGlone, R.B. Jordan, Detection of Brownheart in 'Braeburn' apple by transmission NIR spectroscopy, Postharvest Biol. Technol. 28 (2003) 87–96.
[17] R.M. Balabin, R.Z. Safieva, Gasoline classification by source and type based on near infrared (NIR) spectroscopy data, Fuel 87 (2008) 1096–1101.
[18] Y. Dou, Y. Sun, Y.Q. Ren, P. Ju, Y.L. Ren, Simultaneous non-destructive determination of two components of combined paracetamol and amantadine hydrochloride in tablets and powder by NIR spectroscopy and artificial neural networks, J. Pharm. Biomed. Anal. 37 (2005) 543–549.
[19] H. Schulz, U.H. Engelhardt, A. Wegent, H.H. Drews, S. Lapczynski, Application of near-infrared reflectance spectroscopy to the simultaneous prediction of alkaloids and phenolic substances in green tea leaves, J. Agric. Food Chem. 47 (1999) 5064–5067.
[20] Q.S. Chen, J.W. Zhao, M.H. Liu, J.R. Cai, J.H. Liu, Determination of total polyphenols content in green tea using FT-NIR spectroscopy and different PLS algorithms, J. Pharm. Biomed. Anal. 46 (2008) 568–573.
[21] Q.S. Chen, J.W. Zhao, H.D. Zhang, X.Y. Wang, Feasibility study on qualitative and quantitative analysis in tea by near infrared spectroscopy with multivariate calibration, Anal. Chim. Acta 572 (2006) 77–84.
[22] S. Vittayapadung, J.W. Zhao, Q.S. Chen, R. Chuaviroj, Application of FT-NIR spectroscopy to the measurement of fruit firmness of Fuji apples, Maejo Int. J. Sci. Technol. 2 (2008) 13–23.
[23] X.L. Li, Y. He, Discriminating varieties of tea plant based on Vis/NIR spectral characteristics and using artificial neural networks, Biosyst. Eng. 99 (2008) 313–321.
[24] F. Chauchard, R. Cogdill, S. Roussel, J.M. Roger, V. Bellon-Maurel, Application of LS-SVM to non-linear phenomena in NIR spectroscopy: development of a robust and portable sensor for acidity prediction in grapes, Chemom. Intell. Lab. Syst. 71 (2004) 141–150.
[25] Q.S. Chen, J.W. Zhao, C.H. Fang, D.M. Wang, Feasibility study on identification of green, black and Oolong teas using near-infrared reflectance spectroscopy based on support vector machine (SVM), Spectrochim. Acta Part A 66 (2007) 568–574.
[26] N. Labbe, S.H. Lee, H.W. Cho, M.K. Jeong, N. Andre, Enhanced discrimination and calibration of biomass NIR spectral data using non-linear kernel methods, Bioresour. Technol. 99 (2008) 8445–8452.
[27] V. Centner, O.E. de Noord, D.L. Massart, Detection of nonlinearity in multivariate calibration, Anal. Chim. Acta 376 (1998) 153–168.
[28] V.N. Vapnik, A.Y. Chervone, Uniform convergence of relative frequencies of events to their probabilities, Theory Probab. Appl. 16 (1971) 264–280.

Journal of Pharmaceutical and Biomedical Analysis 60 (2012) 98

Contents lists available at SciVerse ScienceDirect

Journal of Pharmaceutical and Biomedical Analysis

journal homepage: www.elsevier.com/locate/jpba

Reply to Letter to the Editor

First of all we appreciate the valuable comments as they indicate in-depth knowledge and careful evaluation of our manuscript. There definitely is a mismatch concerning the quantitative results provided for "*L. polyphyllus*" as they do not correspond with previously reported ones. A possible explanation is, as already suggested by Dr. Aniszewski himself, a confusion of *L. polyphyllus* with *L. angustifolius*. To show practical applicability of the developed CE-assay we selected a variety of seeds from different *Lupinus* species, provided by Prof. Wink, for analysis in our study. Even *L. polyphyllus* and *L. angustifolius* seeds already differ visually they unfortunately/obviously were confused. The misidentification of lupanine and angustifoline in the electropherograms is not possible as MS data as well as migration times were in agreement with respective standard compounds and literature data (*m*/*z* values). Why the alkaloid level in this particular *L. angustifolius* specimen is uncommonly high is out of our expertise (which is towards analytical method development and validation). Regardless if it is caused by some special genetic variation or breeding peculiarity, relevant data of method validation (e.g., excellent recovery for lupanine) and the results for the remaining *Lupinus* species indicated a correct and trustworthy assay. The confusion regarding peak areas and quantitative results (Table 2 and Fig. 3) is explainable by variant initial weight and very divergent regression equations of angustifoline and lupanine. The sample preparation procedure describes a general approach; yet, for individual solutions the amount of (accurately weighted) sample might vary, which is no problem as quantitative results are stated in relation to "gram plant material" anyway (Table 2). Therefore, the electropherograms shown in Fig. 3 do not allow direct quantitative estimations but a comparison of metabolite patterns and relative compositions only. The electropherogram of a standard solution (Fig. 3) does not permit any quantitative conclusions either, as it shows a randomly selected calibration solution indicating the overall separation of reference compounds. In this respect the comment that a "good standard" should have been used is not appropriate, considering that method validation confirmed the suitability of lupanine for this purpose. To conclude, we apologize for the confusion caused by the mix-up of *L. polyphyllus* and *L. angustifolius*. Accordingly, all data related to *L. polyphyllus* has to be assigned to *L. angustifolius*. This negligence should have been avoided, yet it must not diminish attractiveness of a generally very useful application and novel analytical technique. Major aim of this study was development and validation of the latter rather than a chemosystematic investigation.

M. Ganzera
University of Innsbruck, Department of Pharmacognosy, Inst. of Pharmacy, 6020 Innsbruck, Austria
E-mail address: markus.ganzera@uibk.ac.at

Available online 30 October 2011

DOI of original article: 10.1016/j.jpba.2011.10.025.

doi:10.1016/j.jpba.2011.10.027

Journal of Pharmaceutical and Biomedical Analysis

Author enquiries
For enquiries relating to the submission of articles (including electronic submission) please visit this journals homepage at http://www.elsevier.com/locate/jpba. Contact details for questions arising after acceptance of an article, especially those relating to proofs, will be provided by the publisher. You can track accepted articles at http://www.elsevier.com/trackarticle. You can also check our Author FAQs at http://www.elsevier.com/authorFAQ and/or contact Customer Support via http://support.elsevier.com.

Funding body agreements and policies
Elsevier has established agreements and developed policies to allow authors whose articles appear in journals published by Elsevier, to comply with potential manuscript archiving requirements as specified as conditions of their grant awards. To learn more about existing agreements and policies please visit http://www.elsevier.com/fundingbodies

Orders, claims, and journal enquiries: please contact the Elsevier Customer Service Department nearest you:
St. Louis: Elsevier Customer Service Department, 3251 Riverport Lane, Maryland Heights, MO 63043, USA; phone: (877) 8397126 [toll free within the USA]; (+1) (314) 4478878 [outside the USA]; fax: (+1) (314) 4478077; e-mail: JournalCustomerService-usa@elsevier.com
Oxford: Elsevier Customer Service Department, The Boulevard, Langford Lane, Kidlington, Oxford OX5 1GB, UK; phone: (+44) (1865) 843434; fax: (+44) (1865) 843970; e-mail: JournalsCustomerServiceEMEA@elsevier.com
Tokyo: Elsevier Customer Service Department, 4F Higashi-Azabu, 1-Chome Bldg, 1-9-15 Higashi-Azabu, Minato-ku, Tokyo 106-0044, Japan; phone: (+81) (3) 5561 5037; fax: (+81) (3) 5561 5047; e-mail: JournalsCustomerServiceJapan@elsevier.com
Singapore: Elsevier Customer Service Department, 3 Killiney Road, #08-01 Winsland House I, Singapore 239519; phone: (+65) 63490222; fax: (+65) 67331510; e-mail: JournalsCustomerServiceAPAC@elsevier.com